Optimization-based design of structured LTI controllers for uncertain and infinite-dimensional systems

Raquel Stella da Silva de Aguiar

THÈSE

En vue de l'obtention du

DOCTORAT DE L'UNIVERSITÉ DE TOULOUSE

Délivré par : *l'Institut Supérieur de l'Aéronautique et de l'Espace (ISAE)*

Présentée et soutenue le *(16/10/2018)* **par :**

Raquel Stella DA SILVA DE AGUIAR

Optimization-based design of structured LTI controllers for uncertain and infinite-dimensional systems

---

JURY

Phillippe CHEVREL	Professeur	IMT Atlantique	Rapporteur
Edouard LAROCHE	Professeur	Université de Strasbourg	Rapporteur
Christophe PRIEUR	Directeur de recherche	CNRS	Examinateur
Pierre APKARIAN	Directeur de recherche	Onera	Directeur de thèse
Dominikus NOLL	Professeur d'Université	Université de Toulouse	Directeur de thèse

---

École doctorale et spécialité :
EDSYS : Automatique 4200046
Unité de Recherche :
ONERA - The French Aerospace Lab
Institut de Matèmathiques de Toulouse
Directeurs de Thèse :
Pierre APKARIAN
Dominikus NOLL

Abstract

The control of complex systems often requires model approximation amenable to available theory and computational tools. Synthesis based on overly reduced models in order to comply with limited synthesis techniques may even altogether fail. This may necessitate refining the approximate model. This is specially true for the design of finite-dimension Linear Time-Invariant (FDLTI) controllers for infinite-dimensional systems due to spillover effects. For this reason, either robust control, which takes the mismatch between actual and approximate systems into account, or data-driven control which avoids parametric models altogether, should be employed.

Parametric Robust Control synthesis is a NP-hard problem, where relaxations have to be used. These relaxations come with a degree of conservatism and with adverse effect on closed-loop performance. A main objective of this thesis is therefore to develop novel relaxations for robust structured controller synthesis for systems subject to parametric and complex dynamic uncertainty, which allow to avoid or reduce conservatism.

The first proposed strategy is an outer relaxation technique based on scalings or multipliers in tandem with small gain constraints leading to a single augmented model where scalings and controller are tuned simultaneously. The second approach is an inner relaxation method using worst-case scenarios for performance and stability, based computationally on specialized nonsmooth optimization techniques. This leads to an iterative multi-model synthesis, where all models have the state-space order of the nominal model. Finally, a third method combines the power of inner and outer relaxations in a hybrid technique.

In the data-driven control framework, frequency response based synthesis has already proved its versatility for performance optimization, but restricted to open-loop stable systems or pre-stabilized systems. This precludes dealing with unstable infinite-dimensional systems, whose response may be obtained for example from physical laws. Therefore, the second objective of this thesis is to dispense with open-loop stability and develop new methods for frequency response design of structured control laws for unstable or stable infinite dimensional systems.

To accomplish this goal, firstly a bisection method based on Nyquist stability criteria was produced to estimate the spectral abscissa of such systems. A method to estimate impulse response energy over a finite horizon was also developed. In the following, three techniques for designing stabilizing controllers are introduced based on minimization of the spectral abscissa, the impulse response energy, and of the shifted H_∞-norm of the closed-loop system.

The novel robust control techniques were tested on a bench of challenging examples and compared among others to the well-known μ-synthesis method. The results indicate that while outer relaxations excel on pure dynamic uncertainty cases, the inner relaxation proposed achieves the best certified robust performance in general, followed by the hybrid approach. Similarly, the data-driven control techniques were tested on a variety of unstable and stable systems of finite and infinite dimensions. The three data-driven techniques reached equivalent stabilization success rates.

Résumé

La commande de systèmes complexes requiert le plus souvent une approximation du modèle afin qu'il devienne abordable par la théorie et les outils de calcul disponibles. Les lois de commande conçues à partir de ces approximations peuvent se révéler inefficaces lorsqu'elles sont appliquées au système réel. Elles doivent donc être vérifiées a posteriori et peuvent entraîner une modification de l'approximation du modèle si nécessaire. Ceci est particulièrement vrai dans la conception de compensateurs linéaires à temps invariant de dimension-finie (LTIDF) pour les systèmes de dimension infinie en raison du spillover effect. Pour cette raison, il est recommandé d'utiliser, soit une approche de type commande robuste (qui prend en compte l'écart entre le système réel et le modèle), soit du data-driven control qui s'affranchit complètement des modèles paramétriques.

La synthèse de commande robuste est un problème NP-difficile, donc des relaxations sont ici encore utilisées pour simplifier le problème. Ces relaxations introduisent un certain conservatisme des solutions, dégradant la performance en boucle fermée. Ainsi le premier objectif de cette thèse est de développer de nouvelles relaxations pour la synthèse de compensateurs robustes structurés pour des systèmes soumis à des incertitudes paramétriques et dynamiques afin de réduire autant que possible le conservatisme de l'approche.

La première relaxation proposée est une relaxation externe basée sur des *scalings* ou multiplicateurs et des contraintes de faible gain. Ceci conduit à un modèle augmenté unique où les multiplicateurs et le compensateur sont calculés simultanément. La seconde est une relaxation interne basée sur les estimations de pires cas tant en stabilité qu'en performance par des techniques d'optimisation non-lisse. Ces relaxations conduisent à une synthèse itérative multi-modèle où les modèles ont la même ordre que le modèle nominal. Enfin, une troisième méthode combine des relaxations internes et externes dans une technique hybride.

Dans le domaine du data-driven control, la synthèse à partir de données fréquentielles est dejà utilisée avec succès pour l'optimisation de performance, mais elle est limitée aux systèmes stables en boucle ouverte ou pré-stabilisés. Ceci exclut son utilisation sur des systèmes de dimension infinie instables dont les données fréquentielles sont par exemple obtenues à partir d'un modèle s'appuyant sur les lois physiques. Le deuxième objectif de cette thèse est donc de développer des nouvelles méthodes de conception de lois de commande structurées à partir de la réponse fréquentielle pour des systèmes de dimension infinie stables ou instables.

Pour atteindre cet objectif, une méthode de type bisection basée sur les critères de stabilité de Nyquist a été produite pour estimer l'abscisse spectrale de tels systèmes. Une méthode d'estimation de l'énergie de la réponse impulsionnelle sur un horizon fini a également été développée. Ensuite, trois techniques de conception de compensateurs stabilisants ont été créées en utilisant la minimisation de l'abscisse spectrale, de l'énergie de la réponse impulsionnelle et de la norme H_∞-norm décalée d'un système.

Les techniques de commande robuste ont été évaluées sur de nombreux cas test et comparées entre elles, ainsi qu'à la mu-synthèse plus classique. Les résultats indiquent que si les relaxations externes excellent sur des cas d'incertitude dynamique pure, la relaxation interne proposée atteint une meilleure performance robuste en général, suivie par notre approche hybride. De même, les techniques de data-driven control ont été testées sur une variété de systèmes instables et stables de dimensions finie et infinie. Les trois techniques basées sur les données ont atteint des taux de réussite de stabilisation équivalents.

Table of Contents

List of Figures

List of Tables

List of acronyms and abbreviations

ARE	algebraic Riccati equation.
ARI	algebraic Riccati inequality.
BIBO	bounded input bounded output.
BMI	bilinear matrix inequality.
DGK	DGK-iteration.
DPS	distributed parameter system.
FDLTI	finite dimensional linear time-invariant.
FOPID	fractional order proportional integral derivative controller.
FOS	fractional-order system.
FRD	frequency response data.
IDLTI	infinite dimensional linear time invariant.
IQC	integral quadratic constraint.
KKT	Karush–Kuhn–Tucker.
LFT	linear fractional transformation.
LHP	left half-plane.
LMI	linear matrix inequality.
LPV	linear parameter-Varying.
LQ	linear quadratic.
LQG	linear quadratic gaussian control.
LQR	linear quadratic regulator.
LTI	linear time invariant.
LTV	linear time-variant.
MIMO	multi-input multi output.
ODE	ordinary differential equation.
PDE	partial differential equation.
PID	proportional integral derivative controller.
RHP	right half-plane.
ROM	reduced order model.
RP	robust performance.
RS	robust stability.
SDP	semidefinite programming.
SIP	semi-infinite programming.
SISO	single-input single-output.
SSV	structured singular value.

SVD singular value decomposition.

TDS time-delay system.

List of symbols

[...]	Used to distinguish unities from variables, p.ex. K controller from $[K]$ Kelvin, unity of temperature.
$\|\cdot\|_\infty$	H_∞-norm.
$\|\cdot\|_2$	H_2-norm.
α	Also $\alpha(\mathbf{M})$ - Spectral abcissa of matrix $\mathbf{M}$.
$\mathcal{A}(\beta)$	see (2.1).
$\hat{\mathcal{A}}(\beta)$	Class of Laplace Transform of functions belonging to $\mathcal{A}(\beta)$.
$\hat{\mathcal{A}}_-(\beta)$	see (2.2).
$\hat{\mathcal{A}}_\infty(\beta)$	see (2.3).
$\mathfrak{a}$	Value of frequency-domain translation $F(s+\mathfrak{a})$.
$\hat{\mathcal{B}}_-(\beta)$	Callier-Desoer class of transfer functions. see (2.4).
$\mathbb{C}$	Field of complex numbers.
$\mathbb{C}_\beta^-$	Semiplane with $Re(s) < \beta$.
$\overline{\mathbb{C}_\beta^-}$	Semiplane with $Re(s) \leq \beta$.
$\mathbb{C}^-$	Semiplane with $Re(s) < 0$.
$\mathbb{C}_\beta^+$	Semiplane with $Re(s) > \beta$.
$\overline{\mathbb{C}_\beta^+}$	Semiplane with $Re(s) \geq \beta$.
$\mathbb{C}^+$	Semiplane with $Re(s) > 0$.
Δ	Uncertainty block.
$\mathbf{\Delta}$	Structured uncertainty set.
Δ_d	Dynamic uncertainty block.
Δ_p	Parametric uncertainty block.
$\check{\mathbf{\Delta}}$	$\check{\Delta} \subset \Delta$.
$\tilde{\mathbf{\Delta}}$	$\tilde{\Delta} \supset \Delta$.
$\det(\mathbf{M})$	Determinant of matrix $\mathbf{M}$.
$\delta(.)$	Dirac delta function.
$\mathbb{F}^n$	Space of vectors with dimension n over field $\mathbb{F}$.
$\mathbb{F}^{m\times n}$	Set of matrices with dimension $m \times n$ over field $\mathbb{F}$.
$\mathbb{F}^*$	Non-null numbers of field $\mathbb{F}$.
$\mathbb{F}^+$	Numbers of field $\mathbb{F}$ with positive real part.
$\mathbb{F}^-$	Numbers of field $\mathbb{F}$ with negative real part.
$\dot{f}$	First derivative of function f.
$\ddot{f}$	Second derivative of function f.
$f^{(n)}$	*nth* derivative of function f.
G	Model of a plant.
$\mathcal{H}^2$	Space of frequency-domain square integrable functions analytic on RHP.
$\mathcal{H}^\infty$	Space of frequency-domain functions bounded on $j\mathbb{R}$ and analytic on RHP.

$\mathcal{H}_a^\infty$	Space of frequency-domain functions bounded on $a + j\mathbb{R}$ and analytic on complex semi-plane $Re(s) > a$.
$\mathbf{I}$	Identity matrix; dimension from context.
$\mathbf{I_n}$	Identity matrix of dimension $n \times n$.
index(g, a)	Index of curve g around point a on real axis, by extension index of Nyquist curve of system g.
j	Pure imaginary unity, $j = \sqrt{(-1)}$.
$j\mathbb{R}$	Imaginary axis of complex plane.
K	Model of a control law; by extension the controller structure itself.
κ	Vector of controller parameters.
$\mathcal{L}^2$	Space of time-domain square integrable functions.
$\mathcal{L}^2[0, \infty)$	Subspace of $\mathcal{L}_2$ of causal functions.
$\mathcal{L}^\infty$	.
$\mathcal{L}^1$	Space of time-domain of absolutely integrable functions.
$\mathbf{M}$	Generic matrix notation.
$\mathbf{M_{m\times n}}$	Matrix $\in \mathbb{M}^{m\times n}$.
$\mathbf{M_{i,j}}$	Matrix dummy indexation.
$\mathbf{M^H}$	Matrix hermitian.
$\mathbf{M^{-1}}$	Matrix inverse.
$\mathbf{M}^-$	Matrix inverse in the sense of LFT.
$\mathbf{M_{ij}}$	Matrix partition.
$\mathbf{M^T}$	Matrix transpose.
$\mathbf{M}^*$	Matrix transpose conjugate.
$\mathbf{0_{m\times n}}$	Null matrix $\in \mathbb{M}^{m\times n}$.
μ	Also $\mu(\mathbf{M})$ - Structured singular value.
nb	Number of branch-points on $j\mathbb{R}\backslash\{0\}$.
nb_0	Number of branch-points at origin.
$\mathbb{N}$	Field of natural numbers.
n_p	Number of unstable poles.
n_z	Number of unstable zeros.
n_0	Number of poles at origin.
P	Generalized plant model.
$\mathbb{Q}$	Field of rational numbers.
$\mathcal{RH}^\infty$	Space of frequency-domain rational functions bounded on $j\mathbb{R}$ and analytic on RHP.
$\mathcal{RH}_a^\infty$	Space of frequency-domain rational functions bounded on $a + j\mathbb{R}$ and analytic on complex semi-plane $Re(s) > a$.
$\mathbb{R}$	Field of real numbers.
ρ	Also $\rho(\mathbf{M})$ - Spectral radius of matrix $\mathbf{M}$.
s	Laplace variable, $s = a + j\omega$, $a, \omega \in \mathbb{R}$.
σ	Also $\sigma(\mathbf{M})$ - Singular value of matrix $\mathbf{M}$.
$\overline{\sigma}$	Also $\overline{\sigma}(\mathbf{M})$ - Maximum singular value of matrix $\mathbf{M}$.
$\underline{\sigma}$	Also $\underline{\sigma}(\mathbf{M})$ - Minimum singular value of matrix $\mathbf{M}$.
$M \star N$	Redheffer star product of M, N.
t	Time.
tr	Also $tr(\mathbf{M})$ - Trace of matrix $\mathbf{M}$.

$T_{w \to z}$	Transfer function from input w to output z.
ω	Frequency [rad/s].
$\mathbb{Z}$	Field of integers numbers.

Chapter 1

Introduction

In this introductory chapter, the context of this work is established by presenting the background of control of infinite-dimensional systems, robust control and data-driven control. In the following, the motivation, objectives and main contributions of this thesis are stated. At last, the path to achieve the objectives is exposed by briefing the following chapters.

1.1 Problem

The design of control laws relies on information about the system we have to control. Clearly, if the information provided does not correctly characterize the system, the control law designed will be inappropriate or at least achieves poor performance. This is specially true for the design of Finite-Dimension Linear Time-Invariant (FDLTI) controllers for infinite-dimensional systems due to spillover effects. Depending on how the system information is conveyed for control purposes, two major control approaches are employed: model-based control and data-driven control.

In model-based approaches, controllers are designed for a parametric model whereas in data-driven control they are designed based on system input-output data. Parametric models may be obtained directly from physical laws describing the system or by fitting experimental data from the system to build a model structure. The model obtained from the first method is usually involved and not amenable to computational techniques or tools. On the other hand, models obtained from experimental data may be inaccurate due to noise or poor choice of model structure. Some data-driven control approaches manage noisy and inaccurate experimental data. Other approaches however deal with nonparametric models, like for instance frequency response data. A prominent pitfall of data-driven methods is stability certification and stabilization.

In short, three control challenges are addressed:

- the control of infinite-dimensional systems (as a complex system);
- the control of uncertain systems;
- the system stabilization and control through data-driven control.

The literature on the matter is extensive and various different methods were proposed over recent years. In the following, some of the relevant contributions to this work are briefly presented.

1.2 Background

Infinite-dimensional linear time invariant systems (IDLTI) control

Physical systems are inherently nonlinear, time varying, continuous on time and are distributed parameter systems. This comes from continuity, saturation and non-instantaneous propagation of signals and the fact that system dynamics change over time. Notwithstanding, for the range of interest of signals excursion, for instance, near an equilibrium point, and when system dynamics variations are very slow compared to the interval of observation, systems can be assumed to be linear time invariant (LTI) for control purposes.

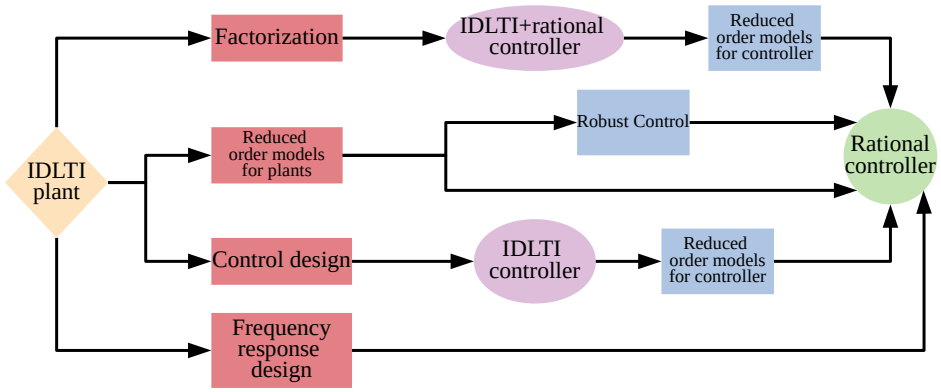

Figure 1.1: Examples of methods for designing rational controllers for IDLTI systems.

The infinite dimensional linear time invariant (IDLTI) systems class comprises among others time-delay system (TDS) and fractional-order system (FOS) and systems described by partial differential equation (PDE). The representation of such systems is not trivial and the existence of one type of representation does not imply existence of another [Curtain, 1989; Zwart, 2004]. The analysis theory of finite dimensional linear time-invariant (FDLTI) systems should be carefully extended to IDLTI. For instance, stability criteria are not as straightforward, not only because pole locations are difficult to calculate, but mainly because the different stability criteria are not necessarily equivalent. For example, a system may have all its poles on left half-plane (LHP) and yet not even be $\mathcal{H}^\infty$ stable [Partington and Bonnet, 2004].

The implementation of systems with irrational transfer functions faces several technical challenges and for this reason, in practice, the control of infinite-dimensional systems employs rational controllers. Gibson [1980] demonstrated that it is not always possible to stabilize an IDLTI system by a finite-dimensional control law. Mikkola and Staffans [2004]; Quadrat [2004a,b] and Mikkola [2005] proved that strong stabilizability of plants is conditioned to the existence of coprime factorization on stable spaces. Earlier, Curtain [1984] showed that IDLTI systems with regular spectral operator with only finitely many eigenvalues on the right half-plane (RHP), finite rank input and output operators and minimal realization can be stabilized by a finite-dimensional controller. It was later shown in Curtain [1985] that the reach of stabilizing control action for infinite-dimensional plants is limited and that there are expected bounds on the order of a stabilizing controller. The controller effect on original system poles is computed by using results of degenerate perturbations to the characteristic equation of IDLTI system.

Similar to the condition presented by Curtain [1984], Balas [1984] proved the dependence of stabilization of IDLTI systems by finite-dimensional controller on existence of plant decomposition in stabilizing subspaces. Curtain [1992] finally proved that if a plant can be decomposed into stable infinite-dimensional space and into a finite-dimensional unstable space and if a controller can stabilize the plant containing the unstable poles, this controller can also stabilize the IDLTI plant, method exploited in Bresch-Pietri et al. [2018].

Curtain [1984, 1985, 1992] and Balas [1982, 1983] proposed the design of rational controllers based on reduced order model (ROM) of IDLTI plants. While Balas focused on Galerkin approximates, Curtain based the approach on modal reduction. Balas [1984] characterized IDLTI plants that can be exponentially stabilized by finite-dimensional controller as the ones having closed, linear and unbounded infinitesimal generator of a strong C_0-semigroup with domain dense on Hilbert space.

Balas [1985] computed the performance degradation by using a finite-dimensional controller instead of optimum infinite-dimensional controller obtained through the solutions of algebraic Riccati equation (ARE) for linear quadratic regulator (LQR) control and infinite Kalman filter. Balas [1986] suggested that, instead of designing finite-dimensional controller based on ROM of the plant, one could obtain a finite-dimensional controller from ROM of an infinite-dimensional controller. The main difference between this approach and that of Balas [1985] is that, in the first, the condition relies on the distance of models whereas Balas [1985] is based on convergence of a series of approximates. He also established the conditions for the equivalence of the controllers obtained by the two methods in terms of stabilization and performance.

Time-delayed systems (TDS-LTI)

TDS and FOS are particular classes of infinite-dimensional systems. Time delay arises from systems with finite propagation of signals or from modeling time elapsed on measurements from sensors, processing time and response time of actuators. Time delay appears as output delays (dead-time systems) or internal delays and may be discrete or distributed. TDS with internal delays can be classified in retarded, neutral and advanced types. For a brief review on the subject refer to Richard [2003]. Even if TDS are used for simplifying models of systems described by PDEs, the stability analysis of TDS is complicated by existence of infinitely many poles. As in the infinite-dimensional general case, analyticity on closed RHP may not be enough to imply bounded input bounded output (BIBO) or even $\mathcal{H}^\infty$ stability [Partington and Bonnet, 2004].

Bonnet and Partington [2000a,b] presented BIBO stability condition for retarded systems with quasi-polynomials of fractional-order with fractional-order delay. In these works they presented coprime factorizations of such systems and the Bézout factors for parametrizing the set of stabilizing controllers. The drawback of this approach is that the controller is infinite-dimensional. Bonnet and Partington [2002, 2007] and Partington and Bonnet [2004] presented necessary and sufficient conditions for BIBO and $\mathcal{H}^\infty$ stability of retarded and neutral systems for integer-order quasi-polynomials with integer-order delays. They proved that a neutral system is stabilizable by a finite-dimensional controller if and only if it admits a coprime factorization on $\mathcal{L}^1+\mathbb{C}\delta(.)$ and, for this reason, advanced systems cannot be stabilizable by a finite-dimensional controller .

For the much simpler case of dead-time systems, the classical approach for single-input single-output (SISO) stable plants with known delays, the control can be based on Smith predictor [Smith, 1957]. The approach was extended to unstable systems in Paor [1985] and Padhan and Majhi [2011]. A comprehensive review on literature about the Smith predictor can be found in O'Dwyer [2005]. In their contributions, Meinsma and Zwart [2000] and Mirkin [2003] obtained $\mathcal{H}^\infty$ controllers for dead-time systems. Even though through different paths, both developed controller synthesis by J-factorization and a causality constraint for a delay-free plant. The two approaches are in fact modified Smith predictors. Additionally, Mirkin [2003] demonstrated the degradation of performance caused by intput delays.

Kashima and Yamamoto [2008a,b] specialized a method for plants characterized by a connection of rational unstable plant and irrational scalar inner function, where dead-time systems are a particular case. They proposed the design of rational controllers by solving two finite-dimension ARE with an additional rank condition. Then the rational controller is paramterized by the inner function.

Fractional-order systems (FOS-LTI)

The second particular case of infinite-dimensional concerns FOS that arise from systems with fractal structure and/or comprising hereditary materials [Oustaloup et al., 2014; Paola and Zingales, 2013]. These are infinite-dimensional systems that admit finite-dimensional pseudo-state representation with pseudo-state fractional derivatives [Matignon, 1998]. The fractional-order transfer functions are multivalued functions hence their analysis is made on Riemman surfaces. This means that branch points and branch cuts should be taken into consideration when studying stability and contours [Mignot et al., 2009].

Using the pseudo-state representation, Matignon [1998] derived stability criteria based on eigenvalues of characteristic equations of the systems. Likewise, Sabatier et al. [2010] developed linear matrix inequality (LMI) stability criteria. Both authors characterize BIBO, $\mathcal{H}^\infty$, exponential and asymptotic stability for this class of systems. In addition, Sabatier et al. [2013] and Trachtler [2016] made analysis based on the Nyquist stability criterion.

In the majority of publications, fractional-order controllers are preferred for FOS control. One successful approach to fractional-order controller design was presented in Oustaloup and Bansard [1993]; Oustaloup et al. [1993] and Lanusse et al. [1993] where they introduced the CRONE (*commande ordre non entière, controller with noninteger order*). Another contribution on this subject was made by Podlubny [1999] who introduced the fractional-order proportional integral derivative controller (PID) controller. Both types of fractional-order controllers were proved to be superior on stabilization and performance for FOS. The use of fractional order proportional integral derivative controller (FOPID) was suggested by Monje et al. [2004] as means to obtain higher degrees of freedom on control. Other approaches to control of FOS include Dorcak et al. [2001], with discretization of system with proportional derivative controller (PID) control, Bhole et al. [2015] with model predictive control and Shirazi

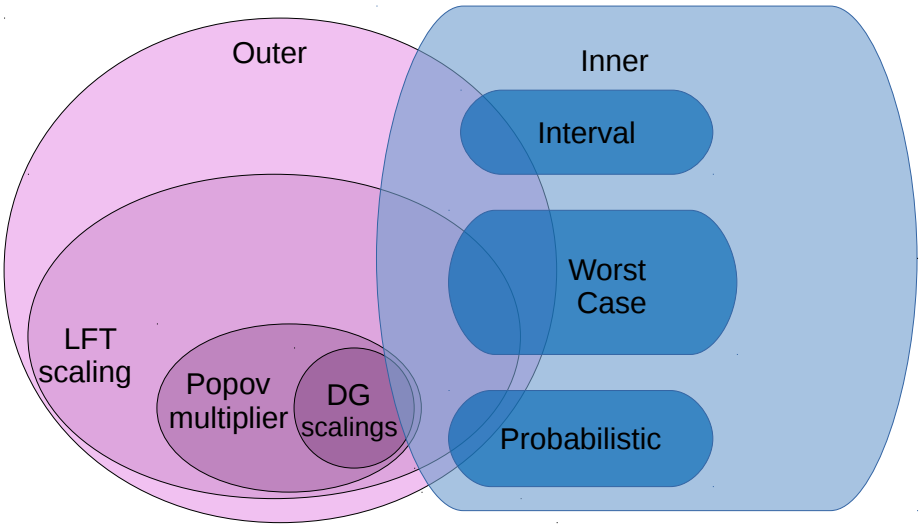

Figure 1.2: Examples of outer and inner relaxation techniques cited in text. Combinations of inner and outer relaxations are possible and will be exploited in this work.

and Ibrir [2016] with static output feedback on pseudo-state representation with solutions derived from LMI.

Robust control

The approximation of an infinite-dimensional system by a finite-dimensional model and the modeling of the mismatch as uncertainty turns the design of finite-dimensional controllers for infinite-dimensional system into the framework of Robust Control theory. This idea was already exploited in Curtain and Glover [1986]. It was shown that if the plant can be decomposed into a finite-dimensional space containing all unstable poles and a stable infinite-dimensional plant, a finite-dimensional controller can be designed for the finite-dimensional part with the mismatch of models playing the role of uncertainty. To this end, the time delay can be replaced by a Padé approximation and fractional-order terms can be approximated using e.g. Oustaloup's method [Vinagre et al., 2000b].

Robust control consists in achieving robust stabilization and robust performance for a system subjected to uncertainties. For the specific case of FDLTI plants subject to FDLTI and stable perturbations, the state of art used to be μ-synthesis for many years. Doyle [1982] introduced the structured singular value of a complex matrix, the μ value, that is a function of the perturbed matrix and of the structure of the perturbation. The objective was to exploit the structure of the uncertaity in order to reduce conservatism of the robustness analysis. The author stated the properties of the new function and, from the relation to other linear algebra functions, lower and upper bounds of μ were established along with scalings to tighten the bounds. The work was extended to mixed structured uncertainties with real and complex blocks in Doyle [1985]. Further developments on bounds, scalings and algorithms to compute the bounds were presented in Fan et al. [1991]; Young [1994]; Young et al. [1991]. Two important theorems are the Small μ Theorem and the Main Loop Theorem, respectively addressing Robust Stability and Robust Performance in terms of μ.

The μ-synthesis is an iterative procedure known as *DK-iteration* consisting mainly of two steps. The first step concerns the optimization of the upper bound of μ value with respect to scalings and the fitting of the scalings with rational realizations. The second is the synthesis of a new unstructured controller for the scaled plant. Each step is convex with respect to the argument of the optimization but the iterative procedure is not guaranteed to converge, even though it is proved to be monotonically non-increasing with respect to μ value.

Chiang and Safonov [1992]; Safonov and Chiang [1993]; Safonov et al. [1993] criticized the *DK-iteration* stating that the fitting of the scalings introduces an unkown amount of conservatism. They proposed to replace scalings by the more general Popov multipliers. The approach is based on a positive-real bilinear transformation, recasting the Small Gain Theorem for stability of interconnected systems as Positive-Real Lemma formulation. The synthesis procedure is also iterative, with one step

concerning maximization of the stability margin with respect to polynomial multipliers and other being synthesis of controller for the augmented plant. The main difference is the use of maximization directly wrt to polynomial multipliers, hence avoiding fitting.

Asai et al. [1996] and Iwasaki and Hara [1998] presented an linear fractional transformation (LFT) scaling derived from the Small Gain Theorem and topological separation for well-posed connected systems. They demonstrated that the scalings of Doyle [1985], Popov multipliers and IQC framework are all particular cases of LFT-scalings. They pondered that computing a separator that satisfies all the constraints may be too hard and proposed inner and outer approximations for the separator class, which lead to lower and upper bounds on robust stability and performance.

The structured singular value represents the largest structured perturbation a stable system can withstand before becoming unstable. The Main Loop Theorem extended the concept to the largest perturbation the system can take while remaining stable and achieving the value of performance.

Although Safonov, Doyle and Iwasaki have different formulations for the problem of finding the largest uncertainty norm a system can take and assure a certain performance level, it is shown that they are equivalent and can all be cast as the problem of finding the μ value in the Main Loop Theorem.

Computing the exact value of μ was proven to be a NP-hard problem [Braatz et al., 1994] and thus a relaxation of the problem is necessary. The approaches of Iwasaki and Hara [1998], Safonov et al. [1993] and Balas [1985], all use outer relaxations, meaning they solve the problem for a larger set that covers the original set of uncertainty by the use of scalings and multipliers. The rationale is that if robust performance and stability are achieved on the larger set, they are also certified for the true set of uncertainties. The drawback is the unknown level of conservatism introduced.

Inner relaxation for robust control

An alternative method to reduce conservatism is the inner approximation as used in Ackermann [1985]. The method consists in a multi-model synthesis for a discrete set of representative plants of the infinite set of uncertain plants. No conservatism is introduce as only uncertainties belonging to original problem are considered. In order to assure stability and the desired level of performance, two major approaches regarding the choice or the number representative perturbed plants prevail: probabilistic and worst-case.

Calafiore and Campi [2006] argumented that basing the analysis on worst-case results in unnecessary conservatism if they are not representative of most of set and a probabilistic choice is more appropriate. Barmish and Lagoa [1996, 1997] and Stengel and Ray [1991] developed analysis of Robust stability and performance on probabilistic grounds. They used Monte Carlo simulation to provide probability of instability and confidence interval, both proved to depend only on the number of samples. In Tempo et al. [1997] it was determined the number of samples of uncertainty necessary to assure a desired Probability level of performance.

Inspired by these results, Calafiore and Campi [2006] developed a robust controller synthesis procedure. First a ϵ-level risk of violation of performance was formulated as a function of the number of samples. This formulation requires even fewer samples than the previous cited methods, typical values reported as being at the order of thousands. Sability and performance certifications are obtained by Monte Carlo simulations. In order to have zero probability of instability, it is necessary an infinite number of samples, meaning the whole set should be tested. So in cases where there is no possibility of failure, the worst-case approach is indicated. The rationale of the approach is that if the controller designed stabilizes and guarantees a performance level for the worst-case perturbed plant of the set, it stabilizes and achieves at least the same level of performance for all the set. The difficulty lies in how to assure the worst-case is picked.

Magni et al. [1998] proposed an iterative method to find these scenarios. It consists in synthesizing a controller for the nominal model and performing a μ analysis to find the uncertainty corresponding to the worst-case scenario. In the sequel, the uncertain model is added to the set of models for which a multi-model control synthesis follows. The procedure is repeated until the performance of worst-case returned is acceptable. The μ-analysis is based on a lower bound of μ, so at the end, a global certification method must follow.

Apkarian et al. [2015b, 2016] proposed a method to find the worst-case scenario of H_∞ performance and stability of systems subject to parametric uncertainty. The worst-case scenario is understood as the scenario corresponding to the largest H_∞ norm for performance and largest spectral abscissa for stability. The uncertainty is constrained in a box and the functions to be maximized are nonsmooth

and nonconvex. They developed then a nonsmooth optimization method. Apkarian et al. [2015a] exploited the results in an iterative procedure for the synthesis of robust controllers similar to Magni et al. [1998], but using the nonsmooth method to find the worst-cases. Apkarian and Noll [2017] showed how to extend the method of Apkarian et al. [2015b] to mixed (complex and real) uncertainty. They transform how to express the constraints on complex uncertainty into box constraints.

H_∞ -control

After the relaxation of the robust control problem, the robust control synthesis is reduced to a control synthesis. In the H_∞ control framework the classical synthesis method is iterative and the controller is parameterized by solutions of ARE, that can be found by LMI solvers. However the controller obtained lacks structure. Unstructured controllers may be of high-order or not even be rational, cases where implementation is limited. Engineering advantages of structured controller, such as simple implementation, easier readjustment and economy, explain their popularity in practical applications as repported in Abroug et al. [2016], Benner et al. [2018] and Zebiri et al. [2013]. Nevertheless, the restriction on controller structure turns the synthesis into a nonconvex problem.Gahinet [1992]; Gahinet and Apkarian [1994] cast the structured H_∞ control using convex formulations with an additional non-convex constraint on the rank of matrix, as did later Iwasaki and Skelton [1993, 1994].

Methods designed specifically to cope with the lost convexity of the already nonsmooth problem were later developed. Mammadov and Orsi [2005a,b] proposed global optimization algorithms that require no gradient information using spectral radius as cost function. On the other hand, Burke et al. [2005] proposed a local optmization method based on gradient sampling for designing stabilizing reduced-order controllers that later would become the basis for MATLAB ™ routines HIFOO [Burke et al., 2006]. In Apkarian et al. [2005] a nonsmooth technique exploiting subdifferentials of the H_∞-norm and bundle methods was employed to H_∞ synthesis of structured controllers. , with further developments in Apkarian and Noll [2006d]. The nonsmooth optmization for multidisk H_∞ synthesis of [Apkarian and Noll, 2006b,d] are the core of MATLAB ™ routines HINFSTRUCT and SYSTUNE . A multidirectional search was also proposed in Apkarian et al. [2004] and Apkarian and Noll [2006c] for the same nonsmooth nonconvex synthesis problem.

In Apkarian and Noll [2006a] and Apkarian et al. [2014] the work of [Apkarian and Noll, 2006d] was extended for multi-disk and multi-model synthesis, on which MATLAB ™ routine SYSTUNE is based. Other approaches on multi-objective design includes Dym et al. [1999, 2002] and Hu et al. [1996] and on multi-model synthesis the works of Magni et al. [1998] by eigenstructure assignment and Ackermann [1985] by simultaneous pole assignement and vectorial performance criteria.

Frequency response data control

As mentioned, robust control is applicable when the structure of the model that fits system's observed behavior is too complex and is alleviated by introduction of uncertainties to a simpler model structure. A natural approach is to avoid model identification and design control laws straight from the input-output behavior in the data-driven approach [Safonov, 1994]. The main distinction among data-driven control methods concerns the implementation of control laws as controller parameters are being tuned, distinguishing adaptive control from the others.

Adaptive control approaches as unfalsified control [Helvoort et al., 2006; Safonov and Tsao, 1997], iterative feedback tuning [Hjalmarsson, 2002], model reference adaptive techniques [Landau, 1974] and learning control [Hunt et al., 1992] constantly update the control law as new data are acquired. This is characterized by the implementation of the controller and realizations of new experiments for acquiring new closed-loop data. This method is not suitable for systems with payload limitation as drones, for example.

Non-adaptive techniques thus rely on the assumption that the available data fully express the system behavior. It means assuming the system is linear, time-invariant, sampled at a rate higher than its bandwidth and long enough to capture slow dynamics. Although these assumptions may seem too restrictive, they are also necessary for identification of LTI models. These conditions are translated as the assumption that the grid data is dense enough. An analysis of intergrid behavior is made by Hamer et al. [2009b] and the limitations on control performance in Vries [1994] and Galdos et al. [2010].

An H_∞ frequency response data (FRD) design of fixed-order controllers for pre-stabilized or stable SISO systems is presented in Galdos et al. [2007]. The method consists in recasting the specifications

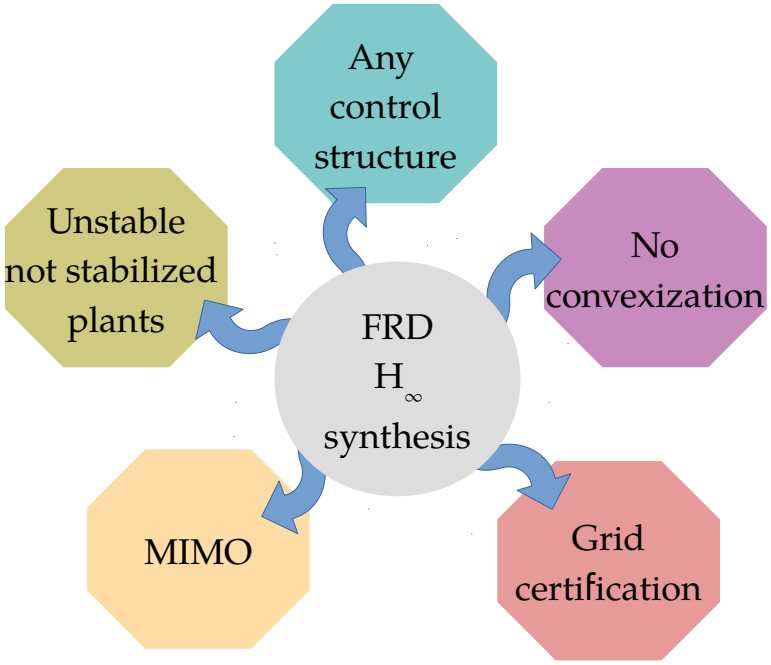

Figure 1.3: Desired features for an FRD H_∞ design method.

as constraints on the Nyquist diagram, limiting the region the curve of the closed-loop system may lay. These constraints are non-convex with respect to linearly parameterized controllers and are convexified by introduction of a reference model. This was later extended to control of multi-model subjected to frequency domain uncertainty in Karimi and Galdos [2010]; Karimi et al. [2008]. Their approach however does not allow free tuning of controller poles and provides a conservative solution due to convexization.

An alternative to obtain linearly parameterized controllers which allows tuning of controller poles is proposed for pre-stabilized or stable SISO systems in Karimi and Zhu [2014]. The method consists in recasting the problem by means of plant coprime factorizations and of linearly parameterized coprime factors of the controller. The non-convex H_∞ constraints are then convexified with respect to the coprime factors.

The extension of FRD design to multi-input multi output (MIMO) systems usually carry out a system decoupling like as the method proposed in Galdos et al. [2009] using Gershgorin bands. As an alternative, Karimi and Kammer [2017] extended the coprime factorization method of Karimi and Zhu [2014] to MIMO systems. In order to convexify the problem, they used Taylor expansion at the initial point, considering a closed-loop stable configuration for a given initial controller. They argued that other model-based techniques also demand initialization, citing nonsmooth optimization based control techniques as examples.

Another contribution to FRD design of structured controller for stable MIMO systems is Solingen et al. [2016]. In their work the authors used the linear parameterization proposed in Karimi and Galdos [2010], but incorporate the basis function into the generalized plant leaving the coefficients of parametrization on a diagonal-structured controller. They used the generalized Nyquist criterion of [MacFarlane and Postlethwaite, 1977] and constraints on Nyquist diagram of the closed-loop system curve to derive a multilinear feasibility problem that can be convexified for some controller structures.

The most recent contribution was made in Apkarian and Noll [2018]. The authors developed an FRD control design for stable or stabilized MIMO for any kind of control structure based on nonsmooth optimization. They also presented a method to verify if the grid of frequencies for which the plant response is available, which allows stability and performance certification. It was also illustrated how the method can be employed in the control of IDLTI MIMO stable or stabilized system. The technique is not conservative as no convexization or linearization is made regardless the nonconvex and nonsmooth character of the problem. However, there is no guaranteed of return of the optimum solution once a local solver is exploited.

The most challenging aspect of data-driven control is to assure closed-loop stability based only on finite samples of open-loop system behavior. Most FRD design techniques and stability tests rely on existence of an initial stabilizing controller, used by occasion of acquisition of experimental data, and so only aim to maintain stability.

Keel and Bhattacharyya [2010] introduced a new characterization of Nyquist criterion in terms of constraints on magnitude, phase and rate change of phase of the controller response. Based on this criterion, it is possible to determine if a controller with a given structure can stabilize a given plant, without tuning. Mohsenizadeh et al. [2012] used the technique to obtain the set of stabilizing PID controllers for a plant. The techniques are applicable to SISO systems, even unstable ones, if the number of unstable poles is known.

Other approaches to FRD stabilization of unstable SISO systems use reference models and try to obtain a stable closed-loop system by minimizing the distance between actual and reference model, as in Heusden et al. [2010]. The main drawback of this technique is that the choice of the reference model is crucial to the success and the problem cannot be convexified unless a initial stabilizing controller is known.

Finally, the work of Hamer et al. [2009a] on FRD design of structured controllers for SISO unstable or stable systems is mentioned. Their design is divided in two steps: performance optimization and stabilization. The stabilization step is based on the gradient of ratio of two functions that points towards the region of stabilizing controllers. They used the mapping between stabilizing controller and stable systems to constrain controller parameters in terms of Cauchy Residue Theorem. In the following they conceived a cost function by the ratio between the residue of a function and the function itself. They showed that the gradient of this cost function points toward the region of stabilizing controllers. The norm minimization is driven by LMI optimization of first order approximations of the norm. The stability in this step is assured by introduction of barrier functions.

1.3 Objective and contributions of the thesis

The available robust control relaxations for the mixed dynamic and parametric structured uncertainty consist in either sampling or enlarging the space of uncertainties. The sample approach, an inner relaxation, will provide robust stability (RS) only if the worst case is among the samples, and worst-case estimators are reported to have problems on challenging parametric uncertainty cases. The outer relaxations available introduce a large amount of conservatism in parametric uncertainty case due to take uncertainty values that were not present in the original problem into consideration. Regarding FRD synthesis, many of the techniques do not address unstable systems unless an initial stabilizing controller is provided by the user. The few methods available for synthesis of structured controller for unstable systems contemplates only SISO case among other limitations. These limitations motivates the two main objectives of this thesis:

Objectives:

- Reduce the conservatism of robust control solutions for the mixed dynamic and parametric structured uncertainty with consequent improvement of performance; and
- Direct synthesis of structured FDLTI controllers for IDLTI, eliminating steps of model reduction and consequent improvement of performance.

To fullfil these objectives, the following contributions resulted from this work:

Main contributions:

- Development of a novel outer relaxation of the robust control problem for the mixed dynamic and parametric structured uncertainty with simultaneous tuning of controller and multipliers with no need to rescale the uncertainty ball;
- Development of a novel inner relaxation of the robust control problem for the mixed dynamic and parametric structured uncertainty based on computation of worst-case scenarios by nonsmooth optimization technique which reduces the conservatism to a very low level;

- Development of a hybrid relaxation of the robust control problem for the mixed dynamic and parametric structured uncertainty with the new inner and outer relaxations developed that is computationally attractive for limited computational power applications;
- Development of a spectral abscissa estimator for meromorphic IDLTI systems;
- Development of three techniques for synthesis of structured FDLTI controllers for unstable and stable IDLTI systems by FRD synthesis, with direct stability and performance estimation.

1.4 Structure of the thesis

Chapter 2 - State-of-art: The theoretical support of the thesis is presented in Chapter 2. The concept of stability and Nyquist stability tests are presented for MIMO FDLTI and IDLTI systems. The multidisk H_∞ control for structured controller synthesis by nonsmooth optimization is briefly presented. The robust control problem is presented in the sequence. The standard relaxations, multipliers and multi-models, are explained. The chapter ends recalling how to choose a grid on frequencies for ensure stability and accuracy of H_∞-norm for data-driven control.

Chapter 3 - Development of outer relaxation for robust control: Chapter 3 contains the first contribution of the thesis to robust control domain. It begins with the development of a novel outer approximation for the robust structured controller synthesis for systems subjected to mixed uncertainty. The approximation is built using multipliers inspired on LFT-scalings and topological separators. The implementation of synthesis is cast as a constrained optimization program that can be solved by nonsmooth techniques. The efficiency of the synthesis procedure is tested by designing robust controllers according to the validation procedure presented in Appendix A. The limitations of the method are discussed and the alternative leads to the next chapter.

Chapter 4- Development of inner relaxation for robust control: - An alternative to avoid the limitations of outer relaxation is presented in chapter 4 . The optimistic estimation of performance by inner relaxations is atenuated by the judicious choice of models that represent the worst-case scenario.The robust control synthesis is then recast as a multi-model synthesis. The validation procedure follows the same procedure as in chapter 3 and introduced in Appendix A. The analysis of the results suggests that a combination of inner and outer relaxations could mitigate the drawbacks of each method while benefiting from their assets. This option is studied in the chapter that follows.

Chapter 5 - Development of hybrid relaxation for robust control: The outer and inner relaxations developed in previous chapters are combined in chapter 5. The rationale is that for dynamic uncertainty outer relaxations perform well whereas inner approximation demands a large number of scenarios. The hybrid method uses multipliers for dynamic uncertainty while addressing the parametric uncertainty by finding worst-case scenarios for a multi-model synthesis. An implementation of the method using nonsmooth solvers is introduced and used to validate the approach according to Appendix A.1. A discussion of the advantages and limitations of the methods developed follows the consolidation of the results. In order to reduce conservatism even further, control synthesis based on the nonparametric model is considered next.

Chapter 6- Development of a method for synthesis of stabilizing controller based on spectral abscissa minimization: A major challenge of H_∞ control based on nonparametric models is to find an initial stabilizing controller for a nominally unstable plant. In chapter 6 a solution to this problem is proposed. Based on equivalence of spectral abscissa and stability of a system, a method for designing structured controllers for unstable infinite-dimensional systems is derived. The task of computing the spectral abscissa of the closed-loop system based on nonparametric model is challenging and is further aggravated when distributed parameter systems are considered. An algorithm for estimation of the spectral abscissa based on shifted frequency-response is then developed. The minimization of the estimate is led by a direct search method in the controller parameter space. The technique is validated on a test set given in Appendix A.1, followed by a discussion about advantages and limitations of the method.

Chapter 7 - Development of a method for synthesis of stabilizing controller based on energy minimization: A second method for data-driven design of structured controller for unstable plants is introduced in chapter 7. The method is based on minimization of the energy of the impulse response of the closed-loop system. The energy is estimated based on shifted frequency-response

and has the advantage of being smooth. The search for the controller parameters that minimize the estimate is cast as a constrained minimization problem. It is shown that whenever the search converges this corresponds to a stabilizing controller.

Chapter 8 - Development of a method for synthesis of stabilizing controller based on H_∞-norm minimization: A third method for designing structured controllers is considered in chapter 8. This method is motivated by the displacement of poles away from imaginary axis when resonant peaks of the H_∞-norm are smoothed. The author proposes a technique to exploit this feature in the case of a nonparametric unstable plant model. As the initial closed-loop systems may be unstable, a shift on H_∞-norm is considered. An iterative method for minimizing H_∞-norm of shifted systems is then developed. The efficiency of the method is tested on a benchmark test presented in Appendix A and the results are discussed.

Chapter 9- Study case: The new methods for structured controller synthesis developed in this work are applied on the control of a tail fin missile in chapter 9.

Chapter 10 - Conclusion: The last chapter of the thesis is dedicate to the contributions of this thesis and the limitations of the presented work. The innovative alternative for the current problems are summarized and the limitations and restrictions of the techniques are supported by analytical and empirical results. In the light of the successful features and limits of techniques, the thesis ends with suggestions for future works.

Chapter 2

Preliminary Concepts

In this chapter

The theory upon which this thesis unrolls is exposed in this chapter. It will be recalled fundamentals and new developments for robust control and control design based on frequency response data.

2.1 Infinite-dimensional Linear Time-Invariant systems

This work is concerned to a particular class of infinite-dimensional systems whose transfer functions belong to the *Callier-Desoer class* $\hat{\mathcal{B}}(\beta)$ [Curtain and Zwart, 1995]. This class is broad enough to comprise most of pratical applications as retarded systems, some neutral systems and fractional-order systems. Most of the theoretical support for the control of this class of systems can be found in Curtain and Zwart [1995] and references therein. This class is of fundamental importance as systems that can be stabilized finite-dimensional controllers are described by functions belonging to this class. In the following, the main concepts regarding control of this class of systems are recalled, as well as stability and stabilizability criteria.

2.1.1 The Callier-Desoer class

The class $\mathcal{A}(\beta)$ is defined as:

$$\mathcal{A}(\beta) = \{f : f(t) = \begin{cases} f_a(t) + \sum_{n=1}^{\infty} f_n \delta(t - t_n), & t \geq 0 \\ 0 & t < 0, \end{cases} \} \tag{2.1}$$

for $t_1 = 0, t_n > 0$ for $n \geq 2$, $\delta(t - t_n)$ is the delta de Dirac at instant t_n, $e^{-\beta} f_a \in \mathcal{L}^1(0, \infty)$ and $f_n \in \mathbb{C}$ such that $\sum_{n=1}^{\infty} |f_n| e^{-\beta t_n} < \infty$.

Let $\hat{\mathcal{A}}(\beta)$ be the class of Laplace transforms of functions belonging to class $\mathcal{A}(\beta)$. $\hat{\mathcal{A}}_-(\beta)$ and $\hat{\mathcal{A}}_\infty(\beta)$, subalgebras of $\hat{\mathcal{A}}(\beta)$, are defined as:

$$\hat{\mathcal{A}}_-(\beta) = \{\hat{f} : \hat{f} \in \hat{\mathcal{A}}(\beta_1) \text{ for some } \beta_1 < \beta\} \tag{2.2}$$

$$\hat{\mathcal{A}}_\infty(\beta) = \{\hat{f} \in \hat{\mathcal{A}}_-(\beta) : \exists \rho > 0 \text{ such that } \inf_{Re(s) > \beta, |s| \geq \rho} |\hat{f}(s)| > 0\}. \tag{2.3}$$

The Callier-Desoer class $\hat{\mathcal{B}}(\beta)$ of transfer functions is then defined as:

$$\hat{\mathcal{B}}(\beta) := \hat{\mathcal{A}}_-(\beta)\hat{\mathcal{A}}_\infty(\beta)^{-1} = \left\{\hat{f} = \hat{n}\hat{m}^{-1} : \hat{n} \in \hat{\mathcal{A}}_-(\beta) \text{ and } \hat{m} \in \hat{\mathcal{A}}_\infty(\beta)\right\} \tag{2.4}$$

Such transfer functions $\hat{f} \in \hat{\mathcal{B}}(\beta)$ are meromorphic and bounded in $\mathbb{C}_\beta^+$ and have only finitely many poles of finite order in $\overline{\mathbb{C}_\beta^+}$. Moreover, transfer functions $\hat{f} \in \hat{\mathcal{B}}(\beta)$ can also be represented as

$$\hat{f} = \hat{n}\hat{m}^{-1} : \hat{n} \in \hat{\mathcal{A}}_-(\beta) \text{ and } \hat{m} \in \mathcal{R}_\infty(\beta), \text{ and} \tag{2.5}$$

$$\hat{f} = \hat{f}_s + \hat{f}_u : \hat{f}_s \in \hat{\mathcal{A}}_-(\beta) \text{ and } \hat{f}_u \text{ strictly proper, rational and holomorphic on} \mathbb{C}_\beta^-, \tag{2.6}$$

where $\mathcal{R}_\infty(\beta)$ is the set of all proper rational transfer functions with complex coefficients, nonzero at ∞ and no poles in $\mathbb{C}_\beta^+$.

For sake of notation, a transfer matrix $G(s)$ of arbitrary dimension with all its elements on $\hat{\mathcal{A}}(\beta), \hat{\mathcal{A}}_-(\beta)$, or $\hat{\mathcal{B}}(\beta)$ will be denoted as belonging to $\hat{\mathcal{A}}(\beta), \hat{\mathcal{A}}_-(\beta)$, or $\hat{\mathcal{B}}(\beta)$, respectively.

If $G(s) \in \hat{\mathcal{B}}(\beta)$, $G(s)$ admits the decomposition $G(s) = G_s(s) + G_u(s)$, where $G_s(s) \in \hat{\mathcal{A}}_-(\beta)$ and $G_u(s)$ is transfer matrix with all elements being strictly proper rational transfer functions holomorphic in $\mathbb{C}_\beta^-$. All $G(s) \in \hat{\mathcal{B}}(\beta)$ are proper on $\overline{\mathbb{C}_\beta^+}$, besides, $G(s)$ has limit G_∞ at infinity if and only if $G_s(s)$ does and $G(s)$ is strictly proper on $\overline{\mathbb{C}_\beta^+}$ if and only if the elements of $G_s(s)$ are Laplace transforms of functions $g(.)$ with $g(.)e^{-\beta} \in L_1(0, \infty)$.

$G(s) \in \hat{\mathcal{B}}(\beta)$ is said to be input-output stable if $G(s) \in \hat{\mathcal{A}}_-(0)$. However many other concepts of input-output stability exists that are equivalente for FDLTI systems but not for IDLTI systems.

2.1.2 Interconnection of systems

Consider the feedback system Σ of two systems G and K in Figure 2.1.

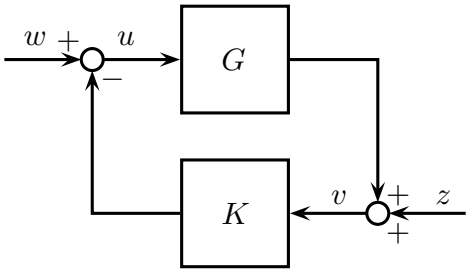

Figure 2.1: System G in feedback with system K.

This system is described in terms of G and K as:

$$\Sigma : \begin{bmatrix} w \\ z \end{bmatrix} = \begin{bmatrix} I & K \\ -G & I \end{bmatrix} \begin{bmatrix} u \\ v \end{bmatrix} \tag{2.7}$$

The well posednes of the feedback system Σ guarantees existence and uniqueness of the solutions u, v . For well posed G and K, the feedback system Σ is said to be well posed if the following two conditions hold [Iwasaki and Hara, 1998]:

1) For each pair of input vectors v, u , there existis a unique pair of vectors z, w satisfiyng equation 2.7.

2) There exists $\gamma > 0$ such that $\left\| \begin{bmatrix} w \\ z \end{bmatrix} \right\| \leq \gamma \left\| \begin{bmatrix} u \\ v \end{bmatrix} \right\|$

In this context, these conditions are analogous to $\det(I+GK)$ be bounded away from zero at infinity in the $\mathbb{C}^+$. Now take $F(s)$ and $T(s)$ the transfer matrix of system Σ and its inverse, respectively:

$$F(s) = \begin{bmatrix} I & K(s) \\ -G(s) & I \end{bmatrix} \tag{2.8}$$

$$T(s) = F^{-1}(s) = \begin{bmatrix} I - K(I+GK)^{-1}G & -K(I+GK)^{-1} \\ (I+GK)^{-1}G & (I+GK)^{-1} \end{bmatrix} \tag{2.9}$$

where the dependence of Laplace variable s was omitted for convenience.

For $G(s)$ and $K(s) \in \hat{\mathcal{B}}(\beta)$ and a well posed feedback system Σ, all elements of $T(s)$ also belong to $\hat{\mathcal{B}}(\beta)$. In addition, Σ is stable if all elements of $T(s)$ are in $\hat{\mathcal{A}}_-(0)$.

If $K(s) \in \hat{\mathcal{A}}_-(0)$, that is, $K(s)$ is stable, the stability analysis is reduced to stability analysis of only one element of $T(s)$ [Zhou and Doyle, 1999]:

$$G(I + KG)^{-1} \tag{2.10}$$

A feedback system Σ is said to satisfy a stability criterion if all elements of $T(s)$ satisfy the corresponding stability criterion.

For a given plant $G(s)$ it can be defined the class of controllers $K(s)$ that leads to a stable feedback system, that is, which class of controllers $K(s)$ stabilizes $G(s)$. The following theorem answer the question of which class of plants $G(s)$ can be stabilized by the class of proper rational controllers.

Theorem 2.1. *[Curtain and Zwart, 1995, Theorem 9.3.17] If $G(s) \in \hat{\mathcal{B}}(0)$, then there exists a finite-dimensional controller $K \in \hat{\mathcal{B}}(0)$ that stabilizes G.*

Once stabilized, the robustness margin of the closed-loop system is defined by:

$$\epsilon_{\max} = \gamma^{-1} = \left(\inf_{\text{K stabilizes G}} \|T(s)\|_\infty \right)^{-1} \tag{2.11}$$

This equation gives the maximum norm of the pertubation that the feedback system can tolerate before becoming unstable. In the case of structured pertubations, Doyle [1982] introduced the structured singular value μ, defined as:

$$\mu = (\min\{\bar{\sigma}(\Delta) : \Delta \in \mathbf{\Delta}, \det(I - M\Delta) = 0\})^{-1}. \tag{2.12}$$

Iwasaki and Hara [1998] recalls that $\mu < 1$ is defined by 1) (page 12) and that 2) is valid if $\mathbf{\Delta}$ is closed and bounded.

2.1.3 Norms of systems

- **H_∞-norm**

The H_∞-norm is defined for systems that are analytic in $\mathbb{C}^+$ and bounded on $\overline{\mathbb{C}^+}$. It is defined as:

$$\|G(s)\|_\infty = \sup_{u \neq 0} \frac{\|Gu\|_2}{\|u\|_2} \tag{2.13}$$

which is determined by:

$$\|G(s)\|_\infty = \sup_{\omega} \overline{\sigma}(G(j\omega)) \tag{2.14}$$

The H_∞-norm represents the largest peak value of maximun gain over all frequencies, simply, the peak gain value. In order to obtain the value of the H_∞-norm , a search must be executed. However is possible to establish a upper bound on H_∞. Define $\Phi(s) := \gamma^2 I - G^T(-s)G(s)$. We have that

$$\|G\|_\infty < \gamma \text{ iff } \Phi(j\omega) > 0 \forall \omega \in \mathbb{R} \tag{2.15}$$

For a system with state-space representation, that is equivalente to state that matrix H

$$H = \begin{bmatrix} A + BR^{-1}D^TC & BR^{-1}B^T \\ -C^T(I + DR^{-1}D^T)c & -(A + BR^{-1}D^TC)^T \end{bmatrix} \tag{2.16}$$

where $R = \gamma I - D^T D$ has no imaginary eigenvalues.

The term H_∞ stable refers to systems that are analytic in $\mathbb{C}^+$ and bounded on $\overline{\mathbb{C}^+}$.

- **H_2-norm**

Let $g(t)$ be a signal defined for $t \geq 0$.

The L_2-norm of $g(t)$ is defined as:

$$|g(t)|_2 := \sqrt{\int_0^\infty tr(g^T(t)g(t))dt} \tag{2.17}$$

Now let $g(t)$ be the impulse response of a system $G(s)$ analytic on $\mathbb{C}^+$. The H_2-norm of $G(s)$ is defined as

$$|G(j\omega)|_2 = \sqrt{\int_0^\infty tr(G^*(j\omega)G(j\omega))d\omega} \tag{2.18}$$

Using Parseval and Plancherel results is possible to verify that for $G(s)$ analytic on $\mathbb{C}^+$:

$$|g(t)|_2 = |G(j\omega)|_2 \tag{2.19}$$

The H_2-norm however is finite only if the transfer function $G(s)$ is strictly proper.

2.1.4 Particular cases of IDLTI systems

Fractional-order systems

Fractional-order systems constitute a particular class of irrational tranfer functions. They are comensurate and non-comensurate given that the exponent is rational or irrational, respectively.

The fractional-order transfer functions are multi-valued functions that unroll on Riemman sheets [Petras, 2009]. Branch points arises in this domain and should be carefully examined regarding stability. The main results for stability of the commensurate type can be found in [Matignon, 1998]. The main result being that a fractional-order system of commensurate type is stable if it has no poles in $\mathbb{C}^+$.

Many approximation methods can be employed to build a rational approximation of a frational-order system, as continued fraction expansion, Carlson's method, Matsuda's method and Charef's method to cite a few. The Oustaloup's method is well accepted and it is a power series expansion based on interlacing of zeros and poles. For a a term $G(s) = s^\alpha, \alpha \in \mathbb{R}$, the approximation $G_{app}(s)$ is given by [Vinagre et al., 2000b]:

$$G_{app}(s) = c \prod_{k=-N}^{N} \frac{1 + s/\omega_k}{1 + s/\omega'_k} \tag{2.20}$$

with $\omega_u = \sqrt{\omega_h \omega_b}; \omega'_0 = a^{-0.5}\omega_u; \omega_0 = a^{0.5}\omega_u; \frac{\omega'_{k+1}}{\omega'_k} = \frac{\omega_{k+1}}{\omega_k} = a\eta > 1; \frac{\omega'_{k+1}}{\omega_k} = \eta > 0; \frac{\omega_k}{\omega'_k} = a > 0; N = \frac{\log(\omega_N/\omega_0)}{\log(a\eta)}; \mu = \frac{\log(a)}{\log(a\eta)}$. or equivalently [Tepljakov et al., 2011]:

$$G_{app}(s) = c' \prod_{k=-N}^{N} \frac{s + \omega_k}{s + \omega'_k} \tag{2.21}$$

with $\omega'_k = \omega_b \left(\frac{\omega_h}{\omega_b}\right)^{\frac{k+N+0.5(1-\alpha)}{2N+1}}; \omega_k = \omega_b \left(\frac{\omega_h}{\omega_b}\right)^{\frac{k+N+0.5(1+\alpha)}{2N+1}}; c' = \omega_h^\alpha$.

The frequency interval of the approximation ω_u and ω_h, as well as the order N of the approximation affects the quality of the approximation and should be chosen case by case. To exemplify, an order $N = 1$ results in a third-order transfer function, while $N = 3$ results in a 7th-order.

Figure 2.2 presents the approximates of function $3.5s^{0.5} + 11.5s^{0.4} + 1$ by Oustaloup approximation for frequency range $[10^{-5}, 10^2]$ for approximate of $N = 1, 2, 3$ for each term and a 3 with an integrator.

Time-Delayed systems

The general transfer function of a system with discrete time delays is

$$G(s) = \frac{r_0(s) + \sum_{k=1}^{n} r_k(s)e^{-\beta_k s} + \sum_{k=1}^{\tilde{n}} \tilde{r}_k(s)e^{-u_k(s)}}{p_0(s) + \sum_{k=1}^{m} p_k(s)e^{-\gamma_k s} + \sum_{k=1}^{\tilde{m}} \tilde{p}_k(s)e^{-v_k(s)}} \tag{2.22}$$

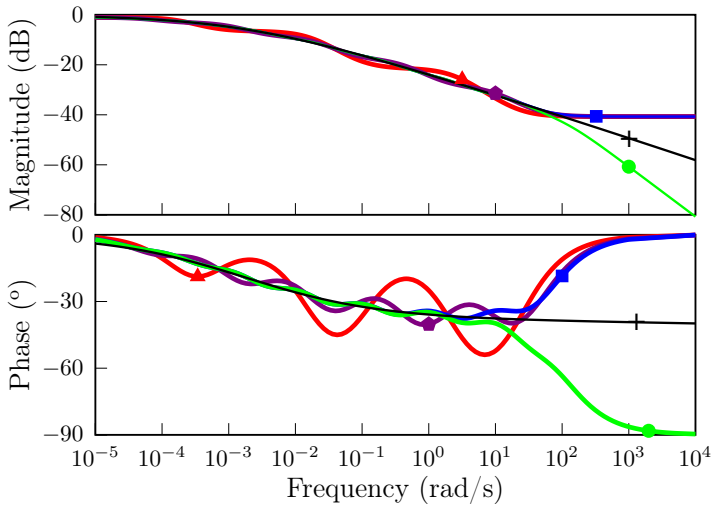

Figure 2.2: Approximations of fractional order system by finite-dimensional systems. Red for 1, purple for 2, blue for 3 and green for 3 plus integrator.

where $r_0, r_k, \tilde{r}_k, p_0, p_k, \tilde{p}_k$ are quasi-polynomials in s of the form $\sum_{m=0}^{n} a_k s^{\alpha_k}$, u_k, v_k are quasi-polynomials in s of the form $\sum_{m=0}^{n} c_k s^{\delta_k}$ with $\delta \in (0, 1]$, and $a_K \in \mathbb{R}$ and $\alpha_k, c_k, \beta_k, \gamma_k \in \mathbb{R}^+$.

For dead-time systems there are no terms $p_k, \tilde{p}_k$. The system is said to be of retarded type if $\deg(p_0(s)) > \deg(p_k(s))$, is of neutral type if $\deg(p_0(s)) = \deg(p_k(s))$ and of advanced type if $\deg(p_0(s)) < \deg(p_k(s))$. The system is said to be proper if $\deg(p_0(s)) \geq \deg(r_0(s))$.

Dead-time and retarded systems as described in eq. 2.22 belong to $\hat{\mathcal{B}}(0)$. Advanced type systems have infinitely many unstable poles, therefore do not belong to $\hat{\mathcal{B}}(0)$ and cannot be stabilized by rational controllers. Neutral systems should be analysed case by case as beloging or not to class $\hat{\mathcal{B}}(0)$.

Bonnet and Partington [2000b] and Bonnet and Partington [2002] proved that a strictly proper and retarded system $G(s)$ is BIBO and $\mathcal{H}^\infty$ stable if and only if $G(s)$ has no poles on closed RHP [Bonnet and Partington, 2000b].

In [Eisenberg, 1971], [Pal, 1979] and [Scott, 1977] a rational approximation for the function representing the delay e^{-s} was derived to become what is known as Padé approximation. Consider the term $G(s) = e^{-hs}$. The Padé approximation is given by:

$$G_{app} = \frac{\sum_{i=0}^{q} (-hs)^i \dfrac{(q+p-i)!q!}{(q-i)!(q+p)!i!}}{\sum_{i=0}^{p} (hs)^i \dfrac{(q+p-i)!q!}{(q-i)!(q+p)!i!}} \tag{2.23}$$

where p and q are the orders of the approximation.

Even if the notion of small or large delay is relative to system's time constant of the rational part, it is usual to use a first and second order approximation for small delays. If the delay is large, high order approximattes are necessary in order to avoid the *spillover effect* in closed-loops with a controller designed for the approximate.

2.2 H_∞ control

The H_∞ mixed-sensitivity approach to controller design is very general and is appropriate for multivariable problems in which several objectives must be taken into account simultaneously [Zhou and Doyle, 1999]. Moreover it is appropriate for uncertainties that cannot be modeled simply as white noise, as in linear quadratic gaussian control (LQG) control. The H_∞ control configuration, Figure 2.3, is defined as an LFT of the generalized plant P and the controller K. In this approach, we define the plant and possibly the model uncertainty, the class of external signals affecting the system and the error signals we want to keep small. Weights are used to describe the expected or known frequency

content of exogenous signals and the desired frequency content of error signals. For more details about how to design filters, please refer to Zhou and Doyle [1999].

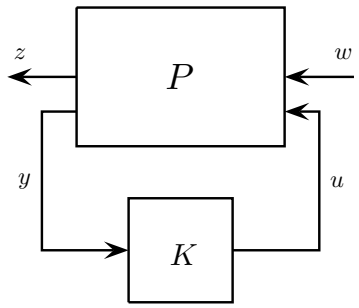

Figure 2.3: H_∞ control problem configuration.

The generalized plant P is defined as:

$$P : \begin{bmatrix} z \\ y \end{bmatrix} = \begin{bmatrix} P_{zw} & P_{zu} \\ P_{yw} & P_{yu} \end{bmatrix} \begin{bmatrix} w \\ u \end{bmatrix}, \tag{2.24}$$

where $w \in \mathbb{R}^{n_w}$ is a vector of exogenous inputs, $z \in \mathbb{R}^{n_z}$ is a vector of regulated outputs, $y \in \mathbb{R}^{n_y}$ is the measured output, and $u \in \mathbb{R}^{n_u}$ is the control input.The H_∞ control problem can then be stated as Problem 1 below.

Problem 1. ***Optimal*** H_∞ ***Control:*** *Find all admissible controllers* $K(s)$ *that stabilize plant* P *and minimize* $\|T_{wz}\|_\infty$.

Unlike optimal H_2 controllers, optimal H_∞ controllers are not obtained as straightforwardly. However, suboptimal controllers that achieve a given H_∞-norm are much simpler to derive. This motivates a simpler formulation for the suboptimal H_∞ control problem.

Problem 1. v1. ***Suboptimal*** H_∞ ***Control:*** *Given* $\gamma > 0$, *find all admissible controllers* $K(s)$, *if any, that stabilize plant* P *and satisfy* $\|T_{wz}\|_\infty < \gamma$.

This problem can be turned into a convex one and standard solutions for the Problem 1.v2 can be obtained by different methods as LMI formulations of Gahinet and Apkarian [1994] and Iwasaki and Skelton [1994], *DGKF* formulation of Doyle et al. [1989] and interpolation approach of Limebeer and Kasenally [1990]. By iteratively reducing the value γ, the controller can achieve values arbitrarily close to the optimal value.

However, what we actually search is a structured controller parameterized by vector κ that can ensure internal stability and a specified level of performance. Typical structures are PIDs, reduced-order controllers, observer-based controllers and notch filters among others [Apkarian and Noll, 2006a]. Unstructured controllers lacks structure and usually have the same dimension as the plant P. For instance, for a structured state-space controller $u(s) = K(\kappa, s)y(s)$ we have:

$$K(\kappa) : \begin{cases} \dot{x}(t) = A_K(\kappa)x(t) + B_K(\kappa)u(t) \\ y(t) = C_K(\kappa)x(t) + D_K(\kappa)u(t). \end{cases} \tag{2.25}$$

where $A_K(\kappa)$, $B_K(\kappa)$, $C_K(\kappa)$, $D_K(\kappa)$ are matrices with entries dependent on parameter vector κ with an arbitrary order $n_x(K)$.

The H_∞ control problem for structured controller is restated as:

Problem 1. v2. ***Suboptimal Structured*** H_∞ ***Control:*** *Given* $\gamma > 0$, *find a structured controller* $K(\kappa, s) \in \mathcal{K}$, *if any, that stabilizes plant* P *and satisfies* $\|T_{wz}\|_\infty < \gamma$.

In this formulation, $\mathcal{K}$ is the set of all controllers $K(\kappa)$ with the desired structure. The problem is now nonconvex with respect to controller and there is no available method for obtaining closed-form solutions for fixed-order controllers. It should be remarked that even if a plant is stabilizable, it should not be assumed that it can be stabilized by a controller with any particular structure [Iwasaki and Skelton, 1994]. Available methods for solving this problem include parametric controller design [Pensar

and Toivonen, 1993], LMI formulations with rank condition [Iwasaki and Skelton, 1994], evolutionary computation [Maruta et al., 2008] and nonsmooth optimization [Apkarian and Noll, 2006a].

Yet another version of the H_∞ control problem is stated for multi-objective, multi-model control where performance is optimized simultaneously for a set of models each with multiple independent performance channels P. Loiseau and Duffal [2016]. Each model P^i of the set of multi-models is defined as:

$$P^i : \begin{bmatrix} z^i \\ y^i \end{bmatrix} = \begin{bmatrix} P^i_{zw} & P^i_{zu} \\ P^i_{yw} & P^i_{yu} \end{bmatrix} \begin{bmatrix} w^i \\ u^i \end{bmatrix}, \tag{2.26}$$

with $w^i \in \mathbb{R}^{n_w}$ a vector of exogenous inputs, partitioned as $w^i = \{w^i_1, \cdots, w^i_{n_l}, w^i_{n_l+1}, \cdots, w^i_{n_l+n_j}\}$, $z^i \in \mathbb{R}^{n_z}$ a vector of regulated outputs, partitioned as $z^i = \{z^i_1, \cdots, z^i_{n_l}, z^i_{n_l+1}, \cdots, z^i_{n_l+n_j}\}$, $y^i \in \mathbb{R}^{n_y}$ the measured output, and $u^i \in \mathbb{R}^{n_u}$ the control input.

The H_∞-norm of performance channels from 1 to n_l are minimized simultaneously while keeping the H_∞-norm of performance channels from $n_l = 1$ to $n_l + n_j = n_w$ inferior to 1.

Problem 1. v3. ***Suboptimal Structured multi-model multi-objective*** H_∞ ***Control:*** *Given* $\gamma > 0$*, find an structured controller* $K(s) \in \mathcal{K}$*, if there is any, that stabilizes all plants* P^i *such that* $\max_{i,l} \|T^i_{w_l z_l}\|_\infty < \gamma$ *and* $\max_{i,j} \|T^i_{w_j z_j}\|_\infty \leq 1$.

This version of H_∞ control is a multidisk design problem regarded as minimizing the maximum of an infinite family of nonconvex functions. An approach to solve such problems is given in Apkarian et al. [2014]. This approach is based on bundle method for nonsmooth optimization introduced in Apkarian and Noll [2006a,b,d].

2.3 Robust control

As discussed in chapter 1, system identification may no be suited to estimate accurately all the parameters and all dynamics of a process. In such cases, in order to ensure that the control designed based on the behavior of the model will achieve the desired performance criteria when implemented on the actual system, the control action must be robust. A robust control guarantees the desired performance of a system when its behavior deviates from its nominal model. The amount and type of model uncertainty a robust control has to handle is also part of the design. The uncertainty should therefore be also estimated, although the concept of modeling for uncertainty maybe a little looser than for models.

In the present work, the uncertainty considered is structured and consists of parametric and dynamic uncertainties. A structured uncertainty has a block diagonal structure where each block accounts for a different uncertainty in the system, as for example multiplicative uncertainties at input and output of a system and uncertainty in one subsystem parameter [Doyle, 1982]. Parametric uncertainties accounts for model parameters that vary in a given range of values and dynamic uncertainties are modeled as complex blocks that affect the plant dynamics as H_∞-norm bounded stable LTI transfer functions.

2.3.1 Uncertain models

The LFT configuration of an uncertain system is represented in Figure 2.4. In this configuration, the structured uncertainty is pulled out from the uncertain system into a block Δ. The uncertain system is then recomposed by $\Delta \star P$.

The generalized plant P from (2.24) now includes the uncertain channel being redefined as:

$$P : \begin{bmatrix} z_\delta \\ z \\ y \end{bmatrix} = \begin{bmatrix} P_{\delta\delta} & P_{\delta w} & P_{\delta u} \\ P_{z\delta} & P_{zw} & P_{zu} \\ P_{y\delta} & P_{yw} & P_{yu} \end{bmatrix} \begin{bmatrix} w_\delta \\ w \\ u \end{bmatrix}, \tag{2.27}$$

with $w \in \mathbb{R}^{n_w}$ a vector of exogenous inputs, $z \in \mathbb{R}^{n_z}$ a vector of regulated outputs, $y \in \mathbb{R}^{n_y}$ the measured output, and $u \in \mathbb{R}^{n_u}$ the control input. The uncertainty channel is defined as

$$w_\delta = \Delta z_\delta, \tag{2.28}$$

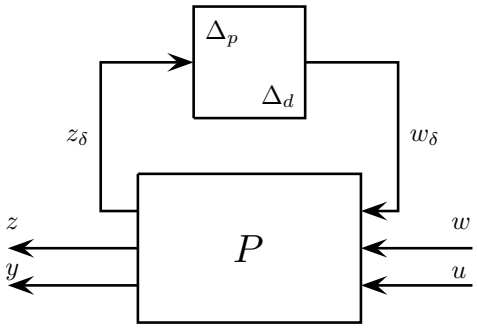

Figure 2.4: Interconnections and signals of uncertain system for a mixed structured uncertainty Δ.

where the uncertain matrix Δ is structured as

$$\Delta = \begin{bmatrix} \Delta_p & 0 \\ 0 & \Delta_d \end{bmatrix}, \tag{2.29}$$

$$\Delta_p := \text{diag}\left[\delta_1 I_{r_1}, \ldots, \delta_{N_p} I_{r_{N_p}}\right], \tag{2.30}$$

for real uncertain parameters $\delta_1, \ldots, \delta_{N_p} \in \mathbb{R}$ and their number of repetitions $r_1, \ldots, r_{N_p}$, and

$$\Delta_d := \text{diag}\left[\Delta_{d1} \ldots, \Delta_{dN_d}\right], \tag{2.31}$$

with $\Delta_{di} \in \mathbb{C}^{n_{p_i} \times n_{q_i}}$, $i = 1, \ldots, N_d$, each Δ_{di} accounting one complex uncertain block.

It is also assumed without loss of generality that the uncertainty is normalized so that Δ belongs to the unit ball

$$\mathbf{\Delta} = \{\Delta : \ \overline{\sigma}(\Delta) \leq 1\}, \tag{2.32}$$

with $\Delta = 0$ representing nominal behavior and $\overline{\sigma}$ denoting the maximum singular value of a matrix. This means $\delta_i \in [-1, 1]$ for real unceratain parameters and $\overline{\sigma}(\Delta_{di}) \leq 1$ for complex blocks. The unit balls

$$\mathbf{\Delta}_p := \{\Delta_p : \ \overline{\sigma}(\Delta_p) \leq 1\}, \ \mathbf{\Delta}_d := \{\Delta_d : \ \overline{\sigma}(\Delta_d) \leq 1\} \tag{2.33}$$

are also defined.

2.3.2 Robust control design

The control of the uncertain system is made through the feedback of the channel $u \to y$ in (2.27) with a structured control law $K(\kappa)$ in (2.25), illustrated by Figure 2.5.

The H_∞ control problem stated in Problem 1 is now modified to the following Robust H_∞ Control Problem:

Problem 2. *Given the compact convex set of parametric and dynamic uncertainties $\mathbf{\Delta}$ in (2.29), including the nominal scenario $\Delta = 0$, the robust structured H_∞ control problem consists in computing a structured output-feedback controller $u = K(\kappa^*)y$ as in (2.25) with the following properties:*

(i) **Robust stability**. *The closed-loop system is well-posed and $K(\kappa^*)$ stabilizes $\Delta \star P$ internally for every $\Delta \in \mathbf{\Delta}$.*

(ii) **Robust performance**. *Given any other robustly stabilizing controller $K(\kappa)$ with the same structure, the optimal controller satisfies*

$$\max_{\Delta \in \mathbf{\Delta}} \|T_{zw}(\Delta, \kappa^*)\|_\infty \leq \max_{\Delta \in \mathbf{\Delta}} \|T_{zw}(\Delta, \kappa)\|_\infty, \text{for all } K(\kappa).$$

Here $T_{zw}(\Delta, \kappa) := \Delta \star P \star K(\kappa)$ is the closed-loop transfer function of the performance channel $w \to z$ of (2.27) when the control loop with $K(\kappa)$ and the uncertainty loop with $\Delta \in \mathbf{\Delta}$ are both closed.

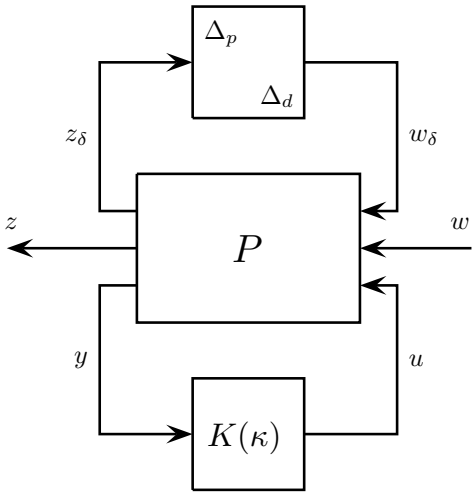

Figure 2.5: Interconnections and signals of the controlled closed-loop uncertain system for a mixed structured uncertainty Δ and a structured control law $K(\kappa)$.

2.3.3 Outer relaxations

The synthesis of robust controllers that solve problem (i)-(ii) from section 2.3.2 is a semi-infinite program by virtue of the maximum over $\boldsymbol{\Delta}$. To become tractable, the problem is usually relaxed. The most common relaxations of the robust control problem are outer relaxations, where a simpler structured $\tilde{\boldsymbol{\Delta}}$ is built to cover the original $\boldsymbol{\Delta}$, that is, $\tilde{\boldsymbol{\Delta}} \supset \boldsymbol{\Delta}$. The rationale is that if the problem is solved on $\tilde{\boldsymbol{\Delta}}$ it is also solved over $\boldsymbol{\Delta}$. The drawback is that scenarios in $\tilde{\boldsymbol{\Delta}} \setminus \boldsymbol{\Delta}$, not included in the original $\boldsymbol{\Delta}$, are now taken into account and thus an unknown amount of conservatism is introduced. Nonetheless, this option is simple and proves to be efficient in a large variety of cases [Chiang and Safonov, 1992; Doyle, 1982, 1985; Fan et al., 1991; Safonov et al., 1993; Young et al., 1991].

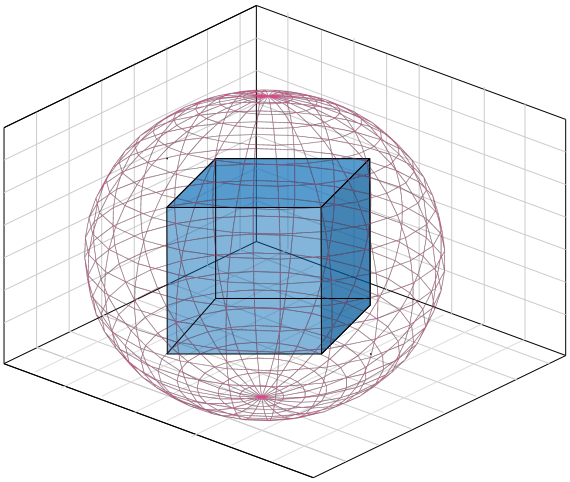

Figure 2.6: Illustration of an outer relaxation (sphere) of the actual domain (cube).

The relaxations suggested in Doyle [1982], Fan et al. [1991] and Safonov et al. [1993], as well as the integral quadratic constraint (IQC) approach [Megretski and Rantzer, 1997] are shown to be particular cases of the topological separator proposed by Iwasaki and Hara [1998].

In this approach, the authors derive robust stability conditions from well-posedness conditions for a feedback system. In the sequel, they show that the system is well-posed if the graphs of the two subsystem are topologically separated. At last, they prove that if these conditions are satisfied, then a topological separator exists, with configuration shown in Figure 2.7. This results in the following theorem extracted from Iwasaki and Hara [1998] :

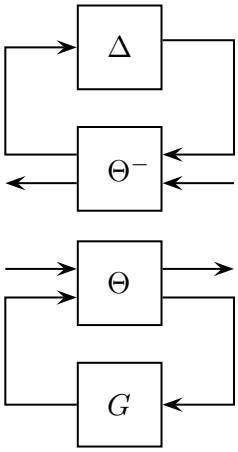

Figure 2.7: LFT scaling Θ for an system G subject to uncertainty Δ.

Theorem 2.2. *[Iwasaki and Hara, 1998, Theorem 4]: Let the uncertainty set $\mathbf{\Delta} \subseteq \mathbb{C}^{m\times n}$ and an $n \times m$ real-rational transfer function G be given. Suppose $0 \in \mathbf{\Delta}$. Then the following statements are equivalent.*

1) The feedback system $\Sigma(\mathbf{\Delta}, G)$ is robustly stable.

2) There exists an $(n+m)\times(m+n)$ real-rational proper invertible transfer function

$$\Theta = \begin{bmatrix} \Theta_{11} & \Theta_{12} \\ \Theta_{21} & \Theta_{22} \end{bmatrix}$$

such that $\Theta_{22}(\infty) = 0 \in \mathbb{R}^{m\times n}$ and

a) the transfer function $\varphi(\Theta, G)$ is stable and

$$\|\Theta \star G\|_\infty < 1 \tag{2.34}$$

b) the feedback system $\Sigma(\Delta, \Theta^-)$ is internally stable and

$$\|\Delta \star \Theta^-\|_\infty \leq 1 \tag{2.35}$$

Moreover, the order of Θ can be chosen to be $\hat{n}$, that is, the order of G. □

The robustness problem now is reduced to find a separator/LFT-scaling Θ that satisfies theorem 2.2 or prove that such scaling does not exist. Please refer to Iwasaki and Hara [1998] for notations and technical details.

2.3.4 Inner relaxations

Inner relaxation of the robust control problem consists in solving the problem for a discrete set $\breve{\mathbf{\Delta}} \subset \mathbf{\Delta}$. The elements $\Delta^i \in \breve{\mathbf{\Delta}}$ are termed scenarios as they are instances of $\Delta \in \mathbf{\Delta}$. It is clear that the certificate over $\breve{\mathbf{\Delta}}$ does not imply a certification on the larger set $\mathbf{\Delta}$. Each worst-case Δ^i results in a plant $P^i_\Delta = \Delta^i \star P$ so that the set $\breve{\mathbf{\Delta}}$ have an associated set of models called a multi-model set.

In chapter 1, the two major approaches to inner relaxation were discussed, the probabilistic approach and the worst-case approach. The worst-case is preferred in cases where a robust stability certification over $\mathbf{\Delta}$ is desired. The rationale behind the worst-case approach to inner relaxation is that, once the models in the multi-model set are controlled simultaneously, the designed controller $K(\kappa^*)$ assures robust stability and performance not only over the set $\breve{\mathbf{\Delta}}$, but over the full scenario set $\mathbf{\Delta}$.

The success of the approach relies on the correct estimation of the worst-case scenarios. Two types of worst-case arise to that end: the robust stability worst-case and the robust performance worst-case. The robust stability worst-case is the instance Δ^i that results on the worst stability margin for the associated $T_{wz}(\Delta^i) = \Delta^i \star P \star K$. The spectral abscissa is used as stability margin as it reflects how far from instability a system is. The robust performance worst-case is the instance Δ^l that results in

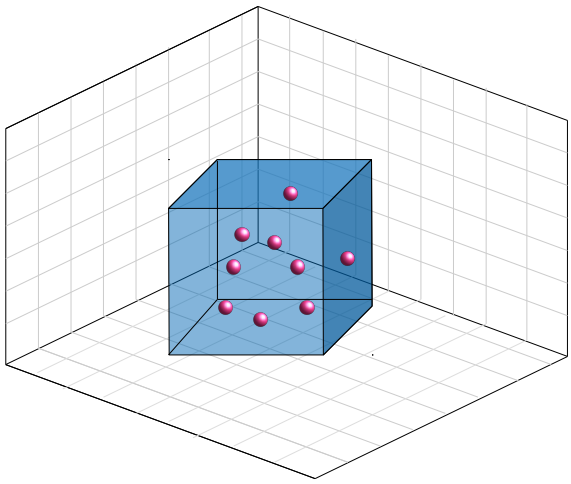

Figure 2.8: Illustration of an inner relaxation (inner dots) of the actual domain (cube).

the largest H_∞-norm for the associated $T_{wz}(\Delta^l) = \Delta^l \star P \star K$. These are expressed as the programs (2.36) and (2.37), respectively.

$$\alpha^* = \max_{\Delta \in \mathbf{\Delta}} \alpha(A(\Delta)) \tag{2.36}$$

$$h^* = \max_{\Delta \in \mathbf{\Delta}} \|T_{wz}(\Delta)\|_\infty. \tag{2.37}$$

where $A(\Delta)$ is the A matrix of the uncertain closed-loop system $T_{wz}(\Delta) = \Delta \star P \star K$. These maximization problems are nonconvex and the functions to be maximized are nonsmooth. Nonsmooth optimization techniques tailored to these problems were developed in Apkarian et al. [2015a,b] for box constrained variables. However, the constraints on $\Delta \in \mathbf{\Delta}$ are of semi-definite type for dynamic uncertainties $\overline{\sigma}(\Delta_d) \leq 1$. Apkarian and Noll [2017] proposed a change of variables allowing the semi-definite constraint in Δ_d to be recast as a box constraint on the new variable x_d. This is based on the fact that complex blocks can be replaced by rank one dyads.

The main results are restated here:

Lemma 2.1. *[Apkarian and Noll, 2017, Lemma 1] Consider an uncertainty structure $\Delta = \text{diag}[\Delta_1, \ldots, \Delta_m] \in \mathbb{C}^{r\times c}$ with real and complex blocks as in (3). Suppose Δ^* check (2.36) everywhere. Then there exist a matrix $\Delta^\# \in \mathbb{C}^{r\times c}$ such that $\overline{\sigma}(\Delta^\#) \leq \overline{\sigma}(\Delta^*) \leq 1$, with the same structure as Δ, but with rank one complex blocks, and which also solves (2.36) globally.*

□

The dyads $\Delta^\#$ are generated by:

$$\Delta_i^\# := \begin{cases} y_i \frac{x_i^H}{\|x_i\|} \text{ with } y_i := \frac{\Delta_i^*}{\|x_i\|} & \text{if } x_i \neq 0 \\ 0 & \text{if } x_i = 0. \end{cases} \tag{2.38}$$

Lemma 2.1 states that the search for Δ_d that solves program (2.36) can be replaced by search for $\Delta_d^\#$ composed of dyad blocks $\Delta_{di}^\# = y_i x_i^H$. The constraints on the decision variable can then be turned from the semi-definite constraint $\overline{\sigma}(\Delta_d) \leq 1$ to unit ball constraints $\|x_i\| \leq 1$, $\|y_i\| \leq 1$. By suitably making a change of variables to polar and spherical coordinates, one gets:

$$\Delta_{di}^\# = \rho_i (v_i \circ e^{j\theta_i^v})(u_i \circ e^{j\theta_i^u})^H. \tag{2.39}$$

where

$$e^{j\theta_i^v} := \begin{bmatrix} e^{j\theta_{i,1}^v} \\ \vdots \\ e^{j\theta_{i,p_i}^v} \end{bmatrix}, \quad e^{j\theta_i^u} := \begin{bmatrix} e^{j\theta_{i,1}^u} \\ \vdots \\ e^{j\theta_{i.q_i}^u} \end{bmatrix} \tag{2.40}$$

and

$$v_i := v_i(\phi^v) := \begin{bmatrix} \cos(\phi^v_{i,1}) \\ \sin(\phi^v_{i,1})\cos(\phi^v_{i,2}) \\ \sin(\phi^v_{i,1})\cdots\sin(\phi^v_{i,p_i-2})\cos(\phi^v_{i,p_i-1}) \\ \sin(\phi^v_{i,1})\cdots\sin(\phi^v_{i,p_i-2})\sin(\phi^v_{i,p_i-1}) \end{bmatrix}, \tag{2.41}$$

and similarly for $u_i := u_j(\phi^u_i)$.

The constraints are now

$$\begin{aligned} &\rho_i \in [0,1], \\ &\theta^v_i \in [0,2\pi]^{p_i}, \\ &\theta^u_i \in [0,2\pi]^{q_i}, \\ &\phi^v_i \in [0,\pi]^{p_i-2} \times [0,2\pi], \text{ and} \\ &\phi^u_i \in [0,\pi]^{q_i-2} \times [0,2\pi]. \end{aligned} \tag{2.42}$$

The decision variable Δ in program (2.36) and program (2.37) can now be replaced by the variable $x = (x_1, \ldots, x_{N_p}, x_{1+N_p}, \ldots x_{N_p+N_d})$ partitioned accordingly to the structure of Δ, with $x_i = \delta_i$ for a real uncertain block Δ_i, and $x_i = (\rho_i, \phi^v_i, \theta^u_i, \phi^u_i, \theta^v_i)$ for a complex block Δ_i. The box-constraints are $x \in \boldsymbol{B}$, where $x_i = \delta_i \in [-1,1]$ for real blocks, and where x_i satisfies 2.39 and 2.42. for complex blocks.

Programs (2.36) and (2.37) are recast as the non-smooth box-constrained optimization programs

$$\alpha^* = \max_{x \in \boldsymbol{B}} \alpha(A(\Delta(x))), \tag{2.43}$$

$$h^* = \max_{x \in \boldsymbol{B}} \|T_{wz}(\Delta(x))\|_\infty. \tag{2.44}$$

In order to apply the nonsmooth optimization technique, one must yet derive the subgradients of functions in (2.43) and (2.44). This is detailed in Apkarian and Noll [2017].

2.4 FRD synthesis

The H_∞ structured control syntheis based on frequency response data does not resort to parametric models. The first concern is how to certify that a system is stable without computation of poles.

2.4.1 Nyquist stability Criterion

The Nyquist Stability Criterion for feedback SISO systems simply states that a feedback system is stable if the number of encirclements of the origin by the curve $1 + GK$ for the Nyquist contour $\mathcal{D}$ in the counter-clockwise direction is equal to $n_z - n_p$, where n_z and n_p are the number of open-loop unstable poles and closed-loop unstable poles, respectively.

For the same Nyquist contour the extension for MIMO systems can be stated as follow. Let $G(s)$ and $K(s) \in \hat{\mathcal{B}}(0)$, with no poles or zeros on the imaginary axis and nu_G and nu_K the number of poles in $\mathbb{C}^+_0$. We assume that $G(s)K(s)$ is proper and has a limit at infinity in $\mathbb{C}^+$. Now consider the system $F(s)$ (2.8) and define $f(s)$ as

$$f(s) = det(F(s)). \tag{2.45}$$

For $f(s) \neq 0$ for all $s \in \mathcal{D}$, define the index, or winding number, of f $\text{ind}(f(s), 0)$ as the number of times $f(s)$ winds around the origin in counterclockwise sense following the contour $\mathcal{D}$. Then the feedback system Σ is stable if $\text{ind}(f(s), 0) = -nu_G + nu_K$.

The $\text{ind}(f(s), 0)$ can be obtained graphicaly by actually counting the number of encirclements. For the cases where $G(s)$ or $K(s)$ have poles on the imaginary axis, the standard approach is to make a small circumvention around the pole including or excluding the pole from the interior of the contour. The inconvenient of this approach is that now the curve closes at the infinity and counting the encirclements graphically is difficult.

Huang et al. [1993] proposed an alternative to handle these cases with poles and zeros on the axis. To this end, consider a rational function $R(s)$ with n_0 poles at the origin and n_{jR} pure imaginary pair of poles at $\pm j\beta_i$, $i = 1, ..., n_{jR}$. $\Psi(s)$ is defined as:

$$\Psi(s) = \left(1 + \frac{1}{s(s+1)}\right)^{n_0} \cdot \prod_{i=1}^{n_{jR}} \left(1 + \frac{1}{(s^2+\beta_i^2)(s+1)}\right)^{n_i}. \tag{2.46}$$

Now $\tilde{R}(s)$ build as

$$\tilde{R}(s) = \frac{R}{\Psi(s)} \tag{2.47}$$

gives that

$$\text{ind}(R(s), 0) = \text{ind}(\tilde{R}(s), 0). \tag{2.48}$$

By taking $R(s)$ as $f(s)$, the condition that $G(s)$ and $K(s)$ have no poles on imaginary axis can now be relaxed. It suffices to use instead $\tilde{f}(s)$, build as in (2.47) with n_0 and n_{jR} of Ψ corresponding the sum of poles of $G(s)$ and $K(s)$ at the origin and on $j\mathbb{R}\backslash\{0\}$, respectively.

Choice of frequency grid

The fact that the Nyquist Stability criterion is in frequency domain, makes it a perfect choice for stability analysis in FRD design. However, the criterion is established for a continuous frequency. A finite grid of frequencies demand careful analysis to verify if the criterion can indeed be applied. The main challenge is to assure that the grid is dense enough to account to account all encirclements of the origin.

Apkarian and Noll [2017] establish a method to determine the coarser grid necessary to compute the correct winding number.

Consider again a function $f(s)$ of (2.45) satisfying conditions that followed or $\tilde{f}(s) = \frac{f(s)}{\Psi(s)}$ in case of $f(s)$ has poles on imaginary axis. We seek the frequencies $\omega_0 = 0 < \omega_1 < \ldots < \omega_N = \infty$ such that the closed polygon $P_f = \{f(-j\omega_N), \ldots, f(0), f(j\omega_1), \ldots, f(j\omega_N)\}$ has the same winding number as that of curve of $f(s)$ for the Nyquist contour $\mathcal{D}$. Let $P_f(j\omega)$ denote the linearly interpolated function associated with the polygon, and $\Delta_{[\omega',\omega'']}\text{arg}f$ denote the change of argument of f along a section $[j\omega', j\omega'']$ of $j\mathbb{R}$. We have that

$$\text{ind}(f(s), 0) = -\frac{1}{2\pi} \sum_{i=-N}^{N-1} \Delta_{[\omega_i,\omega_{i+1}]}\text{arg}f, \tag{2.49}$$

$$\text{ind}(P_f, 0) = -\frac{1}{2\pi} \sum_{i=-N}^{N-1} \Delta_{[\omega_i,\omega_{i+1}]}\text{arg}P_f = -\frac{1}{2\pi} \sum_{i=-N}^{N-1} \text{arg}[\frac{f(j\omega_{i+1})}{f(j\omega_i)}], \tag{2.50}$$

with $\omega_{-i} = -\omega_i$. These two index agree if the nodes ω_i are chosen such that, for every i,

$$\Delta_{[\omega_i,\omega_{i+1}]}\text{arg}f = \text{arg}\left[\frac{f(j\omega_{i+1})}{f(j\omega_i)}\right]. \tag{2.51}$$

Now let $L[.,.|$ be a first-order bound of f where $L[\omega^-, \omega^+| \geq |f'(j\omega)|$ for every $\omega \in [\omega^-, \omega^+]$. For two consecutive nodes $P_f(\omega_i), P_f(\omega_{i+1})$ not passing through 0, if

$$L[\omega_i, \omega_{i+1}](\omega_{i+1} - \omega_i) < |f(j\omega_i)| + |f(j\omega_{i+1})|, \tag{2.52}$$

then (2.51) is satisfied.

With P_f build from the grid generated by (2.52), the winding number of $f(s)$, can be computed by the ray-crossing algorithm. This algorithm consists in counting the number of signed crossings of a ray by the polygon P_f. Provided that this ray does not pass through any of the nodes of P_f, any ray from the origin can be used.

Note that when a grid is built in order to certify the results of the Nyquist stability, this grid is built based on the current $f(s)$ or $\tilde{f}(s)$. An FRD control synthesis should update the grid at each new controller designed, or at least, every time a Nyquist stability test is performed for a new controller. The condition (2.52) can also be employed to build a coarser grid from a denser one in order to simplify the computation of the winding number.

Chapter 3

Development and implementation of novel outer approximations for the synthesis of robust structured controllers

In this chapter

a novel outer relaxation for robust structured controller synthesis is developed and proved to be efficient. Topological separators and LFT-scalings are starting point to the development of new scalings. These scalings and nonsmooth optimization techniques are then employed in the robust synthesis implementation. [Aguiar et al., 2018], [Menezes et al., 2016]

Conclusion

The implementation of the outer relaxation proposed is a good alternative to standard routines as DKSYN. Nevertheless, as most outer relaxations, it may be conservative for systems subjected to repeated parametric uncertainties.

The robust structured H_∞ control problem was restated and its semi-infinite character was remarked in chapter 2. General guidelines for an outer relaxation based on LFT-scalings derived from topological separator [Asai et al., 1996; Iwasaki and Hara, 1998] were also recalled. In this chapter a novel outer relaxation based on LFT-scaling is developed and implemented aiming at a less conservative and computationally tractable robust control synthesis.

3.1 Derivation of multipliers for mixed uncertainty

What is searched is an LFT-scaling that fulfills requirements of Theorem 2.2. If such LFT-scaling can be found, then by Iwasaki and Hara [1998, Theorem 4] it is a topological separator and the robust synthesis in $\mathbf{\Delta}$ has an equivalent in the space on which the scaling is defined.

Consider first only the parametric uncertainty block $\Delta_p \in \mathbf{\Delta}_p$ in (2.30) and (2.33).

The dynamic multipliers $\Phi \in \mathbf{\Phi}$ are defined as:

$$\mathbf{\Phi} := \left\{ \Phi(s) = \operatorname{diag}(\phi_1(s), \ldots, \phi_{N_p}(s)) : \phi_i(s) \text{ stable}, \ \|\phi_i(s)\|_\infty < 1 \right\}, \tag{3.1}$$

where $\Phi(s)$ has the same block diagonal structure as the $\Delta_p \in \mathbf{\Delta}_p$ and therefore commutes with the $\Delta_p \in \mathbf{\Delta}_p$. The Φ defined can be related to Δ_p according the following proposition:

Proposition 3.1. *Given $\Phi \in \mathbf{\Phi}$ defined in (3.1), and $\Delta_p \in \mathbf{\Delta}_p$ defined in (2.30) and (2.33), let*

$$\Gamma(\Phi) := \begin{bmatrix} -\Phi & I+\Phi \\ I-\Phi & \Phi \end{bmatrix}. \tag{3.2}$$

Then the closed loop system $\Delta_p \star \Gamma(\Phi)$ is internally stable and satisfies the estimate

$$\|\Delta_p \star \Gamma(\Phi)\|_\infty \leq 1\,. \tag{3.3}$$

Proof. Since Δ_p and Φ commute, we have

$$\Delta_p \star \begin{bmatrix} -\Phi & I+\Phi \\ I-\Phi & \Phi \end{bmatrix} = (\Delta_p + \Phi)(I + \Phi\Delta_p)^{-1}, \tag{3.4}$$

the expression being well-defined due to $\|\Phi\|_\infty < 1$. Since Δ_p and Φ are structured conformably, one can verify internal stability and the estimate (3.3) in each block $\Delta_p = \delta I$ separately.

Now for $|\delta| \leq 1$, the first term $(\Delta_p + \Phi)$ in (3.4) is stable since Φ is stable. For the second term $(I + \Phi\Delta_p)^{-1}$, internal stability follows from the Small Gain Theorem [Zhou et al., 1996] and the definition of $\mathbf{\Delta}_p$ and $\mathbf{\Phi}$.

To get the estimate (3.3), consider again a single block. For a fixed frequency ω it follows that

$$\overline{\sigma}\left((\delta I + \Phi(j\omega))(I + \delta\Phi(j\omega))^{-1}\right) \leq 1$$

if and only if

$$(\delta I + \Phi(j\omega))^H(\delta I + \Phi(j\omega)) \preceq (I + \delta\Phi(j\omega))^H(I + \delta\Phi(j\omega)),$$

and this is the same as

$$(\delta^2 - 1)(I - \Phi^H(j\omega)\Phi(j\omega)) \preceq 0,$$

where $\preceq 0$ means negative semi-definite. But now the result follows because $|\delta| \leq 1$ and $\|\Phi\|_\infty < 1$ together show that the last condition is satisfied.

□

Proposition 3.1 is now extended to the case where both types of uncertainty are present. For simplicity, assume that complex blocks Δ_i are square, $p_i = q_i$. If need be, this can be achieved by squaring down the plant $P(s)$ in (2.27) with respect to the dynamic uncertainty Δ_d. Let us introduce the set $\mathbf{D}$ of D-scalings

$$\mathbf{D} := \left\{ D(s) = \operatorname{diag}(d_1(s)I_{p_i}, \ldots, d_{N_d}(s)I_{p_{N_d}}) : d_i(s), d_i(s)^{-1} \text{ stable} \right\}. \tag{3.5}$$

Note that $D\Delta_d = \Delta_d D$ due to the block structure of Δ_d and D.

Proposition 3.1 is now extended to

Proposition 3.2. *Given $\Phi(s) \in \mathbf{\Phi}$, $D(s) \in \mathbf{D}$ and $\Delta_p \in \mathbf{\Delta}_p$, $\Delta_d \in \mathbf{\Delta}_d$ defined in (2.30), (2.31) and (2.33), let*

$$\Gamma(\Phi, D) := \begin{bmatrix} -\Phi & 0 & I+\Phi & 0 \\ 0 & 0 & 0 & D \\ I-\Phi & 0 & \Phi & 0 \\ 0 & D^{-1} & 0 & 0 \end{bmatrix}. \tag{3.6}$$

Then the closed loop system $\begin{bmatrix} \Delta_p & 0 \\ 0 & \Delta_d \end{bmatrix} \star \Gamma(\Phi, D)$ is internally stable and satisfies the estimate

$$\left\| \begin{bmatrix} \Delta_p & 0 \\ 0 & \Delta_d \end{bmatrix} \star \Gamma(\Phi, D) \right\|_\infty \leq 1\,. \tag{3.7}$$

Proof. Since Δ_p and Φ commute and $D\Delta_d = \Delta_d D$,

$$\begin{bmatrix} \Delta_p & 0 \\ 0 & \Delta_d \end{bmatrix} \star \begin{bmatrix} -\Phi & 0 & I+\Phi & 0 \\ 0 & 0 & 0 & D \\ I-\Phi & 0 & \Phi & 0 \\ 0 & D^{-1} & 0 & 0 \end{bmatrix} = \begin{bmatrix} (\Delta_p + \Phi)(I + \Phi\Delta_p)^{-1} & 0 \\ 0 & \Delta_d \end{bmatrix}. \tag{3.8}$$

Using the result of proposition 3.1 the first block is internally stable and satisfies (3.3). The second block is stable and has H_∞-norm less than 1 by definition. □

Proposition 3.2 provides an alternative characterization of uncertainty with mixed parametric and dynamic blocks, as it is explained in the sequel. This satisfies condition b) (2.35) of theorem 2.2.

In the sequence, note that the inverse of $\Gamma(\Phi, D)$ regarding the Redheffer star product is obtained by swapping Φ and $-\Phi$ and D and D^{-1} in (3.6). This yields

$$\Gamma(\Phi, D)^{-\star} = \begin{bmatrix} \Phi & 0 & I-\Phi & 0 \\ 0 & 0 & 0 & D^{-1} \\ I+\Phi & 0 & -\Phi & 0 \\ 0 & D & 0 & 0 \end{bmatrix}.$$

Consider the reduced plant P_r with the performance channel $w \to z$ removed:

$$P_r : \quad \begin{bmatrix} z_\delta \\ y \end{bmatrix} = \begin{bmatrix} P_{\delta\delta} & P_{\delta u} \\ P_{y\delta} & P_{yu} \end{bmatrix} \begin{bmatrix} w_\delta \\ u \end{bmatrix}. \tag{3.9}$$

and suppose $K(\kappa)$ stabilizes P_r internally.

Figure 3.1 illustrates the interconnections of the systems.

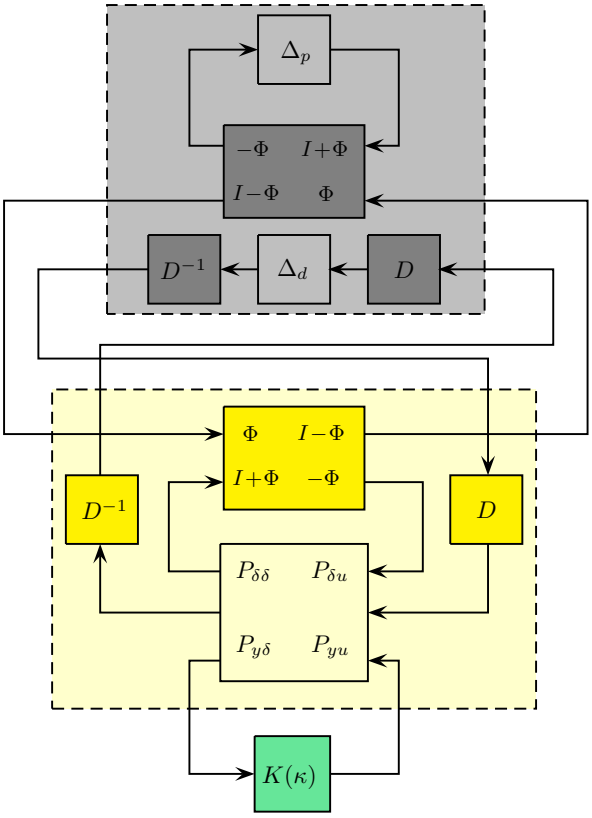

Figure 3.1: Interconnection schema for outer relaxation for robust control.

It follows that if there exist Φ, D and $K(\kappa)$ such that $\Gamma(\Phi, D)^{-\star} \star P_r \star K(\kappa)$ is stable and has H_∞-norm bounded by one, then the closed-loop system $\Delta \star P_r \star K(\kappa)$ is robustly stable. This leads to the next theorem:

Theorem 3.3. *Suppose there exist $\Phi \in \mathbf{\Phi}$, $D \in \mathbf{D}$ and a structured controller $K(\kappa)$ such that the closed-loop system $\Gamma(\Phi, D)^{-\star} \star P_r \star K(\kappa)$ is internally stable and satisfies the estimate*

$$\left\| \Gamma(\Phi, D)^{-\star} \star P_r \star K(\kappa) \right\|_\infty < 1. \tag{3.10}$$

Then the closed-loop system $\Delta \star P_r \star K(\kappa)$ is robustly stable over $\mathbf{\Delta}$. □

The next step is to include robust H_∞-performance into the setup. A scaled performance channel is added leading to the scaled plant P_γ:

$$P_\gamma : \quad \begin{bmatrix} z_\delta \\ z \\ y \end{bmatrix} = \begin{bmatrix} P_{\delta\delta} & P_{\delta w} & P_{\delta u} \\ \frac{1}{\gamma}P_{z\delta} & \frac{1}{\gamma}P_{zw} & \frac{1}{\gamma}P_{zu} \\ P_{y\delta} & P_{yw} & P_{yu} \end{bmatrix} \begin{bmatrix} w_\delta \\ w \\ u \end{bmatrix}. \tag{3.11}$$

Then with the same notations as above and the scaling set $\mathbf{D}$ suitably generalized to account for the new performance block, the following corollary 3.1 is obtained.

Corollary 3.1. *Suppose there exist $\Phi \in \mathbf{\Phi}$, $D \in \mathbf{D}$, and a structured controller $K(\kappa)$ such that $\Gamma(\Phi, D)^{-\star} \star P_\gamma \star K(\kappa)$ is internally stable and satisfies the estimate*

$$\left\|\Gamma(\Phi, D)^{-\star} \star P_\gamma \star K(\kappa)\right\|_\infty < 1. \tag{3.12}$$

Then the closed-loop system $\Delta \star P \star K(\kappa)$ is robustly stable over $\mathbf{\Delta}$, and has worst-case H_∞ performance γ over $\mathbf{\Delta}$. □

The proof of Corollary 3.1 is follows direct from Theorem 3.3.

3.2 Robust control design implementation

In order to implement the robust synthesis technique with the novel outer relaxation, corollary 3.1 should be recast as a 2-disk H_∞-synthesis problem. Gathering all constraints and defining the quantity to be minimized, the synthesis is turned into the following optimization program:

$$\begin{array}{ll} \text{minimize} & \gamma \\ \text{subject to} & \|\Gamma(\Phi, D)^{-\star} \star P_\gamma \star K(\kappa)\|_\infty \leq 1 - \eta \\ & \Gamma(\Phi, D)^{-\star} \star P_\gamma \star K(\kappa) \text{ internally stable} \\ & \|\Phi\|_\infty \leq 1 - \eta \\ & \Phi \in \mathbf{\Phi}, D \in \mathbf{D}, \kappa \in \mathbb{R}^n, \gamma \in \mathbb{R}_+ \end{array} \tag{3.13}$$

where the small threshold $\eta > 0$ is used to emulate the *strictly less than* constraints.

The tunable variables of the program are the matrix Γ, the controller $K(\kappa)$ and the gain γ. The minimization of γ requires all variables to be tuned to their optimum values. This results in a nonconvex and nonsmooth program, with nonsmooth constraints. The options to solve this type of problem were discussed in section 2.2. Following that line, the algorithmic approach to multi-disk synthesis where all H_∞ constraints are handled simultaneously from Apkarian and Noll [2006a] was chosen. An implementation of this approach uses the MATLAB ™ routine SYSTUNE [MathWorks, 2017]. Details about the routine can be found in appendix D.1.

In this set up, the orders of the realizations of scaling D, multiplier Φ and controller K should be determined a priori as well as their structures and parameterizations. In the sequence, all the systems are interconnected into a single parameterized system to be tuned. The performance channel is scaled by parameter γ, the H_∞ gain accounting for closed-loop performance, that will be minimized.

On total, there are seven constraints, enumerated below. Note that the first four constraints are satisfied by construction. The last three should be enforced during optimization and pose additional constraints to the search space.

- $\kappa \in \mathbb{R}^n$ **:** The constraint on κ is a domain constraint, that is, κ belongs to vector space on real numbers. This vector is used to build the controller with a pre-determined structure. Once the structure defined, one should also define the controller parameterization.
- γ **:** This parameter may assume any positive real value. It emulates the performance that will be minimized. Note that γ is used to scale plant P into P_γ.
- $D \in \mathbf{D}$ **:** This constraint specifies that the structure of D should be block diagonal. Each block corresponds to a diagonal matrix whose entries are equal biproper SISO stable minimum-phase systems.
- $\Phi \in \mathbf{\Phi}$ **:** This constraint specifies that the structure of Φ should be block diagonal. Each block corresponds to, possibly MIMO, stable systems.One must also choose a parameterization for Φ.
- $\|\Phi\|_\infty \leq 1 - \eta$ **:** This constraint assures that the Φ multipliers are contained on the unit ball, as required by Theorem 3.3 and Corollary 3.1.

- $\|\Gamma(\Phi, D)^{-\star} \star P_\gamma \star K(\kappa)\|_\infty \leq 1 - \eta$ **:** This constraint assures robust stability over $\mathbf{\Delta}$, Corollary 3.1.
- Internal stability **:** Internal stability is enforced by not allowing closed-loop poles on the right-half plane.

3.3 Numerical Results

The efficiency of the novel outter relaxation with nonsmooth solvers method for robust controllers design is supported by the numerical results for the validation test introduced in Appendix A.1 for a set of test cases (see Appendix B). The term *outer* is used when referring to the implementation of outer relaxation method developed in this section and the term *performance* will be employed in the sense of worst-case H_∞-norm of the closed-loop system. For the sake of readability, some tables were moved to the Appendix of tables at the end of the chapter.

- **Synthesis for the test set**

Table 3.1 shows data of the implementation of the synthesis based on outer approximation developed in this chapter. In all cases, the order of the tridiagonal state-space realizations of D and Φ is 2.

Firstly, it should be verified if the first and third constraints of program (3.13) were satisfied by inspection of columns SG and SG_Φ. The values must be less than 1, but due to numerical precision, values very close to 1 are shown as 1 in the table. As consequence, a value larger than 1 in any of the columns, means that the computation failed as neither stability nor performance are guarantee for the closed-loop system in terms of theorem 3.1. Note that the last four constraints of program (3.13) are satisfied by construction on implementation of the optimization and that the stability constraint is verified by a finite H_∞-norm certification.

Statistics of Table 3.1:

- For test cases 22 and 25, SG and SG_Φ are more than 20 times larger than limit 1 and lower and upper bounds of the certification indicate that the system can be considered unstable or highly degraded. The same is valid for case 9, where the constraints are violated by more than 100%.
- In 23% of the cases, the constraints are violated by less than 3%, but as consequence $\underline{\gamma}$ and γ disagree up to 90%, with a certified performance smaller than the value given by `outer`.
- In case 10, the constraints exceed 1 by more than 30% yet certification attests the system as stable and with a better performance than the value of γ.
- In case 13, the constraints do not exceed 1, but certification and *outer* disagree by 93% in performance, with the certification attesting better performance.
- In those cases where the constraints are not violated, the deviation is 30% in case 29 and it is below 12% for the remaining 57% of the cases.
- The certified values can be considered accurate in all cases except 19, for which the upper bound is infinite whereas the lower bound is 1.

- **Comparison for different controller orders**

The impact of the order of the controller on the performance was studied for state-space controller with order varying between 1 and 5. The results of performance can be found in Table 3.2 on page 33.

Statistics of Table 3.2:

- Analysis of the table reveal that in 53% of the cases increasing the controller order improves the performance.
- In 33% of the cases, the change in the order of the controller does not affect the performance, including cases 22 and 25, that could not be stabilized by the algorithm for any controller order.
- In case 23 increasing the controller order actually degrades the performance. This is attributed to numerical difficulties, altough it is not clear which ones.

Table 3.1: Data from the controller synthesis using the novel outer relaxation for the test set.

Ex	$n_x(K)$	n_K	γ	$\underline{\gamma}$	$\overline{\gamma}$	SG	SG_Φ	t_s	t_a
1	2	12	0.987	0.995	0.997	1	0	7	0.28
2	1	4	0.991	1	1.002	1	0	11	0.26
3	4	29	1.415	1.421	1.424	0.999	0	34	0.28
4	2	16	0.991	0.999	1.001	1	0	11	0.1
5	4	30	1.831	1.614	1.617	0.947	0	29	0.42
6	1	4	0.992	1	1.002	1	0	6	0.25
7	4	48	0.996	1.004	1.007	1	0	45	0.69
8	2	9	1.117	1.127	1.129	1	0.988	9	0.06
9	3	22	104.91	134.2	168.46	1.311	1.310	93	4.59
10	3	14	18.481	3.842	3.865	1.862	1.861	152	6.8
11	4	19	1.417	1.008	1.01	1.009	1.009	84	3.5
12	5	24	1.006	1.016	1.018	0.999	0.998	26	0.2
13	1	4	13.832	1.008	1.01	1	0.995	36	1.08
14	2	12	1.109	1	1.002	1	0.998	47	16.6
15	4	19	9.999	5.091	5.103	0.999	0.999	14	0.06
16	5	37	2.349	1.948	1.951	0.999	0.991	270	0.37
17	3	23	20.119	1.733	1.738	0.999	0.996	83	0.88
18	3	14	10.085	9.16	9.179	1.007	1.007	39	0.18
19	1	4	10.366	1.000	Inf	1.034	1.023	82	2.46
20	3	14	10.093	8.057	8.115	1.009	1.009	451	2.64
21	1	9	0.999	1	1.002	1	1	57	0.56
22	2	9	30.451	49510	49609	4728	4729	239	0.63
23	1	8	40.763	14.777	16.103	1.013	1.013	92	6.69
24	3	14	1.97	1.959	1.963	1	0.9	16	0.18
25	1	8	30.25	217.0	233.6	20.02	20.02	47	4.9
26	1	9	0.999	1	1.002	1	0.999	57	0.25
27	3	14	1.594	1.588	1.592	1	0.998	17	0.29
28	1	6	10.015	2.966	2.973	1.001	1.001	16	0.39
29	4	19	1.278	1.07	1.073	0.999	0.939	29	0.07
30	5	24	7.262	7.078	7.099	0.999	0.945	31	0.12

Legend:

Ex:	Test case	γ :	performance achieved by *outer*
$n_x(K)$:	order of the controller	$\underline{\gamma}$:	lower bound certificate on performance
n_K:	dimension of parameter vector κ	$\overline{\gamma}$:	upper bound certificate on performance
t_s:	time elapsed for synthesis [s]	SG_Φ:	$\|\Phi\|_\infty$
t_a:	time elapsed for certification [s]	SG:	$\|\Gamma(\Phi, D)^{-\star} \star P_\gamma \star K(\kappa)\|_\infty$

◇ In case 9, for first-order and third-order controllers, the closed-loop system is stable but the performance is greater than 100.

- **Comparison for different scaling orders**

The *outer* method was also tested against the variation of performance with respect to variations in the order of D and Φ. The results are presented in Table 3.3 on page 34, for variations on the order of D and in 3.4 on page 34 for variations on order of Φ.

The order of the state-space realizations of the scaling D ranged from 0 to 3 while the order of the realization of Φ was kept constant and equal 2. Cases 8 to 11 are only subject to parametric uncertainties and for this reason the variation on D was not studied. The statistics presented below take these cases into account however.

Statistics of Table 3.3:

◇ In 27% of the cases, modifications in the order of D does not affect the performance.
◇ Among these 27%, 2 cases could not be stabilized by any order of D.
◇ In 47% of the cases, a simple change from a static D to a first-order dynamic D improves the performance, in 30% of the cases by more than 100%.
◇ For the other cases, increasing the order of D results in mild performance improvement.
◇ For 20% of the cases, not every increment on the order of D leads to performance improvement.

◇ In 5 cases a third-order D did not result in the best performance.

The the order of the state-space realization of Φ varies from 1 to 3 while the order of the realization of D was kept 2. Cases 1 to 7 are subject only to dynamic uncertainties hence they were not analysed.

Statistics of Table 3.4:
◇ Only in cases 15, 16 and 25, increase the order of Φ results in a significant improvement on performance.
◇ On the other hand, in 5 cases, 9, 10, 18, 20 and 27, the increase resulted even in a degradation of performance.
◇ Case 23 has an improvement for a change of order of Φ from 1 to 2, but deteriorates from 2 to 3.
◇ For the remaining cases, changing the order of Φ had no impact on performance.

It is worth noting that for most of the cases the synthesis did not succed with a static Φ.

- **Comparison with other synthesis methods**

As *outer* is the first novel method presented, the results from the synthesis based on this outer relaxation are compared only to third-party methods in the present chapter. The comparison with the other techniques developed in this work will take place as they are introduced. The third-party robust synthesis method chosen for comparison is the well-known MATLAB ™ routine DKSYN [MathWorks, 2017] that implements the *DK-iteration* from Doyle [1985]. Note that *DK-iteration* is also based on an outer relaxation. A brief description of DKSYN and more on the how the comparison with DKSYN is carried out can be found in appendix A.1.3. Table 3.5 on page 35 contains the results for both methods on the original test cases.

Statistics of Table 3.5:
◇ The comparison of the methods considering only the performance values, reveals that *outer* has better results in 23% of the cases.
◇ *Outer* is outperformed by DKSYN in 37% of the cases and they are equivalent in 40% of the cases.
◇ Excluding the case of failures, for 4 cases DKSYN outperforms *outer* by more than 100% and in 5 cases *outer* outperforms DKSYN by more than 100%.
◇ The failure cases 9, 22 and 25 by *outer* are handled by DKSYN in cases 9 and 25 with controllers of more than 300 states and corresponds to a failure in case 22. DKSYN fails in case 20, where *outer* achieves a performance of 8 with a third-order controller.
◇ The order of the controllers designed by DKSYN is always larger than the order of the structured controller designed by *outer*, reaching values larger than 100 in some test cases.

It should be kept in mind that the performance returned by DKSYN is not the worst-case H_∞-norm in the modeled $\mathbf{\Delta}$, that is, DKSYN does not assure robust performance and robust stability over $\mathbf{\Delta}$ defined in (2.32). As discussed in appendix A.1.3, $\mathbf{\Delta}$ is rescaled by DKSYN. In order to properly compare the techniques, they should be compared in the same exact problem. This is accomplished by rescaling $\mathbf{\Delta}$ following the procedure in appendix A.1.3. The results of this procedure are now presented in Table 3.6. As DKSYN index of performance refers already to the rescaled $\mathbf{\Delta}$, its results are repeated in Table 3.6 just for the sake of comparison.

Statistics of Table 3.6:
◇ With the rescaled $\mathbf{\Delta}$ *outer* cannot achieve better performance than DKSYN in 36% of the cases up to a 15th-order controller.
◇ From these 36% cases, 4 correspond to cases in which $\mathbf{\Delta}$ was enlarged, to comply with DKSYN rescaled $\mathbf{\Delta}$, and *outer* performs poorer even increasing the order of the controller.
◇ In the other 60% cases, on the new uncertainty bound, *outer* can outperform DKSYN.
◇ With exception of case 10, the order of DKSYN controller is always larger than the order of *outer* controller, exceeding 98 in 7 cases.

Table 3.6: Comparison between synthesis using the novel outer relaxation and DKSYN routine with rescaled Δ

		outer		DKSYN				*outer*		DKSYN	
Ex	$\sigma(\Delta)$	$\underline{\gamma}$	$n_x(K)$	μ	$n_x(K)$	*Ex*	$\sigma(\Delta)$	$\underline{\gamma}$	$n_x(K)$	μ	$n_x(K)$
1	1.007	0.977	4	0.993	13	16	0.825	1.592	15	1.212	98
2	0.99	0.994	1	1.01	16	17	0.053	1.573	1	19.034	9
3	1.117	1.482	10	0.895	38	18	0.053	1.055	1	18.775	6
4	1.017	1.001	14	0.983	20	19	0.224	3.13 0	1	4.466	6
5	0.826	1.044	5	1.21	22	20	x	8.056	3	x	x
6	1.072	0.907	2	0.933	7	21	1.002	0.991	15	0.998	20
7	1.048	0.966	15	0.954	46	22	x	49510	2	x	x
8	0.881	1.020	2	1.135	9	23	0.531	1.442	1	1.882	294
9	0.303	749	15	3.299	445	24	0.941	1.684	10	1.062	34
10	0.382	3.849	7	2.621	10	25	0.555	Inf	15	1.803	304
11	0.224	1.028	1	4.472	253	26	1.068	1.052	15	0.936	24
12	0.612	0.528	2	1.635	27	27	0.589	1.156	1	1.698	25
13	1.005	4.500	13	0.995	99	28	0.005	0.014	1	220	7
14	1.001	0.990	14	0.999	120	29	0.854	0.938	2	1.17 0	18
15	0.936	5.254	10	1.069	30	30	0.914	4.672	10	1.094	30

Legend:

Ex:	Test case	$\sigma(\Delta)$:	new bound on uncertainty Δ
outer :	data for *outer*	DKSYN :	data for DKSYN
$\underline{\gamma}$:	lower bound certificate of *outer*	μ :	performance achieved by DKSYN
$n_x(K)$:	state-space controller order		

- **dksynstruct**

The last numerical test aims to enlighten if the high-order controllers returned by DKSYN are the only ones that satisfy the robust control problem as formulated by *DK-iteration* or if they are result of a choice of design. To this end, the synthesis step was modified so it was executed by a nonsmooth optimization solver for fixed-order controller design, implemented by MATLAB ™ routine HINFSTRUCT. The comparison between the original DKSYN and what was termed *DGK+* considers the performance, the control order and the time elapsed for the whole robust synthesis. The results can be consulted in Table 3.7 on page 35.

Statistics of Table 3.7:

- ◇ for 40% of the cases, the performance obtained for a structured controller were larger than standard DKSYN.
- ◇ The opposite occurs for cases 11, 20, 27 and 28. For case 20, where DKSYN failed, it was possible to design a reduced-order controller.
- ◇ For the 53% remaining cases, the performances differ by less than 10%.
- ◇ For the cases where the performance improved by the structured synthesis, it is worth comparing with the novel techniques. For cases 20 and 28, the performance was at least 6 times higher than the performance achieve by the inner approximation, and more than the double of the lower bound certification for the outer approximation. For case 11, the performance achived is the same for the three approaches.
- ◇ As both, DKSYN and *DGK+* are professional code, one may also be concerned with the time elapsed of synthesis. In 73% of the cases, the synthesis of a structured controller increases the running time by a factor of 6, on average.

Discussion

A new outer relaxation for the Robust Control Synthesis was developed and implemented using nonsmooth optimization. The efficency of the method and comparison to other Robust Control Synthesis methods were evaluated on 30 test cases. It was shown to be efficient, stabilizing and achieving good performance in all test cases but two.

Problem 3.13 is not fully convexified, in contrast to LMI relaxations that introduce conservatism and also lead to numerically difficult solutions due to the presence of Lyapunov and multiplier variables.

Yet, the solutions from the implementation of the novel outer relaxation by nonsmooth optimization techniques are still suboptimal, and thus conservative, in some cases. Possible causes of this suboptimum performance are: small gain constraints being sufficient but not necessary conditions, local solver suboptimal solutions and order of multipliers.

- Small gain constraints 3.1 and 3.12 on program 3.13 are sufficient but not necessary conditions to ensure robust stability and robust performance for robust control problem with the outer relaxation developed. This is noticeable when observing that the code considered to have failed in all cases where the small gain conditions were violated but posterior certification proved the robust controller to be stabilizing and even delivering good performance. Moreover, the implementation seeks to satisfy the constraints at the expense of performance optimization, as they are constraints that ensure stability. It is revealed that in cases where the constraints were indeed conservative, performance optimization was neglected.
- Another possible source of conservatism comes from the fact that local solvers, as the one used for the synthesis, may return suboptimal solutions when many local optima for the problem exist. This affects both the search to satisfy the constraints, that can converge to infeasible local solutions, and the optimization of the performance. A suggestion for these cases is to increase the number of start points.
- It is known that the best performance is achieved by the full-order controller and that using fixed-order controller may degrade performance. In this study, the performance achieved by the synthesis improved with the increase of the controller order in more than half of the cases. For state-space controllers, the number of parameters to be tuned is quadratically dependent of the order of the controller and the solver is expected to deal with the number of parameters for the orders considered.
- Safonov et al. [1993] discussed the advantages of fixed-order realizations of the multipliers opposed to a posterior fitting. The authors argued that the previous choice of the order of the multipliers, if it not helps to decrease conservatism per se, allows to take the degradation of performance due to limited order into account in the controller synthesis step, helping thus to reduce the overall conservatism. The analysis of the variation of the order of the D-scalings points to fact that a dynamic scaling will generally work better than a static one, for only in one case a static scaling had a better performance than dynamic ones. Though inexpensive to calculations, once each full complex uncertainty block only accounts a SISO realization of the scaling, increasing the order above three results in no further improvement of performance.
- The scene is not the same for Φ multiplier. A stabilizing controller cannot even be synthesized if a static multiplier is employed. Because the Φ blocks are full matrices, increasing the order of the realizations of Φ is computationally expensive. For the cases with high number of parametric uncertainties or many repeated parametric uncertainties, increasing the order degrades performance. This happens due to the high number of parameters to be simultaneously tuned in these cases. In cases with a small number of parametric uncertainties and repetitions, one can notice that actually increasing the order of G improves performance.However for the present method, the number of repetitions of parametric uncertainties alone does not explain the failure in such cases or an H_∞-norm above expectation. The failure cases have in common a high number of parametric uncertainty blocks and a high number of repetition in addition to a plant with more than 20 states.

The analysis of results on rescaled uncertainty problems proved that *outer* is very competitive when compared to DKSYN, outperforming DKSYN more often than it was overcome. Moreover, *outer* designed reduced-order controllers, with order not greater than 5, which is always smaller than the order of DKSYN controllers. To beat *outer* , DKSYN requires very high-order controllers. The advantage of *outer* over DKSYN is more pronounced if we consider that implementation of a 253th-order controller will certainly require a model reduction, specially for systems with hardware limitation. If model reduction is applied, the resulting degradation in performance should be computed *a posteriori*, whilst for the presented *outer* method the performance is already assured.

Also observe that *outer* and DKSYN use the same scaling for relaxing the problem in pure complex uncertainty case. The difference between them is that *outer* simultaneously design scaling and controller and use a nonsmooth optimization solver. In these cases, the *outer* method performs better,

showing that the developed synthesis method is preferable to the μ synthesis. When a parametric uncertainty is added, the complex uncertainties are still being scaled in the same way. Iwasaki and Hara [1998] observed that the G-scaling used in DKSYN routine is actually a particular case of topological separator from which Φ multiplier is derived. So for pure parametric uncertainty both methods and multipliers are being compared and results show the equivalence.

Some light is shed upon the matter with the results from comparison from DKSYN and *DGK+*, that uses nonsmooth solvers for structured controller synthesis. The results show that the effort to obtain a fixed-order controller reflected on elapsed time for the overall robust synthesis, larger than original DKSYN in almost all cases. The performance of the new implementation was similar to that of DKSYN, with no failures though. Altogether, the results prove that indeed simultaneously tuning multipliers and controller gain is the best option so far.

Overall, the approach developed in this chapter is still conservative in cases with high repetition of parametric uncertainties. This suggests the use of an alternative strategy to overcome the difficulty of large r_i's. To this end, the inner relaxation is considered and discussed in the next chapter.

Appendix of tables

Table 3.2: Comparison of H_∞-norm obtained by synthesis using the novel outer relaxation for different orders of controller K

$n_x(K)$ *Ex*	1	2	3	4	5	$n_x(K)$ *Ex*	1	2	3	4	5
1	1.017	0.995	0.982	0.989	0.988	16	Inf	Inf	3.349	2.256	1.930
2	1.000	0.999	0.999	0.999	0.999	17	2.1955	3.087	1.739	1.603	6.700
3	11.464	4.635	4.807	1.422	1.167	18	36.27	21.79	9.180	8.718	9.888
4	0.999	0.999	0.999	0.999	0.999	19	0.973	1.000	0.960	1.133	1.185
5	Inf	Inf	1.516	1.614	1.192	20	10.95	9.455	8.057	11.78	7.633
6	1.000	0.867	0.860	0.861	0.880	21	1.000	1.000	1.000	1.000	1.000
7	4.649	2.230	1.145	1.004	1.003	22	40439	49510	6845	Inf	11516
8	2.971	1.127	1.127	1.127	1.128	23	14.77	Inf	Inf	Inf	Inf
9	134.1	139.7	168.5	Inf	197.4	24	1.966	1.986	1.959	1.980	1.958
10	94.87	68.47	41.52	63.91	3.356	25	820	Inf	Inf	Inf	2692
11	x	1.000	1.001	1.008	1.014	26	1.000	1.000	1.000	1.000	1.000
12	Inf	3.376	1.246	1.205	1.018	27	2.527	1.354	1.742	1.797	1.587
13	1.010	1.584	1.450	1.337	2.700	28	3.217	2.982	3.145	2.949	2.980
14	1.012	1.000	1.000	1.000	1.000	29	2.423	1.200	1.180	1.073	1.118
15	19.71	9.628	9.148	6.372	6.874	30	Inf	60.710	22.20	8.611	7.100

Legend:

Ex: Test case $n_x(K)$: state-space controller order

Table 3.3: Comparison of H_∞-norm obtained by synthesis using the novel outer relaxation for different orders of scaling D

$n_x(D)$ *Ex*	0	1	2	3	$n_x(D)$ *Ex*	0	1	2	3
1	1.021	0.995	0.995	0.995	16	4.155	2.081	1.948	1.815
2	2.184	1.000	1.000	1.000	17	3.94	5.934	2.078	12.329
3	42.48	5.934	4.807	6.496	18	1791	36.702	19.636	9.62
4	0.999	0.999	0.999	0.999	19	1.228	1.019	1.000	1.784
5	2.581	1.272	1.614	1.303	20	9.883	23175	8.057	5.11
6	3.633	1.000	1.000	1.000	21	1.000	1.000	1.000	1.000
7	3.481	1.034	1.004	1.001	22	98820	Inf	49510	34489
8	-	-	-	-	23	Inf	Inf	14.777	14.46
9	-	-	-	-	24	2.357	2.007	1.959	1.865
10	-	-	-	-	25	Inf	Inf	2692	Inf
11	-	-	-	-	26	1.000	1.000	1.000	1.000
12	1.726	1.247	1.246	1.238	27	77.591	2.634	1.588	1.574
13	1.002	1.018	1.008	1.009	28	Inf	3.115	3.177	2.964
14	1.000	1.000	1.000	1.000	29	1.114	1.232	1.538	1.221
15	11.911	8.936	9.148	7.192	30	9.964	7.631	7.988	7.64

Legend:

Ex: Test case $n_x(D)$: order of scaling D

Table 3.4: Comparison of H_∞-norm obtained by synthesis usingthe novel outer relaxation for different orders of scaling Φ

$n_x(G)$ *Ex*	1	2	3	$n_x(G)$ *Ex*	1	2	3
1	-	-	-	16	2.484	2.141	1.961
2	-	-	-	17	4.342	2.261	3.604
3	-	-	-	18	20.897	21.789	1794
4	-	-	-	19	1.000	1.000	1.000
5	-	-	-	20	9.699	11.354	13.102
6	-	-	-	21	1.000	1.000	1.000
7	-	-	-	22	Inf	Inf	Inf
8	1.172	1.127	1.127	23	Inf	14.777	Inf
9	120.89	113.2	Inf	24	1.947	1.914	1.899
10	3.738	3.356	Inf	25	Inf	177	271
11	1.008	x	1.018	26	1.000	1.000	1.000
12	1.278	1.246	1.21	27	1.618	1.646	2.48
13	1.002	1.008	1.006	28	2.987	3.075	2.993
14	1.000	1.000	1.001	29	1.22	1.188	1.192
15	7.937	8.516	6.699	30	7.334	7.134	7.083

Legend:

Ex: Test case $n_x(G)$: order of multiplier Φ

Table 3.5: Comparison between synthesis using the novel outer relaxation and DKSYN routine

	outer		DKSYN			*outer*		DKSYN	
Ex	$n_x(K)$	LB_a	$n_x(K)$	μ	*Ex*	$n_x(K)$	LB_a	$n_x(K)$	μ
1	2	0.995	13	0.993	16	5	1.948	98	1.212
2	1	1.000	16	1.010	17	3	2.078	9	19.034
3	5	1.167	38	0.895	18	5	8.732	6	18.775
4	2	0.999	20	0.983	19	1	1.000	6	4.466
5	4	1.614	22	1.210	20	3	8.057	x	x
6	1	1.000	7	0.933	21	1	1.000	20	0.998
7	4	1.004	46	0.954	22	2	49510	x	x
8	2	1.127	9	1.135	23	1	14.778	294	1.882
9	1	396.61	445	3.299	24	3	1.959	34	1.062
10	5	6.097	10	2.621	25	4	2692	304	1.803
11	2	1.000	253	4.472	26	1	1.000	24	0.936
12	3	1.246	27	1.635	27	3	1.588	25	1.698
13	1	1.008	99	0.995	28	1	2.967	7	220
14	2	1.000	120	0.999	29	2	1.538	18	1.17
15	4	6.372	30	1.069	30	5	7.988	30	1.094

Legend:

Ex:	Test case	$n_x(K)$:	state-space controller order
outer :	data for *outer*	DKSYN :	data for DKSYN routine
$\underline{\gamma}$:	lower bound certificate of *outer*	μ :	performance achieved by DKSYN

Table 3.7: Comparison of H_∞-norm obtained by synthesis using DKSYN and DG-iteration plus HINFSTRUCT

	DGK+			DKSYN				*DGK+*			DKSYN		
Ex	$n_x(K)$	μ	t	$n_x(K)$	μ	t	*Ex*	$n_x(K)$	μ	t	$n_x(K)$	μ	t
1	2	0.999	8	13	0.993	4	16	5	1.968	633	98	1.212	90
2	2	0.999	7	16	1.010	6	17	3	23.03	595	9	19.03	100
3	3	1.098	49	38	0.895	4	18	2	1204	17	6	18.77	29
4	2	0.983	4	20	0.983	2	19	3	132.4	352	6	4.466	484
5	4	1.115	377	22	1.210	7	20	3	20.32	171	x	x	x
6	2	0.934	9	7	0.933	3	21	2	0.998	22	20	0.998	7
7	4	1.013	107	46	0.954	10	22	x	x	x	x	x	x
8	2	1.082	23	9	1.135	10	23	3	9.374	2065	294	1.882	130
9	4	15.93	1575	445	3.299	2239	24	3	1.163	52	34	1.062	20
10	3	4.892	90298	10	2.621	11050	25	4	16.13	653	304	1.803	2036
11	2	1.005	2255	253	4.472	4928	26	2	0.937	42	24	0.936	10
12	3	1.958	30	27	1.635	7	27	3	1.496	9	25	1.698	10
13	2	5.364	128	99	0.995	31	28	3	6.943	438	7	220.1	206
14	2	1.004	173	120	0.999	26	29	2	1.123	22	18	1.170	16
15	3	1.693	37	30	1.069	22	30	5	1.123	65	30	1.094	12

Legend:

Ex:	Test case	$n_x(K)$:	state-space controller order
DKSYN :	data for DKSYN routine	*DGK+*:	data for DK-iteration+structured synthesis
μ :	achieved performance	*t*:	time elapsed for synthesis

Chapter 4

Development and implementation of a new inner approximation for the synthesis of robust structured controllers

In this chapter

a novel inner relaxation for robust structured controller synthesis is developed and proved to be efficient. A set of models representing the uncertain model is obtained by an iterative search for the worst case stability and performance scenarios. Then, a nonsmooth optimization technique for multi-disk multi-model structured controller synthesis is employed. [Aguiar et al., 2018], [Menezes et al., 2016]

Conclusion

The inner relaxation approach is shown to be the less conservative among the methods tested and not optimistic. The approach demands a larger number of scenarios in cases with dynamic uncertainty than in cases with pure parametric uncertainty, which may reduce the performance of the technique.

The intractable robust structured H_∞ control problem of chapter 2 was solved by applying an outer relaxation to the problem in chapter 3. The results of chapter 3 indicate that for the cases of a high number of repetitions of parametric uncertainties the outer relaxation is still conservative and prone to failure.

The technique developed in Apkarian and Noll [2017]; Apkarian et al. [2015a] to find worst-case scenarios and recalled in section 2.3.4 is now used for an inner relaxation of robust control problem for mixed uncertainties. The objective is to reduce conservatism.

4.1 Generation of scenarios for mixed uncertainty

The generation of scenarios for the inner relaxation will use the techniques introduced in Apkarian et al. [2015a] for parametric uncertainty and in Apkarian and Noll [2017] for dynamic uncertainty. The generation of worst-case scenarios results from a robust analysis of an uncertain system and naturally demands a nominal stable closed-loop system. To this end, the first step is an H_∞ structured control synthesis for $\Delta = 0$, that is, $\delta_i = 0$ for $i = 1, \ldots, N_p$ in eq. 2.30 and $\Delta_i = \mathbf{0}$ for $i = 1, \ldots, N_d$ in eq. 2.31:

$$\min_{K \in \mathcal{K}, \Delta = 0} \|\Delta \star P \star K(\kappa)\|_\infty \tag{4.1}$$

The $K(\kappa^*)$ corresponds to the solution of program (4.1), that can be solved by methods discussed in section 2.2 as MATLAB ™ routine SYSTUNE [MathWorks, 2017]. One thus proceeds to the generation of scenarios, obtained through program (2.43) and (2.44) recalled below:

$$\alpha^* = \max_{x \in \boldsymbol{B}} \alpha(A(\Delta(x))),$$
$$h^* = \max_{x \in \boldsymbol{B}} \|T_{wz}(\Delta(x))\|_\infty.$$

where x is partitioned accordingly to the structure of Δ, $x = (x_1, \ldots, x_{N_p}, x_{1+N_p}, \ldots x_{N_p+N_d})$ with $x_i = \delta_i$, $i = 1, \ldots, N_p$ and $x_i = (\rho_i, \phi_i^v, \theta_i^u, \phi_i^u, \theta_i^v)$, $i = 1 + N_p, \ldots, N_p + N_d$ and $\boldsymbol{B}$ is the set of box constrained variables x such that

$$\begin{aligned} \boldsymbol{B} = \{x : x_i \in [-1, 1],\ i = 1, \ldots, N_p \text{ and } x_i \in [0, 1] \times [0, 2\pi]^{p_i} \times [0, 2\pi]^{q_i} \times \\ [0, \pi]^{p_i - 2} \times [0, 2\pi] \times [0, \pi]^{q_i - 2} \times [0, 2\pi],\ i = 1 + N_p, \ldots, N_p + N_d\}. \end{aligned} \tag{4.2}$$

Each new scenario generated is included in the set $\boldsymbol{\Delta}_a$ and a new H_∞ synthesis follows in the form of the optimization program:

$$\min_{\kappa} \max_{\Delta \in \boldsymbol{\Delta}_a} \|\Delta \star P \star K(\kappa)\|_\infty, \tag{4.3}$$

which due to the finiteness of $\boldsymbol{\Delta}_a$ is a multi-disk H_∞-synthesis problem in the sense of Apkarian and Noll [2006a].

This seems appealing since program (4.3) can be solved to local optimality with tools like SYSTUNE or HINFSTRUCT [Apkarian et al., 2014],[MathWorks, 2017]. A scheme of the iterative selection of these active scenarios $\Delta \in \boldsymbol{\Delta}_a$ is shown in Figure 4.1.

4.2 Robust control design implementation

The implementation of the proposed robust control synthesis with inner relaxation follows the directives of Algorithm 4.1. Programs α^* in step 3 and program h^* in step 4 are discussed in detail in references Apkarian et al. [2015a,b, 2016]; Ravanbod et al. [2017].

Algorithm 4.1: Robust synthesis by inner approximation

Parameters: $\varepsilon > 0$.

▷ **Step 1** (`Nominal synthesis`).
Initialize the set of active scenarios as $\boldsymbol{\Delta}_a = \{0\}$.

▷ **Step 2** (`Multi-model synthesis`).
Given the current finite set $\boldsymbol{\Delta}_a \subset \boldsymbol{\Delta}$ of active scenarios, compute a structured multi-model H_∞ controller by solving the multi-disk H_∞-program

$$h_* = \min_{\kappa \in \mathbb{R}^n} \max_{\Delta \in \boldsymbol{\Delta}_a} \|\Delta \star P \star K(\kappa)\|_\infty.$$

The solution is the structured multi-model H_∞ controller $K(\kappa^*)$.

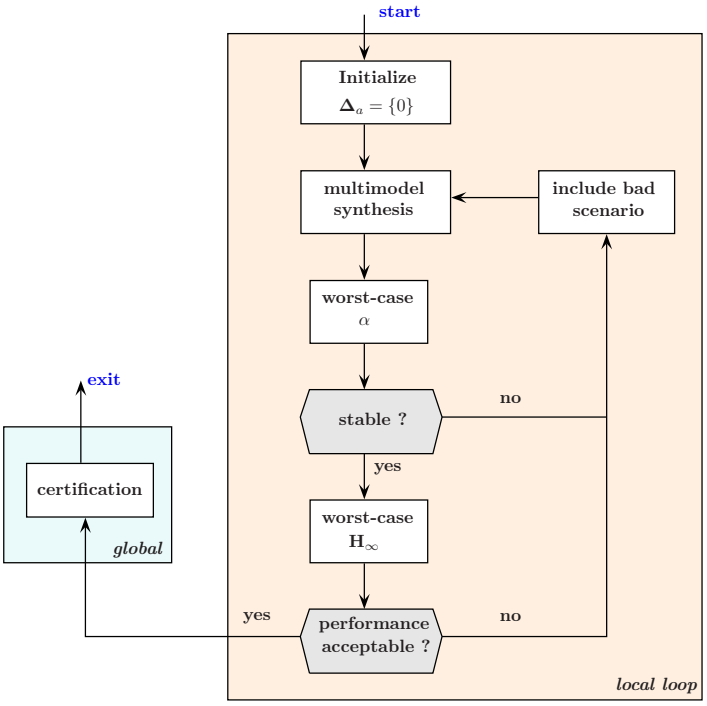

Figure 4.1: Schema of algorithm 4.1 for Robust Control with inner relaxation.

▷ **Step 3** (`Worst-case stability`).
Try to destabilize the closed-loop system $\Delta \star P_r \star K(\kappa^*)$ by computing its worst case spectral abscissa

$$\alpha^* = \max_{\Delta \in \mathbf{\Delta}} \alpha\left(A(\Delta, \kappa^*)\right).$$

The solution is the worst stability scenario Δ^*. If $\alpha^* = \alpha\left(A(\Delta^*, \kappa^*)\right) \geq 0$, then include Δ^* in the set $\mathbf{\Delta}_a$ and go back to step 2. Otherwise continue with step 4.

▷ **Step 4** (`Worst-case performance`).
Try to degrade performance of the closed-loop system $\Delta \star P \star K(\kappa^*)$ by computing its worst case H_∞-norm

$$h^* = \max_{\Delta \in \mathbf{\Delta}} \|\Delta \star P \star K(\kappa^*)\|_\infty.$$

The solution is the worst performance scenario $\Delta^\sharp$.

▷ **Step 5** (`Stopping test`).
If $\alpha(A(\Delta^\sharp, \kappa^*)) < 0$ and $h^* < (1+\varepsilon)h_*$, degradation of performance is marginal. Then exit loop and go to step 6 for posterior certification. Otherwise include $\Delta^\sharp$ in the set $\mathbf{\Delta}_a$ and continue loop with step 2.

▷ **Step 6** (`Certification`).
Use a global solver to certify *a posteriori* that $K(\kappa^*)$ is robustly stable over $\mathbf{\Delta}$ and has robust H_∞-performance h_* over $\mathbf{\Delta}$.

In step 3, $A(\Delta, \kappa)$ denotes the A-matrix of the closed loop system with controller $K(\kappa)$ and the uncertainty block Δ. All programs in the algorithm 4.1 are nonsmooth and they are addressed by bundle trust-region methods. The main difference between α^*, h^* on the one hand, and h_* on the other, is analyzed in Apkarian et al. [2015a, 2016].

It is possible to split the search for worst-case scenarios $\Delta \in \mathbf{\Delta}_a$ into two consecutive steps, where bad scenarios for $\mathbf{\Delta}_p$ and bad scenarios for $\mathbf{\Delta}_d$ are generated separately. In the first half-step, for fixed κ^* and for a fixed complex uncertainty Δ_d^*, a search over $\mathbf{\Delta}_p$ for a worst case Δ_p^* is made based on an optimization program as analyzed in Apkarian et al. [2016]. In the second half-step this scenario Δ_p^*,

along with κ^*, are held fixed, and a search over $\mathbf{\Delta}_d$ for a worst-case Δ_d^* based on WCGAIN is made. The idea to proceed in this way springs from the observation that the function WCGAIN [MathWorks, 2017] works particularly well in the case of sole complex uncertainty $\mathbf{\Delta}_d$, as observed in Newlin and Glavaski [1995], but is less precise in the case of mixed uncertainty or pure real uncertainty.

4.3 Numerical Results

The efficiency of the novel inner relaxation with nonsmooth solvers method for robust controllers design is supported by the numerical results for the validation test introduced in Appendix A.1 for a set of test cases (see Appendix B). The term *inner* is used when referring to the implementation of inner relaxation method developed in this chapter and the term *performance* is employed in the same sense as in previous chapter and refers to worst-case H_∞-norm of the closed-loop system. For the sake of readability, some tables were moved to the Appendix of tables at the end of the chapter.

- **Synthesis for the test set**

Table 4.1: Data from the controller synthesis using inner relaxation for the test set.

Ex	$n_x(K)$	n_K	γ	$\underline{\gamma}$	$\overline{\gamma}$	$\lvert\Delta_a\rvert$	t_s	t_a
1	2	12	0.995	0.995	0.997	11	28	0.15
2	1	4	1.000	0.999	1.001	7	11	0.17
3	3	22	1.005	1.009	1.011	25	279	0.67
4	2	16	0.832	0.999	1.001	3	6	0.33
5	4	30	0.996	0.996	0.999	25	1247	1.06
6	1	4	1.000	1.000	1.002	4	2	0.31
7	4	48	0.999	1.002	1.004	29	1792	0.75
8	2	9	1.000	1.000	1.002	4	2	0.11
9	4	29	1.008	1.008	4.377	5	38	5.05
10	3	14	0.982	0.982	2.777	3	9	21.8
11	1	4	1.000	1.000	1.002	2	3	4.50
12	3	14	1.000	1.000	1.002	11	70	0.43
13	1	4	1.000	1.000	1.001	3	3	1.12
14	2	12	1.006	0.999	1.009	9	16	10.9
15	3	14	0.998	0.996	1.001	8	26	1.01
16	5	37	0.996	1.02 0	1.138	31	1269	6.55
17	3	23	0.998	0.999	1.002	18	151	3.78
18	2	9	0.997	1.007	1.009	7	16	5.98
19	1	4	1.000	1.000	Inf	2	1	1.62
20	3	14	1.000	0.997	5.125	8	62	9.02
21	1	9	1.000	1.000	1.002	3	4	0.19
22	2	9	1.000	0.999	1.002	7	44	6.01
23	3	22	0.994	1.043	1.255	36	578	6.90
24	3	14	1.084	1.088	1.117	8	21	0.99
25	4	29	0.990	0.989	9.112	13	264	5.37
26	1	9	1.000	1.000	1.002	3	3	0.31
27	3	14	1.002	1.002	1.004	8	36	0.33
28	2	12	1.000	1.000	1.011	8	10	14.3
29	2	9	1.000	1.000	1.001	6	6	0.10
30	5	24	1.001	1.001	1.003	13	92	0.42

Legend:

Ex:	Test case		
$n_x(K)$:	order of the controller	$\underline{\gamma}$:	lower bound certificate on performance
n_K:	dimension of parameter κ	$\overline{\gamma}$:	upper bound certificate on performance
γ:	performance achieved by *inner*	t_s:	time elapsed for synthesis [s]
$\lvert\Delta_a\rvert$:	number of scenarios	t_a:	time elapsed for certification [s]

The results of algorithm 4.1 for 30 test cases are shown in Table 4.1.

Statistics of Table 4.1:

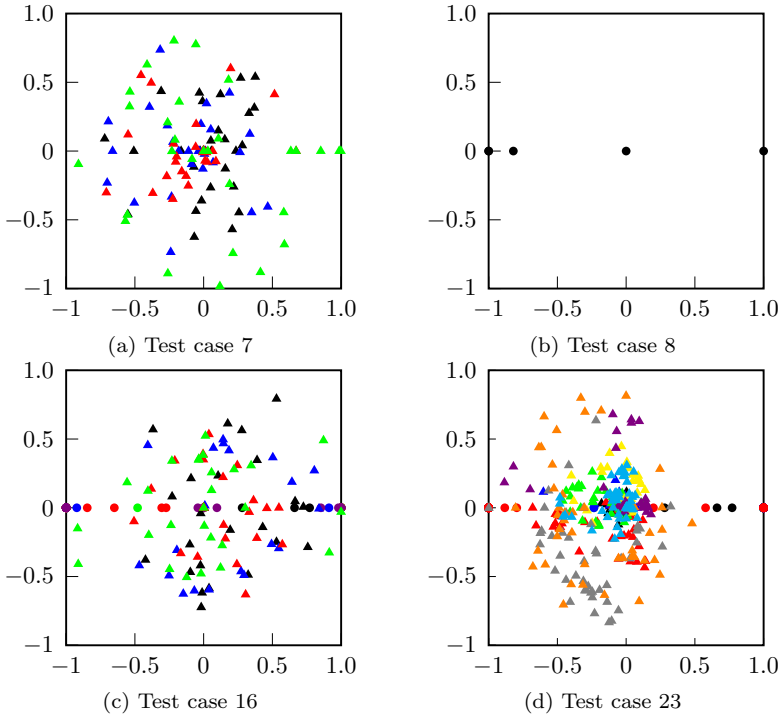

(a) Test case 7 (b) Test case 8

(c) Test case 16 (d) Test case 23

Figure 4.2: Scenarios generated for test cases 7, 8, 16 and 23 on the complex plane, with triangles and circles for complex and real uncertainties, respectively. The instances of an input of an uncertainty block through iterations are plotted in the same color.

- ◇ Within a tolerance of 5%, the lower bound of certification agrees with the γ returned by the method in all cases, except case 4, where the deviation is of 20%.
- ◇ On the other hand, the variation between the γ and the upper bound is less than 5% in 73% of the cases only.
- ◇ In test case 19, the upper bound either fails or attest the system as unstable.
- ◇ In test cases 9,10, 20 and 25 the upper bound is more than the double of γ, and for test cases 4, 16 and 23 the variation is less than 30%.
- ◇ Test cases 3, 5, 7, 16 and 23 demand more than 20 scenarios.
- ◇ The test cases that demand more than 10 and less than 20 scenarios are 1, 12,17,25 and 30.

As illustration of distribution of scenarios, Figure 4.2 shows all scenarios generated for cases 7, 8, 16 and 23 on the complex plane. Note that although more than 20 scenarios are generated for cases 16 and 23, the instances for real parameter assume less than 10 values. This means that they are repeated through iterations while new values are generated only for dynamic uncertainty.

- **Comparison for different controller orders**

The variation of the worst-case H_∞-norm with respect to the order of the controller was analysed for a strcutured state-space controller with order ranging from 1 to 5. The results are shown in Table 4.2.

Statistics of Table 4.2:

- ◇ In 67% of the cases increasing the order of the controller improves the performance of the closed-loop system.
- ◇ In 7 cases the order of K does not affect the performance.
- ◇ In cases 4 and 11 no direct relation between performance and controller order was established.
- ◇ The synthesis was not successfully finished in case 4 for a 1st-order controller and in case 17 for a 2nd-order controller. In cases 16 and 30, for a 1st-order controller, and case 7, for a 2nd-order controller, the algorithm could not find a stabilizing controller with this structure.

- **Comparison to other synthesis methods**

The results for *inner*, *outer* and DKSYN are presented in Table 4.3 for direct comparison.

Table 4.3: Comparison between synthesis using new inner relaxation, new outer relaxation and DKSYN routine.

		inner	*outer*	DKSYN				*inner*	*outer*	DKSYN	
Ex	$n_x(K^1)$	γ	$\underline{\gamma}$	$n_x(K^2)$	μ	Ex	$n_x(K^1)$	γ	$\underline{\gamma}$	$n_x(K^2)$	μ
1	2	0.995	0.995	13	0.993	16	5	1.020	1.948	98	1.212
2	1	0.999	1.000	16	1.01	17	3	0.999	2.078	9	19.034
3	3	1.009	4.807	38	0.895	18	2	1.007	19.636	6	18.775
4	2	0.999	0.999	20	0.983	19	1	1.000	1.000	6	4.466
5	4	0.996	1.614	22	1.21	20	3	0.997	8.057	x	x
6	1	1.000	1.000	7	0.933	21	1	1.000	1.000	20	0.998
7	4	1.002	1.004	46	0.954	22	2	0.999	49510	x	x
8	2	1.000	1.127	9	1.135	23	3	1.043	Inf	294	1.882
9	4	1.008	Inf	445	3.299	24	3	1.088	1.959	34	1.062
10	3	0.982	Inf	10	2.621	25	4	0.989	2692	304	1.803
11	1	1.000	1.546*	253	4.472	26	1	1.000	1.000	24	0.936
12	3	1.000	1.246	27	1.635	27	3	1.002	1.588	25	1.698
13	1	1.000	1.008	99	0.995	28	2	1.000	Inf	7	220.183
14	2	1.006	1.000	120	0.999	29	2	1.000	1.538	18	1.17
15	3	0.996	9.148	30	1.069	30	5	1.001	7.988	30	1.094

Legend:

Ex:	Test case	$n_x(K^1)$:	controller order for *inner* and *outer*
$\underline{\gamma}$:	lower bound certificate of *outer*	γ :	performance achieved by *inner*
μ:	performance achieved by DKSYN	$n_x(K^2)$:	controller order for DKSYN

Statistics of Table 4.3:

◇ *inner* is better than *outer* in 67% of the cases and equivalent in the remaining cases.
◇ *inner* is better than DKSYN in 57% of the cases.
◇ *inner* is outperformed by DKSYN in case 3, but DKSYN needs a controller with order 12 times higher.
◇ *inner* and DKSYN are equivalent in 40% of the cases.
◇ In case 11 the results for *outer* are for a 2-nd order controller, once the synthesis for a one-state controller fails.

Table 4.4: Comparison between new inner relaxation and DKSYN for rescaled Δ

		inner		DKSYN				*inner*		DKSYN	
Ex	$\sigma(\Delta)$	γ	$n_x(K)$	μ	$n_x(K)$	Ex	$\sigma(\Delta)$	γ	$n_x(K)$	μ	$n_x(K)$
1	1.007	0.976	4	0.993	13	16	0.825	1.117	4	1.212	98
2	0.99	0.999	1	1.01	16	17	0.053	0.261	1	19.034	9
3	1.117	0.853	4	0.895	38	18	0.053	0.265	1	18.775	6
4	1.017	1.009	7	0.983	20	19	0.224	1.000	1	4.466	6
5	0.826	1.004	3	1.21	22	20	x	0.997	3	x	x
6	1.072	0.913	2	0.933	7	21	1.002	1.002	8	0.998	20
7	1.048	0.951	7	0.954	46	22	x	0.999	2	x	x
8	0.881	0.926	2	1.135	9	23	0.531	0.677	2	1.882	294
9	0.303	1.504	1	3.299	445	24	0.941	1.044	3	1.062	34
10	0.382	1.426	1	2.621	10	25	0.555	1.202	1	1.803	304
11	0.224	1.000	1	4.472	253	26	1.068	1.052	8	0.936	24
12	0.612	0.466	2	1.635	27	27	0.589	1.092	1	1.698	25
13	1.005	1.002	7	0.995	99	28	0.005	0.012	1	220	7
14	1.001	1.000	8	0.999	120	29	0.854	0.872	2	1.17	18
15	0.936	1.012	2	1.069	30	30	0.914	0.838	5	1.094	30

Legend:

Ex:	Test case	$\sigma(\Delta)$:	new bound on uncertainty Δ
inner :	data for *inner*	DKSYN :	data for DKSYN
$\underline{\gamma}$:	performance by *inner*	μ :	performance by DKSYN
$n_x(K)$:	state-space controller order		

Recall that the results of DKSYN are valid for a rescaled $\boldsymbol{\Delta}$, so robust performance and robust

stability are assured for a different problem. Table 4.4 presents the results of *inner* for the rescaled $\mathbf{\Delta}$, in order to a comparison to DKSYN on the same problem, following the guidelines of Appendix A.1.3. Columns regarding *outer* results are not shown as comparison between *inner* and *outer* were given in Table 4.3. DKSYN results are repeated in Table 4.4 just for the sake of comparison.

Statistics of Table 4.4:

- ◇ For the rescaled $\mathbf{\Delta}$, *inner* can achieve better than DKSYN in case 3 with a 3rd-order controller.
- ◇ The difference between the performance achieved by them differs by 11% in case 26, favoring DKSYN.
- ◇ In cases 4, 13, 14 and 21, *inner* cannot do better than DKSYN with the rescaled $\mathbf{\Delta}$, being equivalent.
- ◇ For the remaining 80% of the cases, *inner* can outperform DKSYN with rescaled $\mathbf{\Delta}$.
- ◇ The order of DKSYN controller is always larger than the order of *outer* controller, exceeding 98 in 7 cases.

- **Alternative to scenario generation**

An alternative to generation of scenarios by nonsmooth techniques presented in Apkarian et al. [2015b] and Apkarian and Noll [2017] was introduced in section 4.1. This alternative suggested the use of WCGAIN for generating dynamic uncertainty scenarios in tandem with the nonsmooth technique for parametric uncertainty scenarios. In Table 4.5 on page 45 the results for syhnthesis with inner relaxation using scenarios generated exclusively by WCGAIN and synthesis using scenarios generated by this mixed approach are presented.

Statistics of Table 4.5:

- ◇ The method $inner_{wcg}$ failed to find a robust stabilizing controller in case 12, whereas in cases 19 and 22 stability is not certified by the upper bound.
- ◇ The method $inner_{mix}$ found a stabilizing solution for all 30 test cases.
- ◇ The difference between lower and upper bounds of the certification was greater than 20% in cases 9, 10, 19, 20, 22, 23 and 25 for $inner_{wcg}$ and in cases 20, 23 and 25 for $inner_{mix}$.
- ◇ The certification bounds of $inner_{wcg}$ met those of *inner* in all but two cases.
- ◇ For test case 22, the method $inner_{wcg}$ has a lower bound of 0.443, but computation of the upper bound reports it as unstable, and for test case 23 the method $inner_{mix}$ method achieves a lower bound of 20% larger.
- ◇ In comparison with $inner_{mix}$, the lower bound of *inner* were certified to be smaller in 4 cases and the upper bound in 3 cases.
- ◇ Whereas in case 19 *inner* was not certified to find a stabilizing controller, method $inner_{mix}$ returned a certified stabilizing controller.
- ◇ The method $inner_{mix}$ needs 10 more scenarios in case 17 and 30 and 12 less scenarios in case 16 in comparison to *inner*.
- ◇ In comparison to *inner* , the method $inner_{wcg}$ needs an equal number of scenarios in 23% of the cases, fewer scenarios in 2 cases, and more in the rest. In 23% of the cases method $inner_{wcg}$ needed more than 10 extra scenarios.

Discussion

An iterative inner relaxation method for the robust control synthesis problem was developed and implemented. The inner relaxation uses limited number of instances of the uncertain plant for the synthesis of one controller in a framework known as multi-model H_∞ synthesis. The instances are iteratively chosen as the worst-case instance of the closed-loop system with the current controller. Both the steps, finding a worst-case instance and the multi-model synthesis for structured controllers, are carried out by nonsmooth optimization.

The method was able to synthesize a controller that met all the specifications for a set of 30 test cases. The comparison with the MATLAB ™ routine DKSYN showed that the novel method can indeed

obtain better performance, with the additional advantage of a structured controller with an order way smaller than the order of the one returned by DKSYN.

Comparison with the outer relaxations methods showed that the certified performance of the inner relaxation is better than the performance of outer relaxations. The discussion about the origins of conservatism of each one of the outer relaxations methods considered was made in chapter 3.

The novel inner relaxation method was also, in general, not optimistic compared to the lower and upper bounds for the H_∞-norm returned by a global certification tool. Compared to the method introduced in chapter 3, it is noticeable that in cases of pure dynamic uncertainty, both performances (achieved H_∞-norm) are similar, whereas for repeated real parametric uncertainties *inner* performs better.

Inner approximations are considered to be an optimistic method and not able to guarantee certificate over the uncertainty set. This is true for stochastic and random methods that sample the space and provide probabilities of violation and confidence intervals of performance. The approach chosen in this thesis is based on worst-case scenario. In this approach, the synthesis objective is stabilization and performance improvement of the worst-case scenario. So, it is reasonable to conclude that if the the controller is able to deliver the desired level of performance and stabilize the worst-case, the requirements for all the other scenarios will be satisfied too. Therefore, for worst-case based inner relaxation method, optimism will occur in so far as that the worst-case estimation fails. This is likely to happen in the method developed for it resorts to a local solver and there is no guarantee that the actual worst-case is returned. This is why posterior certification by a global method in the post-processing step, like the μ analysis of WCGAIN, is needed (see scheme 4.1).

Consider the outer relaxation for robust synthesis based on μ analysis. The μ analysis, considered to deliver true certification, is based on upper and lower bounds of μ. The upper bound is found by a global method, so it provides a true certificate on an upper bound. There is no way to accurately measure the gap between upper bound and the actual value of μ. The computation of lower bound is also done by local solvers and thus provides no certification for the very same reason the worst-case estimator lacks certification. The certification is only possible when the two bounds meet. An outer relaxation based on μ analysis will also lack a certification if based on lower bound of μ. So the claim that outer relaxations provides certification of performance is only valid if the appropriate bound is chosen and it is not a certification of μ, but of an upper bound of μ.

The other inner relaxation by worst-case scenario one finds in the literature [Magni et al., 1998] is based on worst-cases found by μ analysis. However it is based on the lower bound estimation of μ and thus also lacks certificate.

To illustrate what would be to use μ analysis to generate worst-case scenarios for an inner relaxation, this alternative was implemented and tested. For all cases where the bounds meet and μ is considered exact, the results were the same as for *inner*. In only one case it was possible to actually improve the upper bound. No improvement was achieved in the other cases, revealing an overconservative estimation or a mismatch on the region of peak values of lower and upper bounds. Considering only the certified values, the results for synthesis based on worst-case estimation by μ analysis are worse than the one based on nonsmooth optimization. This proves that the local solver of Apkarian et al. [2015a,b] is better suited for finding worst-cases.

Outer relaxations methods as μ analysis have difficulty in handling parametric uncertainties. To verify whether this was the origin of their poorer performance, a test employing μ analysis to generate scenarios for dynamic uncertainty and worst-case estimators for parametric uncertainties was made. The outcome of this combination was worse than the results of each technique applied to the mixed case. This is possibly due to a failure in convergence to a common worst-case mixed uncertainty.

More remarkable is that in the cases where a high number of scenarios is needed, the instances of parametric uncertainties remained on a small set of values while the instances of dynamic uncertainty were distributed on the whole disk. This is a weak point of the developed method, because the more scenarios are needed to achieve robust performance, the more challenging is the multi-model synthesis due to the high number of plants to control simultaneously.

This instigates the study of the use of the outer approximation for dynamic uncertainties while maintaining a inner approximation for the parametric uncertainties. That is the subject of the next chapter.

Appendix of tables

Table 4.2: Comparison of performance obtained by synthesis using inner relaxation for different orders of controller K

$n_x(K)$ Ex	1	2	3	4	5	$n_x(K)$ Ex	1	2	3	4	5
1	1.021	0.995	0.972	0.976	0.991	16	Inf	1224	1.609	1.205	0.996
2	1.000	0.999	0.999	1.000	0.999	17	1.287	x	0.998	0.942	0.942
3	7.799	4.327	1.005	0.800	0.794	18	1.191	0.997	0.994	0.991	0.954
4	x	0.832	1.001	0.907	0.972	19	1.000	1.000	1.000	1.000	1.000
5	135	1.79	2.493	0.996	0.957	20	2.185	1.214	1.000	0.993	0.91
6	1.000	0.86	0.86	0.86	0.859	21	1.000	1.000	1.000	1.000	1.000
7	4.64	Inf	1.144	0.999	0.982	22	1927	1.000	1.004	0.839	0.802
8	2.226	1.000	0.979	0.944	0.938	23	5.223	2.704	0.994	0.721	0.711
9	1.578	1.098	1.024	1.008	1.000	24	1.57	1.068	1.084	0.997	1.097
10	1.492	1.114	0.982	0.971	0.919	25	1.534	1.144	1.030	0.99	0.996
11	1.000	0.724	1.000	0.63	1.000	26	1.000	1.000	1.000	1.000	1.000
12	22.898	3.106	1.000	0.849	0.833	27	2.292	1.084	1.002	0.99	0.974
13	1.000	1.000	1.000	1.000	1.000	28	1.000	1.000	1.001	1.000	1.001
14	1.004	1.000	1.000	1.000	1.000	29	2.188	1.000	0.990	0.911	0.913
15	9.85	1.051	0.998	0.988	0.969	30	Inf	57.017	10.049	2.803	1.001

Legend:

Ex: Test case $n_x(K)$: state-space controller order

Table 4.5: Comparison of performance obtained for inner relaxation with scenarios generated by wcgain and mix of both

		$inner_{wcg}$				$inner_{mix}$			
Ex	$n_x(K)$	$\underline{\gamma}$	$\overline{\gamma}$	t	$\lvert\Delta_a\rvert$	$\underline{\gamma}$	$\overline{\gamma}$	t	$\lvert\Delta_a\rvert$
1	2	0.999	1.001	46	18	-	-	-	-
2	1	1.000	1.002	3	6	-	-	-	-
3	3	1.009	1.011	490	35	-	-	-	-
4	2	0.999	1.001	3	4	-	-	-	-
5	4	1.071	1.075	4508	50	-	-	-	-
6	1	1.000	1.002	6	9	-	-	-	-
7	4	1.004	1.007	769	27	-	-	-	-
8	2	1.000	1.002	3	5	-	-	-	-
9	4	1.001	4.392	67	6	-	-	-	-
10	3	0.982	2.567	28	3	-	-	-	-
11	5	1.000	1.002	2	2	-	-	-	-
12	3	Inf	Inf	10	5	0.964	0.964	24	9
13	1	1.000	1.001	4	3	1.000	1.000	6	3
14	2	1.000	1.002	398	46	1.000	1.000	24	13
15	3	1.000	1.002	37	12	1.020	1.020	19	8
16	5	0.995	1.128	1936	36	1.220	1.220	682	18
17	3	0.995	1.001	520	36	1.298	1.300	249	25
18	2	1.003	1.005	62	15	1.003	1.003	16	9
19	1	1.000	Inf	2	2	1.000	1.000	0	2
20	3	0.999	5.101	58	8	1.052	5.200	58	7
21	1	1.006	1.008	5	6	1.000	1.000	6	6
22	2	0.443	Inf	26	7	1.045	1.047	51	9
23	3	1.007	1.267	1543	51	1.275	1.556	809	34
24	3	1.095	1.109	20	9	1.130	1.130	23	6
25	4	1.036	5.836	316	16	1.094	8.733	273	13
26	1	1.000	1.002	4	3	1.000	1.002	2	3
27	3	0.992	1.024	21	9	1.034	1.034	38	9
28	2	0.999	1.006	95	34	1.000	1.004	10	5
29	2	0.998	1.000	11	8	1.017	1.017	6	6
30	5	1.000	1.002	432	31	1.030	1.032	284	23

Legend:

Ex:	Test case	$n_x(K)$:	state-space controller order
$inner_{wcg}$:	data for WCGAIN generator	$\underline{\gamma}$:	lower bound certificate of performance
$inner_{mix}$:	data for mixed generator	$\overline{\gamma}$:	lower bound certificate of performance
t:	time elapsed for synthesis	$\lvert\Delta_a\rvert$:	number of scenarios

Chapter 5

Development and implementation of a hybrid approximation for the synthesis of robust structured controllers

In this chapter

a hybrid relaxation method for the synthesis of robust structured controllers is derived. It combines the power of inner relaxation for dealing with parametric uncertainties with the simplicity of outer relaxation for dynamic uncertainties. The algorithm is once again implemented with the aid of nonsmooth optimization techniques for simultaneous tuning of scalings and controller for multimodel synthesis. [Aguiar et al., 2018], [Menezes et al., 2016]

Conclusion

The relaxation alleviates the computational burden demanding less scenarios than the pure inner relaxation. In general, the performance of an hybrid relaxation method is comparable to inner, and better than outer.

As discussed in chapter 3, outer relaxations may be overly conservative when applied to systems with parametric uncertainty with a large number of repetitions. The most likely source of conservatism is the associated Φ multiplier that will require a high number of free terms to be tuned. Even though this suggests the use of inner relaxations, it should be kept in mind that the presence of complex uncertainties makes the computation of worst-case scenarios of stability and performance harder than in the case of pure real parametric uncertainty. Computations of worst cases are more onerous, but more severely, the number of active scenarios $\Delta \in \mathbf{\Delta}_a$ needed to cover the set $\mathbf{\Delta}$ may be significantly larger than in the case of pure $\mathbf{\Delta}_p$. This increases the computational burden of the multi-model synthesis that follows.

This rises the question whether the two types of uncertainty could not be handled individually by different methods. In the previous chapter, an approach was tested where scenarios were generated independently for each type of uncertainty. The new approach envisaged fuses the inner relaxation for $\mathbf{\Delta}_p$ and a multiplier approach for $\mathbf{\Delta}_d$. This is what has been termed *hybrid approach* or *hybrid* for short.

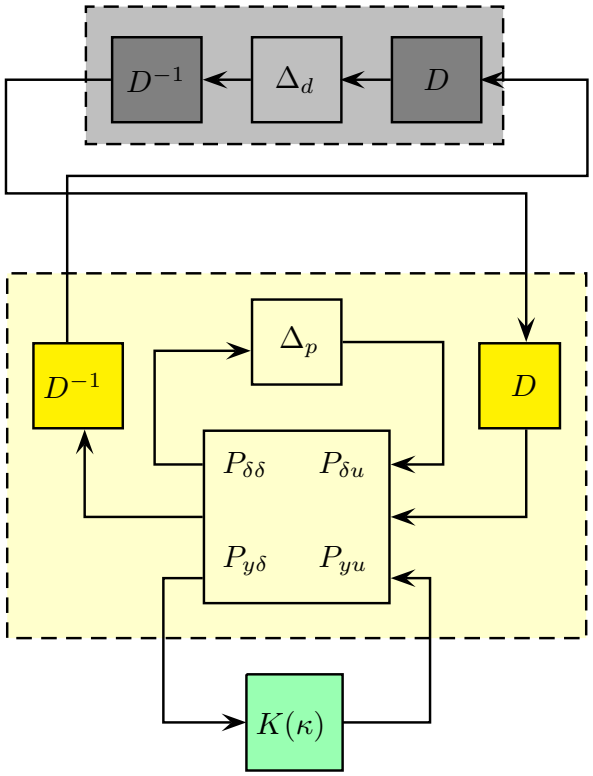

Figure 5.1: Interconnection schema for hybrid relaxation for robust control. The undelerlying layers illustrates the multimodel aspect of the synthesis due to scenarios of parametric uncertainty block.

5.1 Combination of outer and inner relaxation

In order to use the outer approximation derived in chapter 3 only for dynamic uncertainties, the multiplier $\Gamma(\Phi, D)$ from proposition 3.2 should be adapted. The scaling $D \in \mathbf{D}$ remains the same of (3.5) while Φ multiplier is replace by the zero matrix in the Γ multiplier of (3.6) to obtain:

$$\Gamma(0, D) = \begin{bmatrix} 0 & 0 & I & 0 \\ 0 & 0 & 0 & D \\ I & 0 & 0 & 0 \\ 0 & D^{-1} & 0 & 0 \end{bmatrix}. \tag{5.1}$$

Corollary 3.1 of chapter 3 is then adapted to theorem 5.4 below.

Theorem 5.4. *Suppose there exists $D \in \mathbf{D}$ and a structured controller $K(\kappa)$ such that the closed loop system $\Delta_p \star \Gamma(0, D)^{-\star} \star P_\gamma \star K(\kappa)$ is internally stable and satisfies the estimate*

$$\left\| \Delta_p \star \Gamma(0, D)^{-\star} \star P_\gamma \star K(\kappa) \right\|_\infty < 1 \tag{5.2}$$

for all $\Delta_p \in \mathbf{\Delta}_p$. Then the closed-loop system $\Delta \star P \star K(\kappa)$ is robustly stable and has worst-case H_∞ performance γ over $\mathbf{\Delta}$.

Proof. It suffices to note that

$$\Delta_p \star \Gamma(0, D)^{-\star} \star P_\gamma \star K(\kappa) = \begin{bmatrix} D & 0 \\ 0 & I \end{bmatrix} (\Delta_p \star P_\gamma \star K(\kappa)) \begin{bmatrix} D^{-1} & 0 \\ 0 & I \end{bmatrix}. \tag{5.3}$$

It then follows that internal stability of $\Delta_p \star \Gamma(0, D)^{-\star} \star P_\gamma \star K(\kappa)$ in tandem with (5.2) is a complex μ upper bound condition for stability and performance in the sense of Packard and Doyle [1993]. Therefore, for any $\Delta_p \in \mathbf{\Delta}_p$, the system $\Delta_p \star P_\gamma \star K(\kappa)$ is stable and has worst-case H_∞ performance γ for all $\Delta_d \in \mathbf{\Delta}_d$, which concludes the proof. □

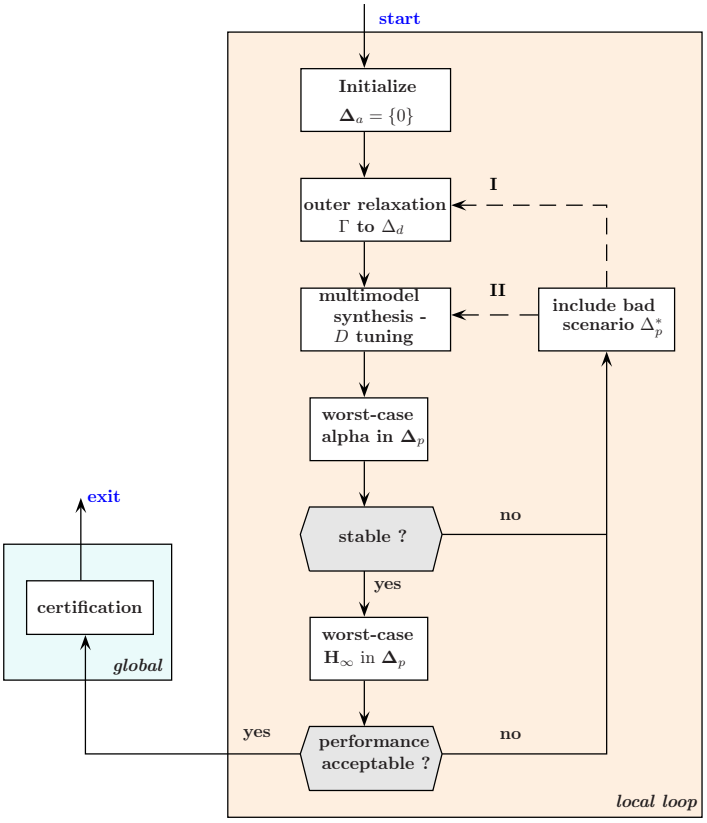

Figure 5.2: Schema of algorithm 5.1 for Robust Control with hybrid relaxation.

Figure 5.1 illustrates the interconnections of system (5.3).

This manages the dynamic uncertainty. Now scenarios should be generated. In chapter 4 scenarios were generated for the closed-loop system $T_{wz}(\Delta(x)) = \Delta \star P \star K(\kappa)$. Now, with the dynamic uncertainty covered by the scaling, the scenarios will be generated for the system: $T_{wz}^D(\Delta_p(x)) = \Delta_p \star \Gamma(0, D)^{-\star} \star P_\gamma \star K(\kappa)$. Programs (4.1) and (4.1) become:

$$\alpha^* = \max_{x \in \boldsymbol{B}'} \alpha(A^D(\Delta_p(x))), \tag{5.4}$$

$$h^* = \max_{x \in \boldsymbol{B}'} \|T_{wz}^D(\Delta_p(x))\|_\infty, \tag{5.5}$$

where x is partitioned according to the structure of Δ_p, $x = (x_1, \ldots, x_{N_p})$ with $x_i = \delta_i$, $i = 1, \ldots, N_p$ and $\boldsymbol{B}'$ is the set of box constrained variables x such that

$$\boldsymbol{B} = \{x : x_i \in [-1, 1],\ i = 1, \ldots, N_p\}, \tag{5.6}$$

and $A^D(\Delta_p)$ is the A matrix of the uncertain closed-loop system $\Delta_p \star \Gamma(0, D)^{-\star} \star P_\gamma \star K(\kappa)$.

The scenarios generated are included in the set $\mathbf{\Delta}_{p,a}$ and a new H_∞ synthesis follows in the form of the optimization program:

$$\begin{array}{ll} \text{minimize} & \gamma \\ \text{subject to} & \|\Delta_p \star \Gamma(0, D)^{-\star} \star P_\gamma \star K(\kappa)\|_\infty \leq 1 - \eta \text{ for all } \Delta_p \in \mathbf{\Delta}_{p,a} \\ & \Gamma(\Phi, D)^{-\star} \star P_\gamma \star K(\kappa) \text{ internally stable} \\ & D \in \mathbf{D}, \kappa \in \mathbb{R}^n, \gamma \in \mathbb{R}_+. \end{array} \tag{5.7}$$

5.2 Control synthesis implementation

The robust control synthesis with hybrid relaxation was recast as program (5.7). The implementation of (5.7) will take elements from the implementation of both outer and inner relaxations. The scheme

of the iterative synthesis with the set of active scenarios $\mathbf{\Delta}_a \subset \mathbf{\Delta}$ in Figure 4.1 for the inner relaxation approach should the be adapted.

The scheme for the hybrid relaxation approach, Figure 5.2, includes the outer relaxation by the Γ multiplier (5.1) for the complex block Δ_d and generation of active scenarios to build set $\mathbf{\Delta}_{p,a} \subset \mathbf{\Delta}_p$. There are two possibities for the application of the outer relaxation: Either a multiplier Γ is used for each plant associated to a $\Delta_p \in \mathbf{\Delta}_{p,a}$, as indicated by arrow I in Figure 5.2, or the same multiplier Γ is used for all the plants associated to set $\mathbf{\Delta}_{p,a}$, as indicated by arrow II. On one hand, the implementation of option I results in less conservativism. On the other hand, this will lead to a polynomial growth of the number of parameters to be tuned for each scenario added.

The synthesis implementation follows the guidelines of Algorithm below:

Algorithm 5.1: Robust synthesis by hybrid approximation

Parameters: $\varepsilon > 0$, $\eta > 0$.

▷ **Step 1** (`Nominal synthesis`).
Initialize set of active real scenarios as $\mathbf{\Delta}_{p,a} = \{0\}$.

▷ **Step 2** (`Multi-model synthesis`).
Given current finite set $\mathbf{\Delta}_{p,a} \subset \mathbf{\Delta}_p$ of active real scenarios, compute structured multi-model H_∞-controller by solving the H_∞-program:

$$\begin{array}{ll} \text{minimize} & \gamma \\ \text{subject to} & \|\Delta_p \star \Gamma(0,D)^{-\star} \star P_\gamma \star K(\kappa)\|_\infty \leq 1-\eta \text{ for all } \Delta_p \in \mathbf{\Delta}_{p,a} \\ & \Gamma(\Phi,D)^{-\star} \star P_\gamma \star K(\kappa) \text{ internally stable} \\ & D \in \mathbf{D}, \kappa \in \mathbb{R}^n, \gamma \in \mathbb{R}_+. \end{array} \tag{5.8}$$

The locally optimal solution $(\gamma_*, D^*, \kappa^*)$ gives rise to the structured multi-scenario H_∞-controller $K(\kappa^*)$.

▷ **Step 3** (`Worst-case stability`).
Try to destabilize the closed-loop system $\Delta_p \star \Gamma(0,D^*)^{-\star} \star P_{\gamma_*} \star K(\kappa^*)$ by computing its worst case spectral abscissa

$$\alpha^* = \max_{\Delta_p \in \mathbf{\Delta}_p} \alpha\left(A(\Delta_p, \kappa^*)\right).$$

The solution is the worst stability scenario Δ_p^*. If $\alpha^* = \alpha\left(A(\Delta_p^*, \kappa^*)\right) \geq 0$, then include Δ_p^* in the set $\mathbf{\Delta}_{p,a}$ and go back to step 2. Otherwise continue with step 4.

▷ **Step 4** (`Worst-case performance`).
Try to degrade performance of the closed-loop system $\Delta_p \star \Gamma(0,D^*)^{-\star} \star P_{\gamma_*} \star K(\kappa^*)$ by computing its worst case H_∞-norm

$$\gamma^* = \max_{\Delta_p \in \mathbf{\Delta}_p} \|\Delta_p \star \Gamma(0,D^*)^{-\star} \star P_{\gamma_*} \star K(\kappa^*)\|_\infty.$$

The solution is the worst performance scenario $\Delta_p^\sharp$.

▷ **Step 5** (`Stopping test`).
If $\alpha(A(\Delta_p^\sharp, \kappa^*)) < 0$ and $\gamma^* < (1+\varepsilon)\gamma_*$, degradation of performance is marginal. Then exit loop and goto step 6 for posterior certification. Otherwise include $\Delta_p^\sharp$ in the set $\mathbf{\Delta}_{p,a}$ and continue loop with step 2.

▷ **Step 6** (`Certification`).
Use μ-analysis tools from MathWorks [2017] to certify *a posteriori* that $K(\kappa^*)$ is robustly stable over $\mathbf{\Delta}$ and has robust H_∞ performance γ_* over $\mathbf{\Delta}$.

The multi-model synthesis in step 2 of algorithm 5.1 on the other hand is executed conformably to program (3.13). The constraints on γ, κ, D and internal stability are exactly the same and reproduced next for convenience of the reader. The only change is on the small gain constraint of the H_∞-norm of the closed loop system, that now are multi-disk constraints, as there will be as many systems as there are active scenarios.

- $\kappa \in \mathbb{R}^n$ **:** The constraint on κ is that κ should belong to vector space on real numbers. This vector is used to build the controller with a pre-determined structure. Once the structure defined, one should also define how the controller is parameterized with respect to κ.
- γ **:** This parameter may assume any positive real value. It emulates the performance that will be minimized. Note that γ is used to scale plant P into P_γ.
- $D \in \mathbf{D}$ **:** This constraint specifies that the structure of D should be block diagonal as in (3.5). Each block corresponds to a diagonal matrix whose entries are equal biproper SISO stable minimum-phase systems.
- Internal stability **:** Internal stability is enforced by not allowing closed-loop poles on the right-half plane.
- $\|\Delta_p \star \Gamma(0, D)^{-\star} \star P_\gamma \star K(\kappa)\|_\infty \leq 1 - \eta$ for all $\Delta_p \in \mathbf{\Delta}_{p,a}$ **:** This constraint assures robust stability over $\mathbf{\Delta}_d$ for each plant associated to one active scenario $\Delta_p \in \mathbf{\Delta}_{p,a}$.

In the present approach the scalings $D \in \boldsymbol{D}$ are chosen independently of $\Delta_p \in \mathbf{\Delta}_{p,a}$. Choosing an individual $D_p = D(\Delta_p)$ for each performance constraint indexed by $\Delta_p \in \mathbf{\Delta}_{p,a}$ would reduce conservatism, but at the same time increase the number of variables in the synthesis program of step 2.

5.3 Numerical Results

The efficiency of the novel hybrid relaxation with nonsmooth solvers method for robust controllers design is supported by the numerical results for the validation test introduced in Appendix A.1 for a set of test cases (see Appendix B). The approach with a unique multiplier Γ for all scenarios was selected. The term *hybrid* is used when referring to the implementation of the hybrid relaxation method developed in this chapter and the term *performance* is employed in the same sense as in previous chapter and refers to worst-case H_∞-norm of the closed-loop system. For the sake of readability, some tables were moved to the Appendix of tables at the end of the chapter.

- **Synthesis for the test set**

Table 5.1 shows data of the implementation of the synthesis based on hybrid approximation developed in this section. In all cases, the order of the tridiagonal state-space realizations of D is 2. The constraint $\|\Delta_p \star \Gamma(0, D)^{-\star} \star P_\gamma \star K(\kappa)\|_\infty \leq 1 - \eta$ for all $\Delta_p \in \mathbf{\Delta}_{p,a}$.

Statistics of Table 5.1:

- ◇ Within a tolerance of 5%, the lower bound of certification agrees with the γ returned by the method in all cases.
- ◇ The variation between γ and the upper bound, on the other hand, is less than 5% in 83% of the cases.
- ◇ In test case 19, the upper bound either fails or attest the system as unstable. In test cases 9,10, 20 and 25 the upper bound is more than the double of γ.
- ◇ The test case 16 is the only one that requires more than 10 scenarios.

As opposed to inner relaxation, none of the cases demands more than 20 scenarios. This reinforce the hypothesis that the extra number of scenarios demanded by *inner* is, as speculated, due to the dynamic uncertainty. Figure 5.3 shows the scenarios generated for test cases 7, 8, 16 and 23. The scenarios are only generated for parametric uncertainties. In case 8, where the uncertainty is pure parametric, the problem is exactly the same for both *inner* and *hybrid* . Case 7 is a pure dynamic uncertainty case, and as such, no scenario is generated in the hybrid approach, while for inner the disk

Table 5.1: Data from the controller synthesis using hybrid relaxation for the test set.

Ex	$n_x(K)$	n_K	γ	$\underline{\gamma}$	$\overline{\gamma}$	$\lvert\Delta_a\rvert$	t_s	t_a
1	2	12	1.006	1.001	1.003	1	5	0.15
2	1	4	1.001	1.000	1.002	1	8	0.09
3	3	22	1.223	1.209	1.212	1	35	0.22
4	2	16	1.005	0.999	1.001	1	10	0.13
5	4	30	2.876	2.426	2.436	1	20	0.34
6	1	4	1.009	1.003	1.005	1	6	0.33
7	4	48	1.033	1.03	1.032	1	35	0.9
8	2	9	1.001	1.000	1.002	4	9	0.13
9	4	29	1.021	1.02	4.461	5	74	5.47
10	3	14	0.981	0.982	3.011	3	23	13.5
11	1	4	1.000	1.000	1.002	3	9	2.35
12	3	14	1.05 0	1.049	1.051	4	22	0.17
13	1	4	1.003	1.000	1.001	3	21	1.09
14	2	12	1.001	1.000	1.002	6	33	24.6
15	3	14	1.007	1.006	1.008	4	36	0.51
16	5	37	1.047	1.043	1.144	19	2165	7.61
17	3	23	1.239	1.2	1.203	4	42	1.94
18	2	9	1.158	1.155	1.158	8	106	3.88
19	1	4	1.000	1.000	Inf	3	10	2.51
20	3	14	1.088	1.083	4.572	5	73	3.99
21	1	9	1.006	1.000	1.002	3	14	0.27
22	2	9	1.396	1.415	1.42	4	105	6.68
23	3	22	3.444	3.27	3.208	3	62	1.93
24	3	14	1.188	1.186	1.189	4	34	0.26
25	4	29	1.058	1.058	5.877	5	92	7.18
26	1	9	1.008	1.000	1.002	3	22	1.05
27	3	14	1.012	1.008	1.012	6	68	0.42
28	2	12	1.001	0.999	1.006	7	38	2.53
29	2	9	0.996	0.995	0.997	4	33	0.08
30	5	24	1.144	1.119	1.122	4	85	0.26

Legend:

Ex:	Test case	γ :	performance achieved by *hybrid*
$n_x(K)$:	order of the controller	$\underline{\gamma}$:	lower bound certificate on performance
n_K:	dimension of parameter vector κ	$\overline{\gamma}$:	upper bound certificate on performance
t_s:	time elapsed for synthesis [s]	$\lvert\Delta_a\rvert$:	number of scenarios
t_a:	time elapsed for certification [s]		

is well sampled. For the mixed structure uncertainty cases 16 and 23 there is one remark that should be made besides the obvious fact the *inner* needs many more scenarios. The scenarios for parametric uncertainties take more values on *inner* synthesis.

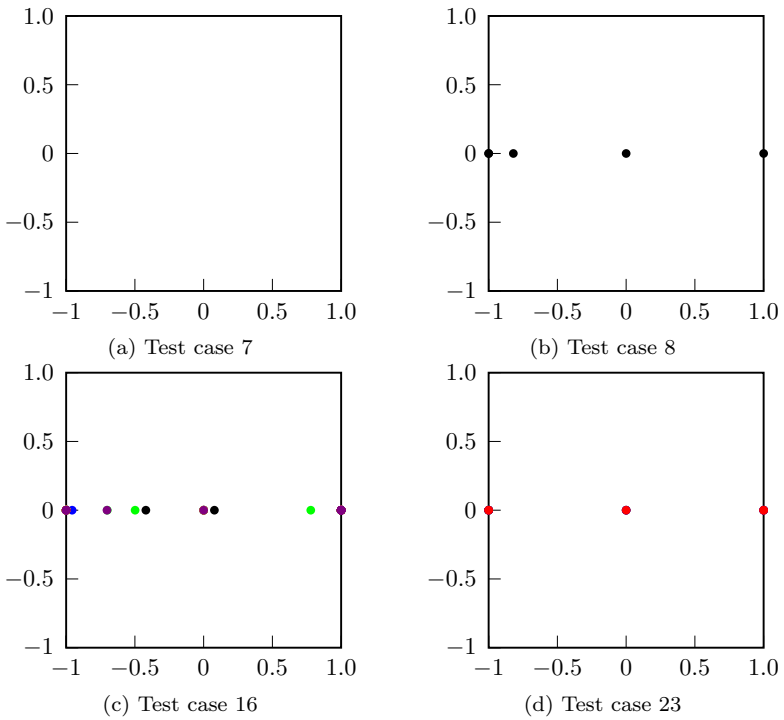

(a) Test case 7 (b) Test case 8

(c) Test case 16 (d) Test case 23

Figure 5.3: Scenarios generated for test cases 7, 8, 16 and 23 on the complex plane, with triangles and circles for complex and real uncertainties, respectively.

- **Comparison for different controller orders**

The variation of the worst-case H_∞-norm with respect to the order of the controller was analysed for a strcutured state-space controller with order ranging from 1 to 5. The results are shown in Table 5.2 on page 55.

Statistics of Table 5.2:

◇ In 63% of the cases increasing the order of the controller improves the H_∞-norm of the closed-loop system.
◇ In 30% of the cases increasing the order of K does not affect the H_∞-norm .
◇ The results for test cases 1 and 20 are inconclusive, probably due to numerical problems.

- **Comparison for different scaling orders**

Table 5.3 on page 56, presents the results for the synthesis for a variation of the order of the scaling from 0 to 3.

Statistics of Table 5.3:

◇ In 23% of the cases the order of D does not affect the performance.
◇ In 36% of the cases, the performance is improved only by increasing the order of D from 0 to 1, and further increasing has no effect.
◇ For the 8 remaining cases, increasing the order of D generally improves the performance, except in cases 3, 5, 22 and 23, where a 2nd-order achieves better than a 3rd-order performs.
◇ Cases 8 to 11 only contain parametric uncertainties, so no D-scaling is necessary.

Table 5.4: Comparison between synthesis using new hybrid, inner and outer relaxations and DKSYN routine

		hybrid		*inner*		*outer*	DKSYN	
Ex	$n_x(K^1)$	γ_i	$\lvert\Delta_{ai}\rvert$	γ_h	$\lvert\Delta_{ah}\rvert$	$\underline{\gamma}$	$n_x(K^2)$	μ
1	2	1.001	1	0.995	11	0.995	13	0.993
2	1	1.000	1	0.999	7	1.000	16	1.010
3	3	1.209	1	1.009	25	4.807	38	0.895
4	2	0.999	1	0.999	3	0.999	20	0.983
5	4	2.426	1	0.996	25	1.614	22	1.210
6	1	1.003	1	1.000	4	1.000	7	0.933
7	4	1.030	1	1.002	29	1.004	46	0.954
8	2	1.000	4	1.000	4	1.127	9	1.135
9	4	1.020	5	1.008	5	Inf	445	3.299
10	3	0.982	3	0.982	3	Inf	10	2.621
11	1	1.000	3	1.000	2	1.546*	253	4.472
12	3	1.049	4	1.000	11	1.246	27	1.635
13	1	1.000	3	1.000	3	1.008	99	0.995
14	2	1.000	6	1.006	4	1.000	120	0.999
15	3	1.006	4	0.996	8	9.148	30	1.069
16	5	1.043	19	1.020	31	1.948	98	1.212
17	3	1.200	4	0.999	18	2.078	9	19.034
18	2	1.155	8	1.007	7	19.636	6	18.775
19	1	1.000	3	1.000	2	1.000	6	4.466
20	3	1.083	5	0.997	8	8.057	x	x
21	1	1.000	3	1.000	3	1.000	20	0.998
22	2	1.415	4	0.999	7	49510	x	x
23	3	3.270	3	1.043	36	Inf	294	1.882
24	3	1.186	4	1.088	8	1.959	34	1.062
25	4	1.058	5	0.989	13	2692	304	1.803
26	1	1.000	3	1.000	3	1.000	24	0.936
27	3	1.008	6	1.002	8	1.588	25	1.698
28	2	0.999	7	1.000	8	162984	7	220.000
29	2	0.995	4	1.000	6	1.538	18	1.170
30	5	1.119	4	1.001	13	7.988	30	1.094

Legend:

Ex:	Test case	$n_x(K^1)$:	controller order for *hybrid* , *inner* and *outer*
γ_h :	performance achieved by *hybrid*	γ_i :	performance achieved by *inner*
$\lvert\Delta_{ah}\rvert$:	number of scenarios for *hybrid*	$\lvert\Delta_{ai}\rvert$:	number of scenarios for *inner*
$\underline{\gamma}$:	lower bound certificate of *outer*	μ:	performance achieved by DKSYN
$n_x(K^2)$:	controller order for DKSYN		

- **Comparison to other synthesis methods**

As in the previous chapters, the approach developed in this section is compared to previous approaches, *outer* and *inner* and DKSYN. The results are displayed in Table 5.4.

Statistics of Table 5.4:

- ◇ *hybrid* is equivalent to *inner* in 76% of the cases and it is outperformed by *inner* in the remaining cases.
- ◇ *hybrid* is better than *outer* in 63% of the cases, it is outperformed in 1 case, and it is equivalent in the remaining cases.
- ◇ *hybrid* is better than DKSYN in 50% of the cases, is outperformned by DKSYN in 4 cases, and they are equivalent in 37% of the cases.

As already mentioned in previous chapters, DKSYN results are valid on a rescaled $\boldsymbol{\Delta}$.Table 5.5 presents the results of *hybrid* for this rescaled $\boldsymbol{\Delta}$, following the procedure of Appendix A.1.3. Columns regarding *outer* and *inner* are omitted as they were already compared in Table 5.4, whereas DKSYN results are repeated for the sake of comparison.

Statistics of Table 5.5:

- ◇ For the rescaled $\boldsymbol{\Delta}$ *hybrid* cannot achieve better performance than dksyn in cases 3 and 26 up to a 15th-order controller.
- ◇ In cases 4, 7, 13, 14 and 21, *hybrid* cannot do better than DKSYN with the rescaled $\boldsymbol{\Delta}$, being equivalent.
- ◇ For the remaining 77% of the cases, *hybrid* can outperform DKSYN with the rescaled $\boldsymbol{\Delta}$.

Table 5.5: Comparison between synthesis using hybrid relaxation and DKSYN routine for the rescaled $\boldsymbol{\Delta}$

		hybrid		DKSYN				*hybrid*		DKSYN	
Ex	$\sigma(\Delta)$	$\underline{\gamma}$	$n_x(K)$	μ	$n_x(K)$	Ex	$\sigma(\Delta)$	$\underline{\gamma}$	$n_x(K)$	μ	$n_x(K)$
1	1.007	0.989	8	0.993	13	16	0.825	1.132	4	1.212	98
2	0.99	1.000	1	1.01	16	17	0.053	0.261	1	19.034	9
3	1.117	1.070	9	0.895	38	18	0.053	0.264	1	18.775	6
4	1.017	1.009	14	0.983	20	19	0.224	1.000	1	4.466	6
5	0.826	1.055	3	1.21	22	20	x	1.083	3	x	x
6	1.072	0.923	2	0.933	7	21	1.002	1.001	10	0.998	20
7	1.048	0.974	15	0.954	46	22	x	1.415	2	x	x
8	0.881	0.926	2	1.135	9	23	0.531	0.981	1	1.882	294
9	0.303	1.507	1	3.299	445	24	0.941	1.017	2	1.062	34
10	0.382	1.426	1	2.621	10	25	0.555	1.206	1	1.803	304
11	0.224	1.000	1	4.472	253	26	1.068	1.052	15	0.936	24
12	0.612	0.474	2	1.635	27	27	0.589	1.091	1	1.698	25
13	1.005	1.002	15	0.995	99	28	0.005	0.012	1	220	7
14	1.001	1.000	10	0.999	120	29	0.854	0.871	2	1.17	18
15	0.936	1.015	2	1.069	30	30	0.914	0.905	5	1.094	30

Legend:

Ex:	Test case	$\sigma(\Delta)$:	new bound on uncertainty Δ
hybrid :	data for *hybrid*	DKSYN :	data for DKSYN
$\underline{\gamma}$:	lower bound certificate of *hybrid*	μ :	performance achieved by DKSYN
$n_x(K)$:	state-space controller order		

Discussion

The hybrid approach developed in this chapter was shown to be efficient in designing robust controllers for systems subjected to structured mixed uncertainty. As expected, for cases with sole dynamic uncertainties, it is equivalent to the outer relaxation introduced in chapter 3 and has a good performance, similar to other outer relaxations. In cases of pure parametric uncertainties it is equivalent to inner relaxation introduced and discussed previously. It is in cases of mixed uncertainties that the novelty is expressed.

An optimistic estimation occurs when the value of the H_∞-norm computed by the method is inferior to certification bounds, indicating a failure to compute the worst-case scenario. In general, the method was not optimistic, with performance meeting the lower bound of the certification method. For cases where the upper bound was not met, the discussion is left open. This may indicate an optimistic estimation from both *hybrid* and the lower bound of certification tool, due to a local minimum that is far from global, or an overly conservative estimation of the upper bound. It should be noticed that in such cases, the uncertainty has a large number of parametric uncertainties and/or parametric uncertainties with high repetition where the certification tool WCGAIN is reported to be prone to failure in such cases.

The hybrid relaxation is very close to inner counterpart regarding performance. The method succeds in cases of mixed uncertainties where the methods based on outer relaxations failed. This is credit to the inner relaxation for the parametric uncertainties. However, one can notice that in such cases a full inner relaxation reaches better performance. Supported by these results, it is concluded that concerning only performance, the full inner relaxation method presented in chapter 4 is the best technique.

Concerning the number of scenarios generated, as expected, the hybrid approach needs fewer scenarios than the inner. This endorses the conjecture that a high number of scenarios is necessary to cover the behavior of dynamic uncertainty. The comparison of the distribution of parametric uncertainty scenarios for inner and hybrid approaches showed that the need for more dynamic uncertainty scenarios increases also the number of values assumed for parametric uncertainty. This is explained by the fact that for each new dynamic uncertainty scenario a different parametric uncertainty value may be associated. This happens because if we fix one uncertainty block while the others vary in the search for the worst-case scenario, the values obtained for the remaining blocks may differ considerably from the values obtained for a different value of the fixed block.

Altogether, the conclusion is that for the cases considered, the number of scenarios do not results on degradation of performance due to the elevated number of models on multi-model synthesis.

Nonetheless, the hybrid approach remains an alternative for limited computational power. Moreover, the results support the hypothesis that the simple alleviation of outer relaxation for parametric uncertainty is enough to improve performance and that indeed the major source of conservatism of outer methods comes from repetitions in parametric uncertainties.

The hybrid approach in the inverse sense, outer relaxation for parametric uncertainties and inner relaxation for dynamic uncertainties was also considered. The results were discouraging. The simple explanation is that the resulting synthesis have to deal at the same time with the high number of scenarios, product of complex uncertainties, and a high number of parameters to be tuned, due to outer relaxation of parametric uncertainties.

The analysis of impact of scaling order on performance shows that it is equal to the outer relaxation case: a dynamic scaling for dynamic uncertainty is proven important, regardless of order.

The last topic is related to similar approaches to hybrid relaxation. The approaches in Nyström et al. [1999] and Karimi et al. [2016] are similar to program 5.7. They all are synthesis based on multi-models subjected to dynamic uncertainties. However these two methods are applied to the problem of a discrete set of multimodels and not to an uncertain system subjected to structured mixed uncertainty. In the latter case, there is an infinity of models, each associated to an instance of the parametric uncertainty. It is the judicious choice of scenarios that leads to a finite set of multimodels, as explained in Algorithm 5.1.

Appendix of tables

Table 5.2: Comparison of H_∞-norm obtained by synthesis using hybrid relaxation for different orders of controller K

$n_x(K)$ Ex	1	2	3	4	5	$n_x(K)$ Ex	1	2	3	4	5
1	1.028	1.006	1.008	0.989	1.006	16	4973	126	1.606	1.268	1.047
2	1.001	1.001	1.000	1.000	1.000	17	1.373	1.169	1.239	1.240	1.205
3	12.289	9.368	1.223	11.370	7.764	18	1.200	1.158	1.054	1.046	1.023
4	1.005	1.005	1.005	1.005	1.005	19	1.000	1.000	1.000	1.000	1.000
5	14.03	11.99	2.804	2.876	1.252	20	2.298	1.833	1.088	1.745	1.079
6	1.009	0.872	0.867	0.867	0.867	21	1.006	1.006	1.005	1.005	1.005
7	4.660	2.255	1.154	1.033	1.014	22	226	1.396	2.951	2.431	1.126
8	2.227	1.001	0.980	0.935	0.935	23	5.217	4.630	3.309	3.128	0.911
9	1.579	1.128	1.021	1.021	0.995	24	1.922	1.128	1.188	1.128	1.101
10	1.492	1.112	0.981	0.973	0.938	25	1.539	1.155	1.067	1.058	1.053
11	1.000	1.000	1.000	1.000	1.000	26	1.008	1.008	1.008	1.008	1.008
12	23.792	3.267	1.050	0.904	0.892	27	2.366	1.093	1.012	1.011	0.981
13	1.003	1.000	1.003	1.003	1.001	28	1.000	1.001	1.001	1.000	1.005
14	1.000	1.001	1.000	1.000	1.000	29	2.186	0.996	0.980	0.913	0.914
15	10.112	1.050	1.007	0.999	0.992	30	147	59.64	10.697	3.44	1.144

Legend:

Ex: Test case $n_x(K)$: state-space controller order

Table 5.3: Comparison of H_∞-norm obtained by synthesis using hybrid relaxation for different orders of scaling D

$n_x(D)$ Ex	0	1	2	3	$n_x(D)$ Ex	0	1	2	3
1	1.028	1.007	1.006	1.005	16	7.013	1.035	1.047	1.019
2	5.415	1.004	1.001	1.001	17	3.674	1.214	1.239	1.041
3	12.468	7.156	1.223	8.702	18	1.136	1.073	1.158	1.066
4	1.005	1.005	1.005	1.005	19	1.000	1.000	1.000	1.000
5	3.308	1.383	2.876	4.198	20	2.024	1.745	1.088	1.056
6	3.743	1.009	1.009	1.009	21	1.006	1.006	1.006	1.005
7	3.848	1.068	1.033	1.014	22	1.473	1.226	1.396	4.808
8	-	-	-	-	23	19.561	5.515	3.309	5.59
9	-	-	-	-	24	3.329	1.101	1.188	1.102
10	-	-	-	-	25	1.233	1.228	1.058	1.051
11	-	-	-	-	26	1.008	1.008	1.008	1.008
12	1.662	1.054	1.05	1.051	27	2.614	1.016	1.012	1.011
13	1.003	1.003	1.003	1.003	28	1.000	1.001	1.001	1.001
14	1.000	1.000	1.001	1.000	29	1.079	0.995	0.996	0.996
15	17.398	1.029	1.007	0.999	30	1.568	1.091	1.144	1.101

Legend:

Ex: Test case $n_x(D)$: order of scaling D

Chapter 6

Development of FRD design of structured controllers based on spectral abscissa minimization

In this chapter

a frequency response data design of structured controllers based on minimization of spectral abscissa is developed and implemented. A technique for estimating spectral abscissa is first derived. Then, the synthesis is implemented using direct search routines.

Conclusion

The technique can effectively design controllers that lead to closed-loop systems with negative spectral abscissa for the class of systems considered. Tests with finite-dimensional systems show that the method loses efficiency when unstable poles accumulates on the axis defined spectral abscissa paralel to $j\mathbb{R}$.

The two major challenges of infinite-dimensional systems control are the intrisic complexity of the systems, that not seldom leads to creation of control techniques specialized on very specific systems, and the nature of the controller to be designed. The implementation of infinite-dimensional controllers is currently limited to certain types, such as controllers with delays. Implementation of general infinite-dimensional controllers demands approximation and this often results in performance degradation. The direct design of finite-dimensional controllers allows to take this degradation into account in the design. Furthermore, not all infinite-dimensional systems can be stabilized by a proper rational controller. The main results concerning the class of systems that can effectively be stabilized by proper rational controllers were recalled in section 2.1.1.

Approaches like the one of Balas [1983] design rational controllers for approximations of infinite-dimensional plants. Another approach [Balas, 1986] relies on rational approximations of an infinite-dimensional controller designed for infinite-dimensional plants. In chapters 3, 4 and 5 the robust control problem of finite-dimensional systems was addressed. As discussed in chapter 1 (Introduction), the control of infinite-dimensional systems can also be addressed in this framework by approximating these systems by finite-dimensional models and modeling uncertainty as the mismatch between infinite and finite-dimensional models [Curtain and Glover, 1986].

In this chapter and the following two, techniques for designing rational structured controllers for infinite dimensional systems are proposed. These techniques are based on the frequency response data of the systems and avoid approximations altogether, for plant and controller. While many techniques based on frequency or time domain response data of systems are already in use successfuly, they

are restricted to stable or pre-stabilized systems. The techniques in the following were developed specifically to overcome this limitation.

6.1 Spectral abscissa estimation

6.1.1 Motivation

The systems that can be stabilized by proper rational controllers are the ones described by functions belonging to the Callier-Desoer class $\hat{\mathcal{B}}(0)$. As recalled in section 2.1.1, such functions are meromorphic and bounded in $\mathbb{C}^+$, have only finitely many poles of finite order in $\overline{\mathbb{C}^+}$ and can be decomposed into a sum of two functions, one belonging to $\hat{\mathcal{A}}_-(0)$, thus infinite-dimensional and stable, and other belonging to space of strictly proper rational functions holomorphic on $\mathbb{C}^-$.

What we aim for is to obtain a structured controller $K(\kappa, s) \in \mathcal{K}$ that in feedback with the system $G(s)$ results in a stable system. This means that the feedback system $T(\kappa, s)$, from (2.9), should belong to $\hat{\mathcal{A}}_-(0)$, like stated in section 2.1.2. Alternatively, the objective can be set as to obtain a structured controller $K(\kappa, s) \in \mathcal{K}$ such that the Nyquist stability test of section 2.4.1 is positive for f defined in (2.45). For the class of systems under consideration, stability can be assured by the negative spectral abscissa of the feedback system, $\alpha(T(\kappa, s)) < 0$.

If such a controller exists, it should be found by a search in the space $\mathcal{K}$. The search ends successfully as soon as a controller $K(\kappa^*, s)$ with $\alpha(T(\kappa^*, s)) < 0$ is found. For the infinite-dimensional cases, a $\alpha(T(\kappa^*, s)) < 0$ is certified by the Nyquist stability test of section 2.4.1. As the spectral abscissa is the criterion to be used, we propose to use it also in a search as the function to be minimized. To proceed with this option, we propose in the following a method to compute the positive spectral abscissas for infinite-dimensional systems in $\hat{\mathcal{B}}_-(0)$.

6.1.2 The shifted Nyquist

In the computation of the spectral abscissa, the controller is fixed, so its dependence on vector κ will be omitted for convenience, as will the dependence on the Laplace variable s, whenever there is no ambiguity.

We begin by recalling that if $G(s), K(s) \in \hat{\mathcal{B}}(0)$, then also $T(s) \in \hat{\mathcal{B}}(0)$. This means $T(s)$ is meromorphic in $\mathbb{C}^+$. Since it has finitely many poles in this half plane, we can take a sufficiently large real constant $\mathfrak{a} > 0$ such that $T(s)$ is now holomorphic in $\mathbb{C}_\mathfrak{a}^+$ and bounded in $\overline{\mathbb{C}_\mathfrak{a}^+}$. If we define $T_\mathfrak{a}(s)$ as

$$T_\mathfrak{a}(s) = T(s + \mathfrak{a}), \tag{6.1}$$

then $T_\mathfrak{a}$ is holomorphic in $\mathbb{C}^+$ and bounded in $\overline{\mathbb{C}^+}$, hence stable. Analogous to the descriptions of $F(s)$ and $T(s)$ in terms of $G(s)$ and $K(s)$ from (2.8) and (2.9), we have:

$$F_\mathfrak{a}(s) = \begin{bmatrix} I & K_\mathfrak{a}(s) \\ -G_\mathfrak{a}(s) & I \end{bmatrix}, \tag{6.2}$$

$$T_\mathfrak{a}(s) = F_\mathfrak{a}^{-1}(s) = \begin{bmatrix} I - K_\mathfrak{a}(I + G_\mathfrak{a} K_\mathfrak{a})^{-1} G_\mathfrak{a} & -K_\mathfrak{a}(I + G_\mathfrak{a} K_\mathfrak{a})^{-1} \\ (I + G_\mathfrak{a} K_\mathfrak{a})^{-1} G_\mathfrak{a} & (I + G_\mathfrak{a} K_\mathfrak{a})^{-1} \end{bmatrix}, \tag{6.3}$$

and

$$f_\mathfrak{a}(s) = \det(F_\mathfrak{a}(s)), \tag{6.4}$$

where $G_\mathfrak{a}(s) = G(s + \mathfrak{a})$ and $K_\mathfrak{a}(s) = K(s + \mathfrak{a})$.

The Nyquist stability test of section 2.4.1 can now be applied to the curve $f_\mathfrak{a}(s)$. What should be noted is that now the number of open-loop poles enclosed by the Nyquist contour may have changed. The poles of $G(s)$ and $K(s)$ contained in the region $\overline{\mathbb{C}^+} \cap \overline{\mathbb{C}_\mathfrak{a}^-}$ are now poles of $G_\mathfrak{a}(s)$ and $K_\mathfrak{a}(s)$ in $\overline{\mathbb{C}^-}$. Therefore only the poles of $G(s)$ and $K(s)$ contained in $\overline{\mathbb{C}_\mathfrak{a}^+}$ correspond to unstable poles of $G_\mathfrak{a}(s)$ and $K_\mathfrak{a}(s)$ in $\overline{\mathbb{C}^+}$. Let pu_G be the set of poles of $G(s)$ in $\overline{\mathbb{C}^+}$. The set of poles $pu_{G_\mathfrak{a}}$ in $\overline{\mathbb{C}_0^+}$ is defined as:

$$pu_{G_\mathfrak{a}} = \{v \in pu_G / Re(v) \geq \mathfrak{a}\}, \tag{6.5}$$

and $pu_{K_\mathfrak{a}}$, the set of poles of K in $\overline{\mathbb{C}^+}$ being defined analogously. Therefore, the number of open-loop unstable poles to be used within the Nyquist stability test for $f_\mathfrak{a}$ is $|pu_{G_\mathfrak{a}}| + |pu_{K_\mathfrak{a}}|$.

It is not necessary to obtain any of these shifted systems explicitly. Since the Nyquist stability test is discretized on a finite grid of frequencies $\omega \in \Omega$, all we need to do is to obtain the frequency response of systems $G(s)$ and $K(s)$ for $s = \mathfrak{a} + j\omega$. The polygon $f_{\omega_\mathfrak{a}} = det(I + G(\mathfrak{a} + j\omega)K(\mathfrak{a} + j\omega))$ is the polygonal approximation of the curve $f(s + \mathfrak{a}) = det(I + G(s + \mathfrak{a})K(s + \mathfrak{a}))$.

6.1.3 Spectral abscissa estimation algorithm

What we search now is the minimum real constant $\mathfrak{a} > 0$ for which the Nyquist stability test of $T_\mathfrak{a}(s)$ is positive. The exact value $\mathfrak{a}$ corresponds to the real part of the rightmost pole of $T(s)$. The simplest way of computing such $\mathfrak{a}$ is to employ a bisection method with the stability as criterion to take the upper or lower current bound, starting from sufficiently large $\overline{\mathfrak{a}} > 0$ and $\underline{\mathfrak{a}} = 0$.

The procedure is implemented through Algorithm 6.1 below, where $\kappa^\sharp$ is fixed and $K(\kappa^\sharp, s)$ is assumed to be stable. The extension to unstable $K(s)$ is straightfoward.

Algorithm 6.1: Estimation of positive spectral abcissa $\alpha(S)$ of a closed-loop system S

Parameters: $\epsilon > 0$.

▷ **Step 1** (`Initialization`).
Apply Nyquist stability test of 2.4.1 to $T(\kappa^\sharp, s)$.
If stable, quit. Else set $\overline{\mathfrak{a}} = 1$, $\underline{\mathfrak{a}} = 0$ and go to Step 2.

▷ **Step 2** (`Finding stabilizing shift`).
Apply Nyquist stability test of 2.4.1 to $\overline{\mathfrak{a}}$-shifted system $T(\kappa^\sharp, s + \overline{\mathfrak{a}})$.
If stable, go to Step 3. Else set $\underline{\mathfrak{a}} = \overline{\mathfrak{a}}$, $\overline{\mathfrak{a}} = 2\overline{\mathfrak{a}}$ and repeat Step 2.

▷ **Step 3** (`Refining estimate`).
$\mathfrak{a} = 0.5 \cdot (\mathfrak{a} + \underline{\mathfrak{a}})$.
Apply Nyquist stability test of 2.4.1 to $\overline{\mathfrak{a}}$-shifted system $T(\kappa^\sharp, s + \mathfrak{a})$.
If stable, $\overline{\mathfrak{a}} = \mathfrak{a}$. Else $\underline{\mathfrak{a}} = \mathfrak{a}$.
Repeat Step 3 until $\overline{\mathfrak{a}} - \underline{\mathfrak{a}} < \epsilon \cdot \max\{10^{-4}, \min\{\underline{\mathfrak{a}}, 1\}\}$. Then return $\overline{\mathfrak{a}}$.

In Algorithm 6.1, ϵ is the tolerance error.To emphasize the fact the spectral abscissa is computed up to a tolerance error ϵ, we write α_ϵ.

Computing the winding number of systems shifted by a real constant is equivalent to compute the winding number of the original system for a countour $\mathcal{D}_\mathfrak{a}$ containing the semiplane $\overline{\mathbb{C}_\mathfrak{a}^+}$.as shown in Figure 6.1. This means the frequency response data are now obtained on the shifted axis $\mathfrak{a} + j\mathbb{R}$.

If $G(s)$ has at least one pole on axis $\mathfrak{a} + j\mathbb{R}$, one cancel out the pole as in (2.47). Another possibility is to pertube slightly the value of the shift $\mathfrak{a}$, once we are interested only in the estimation of $\alpha(G(s))$. This is possible since the systems under consideration have only isolated singularities in $\mathbb{C}^+$.

6.2 Control synthesis implementation

The criterion $\alpha_\epsilon(T(\kappa))$ computed in algorithm 6.1 has now to be minimized until a parameter κ^* with $\alpha_\epsilon(T(\kappa^*)) \leq 0$ is found. As a consequence of using only the plant frequency response data, the only available information about the search criterion $\alpha_\epsilon(T(\kappa))$ is the value of the criterion itself. Therefore direct search methods, not dependent of derivative information, are recomended. The search should also be able to deal with the uncertainty in criterion value, as what is computed is actually $\alpha_\epsilon(T(\kappa)) \in [\underline{\mathfrak{a}}, \overline{\mathfrak{a}}]$. The chosen technique is the multi-directional search , which had already be successfully used in [Apkarian and Noll, 2006c] for H_∞ control of finite dimensional systems. The multidirectional search of Higham [2002] is used in the synthesis implementation and it is briefly described in Appendix D.

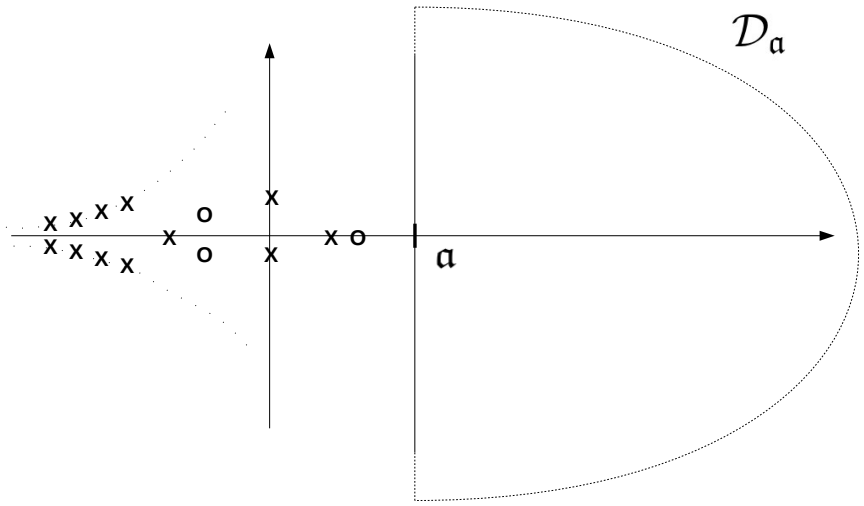

Figure 6.1: Illustration of the contour $\mathcal{D}_\mathfrak{a}$ for Nyquist stability test in spectral abscissa estimation.

It is important to remark that this implementation aims only at the design of a stabilizing controller. As such, the search for a structured stabilizing controller ends as soon as $\alpha(T(\kappa^*, s)) < 0$ is found. Once a stabilizing controller is available, a performance optimization step may follow.

The synthesis fails if no controller can be found such that $\alpha_\epsilon(T(\kappa^*, s)) < 0$. Altough the analytic expression and derivative of the function to be minimized are not available, the function to be minimized is an estimation of the spectral abscissa, known to be nonsmooth . Also the problem is not convex with respect to the structured controller. To circumvent beign stalled at local minima, it may be necessary to restart the search with different seeds.

6.3 Numerical Results

In this section, the new proposed method for FRD design of structured controllers for unstable systems based on spectral abscissa minimization is tested in a variety of finite and infinite-dimensional systems. The method is considered successful for a given system if a controller is designed such that the feedback system $T(s)$ has all its poles on $\mathbb{C}^-$.

- **Finite-dimensional benchmark**

The first set of test cases comprises unstable finite-dimensional systems. The set of systems is described in Appendix C. For all cases the controller designed is a third-order tridiagonal state-space controller. These results are important for they can be compared to results from benchmark methods for finite-dimensional plants without bias of approximation. The benchmark method used is SYSTUNE from MATLAB ™, described briefly in Appendix D.1. The H_∞-norms were normalized by the H_∞-norm obtained by SYSTUNE in each case. The FRD H_∞-norm optimization method that follows the stabilization was the one introduced in Apkarian and Noll [2018].

The results are presented in table 6.1. For this test, the spectral abscissa is estimated with a tolerance error of 1% and a maximum of 4 restarts is allowed. The grid of frequencies is in the interval $[10^{-3}$,$10^{4}]$ rad/s with a maximum density of 50,000 points per decade. Note that the actual grid used in the optimization is coarser due the use of method presented in section 2.4.1 for refining the frequency grid.

Statistics of Table 6.1:

◇ One restart was needed in case 16 to obtain a successfuly solution;
◇ In cases 20 and 21 a stabilizing solution could not be found by the FRD method after 4 restarts;
◇ The final H_∞-norm after optimization reached values similar to the benchmark method SYSTUNE in all stabilized systems except in cases 4 and 36, where the percentual difference was 69% and

Table 6.1: Comparison of results for FRD design based on abscissa minimization and by SYSTUNE for unstable finite-dimensional systems.

		FRD_α					SYSTUNE	
		κ^0	$\kappa^\sharp$		κ^*			
Ex	n_K	α	α	$\|.\|_\infty$	α	$\|.\|_\infty$	α	$\|.\|_\infty$
1	18	62.473	-0.024	549.75	-0.05	1.000	-0.05	1.000
2	18	0.523	-0.045	40.344	-0.049	0.997	-0.048	1.000
3	30	1.292	-0.095	3.738	-0.445	1.000	-0.445	1.000
4	40	3.102	-0.054	6.18e5	-0.045	3.26	-0.084	1.000
5	40	0.634	-0.001	18.257	-0.022	1.003	-0.017	1.000
6	40	0.614	-0.001	46.233	-0.006	1.000	-0.006	1.000
7	18	0.635	-0.016	24.422	-0.017	1.008	-0.148	1.000
8	61	0.248	-0.016	99.73	-0.177	1.000	-0.136	1.000
9	61	3.62	-0.005	268.91	-0.061	1.000	-0.076	1.000
10	33	0.223	-0.038	20.448	-0.089	0.906	-0.042	1.000
11	61	0.239	-0.005	534.1	-0.001	1.002	-0.001	1.000
12	28	1.444	-0.157	4.277	-0.737	1.000	-2.069	1.000
13	23	2.038	-0.021	72.546	-2.162	1.000	-2.972	1.000
14	23	2.504	-0.111	46.471	-1.219	1.002	-2.02	1.000
15	61	6.332	-0.221	14.498	-2.427	1.001	-1.383	1.000
16	23	10.505	-0.003	183.22	-0.39	1.022	-0.218	1.000
17	40	-0.191	-0.191	46.428	-1.094	1.000	-2.084	1.000
18	63	0.155	-0.009	26.566	-0.098	1.001	-0.01	1.000
19	28	14.065	-0.036	1404.51	-0.645	0.998	-0.63	1.000
20	23	12.707	0.34	-	-	-	-2.64	1.000
21	23	132.45	6.464	-	-	-	-3.691	1.000
22	18	1.104	-0.395	3.203	-1.988	0.998	-1.995	1.000
23	33	0.621	-0.01	72.23	-1.413	0.992	-1.776	1.000
24	33	1.429	-0.006	501.88	-2.027	1.002	-1.948	1.000
25	23	42.617	-0.396	1.847	-0.457	1.000	-3.262	1.000
26	23	52.945	-0.235	8.935	-0.564	1.000	-1.638	1.000
27	23	9.828	-0.328	15.56	-1.279	1.000	-1.927	1.000
28	23	12.534	-0.261	6.394	-0.907	1.002	-0.628	1.000
29	23	51.703	-0.041	375.61	-0.544	1.000	-0.879	1.000
30	28	0.46	-0.227	1.47	-0.963	1.001	-0.968	1.000
31	28	0.491	-0.022	221.5	-1.227	1.004	-1.499	1.000
32	33	9.422	-0.061	6.695	-1.185	1.004	-2.204	1.000
33	33	0.244	-0.068	17.57	-3.806	1.001	-3.861	1.000
34	33	0.766	-0.144	2.07	-1.548	1.000	-1.504	1.000
35	33	8.778	-0.141	6.044	-3.525	1.000	-7.346	1.000
36	23	16.985	-0.039	2.087	-0.051	1.443	-0.105	1.000

Legend:

Ex:	Test case	κ^0:	initial control parameter vector
α:	spectral abscissa of $T(\kappa^i, s)$	$\kappa^\sharp$:	control parameter vector after stabilization
$\|.\|_\infty$:	$\|T(\kappa^i, s)\|_\infty$	κ^*:	control parameter vector after optimization
systune:	H_∞-norm obtained by SYSTUNE	FRD_α:	results for FRD method based on abscissa
n_K:	dimension of parameter vector κ		

44%, respectively;

- **Infinite-dimensional academic examples**

The set of infinite-dimensional test cases are described in Appendix C. In order to have a benchmark to which compare the method developed in this chapter, the systems were approximated by rational systems using 2nd- to 10th-order Padé approximations for delayed systems and Oustaloup approximations for fractional-order systems, see Appendix D.4 for details. The benchmark method for H_∞ control of finite-dimensional systems is again SYSTUNE .

The results are presented in table 6.2 for a 10th-order approximation. For this test, it was used a tolerance error of 1% for the spectral abscissa estimation and a maximum of 4 restarts. The grid of frequencies is in the interval $[10^{-3}, 10^{4}]$ rad/s and a maximum density of 50,000 points per decade was used for retrieving a coarser grid for the Nyquist test as explained in section 2.4.1. The initial solution is obtained randomly and stability of the controller is not enforced at the initialization.

Statistics of Table 6.2:

- ◇ The synthesis of a stabilizing controller by SYSTUNE for 10th-order approximate systems failed in 6 test cases for the chosen parameters;
- ◇ In test cases 3,5, 23 and 24, SYSTUNE is succed only for 2nd-order approximate terms;
- ◇ The FRD method based on abscissa minimization failed in 4 test cases.

Table 6.2: Comparison of results for FRD design based on abscissa minimization for infinite-dimensional systems and SYSTUNE for their approximations.

			FRD_α		SYSTUNE	
Ex	K	n_K	$\alpha_0(.)$	$\alpha(.)$	$\alpha_{apx}(.)$	$\alpha_{act}(.)$
1	2-SS	9	91.13	0	-36.49	0
2	2,1-TF	4	1.742	0	-0.005	0
3	3,0-TF	9	5e-6	0	-0.121	6e-5
4	2-SS0	8	u	0	-0.001	0
5	3,1-TF	5	1.382	0	-8e-5	0
6	2,1-TF	4	2.159	1.488	0.965	x
7	2-SS	9	u	0	-0.001	0
8	1-SS	4	0.265	0	-0.109	0
9	1-SS	4	4.072	0	-3.086	0
10	3-SS	14	1.545	0.165	0.004	x
11	3-SS0	19	2.030	2.030	2.298	x
12	2-SS	9	0.442	0	-0.001	0
13	2-SS0	12	u	0	-0.059	0
14	2-SS0	12	3.906	0	-0.398	3.397
15	2-SS0	16	0.812	0	-0.001	0.733
16	2-SS0	20	4.265	0	-0.002	0
17	1-SS0	3	2.726	0	-0.002	0
18	1-SS0	3	4.101	0	-0.001	0
19	1-SS0	3	3.351	0	0.029	0.286
20	1-SS0	3	4.531	0	1.599	1.575
21	3-SS	14	u	0.063	-0.132	0.747
22	3,1-TF	5	0.259	0	0.0483	x
23	1,0-TF	2	1.099	0	-3.055	7.071
24	2-SS0	8	u	0	-2.303	0
25	2-SS	9	u	0	-0.001	0.038

Legend:

Ex:	Test case		
n_K:	dimension of parameter κ	K:	controller structure
SYSTUNE :	results obtained by SYSTUNE	FRD_α:	results for FRD method based on abscissa
$\alpha_{apx}(.)$:	spectral abscissa of approximate $T(\kappa^*, s)$	$\alpha_0(.)$:	spectral abscissa of $T(\kappa^0, s)$
$\alpha_{act}(.)$:	spectral abscissa of actual $T(\kappa^0, s)$	$\alpha(.)$:	spectral abscissa of $T(\kappa^*, s)$
u:	unstable controller	x:	not computed

Discussion

The method for FRD design of stabilizing structured controller based on spectral abscissa minimization was shown to be effective in a variety of cases. It successfuly designed stabilizing structured controllers in aproximately 94% of finite-dimensional test cases and 84% of infinite-dimensional test cases.

The first set of tests comprises only finite-dimensional test cases, so the controller synthesis routine SYSTUNE for finite-dimensional systems based on parametric models could be used as a reliable benchmark. The comparison to the benchmark allowed to verify if and how much the FRD design is efficient in stabilizing and optimizing H_∞-norm. Also, a variety of tools is available for further inspection and certification of the results obtained by the FRD design technique, like computation of the complete set of poles and of actual H_∞-norm of the system. The FRD method failed to find a stabilizing controller where SYSTUNE was successful in only 2 cases. The success of the benchmark also helps to reject the hypotesis that a stabilizing controller with the desired structure may not exist. In these two cases, it was observed that 2 or more rightmost poles align vertically close to the spectral abscissa.

The combination of the FRD design of stabilizing structured controllers with FRD H_∞-norm structured control of Apkarian and Noll [2018] led to similar results of optimum H_∞-norm obtained by the benchmark routine based on parametric models. Analysis of the cases where the percentual difference was greater than 40% reveals that the controller designed by SYSTUNE have high gains while the one designed by FRD method has lower gains. In FRD design, lower gains are desired in order to avoid large modulus poles, that demands a larger frequency cut of the grid frequency, thus increasing the computational complexity. Besides that, tighter bounds on the values that the parameter κ may assume speed up the search and increase the success rate, provided a solution is contained in the limited region.

The tests with infinite-dimensional plants expose the problem of designing controllers for infinite-dimensional systems based on their lower-order approximations. For the same controller structure as the FRD method, SYSTUNE failed in 6 cases for 10th-order approximations of delay and fractional terms. In 4 of these cases, when increasing the controller order, the stabilization is successful. In 6 cases increasing the order of the approximation results in failure of the synthesis. This is readily noted by inspection of the results of the controller designed applied to the actual system. This is a clear example of the *spillover effect* described in Balas [1982].

The FRD design technique introduced in this chapter fails in 4 cases. Further tests are necessary to clarify the causes of failure. Two possible reasons are the use of an inappropriate structure for the controller and failure of the optimization method.

It is opportune to compare the method developed for estimating the spectral abscissa to similar methods in the litterature. As the spectral abscissa is employed as objective function with the sole objective of obtain a spectral abscissa smaller than zero, only positive values are of interest. Also, the number or location of other unstable closed-loop poles is not relevant to the FRD design technique. Nonetheless, the estimation method can be extended to compute negative spectral abscissa provided that the feedback system has only isolated singularities in the interval of computation. This constraint aims to satisfy conditions of application of Nyquist stability test.

Many authors considered the computation of number and location of unstable poles of infinite dimensional systems, which naturally provides the spectral abscissa. One of the objectives of these methods is approximation of unstable infinite-dimensional systems by rational systems as in Gu et al. [1992], based on FFT and Hankel singular values. Other works are specialized in one type of system, as the work of Fioravanti et al. [2010] for neutral systems that uses the analytic expression of the system and several integrations and is employed in the toolbox YALTA [Avanessoff et al., 2013], and the works that resulted in the toolbox CRONE [Lanusse et al., 2013] for non-commensurate fractional order systems. The advantage of the method proposed here is that it may be applied to a more general class of systems and it is of simple application.

Despite the high rate of success of the technique based on spectral abscissa minimization presented in this chapter, the fact that it involves a nonsmooth optmization raised the question of whether a method based on optimization of smooth functions would perform better. This lead us to the object of the next chapter, FRD design based on H_2-norm minimization.

Chapter 7

Development of FRD design of structured controllers based on H_2-norm minimization

In this chapter

a frequency response data synthesis based on minimization of H_2-norm is developed and implemented. The technique consists in estimating the energy of systems from the shifted H_2-norm computed in frequency domain and in minimizing this energy reducing the shift iteratively. The motivation for such technique relies on the the relationship between the energy of impulse response and stability of systems.

Conclusion

The technique effectively designs controllers that results on negative spectral abscissa for the class of systems considered.

In the previous chapter a method for the frequency response data design of structured controllers for infinite-dimensional systems were developed based on minimization of the spectral abscissa of the feedback system. This method is specially attractive in the cases where a stabilizing control law should be designed for an unstable infinite-dimensional system. Altough successful, this methods demands high precision estimation of the spectral abscissa several times. The H_2-norm is proposed as objective function, as an alternative to the spectral abscissa, in this chapter.

7.1 Impulse response energy minimization and stability

7.1.1 Motivation

The impulse response of a system is direct related to its poles. In case of proper rational systems, the impulse response is completly determined by the partial fraction decomposition of the transfer function, that is, by its poles and respective residues, and the inverse Laplace transform. Matignon [1998] also established the impulse response for fractional-order systems of commensurate order as a function of their poles.

Consider $G(s)$ a rational stable system with state-space representation $(A, B, C, 0)$. If all its poles are stable then its impulse response will eventually decay to zero. On the other hand, if at least one of its pole is unstable, then its impulse response increases indefinitetly. This implies that the energy of the impulse response of a rational strictly proper system is finite if it is stable and infinite otherwise.

The energy of the impulse response is the square of the H_2 norm which is computed by (2.17) in time domain. For a stable system, it is possible to compute the H_2 norm, in the frequency domain by (2.18). The H_2-norm of a stable transfer function is smooth and easily computed what renders it easy to minimized by optimization procedures. This places it as an ideal choice for a objective function on an optimization search. Together with the fact that it can be computed in frequency domain motivates the study of this function on FRD design of stabilizing controllers.

7.1.2 Energy of shifted systems

Let $g(t)$ be the impulse response associate to a system $G(s)$. Let the energy of a system $G(s)$ be defined as

$$E(G) = \|g(t)\|_2^2 \tag{7.1}$$

For $G(s)$ strictly proper on $\mathbb{C}^+$, $\lim_{\rho\to\infty} \sup_{Re(s)\geq 0, |s|\geq\rho} |G(s)| = 0$. For a stable proper $G(s)$ with limit at infinity G_∞, the energy of the system minus its limit is

$$E(G) = \int_{-\infty}^{\infty} Tr((G(j\omega) - G_\infty)^H (G(j\omega) - G_\infty))d\omega. \tag{7.2}$$

The discretization of the integral 7.2 on frequency grid Ω leads to the summation

$$E_\omega(G) = \sum_{\omega\in\Omega} Tr(G_p(j\omega)G_p^H(j\omega)) \cdot \Delta\omega \tag{7.3}$$

where $G_p(s) = G(j\omega) - G_\infty$.

Let $q(\omega) = Tr((G(j\omega) - G_\infty)^H (G(j\omega) - G_\infty))$, and $Q_\omega(\omega)$ the linearly interpolating polygon of $q(\omega)$ on grid $0 = \omega_0 < \omega_1 < \cdots < \omega_N = \overline{\omega}$. Then

$$\upsilon_{\overline{\omega}} = 2\int_{\overline{\omega}}^{\infty} q(\omega)d\omega$$

and

$$\upsilon_\omega = 2\left|\int_0^{\overline{\omega}} q(\omega)d\omega - \int_0^{\overline{\omega}} Q_\omega(\omega)d\omega\right|.$$

The error $\upsilon = \|E(G) - E_\omega(G)\|$ between the integral and the summation is the sum of the truncation error $\upsilon_{\overline{\omega}}$ and the interpolation error υ_ω.

As recalled in section 2.1, for an unstable strictly proper transfer function $G(s)$, energy $E(G)$ is not finite and cannot be compute in frequency. As observed in last chapter, for a $G(s) \in \hat{\mathcal{B}}(0)$ there is a sufficiently large real constant $\mathfrak{a} > 0$ such that $G_\mathfrak{a}(s) = G(s + \mathfrak{a})$ is now holomorphic in $\mathbb{C}_\mathfrak{a}^+$ and bounded in $\overline{\mathbb{C}_\mathfrak{a}^+}$. Let $g_\mathfrak{a}(t)$ be the impulse response associate to $G_\mathfrak{a}(s)$. Using Laplace transform properties,

$$g_\mathfrak{a}(t) = g(t)e^{-\mathfrak{a}\,t}. \tag{7.4}$$

We have that $\|g_\mathfrak{a}(t)\|_2 = \|G_\mathfrak{a}(s)\|_2$ and energy $E(G_\mathfrak{a})$ is finite.

The energy $E(G_\mathfrak{a})$ computed for a discrete grid of frequencies Ω is:

$$E_\omega(G_\mathfrak{a}) = \sum_{\omega\in\Omega} Tr(G_p(\mathfrak{a} + j\omega)G_p^H(\mathfrak{a} + j\omega)) \cdot \Delta\omega \tag{7.5}$$

7.2 Control synthesis implementation

Let $T(s)$ defined in (2.9) be the transfer function of the feedback system Σ. We search a structured controller $K(\kappa, s) \in \mathcal{K}$ such that $T(\kappa, s) \in \hat{\mathcal{A}}_-(0)$. In this case, $E(T_\mathfrak{a}(\kappa))$ is defined and finite for $\mathfrak{a} = 0$.

The energy of the closed-loop system $E(T_\mathfrak{a}(\kappa, s))$ is minimized until finding a $K(\kappa^*, s) \in \mathcal{K}$ such that $E(T(\kappa^*, s))$ is finite, that is, $T_\mathfrak{a}(\kappa^*, s) \in \hat{\mathcal{A}}(-\mathfrak{a})$. This means $T(\kappa^*, s) \in H^\infty$.

The method consists then in minimizing $E(T_{\mathfrak{a}}\ (\kappa, s))$ reducing iteratively the value of real constant $\mathfrak{a}$ until $\mathfrak{a} = 0$, constraining $\alpha(T(\kappa, s)) < \mathfrak{a}$ at each iteration.

This is implemented by algorithm 7.1 below:

Algorithm 7.1: Synthesis based on minimization of impulse response energy of closed-loop system.

Parameters: $\varepsilon > 0$.

▷ **Step 1** (`Initialization`).
Randomly choose κ^c.
Apply Nyquist stability test of 2.47 to $T(\kappa^c, s)$.
If stable, return $\kappa^* = \kappa^c$ and quit. Else go to Step 2.

▷ **Step 2** (`Compute Shift`).
Get new $\overline{\mathfrak{a}}$ from spectral abscissa estimator of algorithm 6.1 for $T(\kappa^c, s)$.

▷ **Step 3** (`Minimization of energy`).

$$\begin{array}{ll} \text{minimize} & E(T(\kappa, s + \overline{\mathfrak{a}})) \\ \text{subject to} & \text{positive Nyquist stability test for } T(\kappa, s + \overline{\mathfrak{a}}) \\ & K(\kappa, s) \in \mathcal{K} \end{array} \tag{7.6}$$

using (7.5) for computing energy and with κ^c as initial point and κ^+ as solution.

▷ **Step 4** (`Stop criteria`).
Apply Nyquist stability test of 2.4.1 to $T(\kappa^+, s)$.
If stable, return $\kappa^* = \kappa^+$ and quit. Else make $\kappa^c = \kappa^+$ and go to Step 2.

Program 7.6 for optimization of Step 3 can be solved by routines that implement searches for a minimum of a function. The energy as defined in (7.5) is a smooth function on the parameter search κ. However in FRD design the exact function is not available and neither is the expression for its derivative. Only punctual function estimation is available as information for the search. Iterative methods with Gauss-Newton or quasi-Newton methods can be used, with the energy estimation being computed through (7.5). In the present work the MATLAB ™ routine FMINCON [MathWorks, 2017] was used in the search. The frequency grid is a dense grid but an algorithm for selecting an aproriate frequency grid in order to guarantee a desired tolerance error υ in the estimation of the H_2-norm can be developed similar to what have been done in Apkarian and Noll [2018] for the H_∞-norm .

Recall that the spectral abscissa estimator from 6.1 returns an upper bound estimate $\overline{\mathfrak{a}}$. The use of this estimate assures that the shifted system $T(\kappa, s + \overline{\mathfrak{a}})$ has no poles on $j\mathbb{R}$.

7.3 Numerical Results

In this section, the new proposed method for FRD design of stabilizing controllers for unstable systems based on minimization of H_2-norm is tested in a variety of finite and infinite-dimensional systems. As in the previous chapter, the method is considered successful if a controller is designed such that the feedback system $T(s)$ has all its poles on the right half-plane.

- **Finite-dimensional benchmark**

The set of unstable finite-dimensional test cases is the same used for FRD based on spectral abscissa minimization and is presented in Appendix C. The controllers have also the same structure, third-order tridiagonal state-space. The benchmark method is SYSTUNE from MATLAB ™, described briefly in Appendix D and all H_∞-norms were normalized by the H_∞-norm obtained by SYSTUNE. The FRD H_∞-norm optimization method used was the one introduced in Apkarian and Noll [2018].

The results are presented in table 7.1. For this test the grid of frequencies is in the interval $[10^{-3}$

,10^4] rad/s and 10,000 points logarithmicly distributed and a maximum of 10 restarts. For spectral abscissa estimation it was used a tolerance error of 10% and a grid of frequencies in the same interval with a maximum density of 50,000 points per decade.

Table 7.1: Comparison of results for FRD design based on H_2-norm minimization and SYSTUNE for unstable finite-dimensional systems.

		FRD_2					SYSTUNE	
		κ^0	$\kappa^\sharp$		κ^*			
Ex	n_K	α	α	$\|.\|_\infty$	α	$\|.\|_\infty$	α	$\|.\|_\infty$
1	18	62.473	-0.05	400.54	-0.05	1.000	-0.05	1.000
2	18	0.523	-0.005	1205.13	-0.048	0.99	-0.048	1.000
3	30	1.292	-0.021	14.529	-0.325	0.997	-0.445	1.000
4	40	3.102	-0.002	7.34e6	-0.062	1.056	-0.084	1.000
5	40	0.634	-0.009	71.404	-0.025	1.001	-0.017	1.000
6	40	0.614	-0.003	5.606	-0.006	1.000	-0.006	1.000
7	18	0.635	-0.018	11.844	-0.148	1.002	-0.148	1.000
8	61	0.248	-0.039	5.362	-0.207	0.998	-0.136	1.000
9	61	3.62	-0.174	12.477	-0.056	1.000	-0.076	1.000
10	33	0.223	0.199	-	-	-	-0.042	1.000
11	61	0.239	-0.005	354.21	-0.001	1.000	-0.001	1.000
12	28	1.444	-0.351	2.234	-0.629	1.000	-2.069	1.000
13	23	2.038	-0.005	16.484	-1.599	1.000	-2.972	1.000
14	23	2.504	-0.61	2.327	-0.599	1.002	-2.02	1.000
15	61	6.332	-0.194	5.774	-1.918	0.998	-1.383	1.000
16	23	1.008	1.016	-	-	-	-0.218	1.000
17	40	-0.191	-0.191	46.428	-1.094	1.000	-2.084	1.000
18	63	0.155	-0.127	1.115	-0.129	1.000	-0.01	1.000
19	28	1.9	-0.042	69.434	-0.641	0.998	-0.63	1.000
20	23	12.328	36.041	-	-	-	-2.64	1.000
21	23	6.223	67.23	-	-	-	-3.691	1.000
22	18	1.104	-0.242	2.582	-1.993	0.998	-1.995	1.000
23	33	0.621	-0.027	73.051	-1.363	1.003	-1.776	1.000
24	33	1.429	1.455	-	-	-	-1.948	1.000
25	23	42.617	-0.33	1.909	-0.532	1.000	-3.262	1.000
26	23	52.945	-0.451	3.491	-0.536	1.000	-1.638	1.000
27	23	9.828	-0.506	2.272	-1.042	1.000	-1.927	1.000
28	23	12.534	-0.147	6.575	-0.976	1.003	-0.628	1.000
29	23	51.703	-0.005	4.465	-0.729	1.000	-0.879	1.000
30	28	0.46	-0.097	3.828	-0.936	1.004	-0.968	1.000
31	28	0.491	-0.157	2.174	-1.25	1.005	-1.499	1.000
32	33	9.422	-0.027	17.349	-2.222	1.004	-2.204	1.000
33	33	0.244	-0.704	1.903	-3.859	1.000	-3.861	1.000
34	33	0.766	-0.266	1.743	-1.613	1.000	-1.504	1.000
35	33	8.778	-0.626	2.557	-1.924	1.000	-7.346	1.000
36	23	16.985	-0.04	2.017	-0.046	1.429	-0.105	1.000

Legend:

Ex:	Test case	κ^0:	initial control parameter vector
α:	spectral abscissa of $T(\kappa^i, s)$	$\kappa^\sharp$:	control parameter vector after stabilization
$\|.\|_\infty$:	$\|T(\kappa^i, s)\|_\infty$	κ^*:	control parameter vector after optimization
systune:	H_∞-norm obtained by SYSTUNE	FRD_2:	results for FRD method based on H_2-norm
n_K:	dimension of parameter vector κ		

Statistics of Table 7.1:

◇ In cases 10, 16, 20, 21 and 24 a stabilizing solution could not be found after 10 restarts;

◇ Final H_∞-norm after optimization reached similar values to benchmark method SYSTUNE in all

stabilized systems except in case 36, where the percentual difference was 43%;

- **Infinite-dimensional academic examples**

The validation test of the method for FRD design of structured controller based on energy minimization for a set of infinite-dimensional systems follow the same guidelines of the test in the previous chapter. The test cases are the same described in Appendix C and after stabilization by the method developed, the H_∞ optimization is led by the routine of Apkarian and Noll [2018] for the actual infinite-dimensional systems. The systems were approximated in order to use the benchmark routine SYSTUNE. Padé approximations from (2.23) were used for delayed systems and Oustaloup approximations from (2.21), for fractional-order systems, see Appendix D.4.

For this test the grid of frequencies is in the interval $[10^{-3}$,$10^{4}]$ rad/s and 10,000 points logarithmicly distributed and a maximum of 10 restarts. For spectral abscissa estimation it was used a tolerance error of 1% and a grid of frequencies in the same interval with a density of 50,000 points per decade. For the spectral abscissa estimation, the frequency grid is refined by the method presented in section 2.4.1. The initial solution is obtained randomly but controller stability is enforced from the beginning.

Table 7.2: Comparison of results for FRD design based on H_2-norm minimization for infinite-dimensional systems and SYSTUNE for their approximations.

			FRD_2		SYSTUNE	
Ex	K	n_K	$\alpha_0(.)$	$\alpha(.)$	$\alpha_{apx}(.)$	$\alpha_{act}(.)$
1	2-SS	9	24.37	0	-36.49	0
2	2,1-TF	4	0.437	0	-0.005	0
3	3,0-TF	9	0	0	-0.121	6e-5
4	2-SS0	8	0.21	0	-0.001	0
5	3,1-TF	5	0.305	0	-8e-5	0
6	2,1-TF	4	1.020	1.020	0.965	x
7	2-SS	9	1.437	0	-0.001	0
8	1-SS	4	0.132	0	-0.109	0
9	1-SS	4	1.02	0	-3.086	0
10	3-SS	14	0.988	0.978	0.004	x
11	5-SS0	33	2.326	2.301	2.298	x
12	2-SS	9	1.052	1.021	-0.001	0
13	2-SS0	12	0	0	-0.059	0
14	2-SS0	12	3.906	0	-0.398	3.397
15	2-SS0	16	0.812	0	-0.001	0.733
16	2-SS0	20	4.265	0	-0.002	0
17	1-SS0	3	0	0	-0.002	0
18	1-SS0	3	0	0	-0.001	0
19	1-SS0	3	0.289	0	0.029	0.286
20	1-SS0	3	0	0	1.599	1.575
21	3-SS	14	0.839	0.063	-0.132	0.747
22	3,1-TF	5	0.140	0	0.048	x
23	1,0-TF	2	1.020	0	-3.055	7.071
24	2-SS0	8	0	0	-2.055	0
25	2-SS	9	0	0	-0.001	0.038

Legend:

Ex:	Test case		
n_K:	dimension of parameter κ	K:	controller structure
SYSTUNE :	results obtained by SYSTUNE	FRD_α:	results for FRD method based on abscissa
$\alpha_{apx}(.)$:	spectral abscissa of approximate $T(\kappa^*, s)$	$\alpha_0(.)$:	spectral abscissa of $T(\kappa^0, s)$
$\alpha_{act}(.)$:	spectral abscissa of actual $T(\kappa^0, s)$	$\alpha(.)$:	spectral abscissa of $T(\kappa^*, s)$
u:	unstable controller	x:	not computed

Statistics of Table 7.2:

- ◇ In cases 6, 10, 11, 12 and 21 a stabilizing solution could not be found after 10 restarts;
- ◇ In cases 3, 13, 17, 18, 20, 24 and 25 the initial point is already a stabilizing solution.

Discussion

The method for FRD design of stabilizing structured controller based on H_2-norm minimization was shown to be effective in a variety of cases. It successfuly designed stabilizing structured controllers in aproximately 86% of finite-dimensional test cases and 80% of infinite-dimensional test cases.

This technique obtained the lowest rate of success among the techniques, failing in 2 cases where the other two FRD design techniques introduced succeed for finite-dimensional cases. In 3 cases of these cases, at least one of the other methods also fails. Once stabilized, the subsequent H_∞-norm optimization was able to reach values close of those of SYSTUNE for more systems than the other 2 techniques though. The inspection of the solutions showed that contrary to the method based on spectral abscissa, the cause of failure is not related to alignment of rightmost poles, once that was not the case in the failure cases. What occurred was that the minimization of the H_2-norm did not imply in further reduction of the spectral abscissa. A possible solution is to create new heuristics for the choice of the shift.

Concerning the infinite-dimensional cases, the method failed in all cases where the method based on the spectral abscissa also failed. It succeded in 2 cases where the method based on H_∞-norm failed and it is the only one to fail in one particylar case. The method is also the slowest, due to the high density of the grid frequency.

The good efficiency of the method itself corroborates the empirical argument that by minimizing the energy of shifted can indeed lead to stabilization. Even with lower rates of success than the former method, its objective function, the energy, is easily computed and the search is also simplified by the smoothness of the function. However, the constraint is still difficult to handle.

For comments regarding the performance of SYSTUNE, please refer to the Discussion of chapter 6.

Chapter 8

Development of FRD design of structured controllers based on H_∞-norm minimization

In this chapter

a method for the frequency response data design of structured controllers based on minimization of the shifted H_∞-norm is developed and implemented. The shift is iteratively adjusted to guarantee that the minimization will result in stabilization. It is shown that for appropriate set-up current methods for FRD H_∞-norm optimization can be exploited.

Conclusion

The technique succeded in designing stabilizing controller for a variety of finite and infinite-dimensional systems. The found solution in some cases led to an H_∞-norm greater than previous techniques.

8.1 Connections between H_∞-norm and stability

8.1.1 Motivation

The H_∞-norm is not defined for systems that are not analytic in $\mathbb{C}^+$. Yet, equation $\|G(s)\|_\infty = \sup_{\omega\in\mathbb{R}} \overline{\sigma}(G(j\omega))$ for computing the H_∞-norm of a system $G(s)$ does not provide any direct relationship between the poles and the H_∞-norm of a system. Notwithstanding, some empirical results motivate the study of the conncetions between the H_∞-norm and stability.

Consider $G(s)$ a rational stable system with state-space representation (A, B, C, D). Then $\|G(s)\|_\infty$ gives the worst case amplitude gain of the transfer matrix $G(s)$. Also the singular values $\bar{\sigma}(G(j\omega))$, for $\omega \in \Omega$, are related to the poles of the system in the means that badly-damped poles cause resonance peaks. In many cases, badly-damped poles are very close to the imaginary axes, contributing to a small stability margin. By minimizing the H_∞-norm of a stable system, we end up increasing the damping of the system poles, which in some cases is achived by pushing these badly-damped poles further into $\mathbb{C}^-$ and increasing stability margins.

An indirect relationship between the H_∞-norm and stability can also be obtained through the modulus margin. The modulus margin of a feedback system is the minimum distance between the curve of a feedback system and the origin in the generalised Nyquist plot and it is defined as $\|S(s)\|_\infty^{-1}$, $S(s) = (I + G(s)K(s))^{-1}$. In the SISO case, a good measure of the modulus margin assures good

values for gain and phase margin. In general, the modulus margin is closely related to the stability margin.

Shifted H_∞-norm of unstable systems

As seen in chapter 2, the feedback system Σ is internally stable if all four terms of the matrix in (2.9) belong to $\hat{\mathcal{A}}_\infty(0)$. If $K(s)$ is stable, the condition for internal stability of the feedback system is reduced to $G(I+KG)^{-1}$ belonging to $\hat{\mathcal{A}}_\infty(0)$. We also have that for a system $T(s) \in \mathcal{H}_a^\infty$ the norm is defined as $\|T(s)\|_{\mathcal{H}_a^\infty} = \sup_{s\in\mathfrak{a}+j\mathbb{R}} \overline{\sigma}(T(s))$. This is equivalent to H_∞-norm of the shifted system $T(s+\mathfrak{a})$, $\|T(s+\mathfrak{a})\|_\infty$.

Inspired by the fact that the minimization of the H_∞-norm may increase stability margins and push poles into left half-plane, a method for desiging stabilizing structured controllers $K(\kappa, s)$ for unstable systems exploiting an iterative minimization of the shifted H_∞-norm is developed. The rationale is that once unstable poles of the closed-loop system $T(\kappa, s)$are shifted to the left half-plane close to imaginary axis, the optimization of the H_∞-norm of the shifted system will push them further. This implies that the actual, not shifted, system has a smaller spectral abscissa $\alpha(T(\kappa^*, s)) < \alpha(T(\kappa, s))$.

To maximize the efect of the minimization of H_∞-norm on ressonant peaks caused by badly-damped poles, we ensure that there are poles close enough to the imaginary axis. We achieve this by computing the spectral abscissa $\mathfrak{a}_S$ of the actual closed loop system, through the method by estimator algorithm 6.1, and then shifting the system by $\mathfrak{a}_S + \zeta$. This means the poles, erstwhile corresponding to the spectral abscissa, are now on $\mathbb{C}_\zeta^-$. The smaller the ζ, teh closest the poles are to the imaginary axis. By minimizing the H_∞ norm of the shifted system, we expect to achieve a new κ_{+1} such that $\alpha(S(\kappa_{+1}, s)) = \mathfrak{a}_S - \xi$. We proceed until $\alpha(S(\kappa_{+n}, s)) < 0$.

H_∞-norm minimization constraint

H_∞-norm peaks from closed-loop system ressonant modes are also due to badly-damped controller. These poles, however do not contribute to the stabilizing method. To avoid such controllers, some constraints can be posed to redefine the class $\mathcal{K}$ of controllers with the desired structure. In addition to the structure, we can restrict the controller poles to a conical region in $\mathbb{C}^-$, for stable poles with a miniminal decay $\alpha(K(\kappa, s)) \leq -\tau$ and a fixed damp value $\min\{Re(\lambda)/|\lambda| = \psi$, where λ is a pole of $K(\kappa, s)$.

In order to have the feedback system shifted by $\mathfrak{a}$, the controller must also be shifted, so in fact what is obtained at the end of the search is $K(\kappa, s+\mathfrak{a})$. This affects the design of the controller as a constraint on controller poles should be posed. This is necessary to keep the original constraint of a stable controller. So when the stability of the actual system is evaluated, the controller will be stable after reversing the shift. This implies that the poles of the shifted controller $K(\kappa, s+\mathfrak{a})$ should be located in the semi-plane $\mathbb{C}_{-\mathfrak{a}}^-$.

8.2 Control synthesis implementation

Before synthesis, the structure for the controller $K(s) \in \mathcal{K}$ and its parametrization $K(\kappa, s)$ should be chosen. Due to the fact that the H_∞-norm is defined only for systems analytic in $\mathbb{C}^+$ and bounded in $\overline{\mathbb{C}^+}$, the technique demands the initialization of the procedure with a stable feedback system. So for the first iteration, the technique resorts to the same small gain artifice employed in case of stable systems [Zhou and Doyle, 1999].

In order to use small gain for unstable systems, the technique proposed in this chapter is to make the plant stable by shifting the system by the same amount as the plant's spectral abscissa $\mathfrak{a} = \alpha(G(s))$, known by hypotesis. The controller will be shifted by the same amount leading to a feedback system Σ with $T(\kappa, s+\mathfrak{a})$. It suffices to find an initial controller parameter vector κ^0 such that $\|K(\kappa^0, s+\mathfrak{a})\|_\infty < \|G(s+\mathfrak{a})\|_\infty^{-1}$. This can be easily achieved by picking any κ^{0-} such that $K(\kappa^{0-}, s) \in \mathcal{K}$ and adjusting accordingly the elements of κ^{0-} that affect exclusively the controller gains.

In each step, the actual closed-loop system, i.e., not shifted, should be verified for stability. The stability of $T(\kappa^0, j\omega)$ is evaluated using the *Nyquist stability test* of section 2.4.1 for the responses of $K(\kappa^0, j\omega)$ and $G(j\omega)$. If the closed-loop system is stable, the procedure is terminates successfully and

no optimization is necessary. Otherwise, the spectral abscissa of $T(\kappa, s)$ is estimated by algorithm 6.1 and the iterative method takes place.

These overall synthesis steps are implemented by the algorithm 8.1 below.

Algorithm 8.1: Synthesis based on minimization of shifted H_∞-norm of closed-loop system.

Parameters: $\varepsilon > 0$.

▷ **Step 1** (`Initialization`).
Put $\mathfrak{a} = \alpha(G(s))$.
Find $SG = \max_{\omega\in\Omega} \overline{\sigma}(G(\mathfrak{a} + j\omega))$.
Initialize $K(\kappa^0, s) \in \mathcal{K}$.
Reduce gain of controller $K(\kappa^0, s + \mathfrak{a})$ until $\|K(\kappa^c, s + \mathfrak{a})\|_\infty < SG^{-1}$.
Apply Nyquist stability test of 2.4.1 to $T(\kappa^c, s)$.
If stable, return $\kappa^* = \kappa^c$ and quit. Else go to Step 2.

▷ **Step 2** (`Compute Shift`).
Get new $\mathfrak{a}$ from spectral abscissa estimator of algorithm 6.1 for $T(\kappa^c, s)$.

▷ **Step 3** (`Minimization of` H_∞`-norm`).

$$\begin{aligned} &\text{minimize} && \max_{\omega\in\Omega} \overline{\sigma}(T(\kappa, \mathfrak{a} + \varepsilon + j\omega)) \\ &\text{subject to} && \text{positive Nyquist stability test for } T(\kappa, s + \mathfrak{a}) \\ & && K(\kappa, s) \in \mathcal{K} \end{aligned} \tag{8.1}$$

with κ^c as initial point and κ^+ as solution.

▷ **Step 4** (`Stoping test`).
Apply Nyquist stability test of 2.4.1 to $T(\kappa^+, s)$.
If stable, return $\kappa^* = \kappa^+$ and quit. Else make $\kappa^c = \kappa^+$ and go to Step 2.

In order to address the problem by available data-driven H_∞ control techniques, the matrix T can be obtained by defining:

$$P := \begin{bmatrix} I & \mathbf{0} & -I \\ G & I & -G \\ G & I & -G \end{bmatrix} \tag{8.2}$$

and then obtaining the feedback system as $T = P \star K$, the same as (2.9). In the case of a stable controller:

$$P := \begin{bmatrix} G & -G \\ G & -G \end{bmatrix}. \tag{8.3}$$

Note that the minimal realizations of both $P(s)$ have exactly the same poles as $G(s)$.

Program E.26 of Step 3 for H_∞ optimization can be solved by any H_∞ optimization technique provided the H_∞ norm is computed for a discrete frequency grid. This problem is nonconvex and nonsmooth and among the options discussed in chapter 1, the technique of Apkarian and Noll [2018] is chosen for it does not convexify the problem and it is adapted to discrete and finite frequency grids. In this approach the frequency grid Ω is adapted for each κ, guaranteeing a desired tolerance error for the H_∞-norm. In algorithm 8.1 the grid Ω is updated for each $T(\kappa, s + \varepsilon + \mathfrak{a})$, where $\mathfrak{a}$ is held fixed in Step 3. The small constant ε assures that the system has no poles on $\mathfrak{a} + j\mathbb{R}$.

8.3 Numerical Results

In this section, the new proposed method for FRD design of stabilizing structured controllers for unstable systems based on minimization of H_∞-norm is tested in a variety of finite and infinite-dimensional systems. The method is considered successful for a given system if a controller $K(\kappa^*, s)$ is designed such that the feedback system $T(\kappa^*, s)$ belongs to $\mathcal{H}^\infty$.

- **Finite-dimensional benchmark**

The set of finite-dimensional test cases is the same as in the previous two chapters and is described in Appendix C. As before, the controller structure is a third-order tridiagonal state-space and the benchmark method is SYSTUNE from MATLAB ™, described briefly in Appendix D. The H_∞-norms were normalized by the H_∞-norm obtained by SYSTUNE in each case and the FRD H_∞-norm optimization method used was the one introduced in Apkarian and Noll [2018].

The results are presented in table 8.1 for a maximum of 4 restarts. For this test the grid of frequencies is in the range $[10^{-3}, 10^{3}]$ rad/s for a maximum of 10,000 points logarithmicly distributed, refined iteratively by the method introduced in Apkarian and Noll [2018]. The parameter ε is iteratively updated to 3% of the current shift $\mathfrak{a}$. The spectral abscissa was estimated with a tolerance error of 2% and a grid of frequencies in the same interval with a maximum density of 50,000 points per decade. Note that the actual grid used in the optimization is coarser due the use of method presented in section 2.4.1 for refining the frequency grid for spectal abscissa estimation.

Statistics of Table 8.1:
- ◇ At least one restart was needed in 12 cases to obtain a successfuly solution;
- ◇ In cases 10, 21 and 29 a stabilizing solution could not be found after 4 restarts;
- ◇ The final H_∞-norm after optimization reached similar values to benchmark method SYSTUNE in all stabilized systems except in cases 2, 4, 7, 8, 14, 21, and 36, where the percentual difference was between 25% to 69%;
- ◇ The spectral abscissa increased in 7 cases during H_∞ optimization.

- **Infinite-dimensional academic examples**

The second set of test cases comprises infinite-dimensional systems described in Appendix C. An H_∞ optimization based on routine of Apkarian and Noll [2018] follows the stabilization step where a stabilizing controller with the desired structure is obtained by the FRD design based on H_∞-norm minimization developed in this chapter.

The routine SYSTUNE for finite-dimensional systems was employed as benchmark and is described in Appendix D. Rational approximates for the infinite dimensional systems were build using Padé or Oustaloup approximations, respectivelly for delayed and fractional-order systems. Descriptions of approximation routines for MATLAB ™ can be found in Appendix D.4.

The results are presented in table 8.1. For this test the grid of frequencies is in the interval $[10^{-3}, 10^{3}]$ rad/s for a maximum of 10,000 points logarithmicly distributed. The parameter ε is iteratively updated to 3% of the current shift $\mathfrak{a}$for and a maximum of 4 restarts. The spectral abscissa was estimated with a tolerance error of 2% and a grid of frequencies in the same interval with a maximum density of 50,000 points per decade. The initial solution for this method is obtained after the application of the small gain artifice in Step 1 of algorithm 8.1.

Statistics of Table 8.2:
- ◇ The FRD design method based on H_∞ minimization fails in 6 cases;
- ◇ In 12 cases, a stabilizing controller was obtained after the small gain initial step;
- ◇ The SYSTUNE synthesis based on approximations fails in 12 cases;
- ◇ In test cases 3,5, 23 and 24, SYSTUNE is applied for a 2nd-order term approximations;

Discussion

The FRD design of stabilizing structured controllers based on H_∞-norm minimization was shown to be effective in a variety of cases. It successfuly designed stabilizing structured controllers in aproximately 92% of finite-dimensional test cases and 76% of infinite-dimensional test cases.

The test with unstable rational plants showed that the technique have a rate of success similar to other techniques, worse than for method based on abscissa and better than the one based on H_2-norm. Unexpectedly, this technique is the one that achieves the larger H_∞-norm after optimization, among all 4 techniques, SYSTUNE included.

Table 8.1: Comparison of results for FRD design based on H_∞ minimization and SYSTUNE for unstable finite-dimensional systems.

		FRD_∞					SYSTUNE	
		κ^0	$\kappa^\sharp$		κ^*			
Ex	n_K	α	α	$\|.\|_\infty$	α	$\|.\|_\infty$	α	$\|.\|_\infty$
1	18	2.676	-0.05	67.461	-0.05	1.000	-0.05	1.000
2	18	0.177	-0.007	2249.13	-0.035	1.245	-0.048	1.000
3	30	-0.007	-0.035	331.89	-0.445	1.015	-0.445	1.000
4	40	0.006	-0.088	1.95e7	-0.167	3.311	-0.084	1.000
5	40	0.588	-0.001	121.479	-0.018	1.001	-0.017	1.000
6	40	0.632	-0.006	107.828	-0.006	1.000	-0.006	1.000
7	18	0.08	-0.058	9.782	-0.149	1.369	-0.148	1.000
8	61	0.092	-0.011	224.025	-0.028	1.247	-0.136	1.000
9	61	0.228	-0.007	275.896	-0.071	1.000	-0.076	1.000
10	33	0.242	0.016	-	-	-	-0.042	1.000
11	61	0.243	-0.002	43.797	-0.001	1.058	-0.001	1.000
12	28	2.008	-0.566	1.907	-0.251	1.000	-2.069	1.000
13	23	1.996	-1.19	1.184	-2.616	1.000	-2.972	1.000
14	23	1.754	-0.223	1.864	-0.983	1.220	-2.02	1.000
15	61	1.402	-0.365	5.712	-2.372	1.005	-1.383	1.000
16	23	1.115	-0.929	9.012	-0.383	1.022	-0.218	1.000
17	40	0.007	-4.317	105.073	-1.721	1.003	-2.084	1.000
18	63	-0.002	-0.066	2.121	-0.011	1.006	-0.01	1.000
19	28	3.286	-0.46	168.176	-0.636	1.002	-0.63	1.000
20	23	1.981	0.615	-	-	-	-2.64	1.000
21	23	1.859	-4.116	34.168	-4.109	1.458	-3.691	1.000
22	18	1.059	-0.276	4.797	-1.997	0.998	-1.995	1.000
23	33	0.738	-0.148	16.146	-1.698	0.988	-1.776	1.000
24	33	1.662	-1.148	6.267	-2.043	1.005	-1.948	1.000
25	23	1.333	-20.419	14.291	-2.797	1.000	-3.262	1.000
26	23	0.546	-0.268	9.05	-1.217	1.000	-1.638	1.000
27	23	-2.558	-2.559	8.679	-1.762	1.001	-1.927	1.000
28	23	0.251	0.067	-	-	-	-0.628	1.000
29	23	2.012	-7.614	4.497	-1.073	1.001	-0.879	1.000
30	28	0.139	-0.492	2.162	-0.99	0.999	-0.968	1.000
31	28	0.254	-1.523	1.056	-2.225	1.002	-1.499	1.000
32	33	0.191	-0.414	1.905	-2.222	0.998	-2.204	1.000
33	33	1.629	-1.102	3.045	-3.888	1.002	-3.861	1.000
34	33	0.117	-0.118	2.835	-1.667	1.000	-1.504	1.000
35	33	0.55	-0.523	3.516	-6.014	1.000	-7.346	1.000
36	23	0.26	-0.04	2.01	-0.054	1.482	-0.105	1.000

Legend:

Ex:	Test case	κ^0:	initial control parameter vector
α:	spectral abscissa of $T(\kappa^i, s)$	$\kappa^\sharp$:	control parameter vector after stabilization
$\|.\|_\infty$:	$\|T(\kappa^i, s)\|_\infty$	κ^*:	control parameter vector after optimization
systune:	H_∞-norm obtained by SYSTUNE	FRD_∞:	results for FRD method based on H_∞-norm
n_K:	dimension of parameter vector κ		

Table 8.2: Comparison of results for FRD design based on H_∞-norm minimization for infinite-dimensional systems and SYSTUNE for their approximations.

Ex	K	n_K	FRD_∞ $\alpha_0(.)$	FRD_∞ $\alpha(.)$	SYSTUNE $\alpha_{apx}(.)$	SYSTUNE $\alpha_{act}(.)$
1	2-SS	9	0	0	-36.49	0
2	2,1-TF	4	0	0	-0.006	0
3	3,0-TF	9	1e-4	9e-5	-0.121	6e-5
4	2-SS0	8	0.004	0	-0.001	0
5	3,1-TF	5	0	0	-8e-5	0
6	2,1-TF	4	1.609	1.591	0.965	x
7	2-SS	9	0.712	0	-0.001	0
8	1-SS	4	0.101	0	-0.109	0
9	1-SS	4	1.073	0	-3.086	0
10	3-SS	14	1.196	1.037	0.004	x
11	5-SS0	33	2.300	2.301	2.298	x
12	2-SS	9	0.459	0	-0.001	0
13	2-SS0	12	0	0	-0.060	0
14	2-SS0	12	0	0	-0.398	3.397
15	2-SS0	16	0	0	-0.001	0.733
16	2-SS0	20	0	0	-0.002	0
17	1-SS0	3	0	0	-0.002	0
18	1-SS0	3	0	0	-0.001	0
19	1-SS0	3	0	0	0.029	0.286
20	1-SS0	3	0	0	1.599	1.575
21	3-SS	14	0.839	0.013	-0.132	0.747
22	3,1-TF	5	0.135	0.134	0.048	x
23	1,0-TF	2	1.010	0	-3.055	7.071
24	2-SS0	8	0	0	-2.303	0
25	2-SS	9	0.014	0	-0.001	0.038

Legend:

Ex:	Test case		
n_K:	dimension of parameter κ	K:	controller structure
SYSTUNE :	results obtained by SYSTUNE	FRD_α:	results for FRD method based on abscissa
$\alpha_{apx}(.)$:	spectral abscissa of approximate $T(\kappa^*, s)$	$\alpha_0(.)$:	spectral abscissa of $T(\kappa^0, s)$
$\alpha_{act}(.)$:	spectral abscissa of actual $T(\kappa^0, s)$	$\alpha(.)$:	spectral abscissa of $T(\kappa^*, s)$
x:	not computed		

It is also interesting to note that the technique stabilizes a case where the others couldn't, but fails in a case where they succeded. An insight of these cases may help to improve a future combined FRD stabilizing technique. Unsurprisingly, for the already stable systems, the initial step based on small gain is sufficient to guarantee the design of a stabilizing controller.

For comments regarding the performance of SYSTUNE , please refer to the Discussion of chapter 6.

Chapter 9

Study case

In this chapter

a challenging robust control problem for a tail fin missile is consired. The unceratin system is subjected to a mixed uncertainty block comprising parametric uncertainties with a high number of repetitions. The robust syhnthesis using outer relaxations fails while the techniques based on inner and hybrid relaxation achieves similar performance.

Now it is considered the example of paper Aguiar et al. [2018] of this author, inspired on tail fin controlled missile described in Krueger [1993]. This system is already uncertain and new uncertainties are introduced to parameters of the system in this study. The closed-loop interconnection is presented in Fig. 9.1, showing the controller to be designed, K, the generalized plant P, composed of 5 blocks, the uncertainties, and the weights for the performance channels, W_e and W_d.

The missile dynamics, illustrated in Fig. 9.2, include the rigid body dynamics $G_{\mathtt{r}}$, three flexible modes of the system $G_{\mathtt{f}}$ in parallel with $G_{\mathtt{r}}$, and the actuators and sensors dynamics, which are represented by second-order systems $G_{\mathtt{act}}$,$G_{\mathtt{acc}}$, $G_{\mathtt{gyr}}$. The plant P features two additional performance and robustness filters W_e, W_d, which altogether leads to $n_P = 29$ states. The control input of the missile is the tail fin deflection angle d_f through the actuator $G_{\mathtt{act}}$ and the measured output is $y = [\eta_m \;\; q_m]^{\mathsf{T}}$, with acceleration η_m obtained from the accelerometer $G_{\mathtt{acc}}$ and pitch rate q_m obtained from the gyroscope $G_{\mathtt{gyr}}$. The actuator has a fin deflection limit of 40 deg. and a fin rate limit of 300 deg./s with description $u_{act} = G_{\mathtt{act}} \cdot d_f$ where

$$G_{\mathtt{act}}(s) = \frac{\omega_{\mathtt{act}}^2}{s^2 + 2 \cdot 0.7 \cdot \omega_{\mathtt{act}} s + \omega_{\mathtt{act}}^2}.$$

Similar second-order models are used for the accelerometer $G_{\mathtt{acc}}$ and the gyroscope $G_{\mathtt{gyr}}$, with numerical values given in Table 9.1.

The rigid body dynamics, $G_{\mathtt{r}}$ of the missile is described by the state-space representation below, where the input is provided by the actuator and the output is the vector $[\eta_{rigid} \; q_{rigid}]^{\mathsf{T}}$:

$$G_{\mathtt{r}}: \begin{aligned} \begin{bmatrix} \dot{\alpha} \\ \dot{q} \end{bmatrix} &= \begin{bmatrix} Z_\alpha & 1 \\ M_\alpha & M_q \end{bmatrix} \begin{bmatrix} \alpha \\ q \end{bmatrix} + \begin{bmatrix} Z_d \\ M_d \end{bmatrix} u_{act} \\ \begin{bmatrix} \eta_{\text{rigid}} \\ q_{\text{rigid}} \end{bmatrix} &= \begin{bmatrix} V/kG\, Z_\alpha & 0 \\ 0 & 1 \end{bmatrix} \begin{bmatrix} \alpha \\ q \end{bmatrix} + \begin{bmatrix} V/kG\, Z_d \\ 0 \end{bmatrix} u_{act}. \end{aligned}$$

Three flexible modes are added to represent the bending dynamics of the missile.

$$G_{\mathtt{f}}: \begin{bmatrix} \eta_{\text{flex}} \\ q_{\text{flex}} \end{bmatrix} = \sum_{i=1}^{3} \begin{bmatrix} \eta_i(s) \\ q_i(s) \end{bmatrix} u_{act},$$

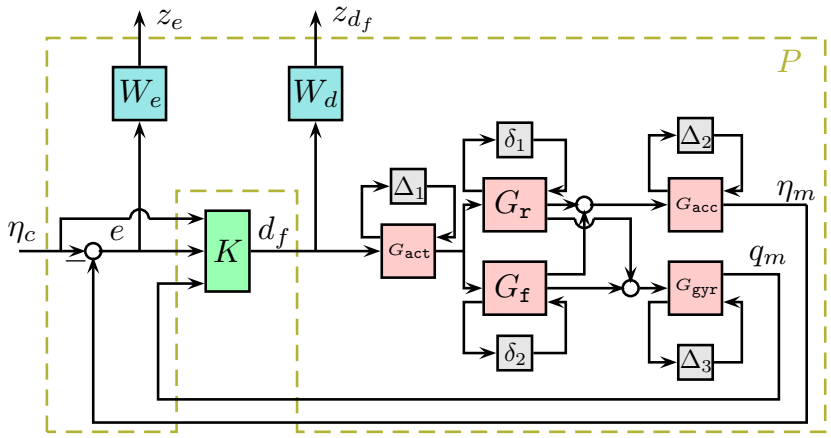

Figure 9.1: Interconnection of plant subsystems, uncertainty blocks and controller.

Table 9.1: Values and uncertainty of the missile parameters

Parameter	Nominal	Uncertainty	Parameter	Nominal	Uncertainty
Z_a	-5.24	$\pm 30\%$	Z_d	-0.73	0
M_a	-46.97	$\pm 15\%$	M_d	-1134	0
M_q	-4.69	$\pm 30\%$	V/kG	1.182	0
ω_1	368	$\pm 15\%$	$\omega_{\mathtt{acc}}$	188.5	0
ω_2	937	$\pm 15\%$	$\omega_{\mathtt{act}}$	377.0	0
ω_3	1924	$\pm 15\%$	$\omega_{\mathtt{gyr}}$	500.0	0
K_{η_1}	-0.943	0	K_{q_1}	1024.1	0
K_{η_2}	0.561	0	K_{q_2}	406.5	0
K_{η_3}	-0.312	0	K_{q_3}	-1408.4	0

where

$$\begin{bmatrix}\eta_i(s)\\ q_i(s)\end{bmatrix} = \frac{1}{s^2 + 2\cdot 0.02\cdot\omega_i s + \omega_i^2}\begin{bmatrix}s^2 K_{\eta_i}\\ sK_{q_i}\end{bmatrix},$$

$i = 1, 2, 3$, and then the overall dynamics are

$$\begin{bmatrix}\eta\\ q\end{bmatrix} = \begin{bmatrix}\eta_{\text{rigid}}\\ q_{\text{rigid}}\end{bmatrix} + \begin{bmatrix}\eta_{\text{flex}}\\ q_{\text{flex}}\end{bmatrix}.$$

The final measured outputs are then $\eta_m = G_{\mathtt{acc}}\cdot\eta$ and $q_m = G_{\mathtt{gyr}}\cdot q$. The values of the parameters of the plant and their respective ranges are presented in Table 9.1.

Unmodeled high frequency dynamics at the actuator and sensor locations are assumed as of 0.1% uncertain at low frequency, and of 100% at high frequency. Explicitly, this corresponds to including the weight

$$W^{\Delta}_{\mathtt{act}}(s) = \frac{(s+\omega_{\mathtt{act}})^2}{(s+10\cdot\omega_{\mathtt{act}})(s+100\cdot\omega_{\mathtt{act}})},$$

for the actuator, and similarly, for accelerometer and gyrometer with their respective frequencies $\omega_{\mathtt{acc}}$ and $\omega_{\mathtt{gyr}}$, shown in Table 9.1.

Gathering all uncertain blocks for the missile yields $\Delta = \text{diag}\,[\Delta_p, \Delta_d]$, with $\Delta_p = \text{diag}\,\left[\delta_{Z_\alpha}, \delta_{M_\alpha}, \delta_{M_q}; \delta_{\omega_1} I_6, \delta_{\omega_2} I_6, \delta\right.$ and $\Delta_d = \text{diag}\,\left[\Delta_{\mathtt{act}}, \Delta_{\mathtt{acc}}, \Delta_{\mathtt{gyr}}\right]$. Table 9.2 summarizes the uncertainty in the system, where negative values represents repetitions of each parametric uncertainty and positive values specifies the dimension of square MIMO LTI dynamic uncertainty. Figure 9.2 illustrates the disturbance in singular values.

Finally, the performance weights were chosen to reflect the following design requirements: Firstly, acceleration η_m should track the command η_c with a rise time of about 0.5 seconds. Hence the weighting function $W_e(s)$ for the transfer function from η_c to the tracking error $e := \eta_c - \eta_m$ was chosen as $W_e(s) := \frac{1}{100}\frac{s/10+100}{s/10+0.05}$.

Table 9.2: Missile Plant

Δ-structure		n_P	z-w	y-u
mixed	-1,-1,-1,-6,-6,-6,1,1,1	29	2 1	3 1

Secondly, for robustness, the high-frequency rate of variation of the control signal and roll-off are captured and penalized through the constraint $||W_d(s)T_{d_f\eta_c}||_\infty \leq 1$, where $W_d(s)$ is a high-pass weighting $W_d(s) := (s/200(0.001s+1))^2$. This also permits to meet the imposed actuator deflection magnitude and rate limits of respectively 40 deg. and 300 deg./sec. Altogether the regulated output is $z = [W_e e \;\; W_d d_f]^\mathsf{T} = [z_e \;\; z_{d_f}]^\mathsf{T}$.

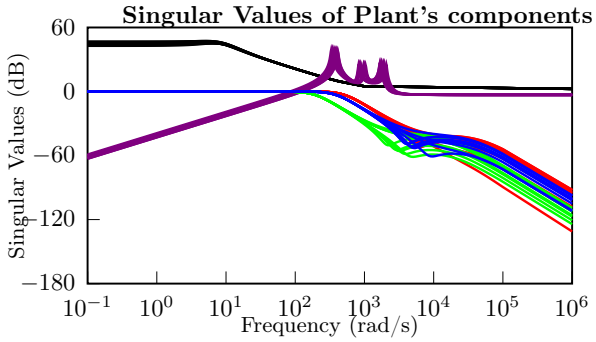

Figure 9.2: Singular values of the uncertain subsystems of the plant.

Using the methods discussed in this work, robust controllers K of order 6 are computed with 3 inputs η_c, $e = \eta_c - \eta_m$, and q_m, and one output d_f.

The results are presented in Table 9.3. The *hybrid* and *inner* relaxation methods found controllers with very similar performance, whereas the *outer* relaxation approach was not able to find a solution. The performance value returned by `DKSYN` was Inf, meaning that it could not find a solution either.

Table 9.3: Results for missile synthesis

n_K	*inner*			*hybrid*			*outer*	
	gain	certified	$\lvert\Delta_a\rvert$	gain	certified	$\lvert\Delta_{p,a}\rvert$	gain	certified
6	0.4310	0.4353	13	0.4416	0.4409	6	-	-

Responses of η_m, q_m and δ_c to η_c step inputs are shown in Fig. 9.3a for *inner* and in Fig. 9.3b for *hybrid* . Both of theses techniques were able to achieve prescribed design requirements.

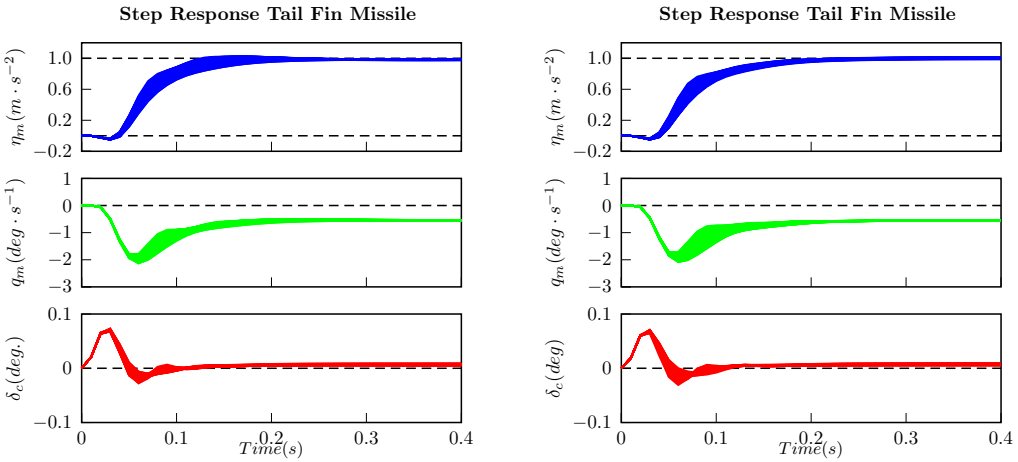

(a) Step responses obtained by inner relaxation technique

(b) Step responses obtained by hybrid relaxation technique

Figure 9.3: Step responses of the closed-loop system for the Tail Fin Missile.

Chapter 10

Discussion and conclusion

In this thesis, it was presented three novel relaxations for the robust control problem implemented by nonsmooth optimization techniques and three new methods for frequency-response data based design of controllers.

10.1 Contributions

The results of this work concern and constitute contributions to domains of robust control, frequency-response data based control, and control of infinite-dimensional systems.

Robust Control

One of the problems studied in this thesis is the H_∞ robust structured control of systems subjected to structured mixed uncertainty. In this subdomain, the structure of the uncertainty and the domain of each block are exploited in order to reduce the conservatism of the control solution. However, dealing with such uncertainties renders the robust control problem highly complex to the point that is not amenable to computation by the current technology. In this context, the main contributions of this thesis are:

- Development of a novel outer approximation with multipliers based on topological separator by nonsmooth optimization. The implementation allows multipliers and controller to be tunned simultaneously to stabilize and improve performance. In addition, the uncertainty is never rescaled during the synthesis and the performance achieved is valid on the modeled uncertainty.
- Development of a novel inner approximation based on worst-case estimation and multi-model synthesis by nonsmooth optimization. This relaxation leads to the best performance achieved among all methods tested in this thesis, including a commercial routine.
- Development of a hybrid relaxation of the robust control problem for mixed dynamic and parametric structured uncertainty with a combination of inner and outer relaxations developed that is computationally attractive on limited computational power applications.

FRD control synthesis

- Development of a spectral abscissa estimator for IDLTI systems that are meromorphic on the left-half complex plane.
- Development of three techniques for synthesis of structured controllers for unstable and stable IDLTI systems by FRD synthesis, with direct stability and performance estimation.

10.2 Limitations

- The main limitation of the outer relaxation developed is common to all outer relaxations: conservatism occurs for systems subjected to structured uncertainty with a large number of blocks

of parametric uncertainties and/or blocks of parametric uncertainty with large number of repetitions. In the presented method, the multipliers required to cover the uncertainty of such systems demand a high number of parameters to be tuned. This leads to optimization problems that can be too challenging for current optimization tools, not even reaching a good local solution.

- The main limitation of FRD design methods, as well as of all data-driven methods, is related to the correct choice of the sampling. In design based on the frequency response this is translated as the choice of frequency grid. The initial grid can be suited for the plant to be controlled but the feedback with a controller may generate new resonant peaks or shift the location of the original ones, and thus analysis on this range may reverberate on stability analysis. This is more critical in design for infinite-dimensional systems that potentially have an infinite number of resonant peaks which may demand a large range of frequency samples. In conclusion, the whole method is built upon the assumption that the necessary samples of the response are available.

- Another limitation of the developed method based on minimization of abscissa spectral is the nonsmooth character of the function to be minimized. Although in the majority of cases this poses no problem, it can be the cause of disruption in specific cases, preventing the search to progress.

10.3 Future work suggestions

- This thesis focus on H_∞ robust control. However the relaxations proposed can be applied to H_2 control with the following considerations. The outer relaxation implementation with an H_2 performance criterion plus small gain conditions, being H_∞ conditions, will lead to a mixed H_2/H_∞ synthesis. This considers that dynamic uncertainty remains bounded LTI systems and parametric uncertainty remains box constrained. The inner relaxation will demand an additional modification. In the iterative procedure, the nonsmooth solver for finding H_∞ worst-cases should be adapted to find H_2 worst-cases. This should not pose a problem considering that H_2 norm is easier to handle due to smoothness of the objective function.

- The spectral estimator can be improved by implementing more sofisticated heuristics instead of bisection algorithm, as tree search, galloping search, not to mention heuristic searches. This would potentially improve the speed of convergence, but according to current experience, not the result itself. Moreover, the estimator could also be extended to estimate spectral abscissa with no prior knowledge of pole locations. This can be made possible through a suitable griding of the plane and an initial sufficiently large shift. This would also allow estimation of negative values of the spectral abscissa.

- Another suggestion for improving results in terms of rate of success of the methods based on energy and spectral abscissa is the specialization of optimization routines. Currently, they were implemented with the aid of generic optimization routines that do not exploit all particularities of each function.

Bibliography

Abroug, N., Lamy, X., and Laroche, E. Human force augmentation: Optimal control parameters tuning using structured h_∞ synthesis. In *Int. Conf. Intelligent Robots and Systems*, Daejeon, South Korea, October 2016. https://doi.org/10.1109/IROS.2016.7759129. 6

Abusaksaka, A. B. and Partington, J. R. BIBO stability of some classes of delay systems and fractional systems. *Systems & Control Letters*, 64:43–46, February 2014. https://doi.org/10.1016/j.sysconle.2013.11.009. X, XII

Ackermann, J. Multi-model approaches to robust control system design. In Ackermann, J., editor, *Uncertainty and Control: Proc. Int. Seminar Organized by Deutsche Forschungs- und Versuchsanstalt für Luft- und Raumfahrt (DFVLR) Bonn, Germany, May, 1985*, volume 70 of *Lecture Notes in Control and Information Sciences*, pages 108–130. Springer, Berlin, Heidelberg, 1985. https://doi.org/10.1007/BFb0007282. 5, 6

Aguiar, R. S. S., Apkarian, P., and Noll, D. Structured robust control against mixed uncertainty. *IEEE Trans. Control Systems Technology*, 26(5):1771–1781, 2018. https://doi.org/10.1109/TCST.2017.2723864. 24, 36, 46, 77, XXII, XXIII, XLII

Apkarian, P. and Noll, D. Nonsmooth optimization for multidisk H_∞ synthesis. *European J. Control*, 12(3):229–244, 2006a. https://doi.org/10.3166/ejc.12.229-244. 6, 16, 17, 27, 37, XIII, XIX, XXIII

Apkarian, P. and Noll, D. Frequency domain H_∞ synthesis using nonsmooth techniques. In *IEEE Conf. Industrial Electronics and Applications*, Singapore, 2006b. https://doi.org/10.1109/ICIEA.2006.257082. 6, 17, XIX

Apkarian, P. and Noll, D. Controller design via nonsmooth multidirectional search. *SIAM J. Control and Optimization*, 44(6):1923–1949, 2006c. https://doi.org/10.1137/S0363012904441684. 6, 59, XXXV

Apkarian, P. and Noll, D. Nonsmooth H_∞ synthesis. *IEEE Trans. Autom. Control*, 51(1):71–86, Jan. 2006d. https://doi.org/10.1109/TAC.2005.860290. 6, 17, XIX

Apkarian, P. and Noll, D. Worst-case stability and performance with mixed parametric and dynamic uncertainties. *Int. J. Robust and Nonlinear Control*, 27(8):1284–1301, May 2017. https://doi.org/10.1002/rnc.3628. 6, 21, 22, 23, 36, 37, 42, XXI, XXVI

Apkarian, P. and Noll, D. Structured H_∞-control of infinite-dimensional systems. *Int. J. Robust and Nonlinear Control*, 28(9):3212–3238, June 2018. https://doi.org/10.1002/rnc.4073. 7, 60, 63, 66, 68, 72, 73, III, XXXV, XXXVIII, XLII

Apkarian, P., Noll, D., and Alazard, D. Controller design via nonsmooth multi-directional search. In *IFAC Proc. Volumes*, volume 37, December 2004. https://doi.org/10.1016/S1474-6670(17)30493-7. 6

Apkarian, P., Noll, D., and Pellanda, P. C. Nonsmooth h_∞ synthesis. In *World Congress on Structural and Multidisciplinary Optimization*, Rio de Janeiro, Brazil, May 2005. http://pierre.apkarian.free.fr/papers/Nonsmooth_Hinf_Conf.pdf. 6

Apkarian, P., Gahinet, P., and Buhr, C. Multi-model, multi-objective tuning of fixed-structure controllers. In *European Control Conf.*, pages 856–861, Strasbourg, France, June 2014. https://doi.org/10.1109/ECC.2014.6862200. 6, 17, 37, XIX

Apkarian, P., Dao, M. N., and Noll, D. Parametric robust structured control design. *IEEE Trans. Autom. Control*, 60(7):1857–1869, July 2015a. https://doi.org/10.1109/TAC.2015.2396644. 6, 21, 36, 37, 38, 43, XXI, XXVI

Apkarian, P., Noll, D., and Ravanbod, L. Computing the structured distance to instability. In *Proc. SIAM Conf. Control and its Applications*, pages 423–430, Paris, France, 2015b. https://doi.org/10.1137/1.9781611974072.58. 5, 6, 21, 37, 42, 43, XXI, XXVI

Apkarian, P., Noll, D., and Ravanbod, L. Nonsmooth bundle trust-region algorithm with applications to robust stability. *Set-Valued and Variational Anal.*, 24(1):115–148, March 2016. https://doi.org/10.1007/s11228-015-0352-5. 5, 37, 38, XXVI

Asai, T., Hara, S., and Iwasaki, T. Simultaneous modeling and synthesis for robust control by LFT scaling. In *IFAC Proc. Volumes*, volume 29, pages 3180–3185, July 1996. https://doi.org/10.1016/S1474-6670(17)58165-3. 5, 24

Avanessoff, D., Fioravanti, A. R., and Bonnet, C. YALTA: a matlab toolbox for the H_∞-stability analysis of classical and fractional systems with commensurate delays. In *IFAC Symp. System Structure and Control*, Grenoble, France, February 2013. https://doi.org/10.3182/20130204-3-FR-2033.00222. 63

Balas, M. J. Trends in large space structure control theory: Fondest hopes, wildest dreams. *IEEE Trans. Automatic Control*, 27(3):522–535, June 1982. https://doi.org/10.1109/TAC.1982.1102953. 2, 63, II, XXXVI

Balas, M. J. The Galerkin method and feedback control of linear distributed parameter systems. *J. of Mathematical Analysis and Applications*, 91(2):527–546, February 1983. https://doi.org/10.1016/0022-247X(83)90167-1. 2, 57

Balas, M. J. Linear distributed parameter systems: Closed-loop exponential stability with a finite-dimensional controller. *Automatica*, 20(3):371–377, May 1984. https://doi.org/10.1016/0005-1098(84)90053-0. 2

Balas, M. J. Suboptimality and stability of linear distributed-parameter systems with finite-dimensional controllers. *J. of Optimization Theory and Applications*, 45(1):1–19, January 1985. https://doi.org/10.1007/BF00940809. 2, 5

Balas, M. J. Finite- dimensional control of distributed parameter systems by Galerkin approximation of infinite dimensional controllers. *J. Mathematical Analysis and Applications*, 114(1):17–36, 1986. https://doi.org/10.1016/0022-247X(86)90062-4. 2, 57

Barmish, B. R. and Lagoa, C. M. The uniform distribution: rigorous justification for its use in robustness analysis. In *Proc. IEEE Conf. Decision and Control*, Kobe, Japan, December 1996. https://doi.org/10.1109/CDC.1996.573689. 5

Barmish, B. R. and Lagoa, C. M. The uniform distribution: A rigorous justification for its use in robustness analysis. *Mathematics of Control, Signal, and Systems*, 10(3):203–222, September 1997. https://doi.org/10.1007/BF01211503. 5

Benner, P., Mitchell, T., and Overton, M. L. Low-Order Control Design using a Reduced-Order Model with a Stability Constraint on the Full-Order Model. *ArXiv e-prints*, March 2018. http://adsabs.harvard.edu/abs/2018arXiv180306549B. 6

Bhole, M., Patil, M., and Vyawahare, V. The design of a non-minimal state space fractional-order predictive functional controller for fractional systems of arbitrary order. *J. of Process Control*, 29:45–56, May 2015. https://doi.org/10.1016/j.jprocont.2015.03.004. 3

Bonnet, C. and Partington, J. R. Coprime factorizations and stability of fractional differential systems. *Systems & Control Letters*, 41(3):167–174, October 2000a. https://doi.org/10.1016/S0167-6911(00)00050-5. 3, X, XII

Bonnet, C. and Partington, J. R. Stabilization of fractional exponential systems including delays. *IFAC Proc. Volumes*, 33(23):57–60, September 2000b. https://doi.org/10.1016/S1474-6670(17)36916-1. 3, 15

Bonnet, C. and Partington, J. R. Analysis of fractional delay systems of retarded and neutral type. *Automatica*, 38(7):1133–1138, July 2002. https://doi.org/10.1016/S0005-1098(01)00306-5. 3, 15

Bonnet, C. and Partington, J. R. Stabilization of some fractional delay systems of neutral type. *Automatica*, 43(12):2047–2053, December 2007. https://doi.org/10.1016/j.automatica.2007.03.017. 3

Bonnet, C., Fioravanti, A. R., and Partington, J. R. Stability of neutral systems with commensurate delays and poles asymptotic to the imaginary axis. *SIAM J. Control and optimization*, 49(2):498–516, 2011. https://doi.org/10.1137/090776275. XII

Braatz, R. P., Young, P. M., Doyle, J., and Morari, M. Computational complexity of μ calculation. *IEEE Trans. Automatic Control*, 39(5):1000–1002, May 1994. https://doi.org/10.1109/9.284879. 5

Bresch-Pietri, D., Prieur, C., and Trélat, E. Feedback stabilization of a 1d linear reaction-diffusion equation with delay boundary control. *IEEE Trans. Automatic Control*, early access, 2018. https://doi.org/10.1109/TAC.2018.2849560. 2

Burke, J. V., Lewis, A. S., and Overton, M. L. A robust gradient sampling algorithm for nonsmooth, nonconvex optimization. *SIAM J. Optimization*, 15(3):751–779, 2005. https://doi.org/10.1137/030601296. 6

Burke, J. V., Henrion, D., Lewis, A. S., and Overton, M. L. HIFOO – a matlab package for fixed-order controller design and H_∞ optmization. *Proc. IFAC Symp. Robust Control Design*, 39:339–344, July 2006. https://doi.org/10.3182/20060705-3-FR-2907.00059. 6

Calafiore, G. C. and Campi, M. C. The scenario approach to robust control design. *IEEE Trans. Autom. Control*, 51(5):742–753, May 2006. https://doi.org/10.1109/TAC.2006.875041. 5

Chiang, R. Y. and Safonov, M. G. Real Km-synthesis via generalized popov multipliers. In *Proc. American Control Conf.*, Chicago, USA, June 1992. https://ieeexplore.ieee.org/document/4792569/. 4, 19, XX

Curtain, R. F. Finite dimensional compensators for parabolic distributed systems with unbounded control and observation. *SIAM J. Control and optimization*, 22(2):255–276, 1984. https://doi.org/10.1137/0322018. 2

Curtain, R. F. Pole assignment for distributed systems by finite-dimensional control. *Automatica*, 21(1):57–67, January 1985. https://doi.org/10.1016/0005-1098(85)90098-6. 2

Curtain, R. F. and Zwart, H. J. *An introduction to Infinite Dimensional Linear systems*. Springer, Berlin, 1995. 11, 13, XIX

Curtain, R. Representations of infinite-dimensional systems. In Nijmeijer, H. and Schumacher, J. M., editors, *Three Decades of Mathematical System Theory*, volume 135 of *Lecture Notes in Control and Information Sciences*. Springer, Berlin, Heidelberg, 1989. https://doi.org/10.1007/BFb0008460. 2

Curtain, R. Finite-dimensional robust controller designs for distributed parameter systems: A survey. In Davisson, L., editor, *Robust Control*, volume 183 of *Lecture Notes in Control and Information Sciences*. Springer, Berlin, Heidelberg, 1992. https://doi.org/10.1007/BFb0114653. 2

Curtain, R. and Glover, K. Robust stabilization of infinite dimensional systems by finite dimensional controllers. *Systems & Control Letters*, 7(1):41–47, February 1986. https://doi.org/10.1016/0167-6911(86)90100-3. 4, 57

Desoer, C. A. and Wang, Y. T. On the generalized Nyquist stability criterion. In *Proc. IEEE Conf. Decision and Control*, Fort Lauderdale, USA, December 1979. https://dx.doi.org/10.1109/CDC.1979.270248. XXI

Dorcak, L., Petras, I., Kostial, I., and Terpak, J. State-space controller design for the fractional-order regulated system. In *Proceedings of ICCC'2001*, Krynica, Poland, May 2001. https://arxiv.org/abs/math/0204189. 3

Doyle, J. C. Analysis of feedback systems with structured uncertainties. *IEE Proc. D - Control Theory and Applications*, 129(6):242–250, November 1982. https://doi.org/10.1049/ip-d:19820053. 4, 13, 17, 19, XIV, XX

Doyle, J. C. Structured uncertainty in control system design. In *Proc. IEEE Conf. Decision and Control*, Fort Lauderdale, USA, December 1985. https://doi.org/10.1109/CDC.1985.268842. 4, 5, 19, 30, XX, XXIV

Doyle, J., Glover, K., Khargonekar, P., and Francis, B. State-space solutions to standard H_2 and H_∞ control problems. *IEEE Trans. Automatic Control*, 34(8):831–847, August 1989. https://doi.org/10.1109/9.29425. 16

Dym, H., Helton, J. W., and Merino, O. Algorithms for solving multidisk problems in H_∞ optimization. In *Proc. IEEE Conf. Decision and Control*, Phoenix, USA, December 1999. https://doi.org/10.1109/CDC.1999.831422. 6

Dym, H., Helton, J. W., and Merino, O. Multidisk problems in H_∞ optimization: A method for analysing numerical algorithms. *Indiana University Mathematics J.*, 51(5):1111–1159, 2002. http://www.jstor.org/stable/24902868. 6

Eisenberg, L. "rational delay-function approximations to e^x. *Electronics Letters*, 7(10):248–249, May 1971. https://doi.org/10.1049/el:19710169. 15

Fan, M. K. H. and Tits, A. L. A measure of worst-case H_∞ performance and of largest acceptable uncertainty. *Systems & Control Letters*, 18(6):409–421, June 1992. https://doi.org/10.1016/0167-6911(92)90044-S. XIV

Fan, M. K. H., Tits, A. L., and Doyle, J. C. Robustness in the presence of mixed parametric uncertainty and unmodeled dynamics. *IEEE Trans. Autom. Control*, 36(1):25–38, January 1991. https://doi.org/10.1109/9.62265. 4, 19, XX

Fioravanti, A. *H_∞ analysis and control of time-delay systems by methods in frequency domain*. Ph.D. dissertation, Université Paris Sud - Paris XI, Paris, France, 2011. https://tel.archives-ouvertes.fr/tel-00627352. X, XII

Fioravanti, A., Bonnet, C., Ozbay, H., and Niculescu, S. A numerical method to find stability windows and unstable poles for linear neutral time-delay systems. *IFAC Proceedings Volumes*, 43(2):183–188, 2010. https://doi.org/10.3182/20100607-3-CZ-4010.00034. 63

Gahinet, P. A convex parametrization of H_∞ suboptimal controllers. In *Proc. IEEE Conf. Decision and Control*, Tucson, USA, December 1992. https://doi.org/10.1109/CDC.1992.371588. 6

Gahinet, P. and Apkarian, P. A linear matrix inequality approach to H_∞ control. *Int. J. Robust and Nonlinear Control*, 4(4):421–448, 1994. https://doi.org/10.1002/rnc.4590040403. 6, 16

Galdos, G., Karimi, A., and Longchamp, R. Robust loop shaping controller design for spectral models by quadratic programming. In *Proc. IEEE Conf. Decision and Control*, New Orleans, USA, December 2007. https://doi.org/10.1109/CDC.2007.4434449. 6

Galdos, G., Karimi, A., and Longchamp, R. H_∞ controller design for spectral MIMO models by convex optimization. In *European Control Conf.*, budapest, Hungary, August 2009. https://ieeexplore.ieee.org/document/7074842. 7

Galdos, G., Karimi, A., and Longchamp, R. H_∞ controller design for spectral MIMO models by convex optimization. *J. of Process Control*, 20(10):1175–1182, December 2010. https://doi.org/10.1016/j.jprocont.2010.07.006. 6

Gibson, J. S. A note on stabilization of infinite dimensional linear oscillators by compact linear feedback. *SIAM J. Control and Optimization*, 18(3):311–316, 1980. https://doi.org/10.1137/0318022. 2

Gu, G., Khargonekar, P. P., Lee, E. B., and Misra, P. Finite-dimensional approximations of unstable infinite-dimensional systems. *SIAM J. Control and Optimization*, 30(3):701–716, 1992. https://doi.org/10.1137/0330039. 63

Hamer, A. J., Weiland, S., and Steinbuch, M. Model-free norm-based fixed structure controller synthesis. In *Proc. IEEE Conf. Decision and Control*, Shanghai, China, December 2009a. https://doi.org/10.1109/CDC.2009.5400924. 8

Hamer, A. J., Weiland, S., and Steinbuch, M. Worst case inter frequency grid behavior of transfer functions identified via finite frequency response data. In *European Control Conf.*, Budapest, Hungary, August 2009b. https://doi.org/10.23919/ECC.2009.7074446. 6

Helvoort, J., Jager, B., and Steinbuch, M. Sufficient conditions for data-driven stability of ellipsoidal unfalsified control. In *Proc. IEEE Conf. Decision and Control*, San Diego, USA, December 2006. https://doi.org/10.1109/CDC.2006.376826. 6

Herrera, J., Ibeas, A., Sen, M., Alcántara, S., and Alonso-Quesada, S. Identification and control of delayed unstable and integrative LTI MIMO systems using pattern search methods. *Advances in Difference Equations*, 2013(331), 2013. https://doi.org/10.1186/1687-1847-2013-331. XI

Heusden, K., Karimi, A., and Bonvin, D. Data-driven controller tuning with integrated stability constraint. *Int. J. Adaptive Control and Signal processing*, 25(4):331–351, September 2010. https://doi.org/10.1002/acs.1212. 8

Higham, N. J. Optimization by direct search in matrix computations. *SIAM J. Matrix Analysis and Applications*, 14(2):317–333, 1993. https://doi.org/10.1137/0614023. XV

Higham, N. J. The matrix computation toolbox, 2002. http://www.ma.man.ac.uk/~higham/mctoolbox. 59, XV, XXXV

Hjalmarsson, H. Iterative feedback tuning: an overview. *Int. J. Adaptive Control Signal Process.*, 16: 373–395, 2002. https://doi.org/10.1002/acs.714. 6

Hu, Z., Salcudean, S. E., and Loewen, P. D. Multiple objective control problems via nonsmooth analysis. In *IFAC Proc. Volumes*, volume 29, pages 1392–1397, July 1996. https://doi.org/10.1016/S1474-6670(17)57861-1. 6

Huang, H. P., Jiang, C. T., and Chao, Y. C. A new Nyquist test for the stability of control systems. *Int. J. Control*, 58(1):97–112, December 1993. https://dx.doi.org/10.1080/00207179308922993. 22, XXI

Hunt, K., Sbarbaro, D., Zbikowski, R., and Gawthorp, P. Neural networks for control systems—a survey. *Automatica*, 28(6), Novemebr 1992. https://doi.org/10.1016/0005-1098(92)90053-I. 6

Iwasaki, T. and Hara, S. Well-posedness of feedback systems: insights into exact robustness analysis and approximate computatios. *IEEE Trans. Autom. Control*, 43(5):619–630, May 1998. https://doi.org/10.1109/9.668829. 5, 12, 13, 19, 20, 24, 33, XX, XXII

Iwasaki, T. and Skelton, R. E. A complete solution to the general H_∞ control problem: LMI existence conditions and state space formulas. In *Proc. American Control Conf.*, San Francisco, USA, June 1993. http://ieeexplore.ieee.org/document/4792928/. 6

Iwasaki, T. and Skelton, R. E. All controllers for the general H_∞ control problem: LMI existence conditions and state space formulas. *Automatica*, 30(8):1307–1317, August 1994. https://doi.org/10.1016/0005-1098(94)90110-4. 6, 16, 17, XIX

Karimi, A. and Galdos, G. Fixed-order H_∞ controller design for nonparametric models by convex optimization. *Automatica*, 46(8):1388–1394, August 2010. https://doi.org/10.1016/j.automatica.2010.05.019. 7

Karimi, A. and Kammer, C. A data-driven approach to robust control of multivariable systems by convex optimization. *Automatica*, 85:227–233, 2017. http://dx.doi.org/10.1016/j.automatica.2017.07.063. 7

Karimi, A. and Zhu, Y. Robust H_∞ controller design using frequency-domain data. In *IFAC Proc.*, pages 4921–4926, Cape Town, South Africa, August 2014. https://doi.org/10.3182/20140824-6-ZA-1003.01802. 7

Karimi, A., Galdos, G., and Longchamp, R. Robust fixed-order H_∞ controller design for spectral models by convex optimization. In *Proc. IEEE Conf. Decision and Control*, Cancun, Mexico, December 2008. https://doi.org/10.1109/CDC.2008.4739130. 7

Karimi, A., Nicoletti, A., and Zhu, Y. Robust H_∞ controller design using frequency-domain data via convex optimization. *Int. J. Robust and Nonlinear Control*, July 2016. https://dx.doi.org/10.1002/rnc.3594. 55

Kashima, K. and Yamamoto, Y. On standard H_∞ control problems for systems with infinitely many unstable poles. *Systems & Control Letters*, 57(4):309–314, April 2008a. https://doi.org/10.1016/j.sysconle.2007.09.008. 3

Kashima, K. and Yamamoto, Y. Finite rank criteria for control of infinite-dimensional systems. *IEEE Trans. Automatic Control*, 53(4):881–893, May 2008b. https://dx.doi.org/10.1109/TAC.2008.920230. 3

Keel, L. H. and Bhattacharyya, S. P. Controller synthesis free of analytical models: Three term controllers. *IEEE Trans. Automatic Control*, 55(11):2650–2654, November 2010. https://doi.org/10.1109/TAC.2010.2067390. 8

Krueger, D. L. *Parametric Uncertainty Reduction in Robust Multivariable Control*. Ph.D. dissertation, Dept. Elect. Comp. Eng., Naval Postgraduate School, Monterey, CA, 1993. 77, XLII

Landau, I. D. A survey of model reference adaptive techniques—theory and applications. *Automatica*, 10(4):353–379, 1974. https://doi.org/10.1016/0005-1098(74)90064-8. 6

Lanusse, P., Oustaloup, A., and Mathieu, B. Third generation CRONE control. In *Int. Conf. Systems, Man and Cybernetics*, pages 1007–1009, Le Touquet, France, October 1993. https://doi.org/10.1109/ICSMC.1993.384864. 3

Lanusse, P., Malti, R., and Melchior, P. CRONE control system design toolbox for the control engineering community: tutorial and case study. *Philosophical Trans. A Mathematical, Physical and Engineering Sciences*, 371(1990), May 2013. https://doi.org/10.1098/rsta.2012.0149. 63

Leibfritz, F. COMPleib:constrained matrix-optimization problemlibrary-a collection of test examples for nonlinear semidefinite programs, control system design and related problems, 2004. http://www.friedemann-leibfritz.de/COMPlib_Data/COMPlib_Main_Paper.pdf. II, IX, XXXV

Limebeer, D. J. N. and Kasenally, E. M. Necessary and sufficient conditions for the existence of H_∞-optimal controllers: An interpolation approach. In Kaashoek, M. A., van Schuppen, J. H., and Ran, A. C. M., editors, *Int. J. Robust and Nonlinear Control*, volume 4 of *Robust Control of Linear Systems and Nonlinear Control. Progress in Systems and Control Theory*, pages 309–316. Birkhäuser Boston, 1990. https://doi.org/10.1007/978-1-4612-4484-4_29. 16

Loiseau, J. J. and Mounier, H. Stabilisation de l'equation de la chaleur commandée en flux. *Proc. ESAIM*, 5:131–144, August 2002. https://doi.org/10.1051/proc:1998003. X

MacFarlane, A. G. J. and Postlethwaite, I. The generalized Nyquist stability criterion and multivariable root loci. *Int. J. Control*, 25(1):81–127, 1977. https://doi.org/10.1080/00207177708922217. 7

Magni, J. F., Gorrec, Y. L., and Chiappa, C. A multimodel-based approach to robust and self-scheduled control design. In *Proc. IEEE Conf. Decision and Control*, Tampa, USA, December 1998. https://doi.org/10.1109/CDC.1998.757950. 5, 6, 43

Mammadov, M. A. and Orsi, R. H_∞ synthesis via a nonsmooth, nonconvex optimization approach. *Pacific J. Optimization*, 1(2):405–420, 2005a. https://www.researchgate.net/publication/228355179_H_synthesis_via_a_nonsmooth_nonconvex_optimization_approach. 6

Mammadov, M. A. and Orsi, R. A nonsmooth optimization approach to H_∞ synthesis. In *Proc. IEEE Conf. Decision and Control and European Control Conf.*, Seville, Spain, December 2005b. https://doi.org/10.1109/CDC.2005.1583271. 6

Maruta, I., H.Kim, T., and Sugie, T. Synthesis of fixed-structure H_∞ controllers via constrained particle swarm optimization. In *IFAC Proc. Volumes*, volume 41, pages 7843–7848, 2008. https://doi.org/10.3182/20080706-5-KR-1001.01326. 17

MathWorks. Matlab, 2017. https://fr.mathworks.com/help. 27, 30, 37, 39, 49, 66, XIII, XV, XXIII, XXIV, XXXVIII

Matignon, D. Stability properties for generalized fractional differential systems. *Proc. ESAIM*, 5: 145–158, 1998. https://doi.org/10.1051/proc:1998004. 3, 14, 64

Megretski, A. and Rantzer, A. System analysis via integral quadratic constraints. *IEEE Trans. Automatic Control*, 42(6):819–830, June 1997. https://doi.org/10.1109/9.587335. 19

Meinsma, G. and Zwart, H. On H_∞ control for dead-time systems. *IEEE Trans. Automatic Control*, 45(2):272–285, February 2000. https://doi.org/10.1109/9.839949. 3, XI

Menezes, E. F. M., Aguiar, R. S. S., Simões, A. M., and Apkarian, P. Structured robust controller design via non-smooth mixed μ synthesis. *IET Control Theory & Applications*, 10(7):2186–2193, November 2016. https://doi.org/10.1049/iet-cta.2016.0570. 24, 36, 46

Mignot, R., Hélie, T., and Matignon, D. On the singularities of fractional differential systems, using a mathematical limiting process based on physical grounds. *Physica Scripta*, 2009. https://doi.org/10.1088/0031-8949/2009/T136/014023. 3

Mikkola, K. and Staffans, O. Coprime factorizations and stabilizability of infinite-dimensional linear systems. In *Mathematical Theory of Networks and Systems (MTNS2004) Katholieke Universiteit Leuven, Belgium*. July 2004. 2

Mikkola, K. M. Coprime factorizations and stabilizability of infinite-dimensional linear systems. In *Decision and Control, 2005 and 2005 European Control Conference. CDC-ECC '05. 44th IEEE Conference on*, Seville, Spain, December 2005. 10.1109/CDC.2005.1582764. 2

Mirkin, L. On the extraction of dead-time controllers and estimators from delay-free parametrizations. *IEEE Trans. Automatic Control*, 48(4):543–553, April 2003. https://doi.org/10.1109/TAC.2003.809802. 3

Mohsenizadeh, N., Darbha, S., Keel, L. H., and Bhattacharyya, S. P. Model-free synthesis of fixed structure stabilizing controllers using the rate of change of phase. *IFAC Proceedings Volumes*, 45 (3):745–750, 2012. https://doi.org/10.3182/20120328-3-IT-3014.00126. 8

Monje, C. A., Calderon, A. J., Vinagre, B. M., Chen, Y., and Feliu, V. On fractional PI^λ controllers: Some tuning rules for robustness to plant uncertainties. *Nonlinear Dynamics*, 38(1-4):369–381, December 2004. 3

Monje, C., Chen, Y., Vinagre, B., Xue, D., and Feliu-Batlle, V. *Fractional-order Systems and controls : Fundamentals and Applications*. Springer-Verlag London, 2010. https://doi.org/10.1007/978-1-84996-335-0. X

Newlin, M. P. and Glavaski, S. T. Advances in the computation of the μ lower bound. In *Proc. American Control Conf.*, pages 442–446, Seatle, June 1995. https://doi.org/10.1109/ACC.1995.529286. 39

Nyström, R. H., Sandström, K. V., Gustafsson, T. K., and Toivonen, H. T. Multimodel robust control of nonlinear plants: a case study. *J. Process Control*, 9(2):135–150, April 1999. https://doi.org/10.1016/S0959-1524(98)00040-7. 55

Oustaloup, A. and Bansard, M. First generation CRONE control. In *Int. Conf. Systems, Man and Cybernetics*, Le Touquet, France, October 1993. https://doi.org/10.1109/ICSMC.1993.384861. 3

Oustaloup, A., Mathieu, B., and Lanusse, P. Second generation CRONE control. In *Int. Conf. Systems, Man and Cybernetics*, pages 1007–1009, Le Touquet, France, October 1993. https://doi.org/10.1109/ICSMC.1993.384862. 3

Oustaloup, A., Mathieu, B., and Lanusse, P. *Diversity and Non-integer Differentiation for System Dynamics*. Control, Systems and Industrial Engineering Series. ISTE - John Wiley & Sons, London, UK - Hoboken-USA, 2014. 3

O'Dwyer, A. A reference guide to Smith predictor based methods for the compensation of dead-time processes. In *Proc. Irish Signals and Systems Conf.*, Dublin, Scothland, September 2005. https://arrow.dit.ie/cgi/viewcontent.cgi?article=1033&context=engscheleart. 3

P. Loiseau, P. Chevrel, M. Y. and Duffal, J. h_∞ multi-objective and multi-model mimo control design for broadband noise attenuation in an enclosure. In *European Control Conf.*, pages 643–648, Aalborg, Denmark, June 2016. https://doi.org/10.1109/ECC.2016.7810361. 17

Packard, A. and Doyle, J. The complex structured singular value. *Automatica*, 29(1):71–109, 1993. https://doi.org/10.1016/0005-1098(93)90175-S. 47

Padhan, D. and Majhi, S. Modified Smith predictor and controller for time delay processes. *Electronics Letters*, 47(17):959–961, August 2011. https://doi.org/10.1049/el.2011.0378. 3, XI

Pal, J. Stable reduced-order padé approximants using the routh-hurwitz array. *Electronics Letters*, 15(8):225–226, April 1979. https://doi.org/10.1049/el:19790159. 15

Paola, M. and Zingales, M. A discrete mechanical model of fractional hereditary materials. *Meccanica*, 48(7):1573–1586, September 2013. https://doi.org/10.1007/s11012-012-9685-4. 3

Paor, A. M. A modified Smith predictor and controller for unstable processes with time delay. *Int. J. Control*, 41(4):1025–1036, 1985. https://doi.org/10.1080/0020718508961181. 3

Partington, J. R. and Bonnet, C. H_∞ and BIBO stabilization of delay systems of neutral type. *Systems & Control Letters*, 52(3-4):283–288, July 2004. https://doi.org/10.1016/j.sysconle.2003.09.014. 2, 3

Pensar, J. A. and Toivonen, H. T. On the design of fixed-structure H_∞ optimal controllers. In *Proc. IEEE Conf. Decision and Control*, San Antonio, USA, December 1993. https://doi.org/10.1109/CDC.1993.325064. 16

Petras, I. Stability of fractional-order systems with rational orders: A survey. *Fractional calculus and applied analysis*, 12(3):269–298, 2009. https://arxiv.org/abs/0811.4102. 14

Podlubny, I. Fractional-order systems and p $I^\lambda D^\mu$-controllers. *IEEE Trans. Automatic Control*, 44 (1):208–214, January 1999. https://doi.org/10.1109/9.739144. 3

Quadrat, A. Every internally stabilizable multidimensional system admits a doubly coprime factorization. 2004a. http://pages.saclay.inria.fr/alban.quadrat/Pubs/Linfinal.pdf. 2

Quadrat, A. "stabilizing" the stabilizing controllers. 2004b. http://www.math.ucsd.edu/~helton/MTNSHISTORY/CONTENTS/2004LEUVEN/CDROM/papers/534.pdf. 2

Ravanbod, L., Noll, D., and Apkarian, P. Branch and bound algorithm with applications to robust stability. *J. Global Optimization*, 67(3):553–579, March 2017. https://doi.org/10.1007/s10898-016-0424-6. 37, XXVI

Richard, J. Time-delay systems: an overview of some recent advances and open problems. *Automatica*, 39(10):1667–1694, October 2003. https://doi.org/10.1016/S0005-1098(03)00167-5. 3

Sabatier, J., Moze, M., and Farges, C. LMI stability conditions for fractional order systems. *Computers & Mathematics with Applications*, 59(5):1594–1609, March 2010. https://doi.org/10.1016/j.camwa.2009.08.003. 3

Sabatier, J., Farges, C., and Trigeassou, J. C. A stability test for non-commensurate fractional order systems. *Systems & Control Letters*, 62(9):739–746, September 2013. https://doi.org/10.1016/j.sysconle.2013.04.008. 3, XI

Safonov, M. G. . Thoughts on identification for control. In Smith, R. and Dahleh, M., editors, *The Modeling of Uncertainty in Control Systems*, Lecture Notes in Control and Information Sciences. Springer, Berlin, Heidelberg, 1994. https://doi.org/10.1007/BFb0036242. 6

Safonov, M. G. . and Tsao, T. C. The unfalsified control concept and learning. *IEEE Trans. Automatic Control*, 42(6):843–847, June 1997. https://doi.org/10.1109/9.587340. 6

Safonov, M. G. and Chiang, R. Y. Real/complex K_m-synthesis without curve fitting. In Leondes, C., editor, *Control and Dynamic Systems: Advances in Theory and Applications*, volume 56 of *Digital and Numeric Techniques and Their Applications in Control Systems*, pages 303–324. Academic Press, New York, 1993. https://doi.org/10.1016/B978-0-12-012756-6.50013-X. 4

Safonov, M. G., Ly, J. H., and Chiang, R. Y. μ-synthesis robust control: What's wrong and how to fix it? In *Proc. IEEE Regional Conf. Aerospace Control Systems*, Westlake Village,USA, May 1993. https://doi.org/10.1109/AEROCS.1993.720997. 4, 5, 19, 32, XX

Scott, R. Low order rational approximations to the delay operator. *IEEE Trans. Industrial Electronics and Control Instrumentation*, 24(1):61–65, February 1977. https://doi.org/10.1109/TIECI.1977.351443. 15

Shirazi, M. M. and Ibrir, S. Sufficient conditions for static-output feedback control of fractional-order linear systems. In *Proc. IEEE Int. Symp. Intelligent Control*, Buenos Aires, Argentina, September 2016. https://dx.doi.org/10.1109/ISIC.2016.7579980. 3

Smith, O. J. M. Closer control of loops with dead time. *Chemical Engineering Progress*, 53(9):217–219, 1957. 3

Solingen, E., Wingerden, J. W., and Oomen, T. A. E. Frequency-domain optimization of fixed-structure controllers. *Int. J. Robust and Nonlinear Control*, November 2016. https://doi.org/10.1002/rnc.3699. 7

Stengel, R. F. and Ray, L. R. Stochastic robustness of linear time-invariant control systems. *IEEE Trans. Automatic Control*, 36(1):82–87, January 1991. https://doi.org/10.1109/9.62270. 5

Tempo, R., Bai, E. W., and Dabbene, F. Probabilistic robustness analysis: Explicit bounds for the minimum number of samples. *Systems & Control Letters*, 30(5):237–242, June 1997. https://doi.org/10.1016/S0167-6911(97)00005-4. 5

Tepljakov, A., Petlenkov, E., and Belikov, J. FOMCON: a MATLAB toolbox for fractional-order system identification and control. *Int. J. Microelectronics and Computer Science*, 2(2):51–62, 2011. http://yadda.icm.edu.pl/baztech/element/bwmeta1.element.baztech-article-LOD7-0029-0056?q=bwmeta1.element.baztech-volume-2080-8755-international_journal_of_microelectronics_and_computer_science-2011-vol__2_nr_2;2&qt=CHILDREN-STATELESS. 14, XIV, XL

Trachtler, A. On BIBO stability of systems with irrational transfer function. *Cornell University Library*, March 2016. https://arxiv.org/pdf/1603.01059.pdf. 3

Vinagre, B. M., Podlubny, I., Hernández, A., and Feliu, V. Some approximations of fractional order operators used in control theory and applications. *J. Fractional Calculus and Applied Analysis*, 3(3):231–248, 2000a. http://citeseerx.ist.psu.edu/viewdoc/download?doi=10.1.1.452.5372&rep=rep1&type=pdf. XIV

Vinagre, B. M., Podlubny, I., Hernández, A., and Feliu, V. Some approximations of fractional order operators used in control theory and applications. *J. Fractional Calculus and Applied Analysis*, 3(3):231–248, 2000b. http://citeseerx.ist.psu.edu/viewdoc/download?doi=10.1.1.452.5372&rep=rep1&type=pdf. 4, 14

Vries, D. *Identification of model uncertainty for control design.* Ph.D. dissertation, Delft University of Technology, Faculty of Mechanical Engineering and Marine Technology, Delft, Netherlands, 1994. https://repository.tudelft.nl/islandora/object/uuid:5f96c4ea-efc0-46d6-a2ac-782935132498?collection=research. 6

Xiong, Q. and Cai, W. J. Effective transfer function method for decentralized control system design of multi-input multi-output processes. *J. of Process Control*, 16:773–784, 2006. https://doi.org/10.1016/j.jprocont.2006.04.001. XI, XII

Young, P. M. Controller design with mixed uncertainties. In *American Control Conf.*, Baltimore, USA, July 1994. https://doi.org/10.1109/ACC.1994.752496. 4

Young, P. M., Newlin, M. P., and Doyle, J. C. μ analysis with real parametric uncertainty. In *Proc. IEEE Conf. Decision and Control*, Brighton, UK, December 1991. https://doi.org/10.1109/CDC.1991.261579. 4, 19, XX

Yuan, X., Efe, M., and Özbay, H. On delay-based linear models and robust control of cavity flows. In Niculescu, S. and Gu, K., editors, *Advances in Time-Delay Systems*, volume 38 of *Lecture Notes in Computational Science and Engineering*, pages 287–298. Springer, Berlin, Heidelberg, 2004. https://doi.org/10.1007/978-3-642-18482-6_21. X

Zebiri, H., Mourllion, B., and Basset, M. Balanced truncation techniques for active suspension reduced-order h_∞-controller. *IFAC Proc. Volumes*, 46(25):123–128, 2013. ISSN 1474-6670. https://doi.org/10.3182/20130916-2-TR-4042.00043. IFAC Workshop on Advances in Control and Automation Theory for Transportation Applications. 6

Zhou, K. and Doyle, J. C. *Essentials of Robust Control.* Prentice Hall, 1999. 13, 15, 16, 71

Zhou, K., Doyle, J. C., and Glover, K. *Robust and Optimal Control.* Prentice Hall, Englewood Cliffs, New Jersey, 1996. 25

Zwart, H. Transfer functions for infinite-dimensional systems. *Systems & Control Letters*, 52(3-4): 247–255, july 2004. https://doi.org/10.1016/j.sysconle.2004.02.002. 2

Appendix A

Validation

All computations in this work were performed on MATLAB ™ R2016b running in CentOS Linux 7, Intel Xeon(R) E5-1620 @ 3.50GHz and 7.6 GB RAM. All mentions to MATLAB ™ routines refer to the versions for MATLAB ™ R2016b.

A.1 Validation tests for robust control

In order to validate the robust control techniques developed in this work, two aspects were taken into consideration: the power of the technique in synthesizing a controller that meets the specifications for RS and robust performance (RP) stated in subsection 2.3.2, and competitivity of the results regarding other techniques.

The potential of the technique in synthesizing controllers that meet the robust specifications is verified by analysis of the closed-loop system. As the optimization methods used in this work provide only local solutions, as explained in chapter 2, an additional analysis step is performed to certify that RS and RP are guaranteed. The competitivity of three robust control techniques developed is assessed by comparing them among themselves and to third-party routines.

The validation is based on a set of 30 tests cases with different types of uncertainty and structure (see Appendix B). For each test case, five controllers were designed. The controllers have a state-space structure with order n_x ranging from 1 to 5. Following the notation of chapter 2, the matrix $A_K \in \mathbb{R}^{n_x \times n_x}$ is tridiagonal, and matrices B_K, C_K and D_K are full matrices with appropriate dimensions. This means that for control output ans input of dimensions n_y and n_u, respectively, the parameterization of $K(\kappa)$ takes $n_K = n_x(3 + n_y + n_u) + n_y n_u - 2$ parameters, that is, $\kappa \in \mathbb{R}^{n_K}$.

For instance, for a strictly proper SISO tridiagonal 2nd-order state-space controller one has:

$$K(\kappa): \begin{cases} \dot{x}(t) = \begin{bmatrix} \kappa_1 & 0 \\ 0 & \kappa_2 \end{bmatrix} x(t) + \begin{bmatrix} \kappa_3 \\ \kappa_4 \end{bmatrix} u(t) \\ y(t) = \begin{bmatrix} \kappa_5 & \kappa_6 \end{bmatrix} x(t). \end{cases}$$

In the following more details about the validation are provided.

A.1.1 Normalization

The generalized plants and their respective uncertainties follow the exposion in subsection 2.3.1. It should be recalled that the uncertainty channel is scaled so that $\overline{\sigma}(\Delta_i) \leq 1$ for each block $\Delta_i \in \mathbf{\Delta}$.

In order to render the comparison straightforward and to simplify the reading of tables, the performance channel of the systems is rescaled so at least one of the techniques returns H_∞-norm equals 1. The inner H_∞-norm was chosen to be the scaling value. In this set up, a technique that returns an H_∞-norm smaller than 1 means the technique performs better than inner in the particular test case. On the other hand, if a technique returns an H_∞-norm greater than 1, one concludes that inner performs better.

A.1.2 Global certification

In order to certify that the controller returned by the techniques developed provides robust stability and robust performance over $\mathbf{\Delta}$, the closed-loop system was subjected to a robust analysis tool with global certification. It should be kept in mind that, due to the NP-hardness of the robust analysis problem, the certification is sometimes conservative. This means the certification are made for the upper bound estimate of performance and worst-case estimation of stability. Certification of the exact value is assured whenever lower and upper bound coalesce.

A.1.3 Comparison of techniques

The competitivity of the methods was addressed to understand which technique would be preferable in general. The criteria for choosing the best technique are smaller H_∞-norm, consistency of results, and implementability of the controller. As the objectives of the synthesis are RS and RP, it is natural to employ the H_∞-norm of the closed-loop system as the main criterion. The consistency of results aims at evaluating if a technique performs better than the others in some cases, but has very poor results on other cases. The implementability of the controller refers to how simple is the structure of the controller designed. This will be evaluated by the order of the controller returned. For numerical analysis, values that differ by less than 10% will be considered as the same and the difference will be considered as due to numerical precision on computation.

- **Third party routine for robust synthesis**

The most popular robust control synthesis routine is DKSYN, available in the Robust Control Toolbox of MATLAB ™. This is witnessed by the large number of works that reference the procedure on which the routine is based, the *DK-iteration* [Balas, 1982].

The catch is that, according to the documentation of the routine, the performance value returned is the inverse of the lower bound of the robust performance margin. The robust performance margin is the maximum H_∞-norm the uncertainty may assume such that the nominal performance is not degraded further than a given value. Still according to the MATLAB ™ documentation, the performance corresponds to the point where the robust performance margin equals the inverse of the normalized degradation. That means that the performance value bnd returned by DKSYN corresponds to the worst-case closed-loop H_∞-norm for an uncertainty $\overline{\sigma}(\Delta) \leq 1/bnd$. As a result, nothing can be conclued about robust stability for the actual problem when $bnd > 1$.

In order to compare the novel techniques to DKSYN on the same problem, $\mathbf{\Delta}$ should be rescaled so that it corresponds to the scaled unit ball $\mathbf{\Delta} = \{\Delta : \overline{\sigma}(\Delta) \leq 1/bnd\}$. Another aspect worthy to note is that as DKSYN returns unstructured controllers, the controller order may be higher than the order of the structured controllers designed by the novel techniques. So, for the uncertain system with the new rescaled $\mathbf{\Delta}$, a new reduced order structured state-space controller were designed by each new technique. Starting from controller order 1, if worst-case H_∞-norm achieved is larger than bnd, the order of the controller $n_x(K)$ is incremented until worst-case H_∞-norm $<bnd$ or the controller order reaches the smallest value among: 15, the controller order of unstructured controller designed by DKSYN, and the order of the uncertain plant (with multipliers). The limit of a 15th-order controller is justified by the consequent increasing in the dimension of the parameter vector κ, that may cause a computational burden to the optimization methods employed.

A.2 Validation tests for data driven control

The methods developed for FRD design of stabilizing structured controllers for stable and unstable systems are evaluated by the success rate at finding a stabilizing controller. Since the only objective of these methods is to achieve stability, no other quantitative analysis is performed. Measures as stability margins or H_∞-norm are not considered as these methods are supposed to be followed by an H_∞-norm optimization step that will improve performance as well as stability margins.

Two sets of test cases are used for numerical evaluation. The first set of test cases is extracted from *COMPl$_e$ib* (Constrained matrix–optimization problem library) [Leibfritz, 2004]. It consists in 37 unstable finite-dimensional plants with moderate number of states. The relevant data for the selected examples can be found in Table C.1.

The structure of the controllers designed is a tridiagonal state-space structure with order 3. Using the equation of section A.1, the parameterization of this controller $K(\kappa)$ takes $n_K = 7+3\cdot(n_y+n_u)+n_y n_u$ parameters, where n_y and n_u are the control input and output signs dimensions. The dimension of parameter κ for each example is displayed in Table C.1.

The second set of test cases consists of stable and unstable infinite-dimensional systems. The parametric models that generate the frequency domain data for each of the systems are presented in Appendix C. It comprises retarded, neutral and dead-time systems, as well as fractional systems, with SISO and MIMO examples. The structure of the controller is chosen accordingly to the system to be stabilized. The structures are chosen among PID, state-space and rational functions of frequency variable s.

A.2.1 Certification

The feedback systems are certified stable when their rightmost pole is in $\mathbb{C}^-$. For finite-dimensional cases, this is verified by computing their poles using routines from MATLAB ™ for parametric models. The infinite-dimensional systems are certified to be stable if the Nyquist test is positive for a frequency grid in the range $[10^{-7}, 10^{7}]$ with a density of 50,000 points per decade. The H_∞-norm of finite-dimensional systems is verified using MATLAB ™ routines for parametric models.

A.2.2 Comparison of techniques

The success rates of the methods are compared mainly among the three methods developed. The novelty of using only FRD in cases for which no stabilizing controller is available limits the number of available methods to be used as benchmark. The option is to compare the results of FRD design to results of design based on rational approximations of the systems. The routine selected for the H_∞ synthesis is SYSTUNE, which exploits parametric models of finite-dimensional systems in the synthesis. More details about this routine can be found in Appendix D.

The approximations for delayed systems are obtained by replacing the delay terms e^{-as} by an all-pass rational transfer functions obtained by Padé approximations, as recalled in section 2.1.4 equation 2.23. The approximation for each delay term is of order. The MATLAB ™ routine PADE is employed for computation of the coefficients of the approximate term. The approximations for fractional-order systems are obtained using the Oustaloup approximation from section 2.1.4 equation 2.21 for fractional terms on s. The computation of the coefficients of each approximate term applies the Oustaloup approximation implemented by routine OUSTAPP, from FOMCON toolbox for MATLAB ™. This routine is briefly described in Appendix D.

In addition to the stabilization success rate of the techniques, the H_∞ norms of feedback systems are also compared for the rational cases. In order to do so, a complementary H_∞-norm optimization step from Apkarian and Noll [2018] is performed after stabilization using the stabilizing controller as initial controller. The values of all H_∞ norms are normalized by the H_∞-norm achieved by SYSTUNE . In this context, the H_∞-norm from systune are displayed as 1.000 and an H_∞-norm inferior to 1 means a better performance. As the controller structure is the same for both FRD design and SYSTUNE design, the only comparison criteria are stabilization of the feedback system and its H_∞-norm . It should be stressed that stabilization is the primary objective of the techniques developed in this thesis.

Appendix B

Test cases for robust control design

This appendix provides information about the benchmark of 30 test cases used for validation of the robust control methods developed in this work. A table with the dimensions regarding the cases and plots of the open-loop uncertain generalized plant behavior is presented.

Table B.1 presents the data for each of the 30 systems in the directory. The column n_x shows the number of states of the generalized plant P. The dimensions of the exogenous and control input vectors are given in columns n_w and n_u while the dimensions of the performance and measured output vectors are given by columns n_z and n_y. The columns n_p and n_q give the total dimension of the uncertainty Δ. Each block shown on column Δ_p accounts for one uncertain parameter while the size of the matrix gives the number of repetitions r_i of this uncertainty. Under the column Δ_d each full matrix $C^{n_{p_i} \times n_{q_i}}$ accounts for one dynamic uncertainty where the dimension $n_{p_i} \times n_{q_i}$ gives the size of the block.

Note that the of test cases in MATLAB ™ format are available at http://rss-aguiar.site88.net/.

Table B.1: Relevant data of the test cases for robust control design.

Ex	n_x	n_w	n_z	n_u	n_y	n_p	n_q	Δ_p	Δ_d
1	9	3	3	1	2	1	1	-	$C^{1\times1}$
2	7	2	1	1	1	3	3	-	$C^{3\times3}$
3	8	4	4	1	3	3	3	-	$C^{3\times3}$
4	12	2	6	2	2	8	8	-	$C^{8\times8}$
5	22	2	2	2	2	2	2	-	$C^{1\times1}$ $C^{1\times1}$
6	3	1	1	1	1	1	1	-	$C^{1\times1}$
7	26	5	6	2	5	2	2	-	$C^{2\times2}$
8	3	3	2	1	1	1	1	I_1	-
9	23	2	3	1	3	20	20	$I_2 I_{18}$	-
10	10	1	2	1	1	20	20	I_{20}	-
11	5	2	2	1	1	21	21	I_{21}	-
12	9	1	1	1	1	3	3	$I_1 I_1$	$C^{1\times1}$
13	7	2	4	1	1	5	5	$I_2 I_2$	$C^{1\times1}$
14	8	4	3	1	2	5	5	$I_3 I_1$	$C^{1\times1}$
15	8	4	2	2	2	2	2	I_1	$C^{1\times1}$
16	14	2	6	2	2	8	8	$I_1 I_1 I_1 I_1 I_1 I_1$	$C^{2\times2}$
17	9	1	2	1	1	8	8	$I_1 I_1 I_1 I_3 I_1$	$C^{1\times1}$
18	6	1	2	1	1	6	6	$I_1 I_2 I_2$	$C^{1\times1}$
19	6	2	2	1	1	15	15	$I_1 I_3 I_3 I_3 I_1 I_3$	$C^{1\times1}$
20	11	1	2	1	1	21	21	$I_1 I_3 I_3 I_3 I_3 I_1 I_1 I_1 I_1$	$C^{1\times1}$
21	8	2	6	2	2	8	8	$I_1 I_1 I_1 I_1$	$C^{4\times4}$
22	19	3	2	1	1	16	16	$I_1 I_1 I_1 I_2 I_2 I_2 I_2 I_1 I_1 I_1 I_1$	$C^{1\times1}$
23	8	4	4	1	3	11	11	$I_1 I_6 I_1$	$C^{3\times3}$
24	7	2	1	1	1	4	4	I_1	$C^{3\times3}$
25	24	2	3	1	3	22	22	$I_1 I_1 I_1 I_6 I_6 I_6$	$C^{1\times1}$
26	8	2	6	2	2	8	8	$I_1 I_1 I_1 I_1$	$C^{1\times1}$ $C^{1\times1}$ $C^{1\times1}$ $C^{1\times1}$
27	7	2	2	1	1	2	2	I_1	$C^{1\times1}$
28	7	3	2	1	2	7	7	$I_1 I_5$	$C^{1\times1}$

29	4	3	2	1	1	2	2	I_1	$C^{1\times1}$
30	8	2	2	1	1	2	2	I_1	$C^{1\times1}$

To illustrate the behavior of each of the open-loop uncertain generalized plant, Figures B.1 to B.7 present the singular value plot for 50 samples of each uncertain system of the benchmark.

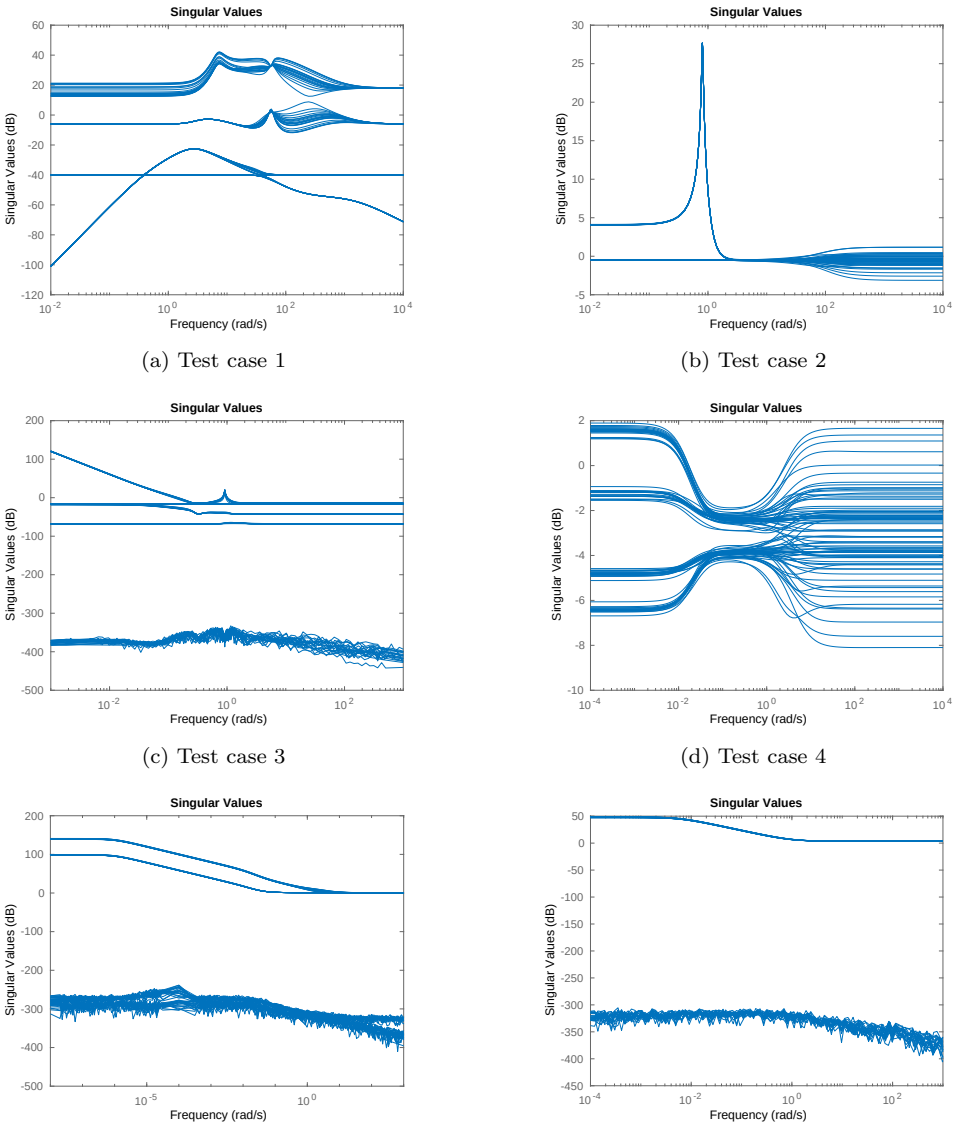

(a) Test case 1

(b) Test case 2

(c) Test case 3

(d) Test case 4

(e) Test case 5

(f) Test case 6

Figure B.1: Singular values of uncertain systems of test cases from 1 to 6.

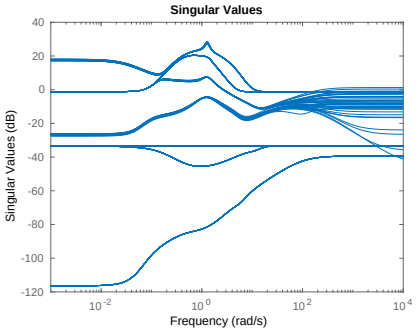

(a) Test case 7

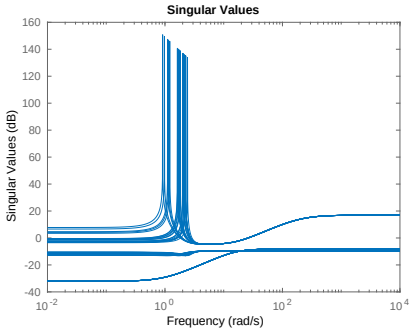

(b) Test case 8

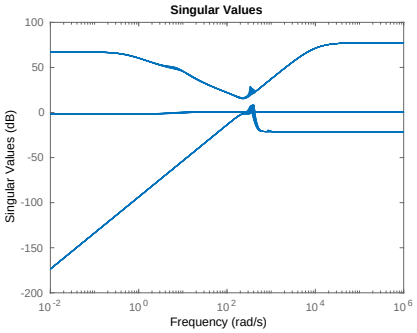

(c) Test case 9

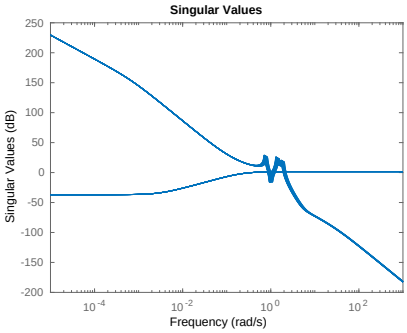

(d) Test case 10

Figure B.2: Singular values of uncertain systems of test cases from 7 to 10.

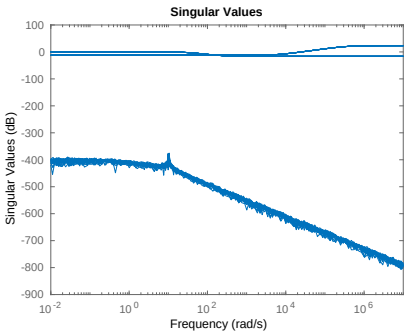

(a) Test case 11

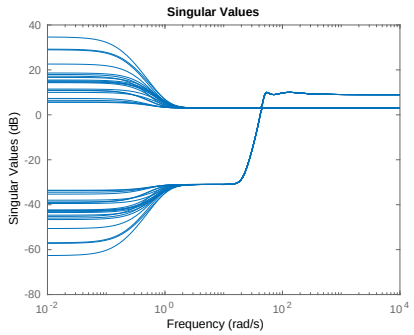

(b) Test case 12

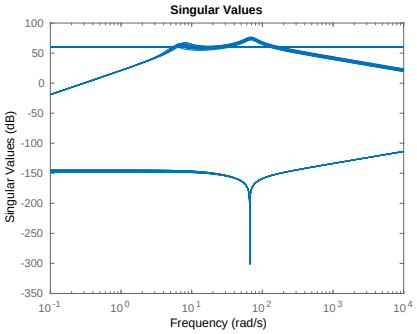

(c) Test case 13

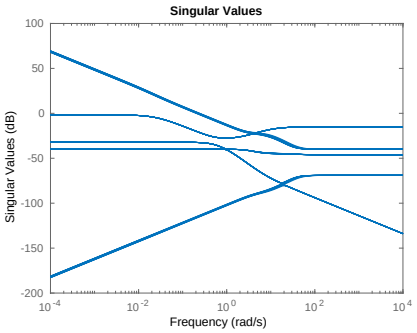

(d) Test case 14

Figure B.3: Singular values of uncertain systems of test cases from 11 to 14.

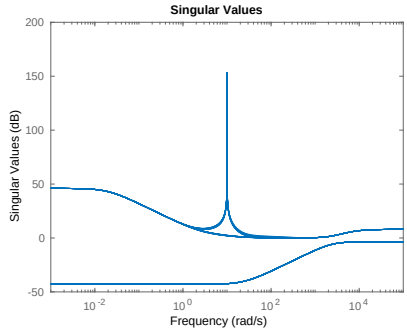

(a) Test case 15

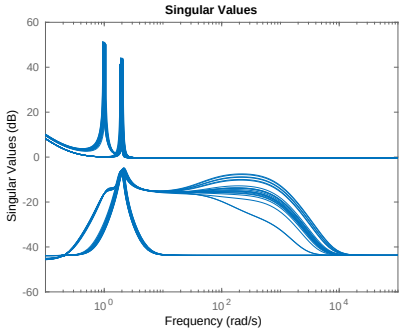

(b) Test case 16

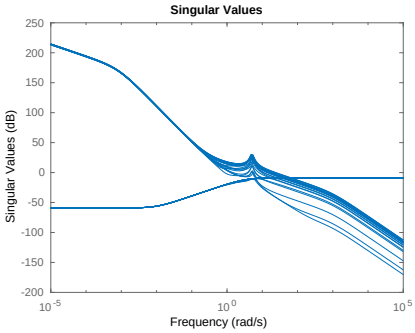

(c) Test case 17

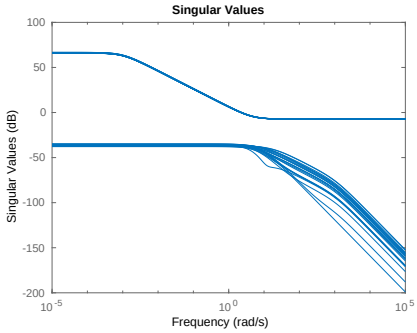

(d) Test case 18

Figure B.4: Singular values of uncertain systems of test cases from 15 to 18.

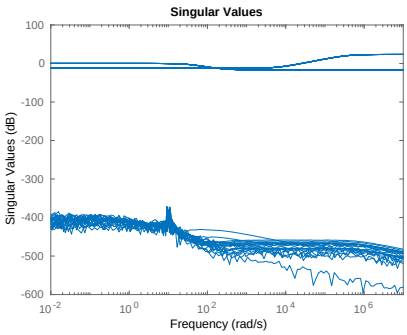

(a) Test case 19

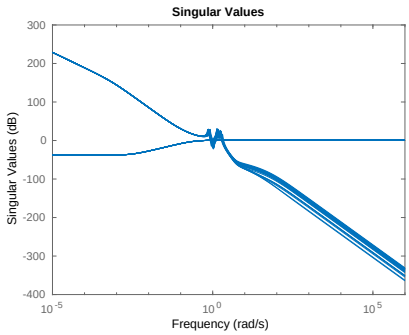

(b) Test case 20

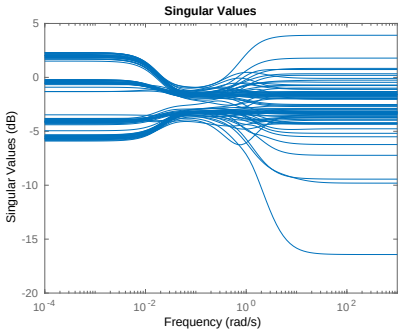

(c) Test case 21

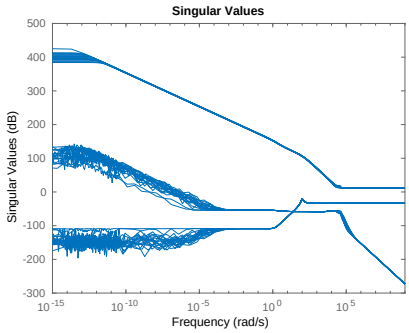

(d) Test case 22

Figure B.5: Singular values of uncertain systems of test cases from 19 to 22.

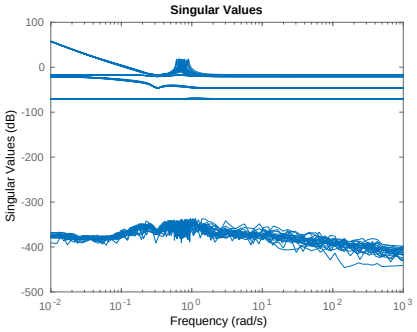

(a) Test case 23

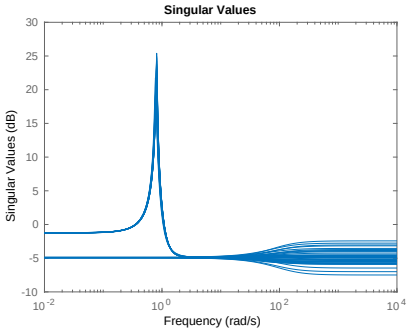

(b) Test case 24

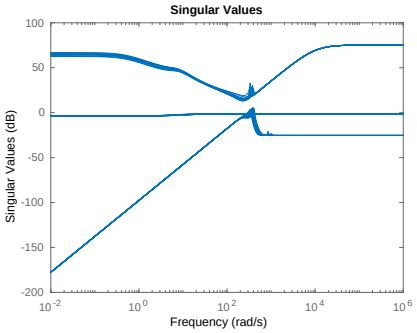

(c) Test case 25

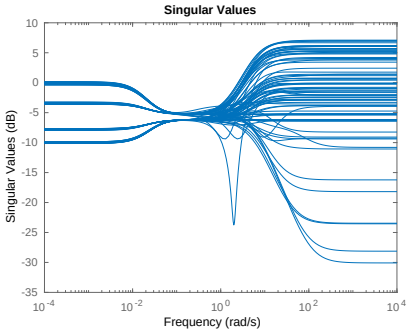

(d) Test case 26

Figure B.6: Singular values of uncertain systems of test cases from 23 to 26.

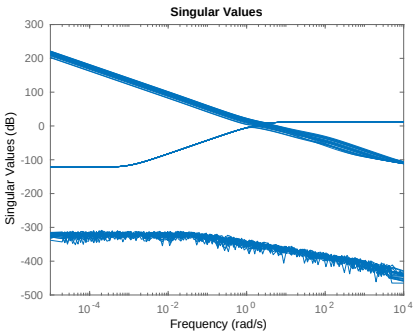

(a) Test case 27

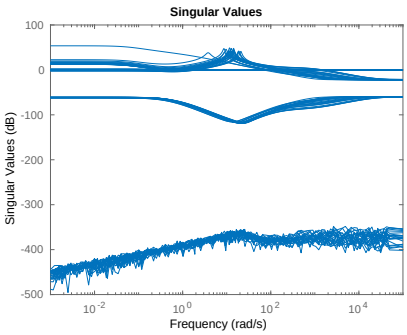

(b) Test case 28

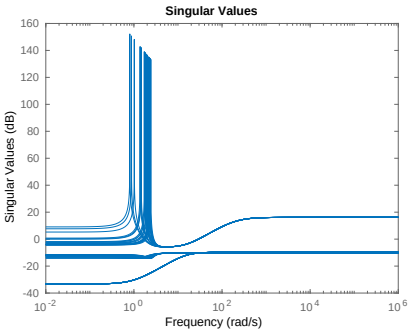

(c) Test case 29

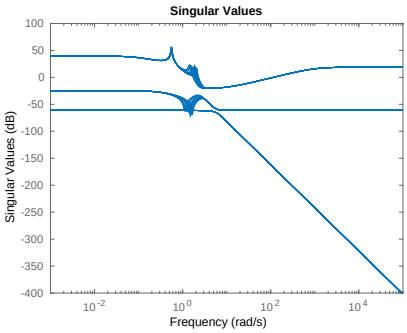

(d) Test case 30

Figure B.7: Singular values of uncertain systems of test cases from 27 to 30.

Appendix C

Test cases for frequency response data design

Finite-dimensional systems

The set of finite-dimensional test cases comprises 37 unstable systems from COMPl$_e$ib (Constrained matrix–optimization problem library) [Leibfritz, 2004]. They are test cases number 4, 7, 8, 11-13, 18, 20-23, 28, 29, 33, 35, 36, 39, 46, 65, 66, 69, 70, 73-82 and 85-89 from set *Exsmall*. Table C.1 displays some information about these systems, renumbered from 1 to 37, including the dimension of tunable controller parameter κ for a third-order tridiagonal state-space controller.

Column n_x shows the number of states of the generalized plant P. The dimensions of the exogenous and control input vectors are given in columns n_w and n_u while the dimensions of the performance and measured output vectors are given by columns n_z and n_y. Column $\alpha(G)$ shows the spectral abscissa of the plant $G(s)$ whereas column $|pu_G|$ displays the number of unstable poles of $G(s)$. At last, column $|\kappa|$ presents the number of parameters to be tuned in the design of a third-order tridiagonal state-space controller for the respective system.

Table C.1: Relevant data of the test cases for FRD design.

Ex	n_x	n_w	n_z	n_u	n_y	$\alpha(G)$	$\lvert pu_G\rvert$	$\lvert\kappa\rvert$
1	4	2	2	1	2	2.579208	1	18
2	9	4	1	1	2	0.172371	2	18
3	9	10	2	1	5	0.012221	1	30
4	4	3	1	3	4	0.579932	1	40
5	28	28	28	3	4	0.579932	1	40
6	40	4	11	3	4	0.579932	1	40
7	4	2	2	2	1	0.27579	2	18
8	8	1	10	4	6	0.08713	4	61
9	8	8	12	4	6	0.234198	2	61
10	8	3	4	4	2	0.234198	2	33
11	20	6	16	4	6	0.234198	2	61
12	4	4	4	2	3	1.99096	2	28
13	4	4	4	2	2	2.010957	2	23
14	3	3	3	2	2	1.675471	2	23
15	6	6	6	4	6	1.441594	3	61
16	4	3	3	2	2	1.019186	4	23
17	10	10	10	3	4	0.008188	1	40
18	20	1	12	2	10	0	1	63
19	5	2	4	3	2	3.280936	4	28
20	8	3	2	3	3	2.300155	6	34
21	6	3	3	2	2	1.944915	2	23
22	6	3	3	2	2	1.944915	2	23
23	3	1	2	2	1	1.170086	1	18

24	5	5	7	2	4	0.689221	1	33
25	5	5	7	2	4	1.707219	1	33
26	5	5	7	2	2	1.292408	1	23
27	5	5	7	2	2	0.508954	1	23
28	7	7	9	2	2	1.02924	1	23
29	7	7	9	2	2	0.231384	1	23
30	7	7	9	2	2	1.974581	1	23
31	5	5	7	2	3	0.132268	1	28
32	5	5	7	2	3	0.249863	1	28
33	5	5	7	2	4	0.224117	1	33
34	5	5	7	2	4	1.560333	1	33
35	5	5	7	2	4	0.11349	1	33
36	5	5	7	2	4	0.54237	1	33
37	5	5	7	2	2	0.280775	1	23

SISO stable integer-order delayed systems

1. Example from Yuan et al. [2004] - Neutral system

$$G(s) = \frac{66000e^{-0.0205s}}{s^2 + 2380s + 40000 - (0.1s^2 + 38s + 4000)e^{-0.002s} - 2.6928e4e^{-0.0205s}}$$

2. Example from Bonnet and Partington [2000a]

$$G(s) = \frac{1}{2s^{0.5} - (s^{0.5} + 1)e^{-s}};$$

   Unstable pole: 0.32245484454

3. from Loiseau and Mounier [2002]

$$G(s) = \frac{2e^{-401s^{0.5}}}{401s^{0.5}(1 - e^{-802s^{0.5}})};$$

   Unstable pole: 0

4. Example from Fioravanti [2011]

$$G(s) = \frac{1}{s^{5/6} + (s^{0.5} + s^{1/3})e^{-10s} + e^{-20s}};$$

   Unstable poles: real part of the pair at 0.0256457;

5. Example from Abusaksaka and Partington [2014]

$$G(s) = \frac{1}{s^{0.5} + e^{-150s^{0.5}}};$$

   Unstable poles: real part of the pair at 0.000275

6. Example from Fioravanti [2011] - Neutral system

$$G(s) = \frac{1}{2s^3 - 6s^2 + 4s + (s^3 - 2s^2 - s + 2)e^{-s} + (s^2 - 3s + 2)e^{-2s}};$$

   Unstable poles: 1 and 2

7. Example from Monje et al. [2010]

$$G(s) = \frac{1}{s - 2s^{0.5} + 1.25};$$

   Unstable poles: real part of the pair at 0.75

8. Example from Padhan and Majhi [2011] - Dead-time systems

$$G(s) = \frac{2e^{-5s}}{10s - 1};$$

Unstable pole: 0.1

9. Example from Meinsma and Zwart [2000] - Dead-time systems

$$G(s) = \frac{e^{-0.2s}}{s - 1}$$

Unstable pole: 1

10.

$$G(s) = \frac{e^{-2*s}}{s - 1}$$

Unstable poles: 1

11. Example from Herrera et al. [2013]

$$G(s) = \begin{bmatrix} \frac{4e^{-15.5s}}{s-1} & \frac{2.3e^{-3.4s}}{s+2} \\ \frac{2.5e^{-7.6s}}{s+1.5} & \frac{3.8e^{-11.8s}}{s-2.3} \end{bmatrix}$$

Unstable poles: 1 and 2.3

12. Example from Sabatier et al. [2013]

$$G(s) = \frac{1}{(1 - s^{0.2})(5s^{\sqrt{3}} + 1)};$$

Unstable pole: 1

13. Example from Xiong and Cai [2006]

$$G(s) = \begin{bmatrix} \frac{5}{4s+1}e^{-3s} & \frac{2.5}{15s+1}e^{-5s} \\ \frac{-4}{20s+1}e^{-6s} & \frac{1}{5s+1}e^{-4s} \end{bmatrix}$$

14. Example from Xiong and Cai [2006]

$$G(s) = \begin{bmatrix} \frac{22.89}{4.572s+1}e^{-0.2s} & \frac{-11.64}{1.807s+1}e^{-0.4s} \\ \frac{4.689}{2.174s+1}e^{-0.2s} & \frac{5.8}{1.801s+1}e^{-0.4s} \end{bmatrix}$$

15. Example from Xiong and Cai [2006]

$$G(s) = e^{-5s} \cdot \begin{bmatrix} \frac{119}{21.7s+1} & \frac{153}{337s+1} & \frac{-2.1}{10s+1)} \\ \frac{37}{500s+1} & \frac{76.7}{28s+1} & \frac{-5}{10s+1} \\ \frac{93}{500s+1} & \frac{-66.7}{166s+1} & \frac{-103.3}{23s+1} \end{bmatrix}$$

16. Example from Xiong and Cai [2006]

$$G(s) = \begin{bmatrix} \frac{-9.811}{(11.36s+1)}e^{-1.59s} & \frac{0.374}{(22.22s+1)}e^{-7.75s} & \frac{-2.368}{(33.3s+1)}e^{-27.33s} & \frac{-11.3}{(21.74s+1)}e^{-3.79s} \\ \frac{5.984}{(14.29s+1)}e^{-2.24s} & \frac{-1.986}{(66.67s+1)}e^{-0.71s} & \frac{0.422}{(250s+1)^2}e^{-8.72s} & \frac{5.24}{(400s+1)}e^{-60s} \\ \frac{2.38}{(1.43s+1)^2}e^{-0.42s} & \frac{0.0204}{(7.14s+1)^2}e^{-0.59s} & \frac{0.513}{(s+1)}e^{-s} & \frac{-0.33}{(2.38s+1)^2}e^{-0.68s} \\ \frac{-11.3}{(21.74s+1)^2}e^{-3.79s} & \frac{-0.176}{(6.9s+1)^2}e^{-0.48s} & \frac{15.54}{(s+1)}e^{-s} & \frac{4.48}{(11.11s+1)}e^{-0.52s} \end{bmatrix}$$

17. Example from Abusaksaka and Partington [2014]

$$G(s) = \frac{1}{(s+1)(1+s(1-e^{-s}))};$$

18. Example from Abusaksaka and Partington [2014]

$$G(s) = \frac{1}{(s+1)^2(1+s(1-e^{-s}))};$$

19. Example from Bonnet et al. [2011]

$$G(s) = \frac{2s+3}{(s+1)(s^2+s+(s^2+s)e^{-s}-(0.5s+1)e^{-2s})}$$

20. Example from Bonnet et al. [2011]

$$G(s) = \frac{s^2+s}{(s^2+s+1+(-s^2+3s+2)e^{-s})(s^2+2+(s^2+s+1)e^{-s})}$$

21. Example from Bonnet et al. [2011]

$$G(s) = \frac{1}{s^2+s+4e^{-s}+(s^2+1.1s+7)e^{-2s}}$$

Unstable poles: $0.666 \pm j1.0325$

22. Example from Bonnet et al. [2011]

$$G(s) = \frac{s}{s^2+2+(s^2+s+1)e^{-10s}}$$

Unstable poles: $0.0420269 \pm j1.10204$, $0.139099 \pm j1.55329$

23. Example from Bonnet and Partington [2000a]

$$G(s) = \frac{e^{-s^{0.5}}}{s-1};$$

Unstable pole: 1

24. Example from Bonnet and Partington [2000a]

$$G(s) = \frac{2(1-e^{-s^{0.5}})}{s^{1.5}(1+e^{-s^{0.5}})};$$

Unstable pole: 0

25. Example from Fioravanti [2011]

$$G(s) = \frac{1}{s^{5/6}+(s^{0.5}+s^{1/3})e^{-40s}+e^{-80s}};$$

Unstable poles: real part of the pair at 0.010483 and second pair at 0.015818;

Appendix D

Third Party Routines

D.1 Multi-model, multi-objective synthesis of structured controllers

The routine SYSTUNE of the MATLAB ™ Control Toolbox is based on the work of Apkarian and Noll [2006a] for multi-disk H_∞ synthesis for rational parametric models using nonsmooth optimization. It simultaneously handles nonlinear, nonconvex and nonsmooth constraints while minimizing multiple objectives. The multi-model synthesis is successful if all constraints are satisfied for all plants in the set, otherwise the problem is consided infeasible for the set of requirements. In this thesis it is used to tune parameters of control structures, as multipliers and controllers, for one or multiple models simultaneously, resulting in structured control laws. It is also used to obtain reference values for the control of infinite-dimensional systems, in this case, using approximations.

The first step to use SYSTUNE is to choose a structure for the controller and parameterize this structure with respect to parameter vector κ. Next each plant is connected to the controller generating a set of parameterized closed-loop systems.

The objective function and constraints should be expressed as requirements that will be optimized with respect to κ. Among the many requirements available for direct assignment, the ones used in this work are the H_∞-norm of a channel, constraints on controller poles, and constraints on closed-loop poles.

SYSTUNE takes as input the parametrized closed-loop system *CL0*, a vector of objectives (cost functions) to be minimized *SoftGoals*, a vector of constraints for the synthesis *HardGoals* and a set of options for the procedure *opt*.

The outputs are the closed-loop system *CL* with the parameters set to the values of the optimum solution, the vector of optimum values of the objectives *fSoft* and the constraint values *gHard* for the solution. A constraint value smaller than 1 indicates that this constraint is satisfied.

$$[\boldsymbol{CL,\ fSoft,\ gHard}] = \mathbf{systune}(\boldsymbol{CL0,\ SoftGoals,\ HardGoals,\ opt})$$

As we work in the H_∞ framework, all our specifications are expressed as H_∞-norm 's. Objectives and constraints in H_∞-norm are described as gains from a particular input to a particular output. The requirements on controller and closed-loop poles are constraints on the minimum decay and minimum damping of the respective poles.

The options of systune exploited in differ from the default in the number of *random starts*. The *random start* value is the number of times the optimization routine reruns using different initial random vector κ.

D.2 Robust stability and performance analysis

In order to certify RS and RP over the uncertainty set $\boldsymbol{\Delta}$, we submit the closed-loop system to a robust analysis tool with global certification. The tool chosen was WCGAIN routine available in Robust Control Toolbox of MATLAB ™ [MathWorks, 2017]. This routine computes lower and upper bounds of the structured singular value (SSV) of a system with respect to the given uncertainty

structure [Doyle, 1982; Fan and Tits, 1992]. The exact value of the SSV is guaranteed to lie between these bounds.

Lower bounds are usually optimistic estimates and do not provide certification unless equal to the upper bound. This is due to the fact that the methods employed in the calculation of the lower bound converge to local maxima. The upper bound provides a certification of stability if the value returned is not *Inf* but it can still be overly conservative regarding performance. The larger the gap between upper and lower bounds, the less can be concluded about the performance of the system. For instance, consider the case where the upper bound is returned *Inf* and lower bound is a finite value close to 1. In this case stability is not certified, but it is not sure if this corresponds to a conservative estimate from upper bound methods or if the local lower bound methods failed to find a unstable instance of the closed-loop system.

WCGAIN takes as input the uncertain closed-loop system *UCL*. The outputs are the lower and upper bounds on worst-case H_∞-norm over all frequencies ω and $\mathbf{\Delta}$ and the Δ and frequency ω where the peak of the lower bound occurs.

The call sequence is

$$[\boldsymbol{wcg},\ \boldsymbol{wcu}] = \mathbf{wcgain}(\boldsymbol{UCL})$$

The outputs are the structure *wcg* that contains the bounds and the structure *wcu* that contains the worst-case estimate of Δ.

D.3 Robust control synthesis

The most popular robust synthesis routine is DKSYN available in the MATLAB ™ Robust Control Toolbox. The *DK-iteration* procedure iteratively optimize the maximum μ value of the system with respect to *DG-scalings* over all frequencies ω and the H_∞-norm with respect to controller K. The optimization of H_∞-norm is carried by the routine HINFSYN, a LMI-based H_∞ synthesis.

The routine DKSYN returns an unstructured robust controller certified to "guarantee a degradation level" on H_∞-norm also returned by the routine.

The routine takes as inputs the uncertain generalized plant P and the dimensions of the controlled inputs and measured outputs *ncont, nmeas*. It is also possible to choose some options for the procedure through an input options variable *opt*. The outputs are the unstructured robust controller K, the performance value *bnd*, the closed-loop uncertain system *CLP* and information about the parameters of the synthesis *dkinfo*, such as the realizations of the scaling matrices for the worst-case uncertainty.

$$[\boldsymbol{K},\ \boldsymbol{CLP},\ \boldsymbol{bnd},\ \boldsymbol{dkinfo}] = \mathbf{dksyn}(\boldsymbol{P},\ \boldsymbol{nmeas},\ \boldsymbol{ncont},\boldsymbol{opt})$$

The only default option changed in this work was set 'MixedMu' option 'on' so the synthesis accounts for parametric uncertainties without covering.

D.4 Finite-dimensional approximation of fractional-order models

In order to apply robust control of finite-dimensional system in the design of rational structured controllers for fractional-order systems, one should first build approximations of the fractional-order systems and estimate the mismatch. The Oustaloup algorithm for approximation of FOS [Vinagre et al., 2000a] was implemented in the routine OUSTAPP of toolbox FOMCON (Fractional-order modeling and control) [Tepljakov et al., 2011] for MATLAB ™. The approximation is obtained from equation 2.21 in section 2.1.4. In fact, the routine builds an approximate for each fractional-order term of the transfer function G. The routine takes as input the fractional-order transfer function G, the lower and upper bounds of the frequency interval for approximation *wb*, *wh*, the order of the approximation N, and the method to be employed.

$$[\boldsymbol{Ga}] = \mathbf{oustapp}(\boldsymbol{G},\ \boldsymbol{wb},\ \boldsymbol{wh},\ \boldsymbol{N},\ \boldsymbol{method})$$

The output is *Ga*, the rational approximation of G.

D.5 Optimization

The methods developed in this thesis for FRD synthesis of FDLTI structured controller are based on minimization of functions of the closed-loop system. Three optimization methods are used, two of them are already implemented in third-party routines and their use is briefly described in the following.

- **Constrained minimization**

The MATLAB ™ routine FMINCON from MathWorks [2017] searches the minimum of a constrained nonlinear multivariable function *fun(x)* with respect to parameter vector x. The routine proceeds to minimization by iteratively updating gradients and Hessians at each parameter space point tested, where tha function is evaluated. The evaluations of the function at these points are the only information about the function that the routine has.

The constraints of the parameter space can be posed linear as $A_{eq}x = b_{eq}$ or $Ax \leq b$ or nonlinear inequalities or equality *cf(x)*, that will be evaluated at x and tested to be less or equal zero. A starting point could also be provided by the user.

The call of the routine is:

$$[\boldsymbol{x, fval, exitflag, output}] = \textbf{fmincon}(\boldsymbol{fun, x0, A, b, Aeq, beq, lb, ub, cf, options})$$

where *A*,*b*, *Aeq*, *beq*, *fun*, *cf* are as above. The lower and upper bounds for each element of the parameter vector are passed as the vectors *lb* and *ub*, respectively. The outputs are the minimum value of the function *fval*, the parameter value x that minimizes the function and information about the running as number of function evaluations.

The options for the minimization, passed as variable *opt*, are vast and can be checked in the documentation of MATLAB ™ version 2016a. In this work the options were modified from default values to use '*sqp*' and '*interior-point*' variants of the search.

- **Multidirectional search**

The routine MDSMAX from the The Matrix Computation Toolbox for MATLAB [Higham, 1993, 2002] is a multidirectional direct search method. It searches the maximum of a real function *fun(x)* of vector x using only the evaluations of the function at points of the search space. The inputs of the routine are the function to be maximized *fun*, the starting value *x0* of the search, and options to the search *opt*.

$$[\boldsymbol{x, fmax, nf}] = \textbf{mdsmax}(\boldsymbol{fun, x0, opt})$$

The outputs are the value x that maximizes the function, the maximum value *fmax* and the number of evaluations *nf* of the function until reaching the maximum. The options are the relative size of the simplex, maximum number of function evaluations that may be performed, a minimum value to be reached and the type of the simplex to be used.

Université de Toulouse

THÈSE

En vue de l'obtention du

DOCTORAT DE L'UNIVERSITÉ DE TOULOUSE

Délivré par : *l'Institut Supérieur de l'Aéronautique et de l'Espace (ISAE)*

Présentée et soutenue le *(16/10/2018)* **par :**

Raquel Stella DA SILVA DE AGUIAR

Conception de compensateurs LTI structurés basée sur l'optimisation pour des systèmes incertains et de dimension infinie. Version provisoire

JURY

Phillippe CHEVREL	Professeur	IMT Atlantique	Rapporteur
Edouard LAROCHE	Professeur	Université de Strasbourg	Rapporteur
Christophe PRIEUR	Directeur de recherche	CNRS	Examinateur
Pierre APKARIAN	Directeur de recherche	Onera	Directeur de thèse
Dominikus NOLL	Professeur d'Université	Université de Toulouse	Directeur de thèse

École doctorale et spécialité :
EDSYS : Automatique 4200046
Unité de Recherche :
ONERA - The French Aerospace Lab
Institut de Matèmathiques de Toulouse
Directeurs de Thèse :
Pierre APKARIAN
Dominikus NOLL

Appendix E

E.1 Introduction

La commande de systèmes complexes requiert le plus souvent une approximation du modèle afin qu'il devienne abordable par la théorie et les outils de calcul disponibles. Les lois de commande conçues à partir de ces approximations peuvent se révéler inefficaces lorsqu'elles sont appliquées au système réel. Elles doivent donc être vérifiées a posteriori et peuvent entraîner une modification de l'approximation du modèle si nécessaire. Ceci est particulièrement vrai dans la conception de compensateurs linéaires invariant dans le temps de dimension finie (en anglais, FDLTI) pour les systèmes de dimension infinie en raison du *spillover effect*. Pour cette raison, il est recommandé d'utiliser, soit une approche de type commande robuste (qui prend en compte l'écart entre le système réel et le modèle), soit du data-driven control qui s'affranchit complètement des modèles paramétriques.

La synthèse de commande robuste est un problème NP-difficile, donc des relaxations sont ici encore utilisées pour simplifier le problème. Les relaxations pour la commande robuste disponibles pour l'incertitude mixte et structurée consistent soit à échantillonner, soit à agrandir l'espace de incertitudes. L'approche de l'échantillon, une relaxation interne, fournira une stabilité robuste (RS) seulement si le pire des cas se situe parmi les échantillons, tandis que les relaxations externes introduisent consevatism dans les cas d'incertitude paramétrique en raison de la prise en compte de valeurs d'incertitude qui n'étaient pas présentes dans le problème initial.

Dans le domaine du data-driven control, la synthèse à partir de données fréquentielles est dejà utilisée avec succès pour l'optimisation de performance, mais elle est limitée aux systèmes stables en boucle ouverte ou pré-stabilisés. Ceci exclut son utilisation sur des systèmes de dimension infinie instables dont les données fréquentielles sont par exemple obtenues à partir d'un modèle s'appuyant sur les lois physiques. Les quelques méthodes disponibles pour les systèmes instables n'envisage que les systèmes mono-entrée/mono-sortie (en anglais, SISO), entre autres limitations.

L'un des principaux objectifs de cette thèse est de développer de nouvelles relaxations pour la synthèse de compensateurs robustes structurés pour des systèmes soumis à des incertitudes paramétriques et dynamiques afin de réduire autant que possible le conservatisme de l'approche. Ceci est réalisé par le développement de trois nouvelles techniques de relaxation pour la commande robuste.

La première stratégie est le développement d'une relaxation externe où les multiplieurs et le compensateur sont calculés simultanément sans qu'il soit nécessaire de redimensionner l'incertitude. La deuxième contribution est la dérivation d'une relaxation interne basée sur les estimations de pires cas tant en stabilité qu'en performance par des techniques d'optimisation non-lisse qui réduisent le conservatisme à un niveau très bas. La troisième relaxation développé est une relaxation hybride où les nouvelles relaxations intérieure et extérieure sont combinées et qui est plus efficace en termes de génération de scénarios du pire des cas.

Le deuxième objectif de cette thèse est donc de développer des nouvelles méthodes de conception de lois de commande structurées à partir de la réponse fréquentielle pour des systèmes de dimension infinie stables ou instables. Pour atteindre cet objectif, un estimateur d'abscisse spectrale pour les systèmes IDLTI méromorphes est développé et exploité dans une technique de conception basée sur la minimisation d'abscisse spectrale. Deux autres nouvelles techniques de conception basées sur la minimisation des normes H_2 et H_∞ décalées à l'aide de l'estimateur sont également développées.

La section suivante présente le support théorique de ce travail. La section E.3 présente la nouvelle approximation externe pour la synthèse de correcteur structuré robuste pour les systèmes soumis à des incertitudes mixtes. Cette approche est basées sur des multiplieurs et des contraintes de faible gain

conduisant à un seul modèle augmenté où les scalings et le correcteur sont calculés simultanément. La nouvelle méthode de relaxation interne est présentée dans la section E.4. La technique est un algorithme itératif entrelaçant le calcul des scénarios de pire des cas et la synthèse multi-modèles. Les relaxations externe et interne développées sont combinées en une relaxation hybride dans la section E.5. Dans la section E.6 une méthode de bissection utilisant le critère de stabilité de Nyquist a été produit pour estimer l'abscisse spectrale des systèmes de dimension infinie instables et utilisé pour la conception de correcteurs structurés basé sur la minimisation de l'abscisse spectrale. Cet estimateur est de nouveau utilisé dans les deux sections suivantes pour calculer les normes décalées des systèmes. Dans la section E.7, une technique permettant d'exploiter la norme H_2 décalé pour la stabilisation des systèmes est développée tandis que dans la section E.8, une autre nouvelle technique développée exploite la norme H_∞ décalée. Les techniques de commande robustes sont appliquées à la commande d'un missile dans la section E.9, suivi des remarques de conclusion de la section E.10.

E.2 Concepts préliminaires

Cette section présente les concepts et les résultats de la littérature utilisés dans l'élaboration des nouvelles techniques de conception de lois de commande introduites dans cette thèse.

Considérons la classe $\mathcal{A}(\beta) = \{f : f(t) = f_a(t) + \sum_{n=1}^{\infty} f_n \delta(t - t_n),\ \text{si } t \geq 0,\ \text{et 0 autrement }\}$, avec $t_1 = 0$, $t_n > 0$ pour $n \geq 2$, $\delta(t - t_n)$ la distribution de Dirac à l'instant t_n, $e^{-\beta} f_a \in \mathcal{L}^1(0, \infty)$ et $f_n \in \mathbb{C}$ tel que $\sum_{n=1}^{\infty} |f_n| e^{-\beta t_n} < \infty$. Soit $\hat{\mathcal{A}}(\beta)$ être la classe de transformées de Laplace des fonctions appartenant à la classe $\mathcal{A}(\beta)$. Considérons également les sous-algèbres de $\hat{\mathcal{A}}(\beta)$ définies par $\hat{\mathcal{A}}_-(\beta) = \{\hat{f} : \hat{f} \in \hat{\mathcal{A}}(\beta_1)$ pour un $\beta_1 < \beta\}$ et $\hat{\mathcal{A}}_\infty(\beta) = \{\hat{f} \in \hat{\mathcal{A}}_-(\beta) : \exists \rho > 0$ tel que $\inf_{Re(s)>\beta, |s|\geq\rho} |\hat{f}(s)| > 0\}$.

La classe Callier-Desoer $\hat{\mathcal{B}}(\beta)$ des fonctions de transfert est alors définie comme :

$$\hat{\mathcal{B}}(\beta) := \hat{\mathcal{A}}_-(\beta)\hat{\mathcal{A}}_\infty(\beta)^{-1} = \left\{\hat{f} = \hat{n}\hat{m}^{-1} : \hat{n} \in \hat{\mathcal{A}}_-(\beta) \text{ and } \hat{m} \in \hat{\mathcal{A}}_\infty(\beta)\right\}. \tag{E.1}$$

Les fonctions de transfert $\hat{f} \in \hat{\mathcal{B}}(\beta)$ sont méromorphiques et bornées en $\mathbb{C}_\beta^+$ et n'ont qu'un nombre fini de pôles d'ordre fini en $\overline{\mathbb{C}_\beta^+}$. De plus, les fonctions de transfert $\hat{f} \in \hat{\mathcal{B}}(\beta)$ peuvent également être représentée par $\hat{f} = \hat{n}\hat{m}^{-1}$, avec $\hat{n} \in \hat{\mathcal{A}}_-(\beta)$ et $\hat{m}$ rationelle, propre, non nule sur ∞ et holomorphe en $\mathbb{C}_\beta^+$ ou par $\hat{f} = \hat{f}_s + \hat{f}_u$, avec $\hat{f}_s \in \hat{\mathcal{A}}_-(\beta)$ et $\hat{f}_u$ strictement propre, rationnel et holomorphe en $\mathbb{C}_\beta^-$.

Une matrice de transfert $G(s)$ de dimension arbritaire avec tous ses éléments sur $\hat{\mathcal{A}}(\beta)$, $\hat{\mathcal{A}}_-(\beta)$, ou $\hat{\mathcal{B}}(\beta)$ sera dite appartenant à $\hat{\mathcal{A}}(\beta)$, $\hat{\mathcal{A}}_-(\beta)$, ou $\hat{\mathcal{B}}(\beta)$, respectivement. Tout les $G(s) \in \hat{\mathcal{B}}(\beta)$ sont propres en $\overline{\mathbb{C}_\beta^+}$, en plus, $G(s)$ a une limite G_∞ à l'infini si et seulement si $G_s(s)$ a une limite et $G(s)$ est strictement propre en $\overline{\mathbb{C}_\beta^+}$ si et seulement si les éléments de $G_s(s)$ sont des transformées de Laplace de fonctions $g(.)$ avec $g(.)e^{-\beta} \in L_1(0, \infty)$. $G(s) \in \hat{\mathcal{B}}(\beta)$ est dite stable au sens entrée-sortie (en anglais, BIBO) si $G(s) \in \hat{\mathcal{A}}_-(0)$.

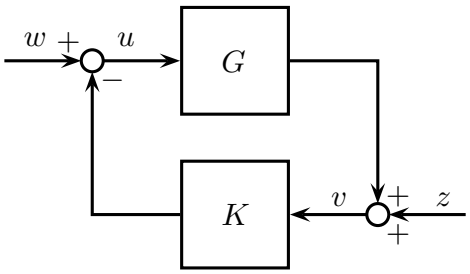

Figure E.1: System G in feedback with system K.

Le système asservi Σ des systèmes $G(s), K(s) \in \hat{\mathcal{B}}(\beta)$, illustré à la Figure E.1, peut se mettre sous la forme $F(s)$ d'entrées u, v et sorties w, z:

$$F(s) = \begin{bmatrix} I & K(s) \\ -G(s) & I \end{bmatrix} \tag{E.2}$$

L'inverse de $F(s)$ est la matrice de transfert $T(s)$:

$$T(s) = F^{-1}(s) = \begin{bmatrix} I - K(I+GK)^{-1}G & -K(I+GK)^{-1} \\ (I+GK)^{-1}G & (I+GK)^{-1} \end{bmatrix} \tag{E.3}$$

où la dépendance de la variable de Laplace s a été omise par commodité.

Pour un système asservi bien posé Σ, c'est-à-dire, $\det(I+GK)$ borné loin de zéro à l'infini en $\mathbb{C}^+$, tous les éléments de $T(s)$ appartiennent également à $\hat{\mathcal{B}}(\beta)$ et Σ est dit stable si tous les éléments de $T(s)$ appartienent à $\hat{\mathcal{A}}_-(0)$. Dans ce contexte, $K(s)$ est dit stabiliser $G(s)$. En Curtain and Zwart [1995, Theorem 9.3.17] les auteurs prouvent que si $G(s) \in \hat{\mathcal{B}}(0)$, alors il existe un correcteur de dimension finie $K(s) \in \hat{\mathcal{B}}(0)$ qui stabilise $G(s)$.

La configuration de la commande H_∞ pour correcteurs structurés, Figure E.2, est une transformation linéaire fractionaire (en anglais, LFT) d'un système P avec un correcteur structuré $K(\kappa)$. Le système P est defini par:

$$P : \begin{bmatrix} z \\ y \end{bmatrix} = \begin{bmatrix} P_{zw} & P_{zu} \\ P_{yw} & P_{yu} \end{bmatrix} \begin{bmatrix} w \\ u \end{bmatrix}, \tag{E.4}$$

avec $w \in \mathbb{R}^{n_w}$ le vecteur d'entrées, partitionné en $w = \{w_1, \cdots, w_{n_l}, w_{n_l+1}, \cdots, w_{n_l+n_j}\}$, $z \in \mathbb{R}^{n_z}$ le vecteur de sortie, partitionné en $z = \{z_1, \cdots, z_{n_l}, z_{n_l+1}, \cdots, z_{n_l+n_j}\}$, $y \in \mathbb{R}^{n_y}$ le signal à asservir, et $u \in \mathbb{R}^{n_u}$ le signal de commande. Structures de commande typiques sont, entre autres, des PID, des correcteurs d'ordre réduit et des correcteurs basés sur l'observation [Apkarian and Noll, 2006a]. Par example, un correcteur d'ordre reduite $n_x(K)$ en representation d'état est décrit par:

$$K(\kappa) : \begin{cases} \dot{x}(t) = A_K(\kappa)x(t) + B_K(\kappa)u(t) \\ y(t) = C_K(\kappa)x(t) + D_K(\kappa)u(t). \end{cases} \tag{E.5}$$

où $A_K(\kappa)$, $B_K(\kappa)$, $C_K(\kappa)$, $D_K(\kappa)$ sont des matrices dont les entrées dépendent du paramètre κ.

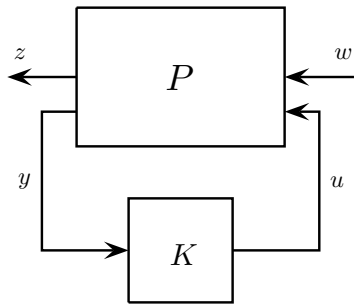

Figure E.2: Configuration du problème de commande H_∞.

Le problème de commande H_∞ structuré sous-optimal multi-modèle et multi-objectif consiste à trouver un $K(s) \in \mathcal{K}$, s'il y en a un, qui stabilise simultanément toutes les systèmes P^i dans un ensemble donné tel que $\max_{i,l} \|T^i_{w_l z_l}\|_\infty < \gamma$ et $\max_{i,j} \|T^i_{w_j z_j}\|_\infty \leq 1$ pour un certain γ et $T^i = P^i \star K(\kappa)$.

Ce problème n'est pas convexe et il n'existe pas de méthode disponible pour l'obtenir des formules pour les correcteurs structurés. Il convient de noter que même si un système est stabilisable, il ne faut pas supposer qu'il peut être stabilisé par un correcteur avec un structure particulière [Iwasaki and Skelton, 1994]. Une approche pour résoudre tels problèmes est donnée dans Apkarian et al. [2014]. Cette approche est basé sur des *bundle methods* pour l'optimisation non lisse introduites dans Apkarian and Noll [2006a,b,d].

Pour les systèmes qui s'écartent de son modèle nominal, l'approche connue sous le nom de commande robuste, Figure E.3, garantit la performance et la stabilité pour le degré d'incertitude du système. Dans le présent travail, l'incertitude considérée est structurée et consiste en des incertitudes paramétrique et des incertitudes dynamiques. Le système P de (E.4) est redefini par:

$$P : \begin{bmatrix} z_\delta \\ z \\ y \end{bmatrix} = \begin{bmatrix} P_{\delta\delta} & P_{\delta w} & P_{\delta u} \\ P_{z\delta} & P_{zw} & P_{zu} \\ P_{y\delta} & P_{yw} & P_{yu} \end{bmatrix} \begin{bmatrix} w_\delta \\ w \\ u \end{bmatrix}, \tag{E.6}$$

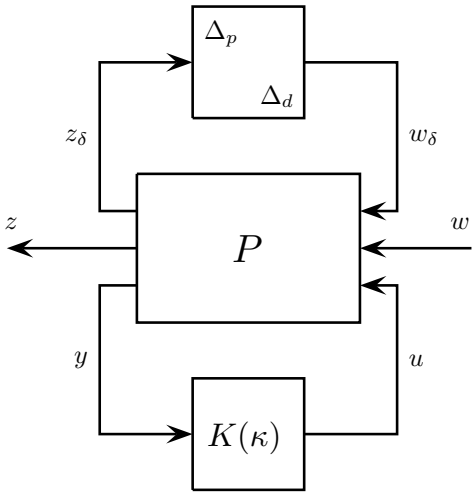

Figure E.3: Interconnexions et signaux d'un système incertain en boucle fermée avec une incertitude structurée mixte Δ et une loi de commande structurée $K(\kappa)$.

où $w_\delta = \Delta z_\delta$. La matrice d'incertitude Δ est structurée $\Delta = \begin{bmatrix} \Delta_p & 0 \\ 0 & \Delta_d \end{bmatrix}$, avec $\Delta_p := \text{diag}\left[\delta_1 I_{r_1}, \ldots, \delta_{N_p} I_{r_{N_p}}\right]$ pour les paramètres incertains réels $\delta_1, \ldots, \delta_{N_p} \in \mathbb{R}$ et leur nombre de répétitions $r_1, \ldots, r_{N_p}$, et $\Delta_d := \text{diag}\left[\Delta_{d1} \ldots, \Delta_{dN_d}\right]$ avec $\Delta_{di} \in \mathbb{C}^{n_{p_i} \times n_{q_i}}$, $i = 1, \ldots, N_d$, chaque Δ_{di} un bloc complexe incertain.

L'incertitude est supposée normalisée de sorte que Δ appartient à la boule unitaire $\mathbf{\Delta} = \{\Delta : \overline{\sigma}(\Delta) \leq 1\}$, avec $\Delta = 0$ représentant le comportement nominal du système. Cela signifie $\delta_i \in [-1, 1]$ pour les paramètres réels d'unceratain et $\overline{\sigma}(\Delta_{di}) \leq 1$ pour les blocs complexes.

Le problème de commande robuste H_∞ structuré consiste à calculer un correcteur structuré avec la lois de commande $u = K(\kappa^*)y$ de telle sorte que le système en boucle fermée soit bien posé, $K(\kappa^*)$ stabilise $\Delta \star P$ pour tout $\Delta \in \mathbf{\Delta}$ et pour tout autre correcteur $K(\kappa)$ avec la même structure, ce correcteur satisfait $\max_{\Delta \in \mathbf{\Delta}} \|T(\kappa^*)\|_\infty \leq \max_{\Delta \in \mathbf{\Delta}} \|T(\kappa)\|_\infty$, où dans ce contexte, $T(\kappa) := \Delta \star P \star K(\kappa)$.

La synthèse de correcteurs robustes est un programme semi-infini. Pour devenir résoluble, le problème est généralement approximé en utilisant des relaxations externes, où un $\tilde{\mathbf{\Delta}}$ plus simple et structuré est construit de telle sorte que $\tilde{\mathbf{\Delta}} \supset \mathbf{\Delta}$. Le raisonnement est que si le problème est résolu sur $\tilde{\mathbf{\Delta}}$, il est également résolu sur $\mathbf{\Delta}$. Même si une quantité inconnue de conservatisme est introduite, cette approche reste simple et s'avère efficace dans une grande variété de cas [Chiang and Safonov, 1992; Doyle, 1982, 1985; Fan et al., 1991; Safonov et al., 1993; Young et al., 1991].

Iwasaki and Hara [1998] ont proposé une approche basée sur des séparateurs topologiques et ont dérivé des conditions de stabilité robustes à partir des conditions pour qu'un système asservi soit bien posé. Dans la suite, ils montrent que le système est bien posé si les graphiques des deux sous-systèmes sont séparés topologiquement. Enfin, ils prouvent que si ces conditions sont remplies, il existe alors un séparateur topologique, avec configuration illustrée à la Figure E.4. Le problème de robustesse est alors réduit à trouver un séparateur (*LFT-scaling*) qui remplisse ces conditions ou prouver qu'un tel séparateur n'existe pas.

Une autre relaxation utilisée est la relaxation interne qui consiste à résoudre le problème pour un ensemble discret de scénarios $\check{\mathbf{\Delta}} \subset \mathbf{\Delta}$. Chaque scénario Δ^i résulte en un système $P^i = \Delta^i \star P$ de sorte que l'ensemble $\check{\mathbf{\Delta}}$ dispose d'un ensemble de modèles associés appelé ensemble multi-modèle. Cet ensemble $\check{\mathbf{\Delta}}$ peut être construit par l'approche probabiliste ou par l'approche du pire des cas. L'approche du pire des cas est préférable dans les cas où l'on désire une certification de stabilité robuste sur $\mathbf{\Delta}$. La justification pour l'approche du pire des cas, c'est qu'une fois que les modèles de l'ensemble multi-modèles des pire des cas sont commandés en même temps, le correcteur conçu $K(\kappa^*)$ assure la robustesse en stabilité et en performances sur l'ensemble $\mathbf{\Delta}$.

Deux types de pires scénarios se présentent à cette fin: le pire scénario de stabilité et le pire scénario de performance. Le pire des cas de stabilité est l'instance qui se traduit par la pire marge de la stabilité, soit $T^i = \Delta^i \star P \star K$. L'abscisse spectrale est utilisée comme marge de stabilité une fois qu'elle reflète le degré d'instabilité d'un système. Le pire des cas de performance est l'instance Δ^l qui

donne la plus grande norme H_∞, soit $T^l = \Delta^l \star P \star K$. Les calculs de ceux-ci sont exprimés en tant que programmes (E.7) et (E.8), respectivement:

$$\alpha^* = \max_{\Delta \in \mathbf{\Delta}} \alpha(A(\Delta)) \tag{E.7}$$

$$h^* = \max_{\Delta \in \mathbf{\Delta}} \|T\|_\infty. \tag{E.8}$$

où $A(\Delta)$ est la matrice A du système en boucle fermée incertain.

Ces problèmes de maximisation sont non convexes et les fonctions à maximiser sont non lisses. Des techniques d'optimisation non lisses adaptées à ces problèmes ont été développées en Apkarian et al. [2015a,b] pour les variables limité dans un hypercube. Cependant, les contraintes sur $\Delta \in \mathbf{\Delta}$ sont du type semi-défini pour les incertitudes dynamiques $\overline{\sigma}(\Delta_d) \leq 1$. Apkarian and Noll [2017] a proposé un changement de variables permettant de modifier la contrainte semi-définie dans Δ_d dans une nouvelle variable x_d limité dans un hypercube. Programmes (E.7) et (E.8) peuvent alors être refondus en programmes d'optimisation non lisses limité dans un hypercube.

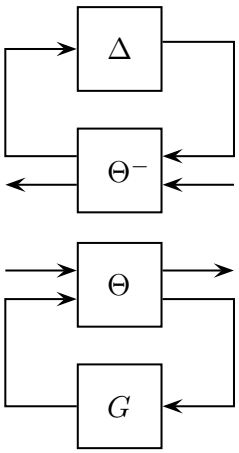

Figure E.4: *LFT-scaling* Θ pour un système G soumis à l'incertitude Δ.

La synthèse H_∞ des correcteurs structurés basée sur la réponse frequentielle ne recours pas aux modèles paramétriques. Le critère de stabilité Nyquist discret est ensuite utilisé pour l'analyse de stabilité.

Soit $G(s), K(s) \in \hat{\mathcal{B}}(0)$, sans pôles ni zéros sur l'axe imaginaire et nu_G et nu_K le nombre de pôles en $\mathbb{C}_0^+$. On suppose que $G(s)K(s)$ est propre et il a une limite à l'infini en $\mathbb{C}^+$. Considérons maintenant le système $F(s)$ (E.2) et définissons $f(s)$ comme:

$$f(s) = det(F(s)). \tag{E.9}$$

Pour $f(s) \neq 0$ pour tout $s \in \mathcal{D}$, l'indice de $f(s)$, $\text{ind}(f(s), 0)$, est défini comme le nombre de fois que $f(s)$ s'enroule autour de l'origine dans le sens inverse des aiguilles d'une montre en suivant le contour $\mathcal{D}$. Le système asservi Σ est stable si $\text{ind}(f(s), 0) = -nu_G + nu_K$ [Desoer and Wang, 1979].

Huang et al. [1993] a proposé une alternative pour traiter les cas avec des pôles et des zéros sur l'axe imaginaire. Pour cela, considérons la fonction $f(s)$ avec n_0 et n_{jR} correspondant à la somme du nombre de pôles de $G(s)$ et $K(s)$ à l'origine et sur $j\mathbb{R}\backslash\{0\}$, respectivement. $\Psi(s)$ est défini comme suit:

$$\Psi(s) = \left(1 + \frac{1}{s(s+1)}\right)^{n_0} \cdot \prod_{i=1}^{n_{jR}} \left(1 + \frac{1}{(s^2 + \beta_i^2)(s+1)}\right)^{n_i}. \tag{E.10}$$

Maintenant pour $\tilde{f}(s) = \frac{f}{\Psi(s)}$ on a que $\text{ind}(f(s), 0) = \text{ind}(\tilde{f}(s), 0)$.

L'utilisation du critère de stabilité de Nyquist pour une grille discrète et finie de fréquences exige une analyse minutieuse pour vérifier si la grille est assez dense pour tenir compte de tous les tours autour de l'origine. Apkarian and Noll [2017] ont établi une méthode pour déterminer la grille plus grossière nécessaire pour calculer l'indice correct.

Considérons à nouveau la fonction $f(s)$ de (E.9) satisfaisant aux conditions qui ont suivi ou $\tilde{f}(s) = \frac{f(s)}{\Psi(s)}$ dans le cas où $f(s)$ a des pôles sur l'axe imaginaire. On recherche les fréquences $\omega_0 = 0 < \omega_1 < \ldots < \omega_N = \infty$ de sorte que le polygone fermé $P_f = \{f(-j\omega_N), \ldots, f(0), f(j\omega_1), \ldots, f(j\omega_N)\}$ a le même indice de $f(s)$ pour le contour de Nyquist $\mathcal{D}$. Soit $P_f(j\omega)$ désignant la fonction interpolée linéairement associée au polygone, et $\Delta_{[\omega',\omega'']}\arg f$ indiquant le changement d'argument de f dans la section $[j\omega', j\omega'']$ de $j\mathbb{R}$. On a que $\mathrm{ind}(f(s), 0) = \mathrm{ind}(P_f, 0)$ si les nodes ω_i sont choisis de telle sorte que, pour chaque i,

$$\Delta_{[\omega_i,\omega_{i+1}]}\arg f = \arg\left[\frac{f(j\omega_{i+1})}{f(j\omega_i)}\right]. \tag{E.11}$$

Soit maintenant $L[.,.|$ une borne de premier ordre de f où $L[\omega^-, \omega^+| \geq |f'(j\omega)|$ por chaque $\omega \in [\omega^-, \omega^+]$. Pour deux nœuds consécutifs $P_f(\omega_i), P_f(\omega_{i+1})$ ne passant pas par 0, si

$$L[\omega_i, \omega_{i+1}](\omega_{i+1} - \omega_i) < |f(j\omega_i)| + |f(j\omega_{i+1})|, \tag{E.12}$$

alors (E.11) est satisfait.

Notez que lorsqu'une grille est construite afin de certifier les résultats du test de stabilité de Nyquist, ceci est construite pour la $f(s)$ ou $\tilde{f}(s)$ actuele. La grille doit être mise à jour à chaque nouveau correcteur conçu, ou au moins à chaque fois que le test de stabilité de Nyquist est effectué pour un nouveau correcteur. La condition (E.12) peut également être utilisée pour construire une grille peu dense à partir d'une grille plus dense afin de simplifier le calcul de l'indice.

E.3 Développement et implémentation d'une nouvelle approximation externe pour la synthèse de correcteurs structurés robustes

On recherche des *LFT-scalings* qui répondent aux conditions établies dans [Iwasaki and Hara, 1998, Theorem 4]. Pour cela, on définie les multiplieurs dynamiques $\Phi \in \mathbf{\Phi}$ comme:

$$\mathbf{\Phi} := \left\{\Phi(s) = \mathrm{diag}(\phi_1(s), \ldots, \phi_{N_p}(s)) : \phi_i(s) \text{ stable}, \ \|\phi_i(s)\|_\infty < 1\right\}, \tag{E.13}$$

où $\Phi(s)$ a la même structure diagonale en bloc que $\Delta_p \in \mathbf{\Delta}_p$ et donc commute avec $\Delta_p \in \mathbf{\Delta}_p$.

Introduisons l'ensemble $\mathbf{D}$ de D-*scalings*:

$$\mathbf{D} := \left\{D(s) = \mathrm{diag}(d_1(s)I_{p_i}, \ldots, d_{N_d}(s)I_{p_{N_d}}) : d_i(s), d_i(s)^{-1} \text{ stable}\right\}. \tag{E.14}$$

Notez que $D\Delta_d = \Delta_d D$ en raison de la structure en blocs de Δ_d et D.

Proposition E.1. *Soit $\Phi(s) \in \mathbf{\Phi}$, $D(s) \in \mathbf{D}$ et $\Delta_p \in \mathbf{\Delta}_p$, $\Delta_d \in \mathbf{\Delta}_d$ comme défini ci-dessus, définissons*

$$\Gamma(\Phi, D) := \begin{bmatrix} -\Phi & 0 & I+\Phi & 0 \\ 0 & 0 & 0 & D \\ I-\Phi & 0 & \Phi & 0 \\ 0 & D^{-1} & 0 & 0 \end{bmatrix}. \tag{E.15}$$

Alors le système en boucle fermée $\begin{bmatrix}\Delta_p & 0 \\ 0 & \Delta_d\end{bmatrix} \star \Gamma(\Phi, D)$ *est stable et satisfait à l'estimation*

$$\left\| \begin{bmatrix}\Delta_p & 0 \\ 0 & \Delta_d\end{bmatrix} \star \Gamma(\Phi, D) \right\|_\infty \leq 1. \tag{E.16}$$

La preuve peut être trouvée dans Aguiar et al. [2018].

Dans la séquence, notez que l'inverse de $\Gamma(\Phi, D)$ concernant le produit-étoile de Redheffer est obtenu en échangeant Φ par $-\Phi$ et D par D^{-1} dans (E.15). Cela donne

$$\Gamma(\Phi, D)^{-\star} = \begin{bmatrix} \Phi & 0 & I-\Phi & 0 \\ 0 & 0 & 0 & D^{-1} \\ I+\Phi & 0 & -\Phi & 0 \\ 0 & D & 0 & 0 \end{bmatrix}.$$

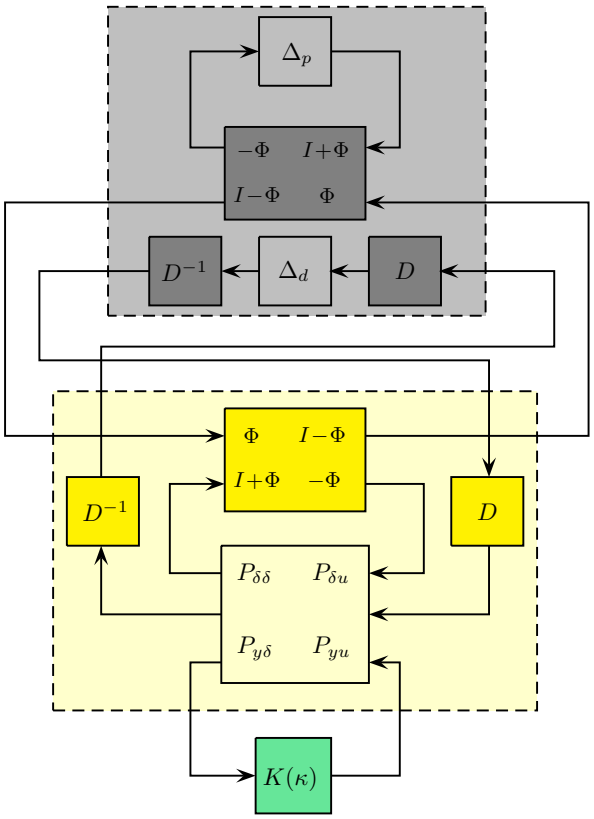

Figure E.5: Schéma d'interconnexion pour la relaxation externe pour un correcteur robuste.

Soit le système P_γ défini depuis P avec les entrées-sorties de la performance escalonées:

$$P_\gamma : \quad \begin{bmatrix} z_\delta \\ z \\ y \end{bmatrix} = \begin{bmatrix} P_{\delta\delta} & P_{\delta w} & P_{\delta u} \\ \frac{1}{\gamma}P_{z\delta} & \frac{1}{\gamma}P_{zw} & \frac{1}{\gamma}P_{zu} \\ P_{y\delta} & P_{yw} & P_{yu} \end{bmatrix} \begin{bmatrix} w_\delta \\ w \\ u \end{bmatrix}. \tag{E.17}$$

Puis avec les mêmes notations que ci-dessus et l'ensemble de *scalings* $\mathbf{D}$ convenablement généralisé pour prendre en compte le nouveau bloc de performance, on obtient le théorème E.1 [Aguiar et al., 2018].

Théorème E.1. *Supposons qu'il existe $\Phi \in \mathbf{\Phi}$, $D \in \mathbf{D}$, et un correcteur structuré $K(\kappa)$ tel que $\Gamma(\Phi, D)^{-\star} \star P_\gamma \star K(\kappa)$ est stable de façon interne et satisfait à l'estimation*

$$\left\|\Gamma(\Phi, D)^{-\star} \star P_\gamma \star K(\kappa)\right\|_\infty < 1. \tag{E.18}$$

Alors le système bouclé $\Delta \star P \star K(\kappa)$ est robustement stable sur $\mathbf{\Delta}$, et son pire des cas de performance H_∞ sur $\mathbf{\Delta}$ est γ. □

La commande H_∞ robuste structuré peut être formulé comme le programe d'optimisation:

$$\begin{array}{ll} \text{minimiser} & \gamma \\ \text{soumis à} & \|\Gamma(\Phi, D)^{-\star} \star P_\gamma \star K(\kappa)\|_\infty \leq 1 - \eta \\ & \Gamma(\Phi, D)^{-\star} \star P_\gamma \star K(\kappa) \text{ stable de façon interne} \\ & \|\Phi\|_\infty \leq 1 - \eta \\ & \Phi \in \mathbf{\Phi}, D \in \mathbf{D}, \kappa \in \mathbb{R}^n, \gamma \in \mathbb{R}_+ \end{array} \tag{E.19}$$

où le petit seuil $\eta > 0$ est utilisé pour assurer les contraintes des inegalités.

Il en résulte un programme non convexe et non lisse, avec des contraintes non lisses. Pour gérer ce programme, l'approche algorithmique de la synthèse multi-disque où tous les contraintes H_∞ sont manipulées simultanément de Apkarian and Noll [2006a] a été choisi en utilisant la routine MATLAB ™ SYSTUNE [MathWorks, 2017] pour implémenter l'approche.

Table E.1: Données de la synthèse de correcteurs robustes utilisant la nouvelle relaxation externe pour l'ensemble de cas de test.

Ex	$n_x(K)$	n_K	γ	$\underline{\gamma}$	$\overline{\gamma}$	SG	SG_Φ	t_s	t_a
1	2	12	0.987	0.995	0.997	1	0	7	0.28
2	1	4	0.991	1	1.002	1	0	11	0.26
3	4	29	1.415	1.421	1.424	0.999	0	34	0.28
4	2	16	0.991	0.999	1.001	1	0	11	0.1
5	4	30	1.831	1.614	1.617	0.947	0	29	0.42
6	1	4	0.992	1	1.002	1	0	6	0.25
7	4	48	0.996	1.004	1.007	1	0	45	0.69
8	2	9	1.117	1.127	1.129	1	0.988	9	0.06
9	3	22	104.91	134.2	168.46	1.311	1.310	93	4.59
10	3	14	18.481	3.842	3.865	1.862	1.861	152	6.8
11	4	19	1.417	1.008	1.01	1.009	1.009	84	3.5
12	5	24	1.006	1.016	1.018	0.999	0.998	26	0.2
13	1	4	13.832	1.008	1.01	1	0.995	36	1.08
14	2	12	1.109	1	1.002	1	0.998	47	16.6
15	4	19	9.999	5.091	5.103	0.999	0.999	14	0.06
16	5	37	2.349	1.948	1.951	0.999	0.991	270	0.37
17	3	23	20.119	1.733	1.738	0.999	0.996	83	0.88
18	3	14	10.085	9.16	9.179	1.007	1.007	39	0.18
19	1	4	10.366	1.000	Inf	1.034	1.023	82	2.46
20	3	14	10.093	8.057	8.115	1.009	1.009	451	2.64
21	1	9	0.999	1	1.002	1	1	57	0.56
22	2	9	30.451	49510	49609	4728	4729	239	0.63
23	1	8	40.763	14.777	16.103	1.013	1.013	92	6.69
24	3	14	1.97	1.959	1.963	1	0.9	16	0.18
25	1	8	30.25	217.0	233.6	20.02	20.02	47	4.9
26	1	9	0.999	1	1.002	1	0.999	57	0.25
27	3	14	1.594	1.588	1.592	1	0.998	17	0.29
28	1	6	10.015	2.966	2.973	1.001	1.001	16	0.39
29	4	19	1.278	1.07	1.073	0.999	0.939	29	0.07
30	5	24	7.262	7.078	7.099	0.999	0.945	31	0.12

Légende:

Ex:	Cas de test	γ :	performance atteinte par *outer*
$n_x(K)$:	ordre du correcteur	$\underline{\gamma}$:	borne inférieure du certificat sur la performance
n_K:	dimension du paramètre κ	$\overline{\gamma}$:	borne supérieure du certificat sur la performance
t_s:	temps ecoulé pour la synthèse [s]	SG_Φ:	$\|\Phi\|_\infty$
t_a:	temps ecoulé pour la certification [s]	SG:	$\|\Gamma(\Phi, D)^{-\star} \star P_\gamma \star K(\kappa)\|_\infty$

Le Tableau E.1 présente les résultats de la mise en œuvre du programme (E.19) pour un ensemble de 30 cas de tests. Dans tous les cas, l'ordre de la répresentation d'état de D et Φ est 2. Les valeurs des colonnes SG et SG_Φ représentent les valeurs des première et troisième contraintes du programe (E.19) et doivent être inférieur à 1. En raison de la précision numérique, les valeurs très proches à 1 sont indiqués par 1 dans le tableau. Une valeur supérieure à 1 dans l'une ou l'autre de ces colonnes signifie que la synthèse a échoué car la stabilité n'est pas garantie. Pour les cas de test 22 et 25, SG et SG_Φ sont plus de 20 fois plus grandes que la limite 1 et les valeurs de la certification indiquent que le système peut être considéré comme instable ou très dégradé. Il en va de même pour le cas 9, où les contraintes sont violées de plus de 100%. Dans 23% de cas les contraintes sont violées de moins de 3%, mais en conséquence $\underline{\gamma}$ et γ sont en désaccord à 90%, avec une performance certifiée inférieure à la valeur donnée par l'approche. Dans le cas 10, les contraintes dépassent 1 de plus de 30% mais la certification atteste que le système est stable et il a une meilleure performance que la valeur retounée par l'approche. Dans le cas 13, les contraintes ne dépassent pas 1, mais l'approche et la certification sont en désaccord de 93% sur les performances, la certification attestant une meilleure performance. Dans les cas où les contraintes ne sont pas violées, l'écart est de 30% dans le cas 29 et l'écart est inférieur à 12% pour les 57% de cas restants. Les valeurs certifiées peuvent être considérée comme exacte dans tous les cas sauf 19, pour lequel la borne supérieure est infinie alors que la limite inférieure est 1.

La nouvelle méthode développée est comparée à la méthode de synthèse robuste DKSYN [MathWorks, 2017] qui implémente le *DK-iteration* de Doyle [1985]. Notez que le *DK-iteration* est également

Table E.2: Comparaison entre la nouvelle relaxation externe et la routine DKSYN pour $\mathbf{\Delta}$ redimensionné.

		outer		DKSYN				*outer*		DKSYN	
Ex	$\sigma(\Delta)$	$\underline{\gamma}$	$n_x(K)$	μ	$n_x(K)$	*Ex*	$\sigma(\Delta)$	$\underline{\gamma}$	$n_x(K)$	μ	$n_x(K)$
1	1.007	0.977	4	0.993	13	16	0.825	1.592	15	1.212	98
2	0.99	0.994	1	1.01	16	17	0.053	1.573	1	19.034	9
3	1.117	1.482	10	0.895	38	18	0.053	1.055	1	18.775	6
4	1.017	1.001	14	0.983	20	19	0.224	3.13 0	1	4.466	6
5	0.826	1.044	5	1.21	22	20	x	8.056	3	x	x
6	1.072	0.907	2	0.933	7	21	1.002	0.991	15	0.998	20
7	1.048	0.966	15	0.954	46	22	x	49510	2	x	x
8	0.881	1.020	2	1.135	9	23	0.531	1.442	1	1.882	294
9	0.303	749	15	3.299	445	24	0.941	1.684	10	1.062	34
10	0.382	3.849	7	2.621	10	25	0.555	Inf	15	1.803	304
11	0.224	1.028	1	4.472	253	26	1.068	1.052	15	0.936	24
12	0.612	0.528	2	1.635	27	27	0.589	1.156	1	1.698	25
13	1.005	4.500	13	0.995	99	28	0.005	0.014	1	220	7
14	1.001	0.990	14	0.999	120	29	0.854	0.938	2	1.17 0	18
15	0.936	5.254	10	1.069	30	30	0.914	4.672	10	1.094	30

Légende:

Ex:	Cas de test	$\sigma(\Delta)$:	nouvelle borne pour l'incertitude Δ
outer :	données de *outer*	DKSYN :	données de DKSYN
$\underline{\gamma}$:	borne inférieure du certificat pour *outer*	μ :	performance atteinte par DKSYN
$n_x(K)$:	ordre du correcteur		

basée sur une relaxation externe. Il faut garder à l'esprit que DKSYN n'assure pas une performance robuste et une stabilité robuste sur $\mathbf{\Delta}$, mais plutôt à une boule rédimensionée. Afin de comparer correctement les techniques, on a utilisé le même $\mathbf{\Delta}$ redimensionné pour une nouvelle synthèse avec la nouvelle relaxation externe. Les résultats sont présentés au Tableau E.2. Sur le nouveau $\mathbf{\Delta}$ l'approche ne peut pas atteindre de meilleures performances que DKSYN dans 36% des cas pour un correcteur d'orde jusqu'au 15. Dans les autres cas (60 %), sur l'incertitude rédimensioné, l'approche est meilleur que DKSYN . A l'exception du cas 10, l'ordre du correcteur conçu par DKSYN est toujours plus grand que celui du correcteur conçu par la nouvelle approche.

La nouvelle relaxation externe pour la synthèse des correcteurs robustes structurés s'est avérée efficace, en stabilisant et en obtenant de bonnes performances dans tous les cas de test sauf deux. Les solutions de la mise en œuvre de la nouvelle relaxation externe par des techniques d'optimisation non lisses sont encore sous-optimale, et donc conservative, dans certains cas. Les causes possibles de cette performance sous-optimale sont: les contraintes de faible gain étant des conditions suffisantes mais non nécessaires, des solutions locales et basse ordre de multiplieurs.

Essais supplémentaires concernant la variation de l'ordre des multiplieurs Φ et des *D-scalings* indiquent que un *scaling* dynamique fonctionnera généralement mieux qu'un statique. Pour les cas avec un nombre élevé d'incertitudes paramétriques ou de nombreuses incertitudes paramétriques répétées, l'augmentation de l'ordre de Φ dégrade les performances en raison du nombre élevé de paramètres à prendre en compte simultanément. Dans le cas d'un petit nombre d'incertitudes paramétriques et des répétitions, on peut remarquer qu'en augmentant l'ordre de G, on améliore les performances.

L'analyse des résultats sur les problèmes d'incertitude redimensionnés a prouvé que l'approche de relaxation externe developpé est très compétitif par rapport à DKSYN , surperformant DKSYN plus souvent qu'il n'a été surmonté. En outre, l'ordre des correcteurs conçu par l'approche, dont l'ordre n'est pas supérieur à 5, est toujours plus petit que l'ordre des correcteurs de DKSYN . Les résultats prouvent qu'en effet le calcul simultané des multiplieurs et du correcteur est la meilleure option jusqu'à présent.

E.4 Développement et implémentation d'une nouvelle approximation interne pour la synthèse de correcteurs structurés robustes

L'approche de relaxation externe développée est encore conservative dans les cas de répétition élevée des incertitudes paramétriques. Pour cette raison, une nouvelle relaxation interne est envisagée et discutée.

La stratégie commence par la conception d'un correcteur pour le modèle nominal. Dans ce qui suit, un procédure itérative vérifie si une incertitude dans l'ensemble $\mathbf{\Delta}$ peut déstabiliser le système ou dégrader la performance au-delà d'un seuil. Dans le cas positif, l'incertitude qui implique le cas le plus défavorable à la déstabilisation ou à la dégradation est estimée et le système pertubée correspondant est ajoutée à un ensemble de systèmes. Un nouveau correcteur est conçu pour la commande simultanée de toutes les systèmes dans l'ensemble et une nouvelle incertitude est estimée. La procédure prend fin si une telle incertitude n'existe pas. Cette stratégie est similaire à celle présentée dans Apkarian et al. [2015b] pour les incertitudes purement paramétriques. L'Algorithme E.1 ci-dessous étend l'approche aux systèmes soumis à des incertitudes mixtes en utilisant les résultats de Apkarian and Noll [2017] pour convertir les contraintes semi-définies en contraintes dans un hypercube.

Une synthèse de commande robuste utilisant des relaxations internes comme celle développée ici nécessite d'une certification sur $\mathbf{\Delta}$ *a posteriori*. Ceci est nécessaire car les relaxations internes assurent la robustesse de performance et de stabilité pour un ensemble $\check{\mathbf{\Delta}} \in \mathbf{\Delta}$.

Algorithme E.1: Synthése de lois de commande robuste par l'approximation interne

Données: $\varepsilon > 0$.

▷ **Instruction 1** (`Synthèse Nominale`)**.**
Initialisez l'ensemble des scénarios actifs en tant que $\mathbf{\Delta}_a = \{0\}$.

▷ **Instruction 2** (`Synthèse Multimodèle`)**.**
Compte tenu de l'ensemble fini des scénarios actifs $\mathbf{\Delta}_a \subset \mathbf{\Delta}$, concevez un correcteur structuré $K(\kappa^*)$ en résolvant le programme multi-disques H_∞

$$h_* = \min_{\kappa \in \mathbb{R}^n} \max_{\Delta \in \mathbf{\Delta}_a} \|\Delta \star P \star K(\kappa)\|_\infty.$$

La solution est le correcteur structuré $K(\kappa^*)$.

▷ **Instruction 3** (`Calcul du pire des cas de stabilité`)**.**
Essayez de déstabiliser le système bouclé $\Delta \star P_r \star K(\kappa^*)$ en calculant son pire des cas pour l'abscissa spectrale:

$$\alpha^* = \max_{\Delta \in \mathbf{\Delta}} \alpha\left(A(\Delta, \kappa^*)\right).$$

La solution est le pire scénario de stabilité Δ^*. Si $\alpha^* = \alpha\left(A(\Delta^*, \kappa^*)\right) \geq 0$, incluez Δ^* dans l'ensemble $\mathbf{\Delta}_a$ et revenez à l'instruction 2. Sinon, passez à l'instruction 4.

▷ **Instruction 4** (`Calcul du pire des cas de performance`)**.**
Essayez de dégrader la performance du système bouclé $\Delta \star P \star K(\kappa^*)$ en calculant son pire des cas de la norme H_∞ :

$$h^* = \max_{\Delta \in \mathbf{\Delta}} \|\Delta \star P \star K(\kappa^*)\|_\infty.$$

La solution est le pire scénario de performance $\Delta^\sharp$.

▷ **Instruction 5** (`Critère d'arrêt`)**.**
Si $\alpha(A(\Delta^\sharp, \kappa^*)) < 0$ et $h^* < (1+\varepsilon)h_*$, la dégradation de performance est marginale; sortez de la boucle et passez à l'étape **??** pour la certification postérieure. Sinon incluez $\Delta^\sharp$ dans l'ensemble $\mathbf{\Delta}_a$ et revenez à l'instruction 2.

▷ **Instruction 6** (`Certification`)**.**
Utiliser un solveur global pour certifier *a posteriori* que $T(\kappa^*)$ est robuste en performance et en stabilité $\mathbf{\Delta}$ sur l'ensemble $\mathbf{\Delta}$.

Tous les programmes de l'Algorithme E.1 ne sont pas lisses et sont adressés par des methodes de *bundle et trust-region*. Les programmes α^* à l'étape 3 et h^* à l'étape 4 sont discutés en détail dans les références Apkarian et al. [2015a,b, 2016]; Ravanbod et al. [2017].

Les résultats de la synthèse pour 30 cas de test utilisant l'implémentation de l'Algorithme E.1 est présenté dans le Tableau E.3. Dans la tolérance de 5%, la borne inférieure de la certification est égale à γ retourné par la méthode dans tous les cas, sauf le cas 4, où l'écart est de 20%. En revanche, l'écart entre γ et la borne supérieure est inférieur à 5 % dans 73 % des cas. Dans le cas de test 19, la borne supérieure échoue ou atteste que le système est instable. Dans les cas de test 9, 10, 20 et 25, la borne supérieure est plus que le double de γ, et pour les cas de test 4, 16 et 23, la variation est inférieure à 30 %. Les cas de test 3, 5, 7, 16 et 23 exigent plus de 20 scénarios et les cas de test qui exigent plus de 10 et moins de 20 scénarios sont 1, 12, 17, 17, 25 et 30.

Table E.3: Données de la synthèse de correcteurs robustes utilisant la nouvelle relaxation interne pour l'ensemble de cas de test.

Ex	$n_x(K)$	n_K	γ	$\underline{\gamma}$	$\overline{\gamma}$	$\lvert\Delta_a\rvert$	t_s	t_a
1	2	12	0.995	0.995	0.997	11	28	0.15
2	1	4	1.000	0.999	1.001	7	11	0.17
3	3	22	1.005	1.009	1.011	25	279	0.67
4	2	16	0.832	0.999	1.001	3	6	0.33
5	4	30	0.996	0.996	0.999	25	1247	1.06
6	1	4	1.000	1.000	1.002	4	2	0.31
7	4	48	0.999	1.002	1.004	29	1792	0.75
8	2	9	1.000	1.000	1.002	4	2	0.11
9	4	29	1.008	1.008	4.377	5	38	5.05
10	3	14	0.982	0.982	2.777	3	9	21.8
11	1	4	1.000	1.000	1.002	2	3	4.50
12	3	14	1.000	1.000	1.002	11	70	0.43
13	1	4	1.000	1.000	1.001	3	3	1.12
14	2	12	1.006	0.999	1.009	9	16	10.9
15	3	14	0.998	0.996	1.001	8	26	1.01
16	5	37	0.996	1.02 0	1.138	31	1269	6.55
17	3	23	0.998	0.999	1.002	18	151	3.78
18	2	9	0.997	1.007	1.009	7	16	5.98
19	1	4	1.000	1.000	Inf	2	1	1.62
20	3	14	1.000	0.997	5.125	8	62	9.02
21	1	9	1.000	1.000	1.002	3	4	0.19
22	2	9	1.000	0.999	1.002	7	44	6.01
23	3	22	0.994	1.043	1.255	36	578	6.90
24	3	14	1.084	1.088	1.117	8	21	0.99
25	4	29	0.990	0.989	9.112	13	264	5.37
26	1	9	1.000	1.000	1.002	3	3	0.31
27	3	14	1.002	1.002	1.004	8	36	0.33
28	2	12	1.000	1.000	1.011	8	10	14.3
29	2	9	1.000	1.000	1.001	6	6	0.10
30	5	24	1.001	1.001	1.003	13	92	0.42

Légende:

Ex:	Cas de test		
$n_x(K)$:	ordre du correcteur	$\underline{\gamma}$:	borne inférieure du certificat sur la performance
n_K:	dimension du paramètre κ	$\overline{\gamma}$:	borne supérieure du certificat sur la performance
γ:	performance atteinte par *inner*	t_s:	temps ecoulé pour la synthèse [s]
$\lvert\Delta_a\rvert$:	nombre de scénarios	t_a:	temps ecoulé pour la certification [s]

Comme illustration de la distribution des scénarios, la Figure E.6 montre tous les scénarios générés pour le cas 7, 8, 16 et 23 sur le plan complexe. Il est à noter que même si plus de 20 scénarios sont générés pour les cas 16 et 23, les instances de l'incertitude parametrique prennent moins de 10 valeurs. Cela signifie qu'elles sont répétées par itérations alors que des nouvelles valeurs sont générées seulement pour l'incertitude dynamique.

Les résultats de la synthèse par les nouvelles relaxations internes et externes et par DKSYN sont présentées au Tableau E.4 à des fins de comparaison directe. La synthèse par la relaxation interne est meilleure que la synthèse par relaxation externe dans 67% des cas et équivalent dans les autres cas. La synthèse par relaxation interne est meilleure que celle par DKSYN dans 57% des cas, il est surperformé par DKSYN dans le cas 3, mais DKSYN a besoin d'un correcteur avec ordre 12 fois plus élevées, et elles sont équivalentes dans 40% des cas.

On rappele que les résultats de DKSYN sont valides pour un $\boldsymbol{\Delta}$ redimensioné. Afin de comparer

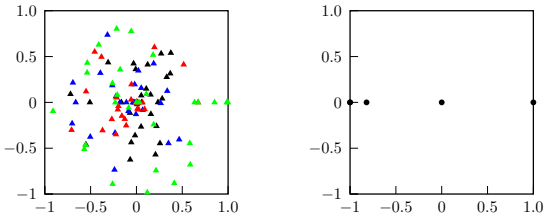

(a) Cas de test 7 (b) Cas de test 8

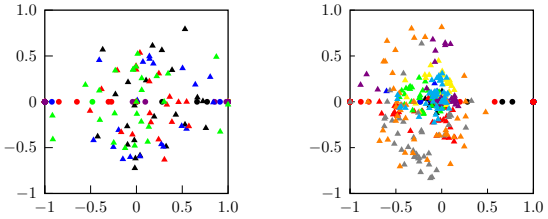

(c) Cas de test 16 (d) Cas de test 23

Figure E.6: Scénarios générés pour les cas de test 7, 8, 16 et 23 sur le plan complexe, avec des triangles et des cercles pour les incertitudes complexes et réelles, respectivement. Les instances d'un bloc d'incertitude par itérations sont tracées dans la même couleur.

Table E.4: Comparaison entre la synthèse utilisant la nouvelle relaxation interne, la nouvelle relaxation externe et la routine DKSYN .

Ex	$n_x(K^1)$	*inner* γ	*outer* $\underline{\gamma}$	DKSYN $n_x(K^2)$	DKSYN μ	Ex	$n_x(K^1)$	*inner* γ	*outer* $\underline{\gamma}$	DKSYN $n_x(K^2)$	DKSYN μ
1	2	0.995	0.995	13	0.993	16	5	1.020	1.948	98	1.212
2	1	0.999	1.000	16	1.01	17	3	0.999	2.078	9	19.034
3	3	1.009	4.807	38	0.895	18	2	1.007	19.636	6	18.775
4	2	0.999	0.999	20	0.983	19	1	1.000	1.000	6	4.466
5	4	0.996	1.614	22	1.21	20	3	0.997	8.057	x	x
6	1	1.000	1.000	7	0.933	21	1	1.000	1.000	20	0.998
7	4	1.002	1.004	46	0.954	22	2	0.999	49510	x	x
8	2	1.000	1.127	9	1.135	23	3	1.043	Inf	294	1.882
9	4	1.008	Inf	445	3.299	24	3	1.088	1.959	34	1.062
10	3	0.982	Inf	10	2.621	25	4	0.989	2692	304	1.803
11	1	1.000	1.546*	253	4.472	26	1	1.000	1.000	24	0.936
12	3	1.000	1.246	27	1.635	27	3	1.002	1.588	25	1.698
13	1	1.000	1.008	99	0.995	28	2	1.000	Inf	7	220.183
14	2	1.006	1.000	120	0.999	29	2	1.000	1.538	18	1.17
15	3	0.996	9.148	30	1.069	30	5	1.001	7.988	30	1.094

Légende:

Ex:	Cas de test	$n_x(K^1)$:	ordre du correcteur pour *inner* et *outer*
$\underline{\gamma}$:	borne inférieure du certificat pour *outer*	γ :	performance atteinte par *inner*
μ:	performance atteinte par DKSYN	$n_x(K^2)$:	ordre du correcteur pour DKSYN

la nouvelle technique de synthèse de commande robuste utilisant la relaxation interne et DKSYN , on utilise le même $\boldsymbol{\Delta}$ redimensioné par DKSYN . Les résultats des deux méthodes sont présentés dans le Tableau E.5. Pour le $\boldsymbol{\Delta}$ redimensionné, la nouvelle technique de relaxation interne est équivalente à DKSYN dans les cas 4, 13, 14 et 21 et il est meilleur que DKSYN dans 80% des cas, malgré le fait que l'ordre du correcteur par DKSYN est toujours plus grand que celui de la technique de relaxation interne.

La comparaison avec les méthodes de relaxation externe a montré que la performance certifiée de la méthode de relaxation interne est meilleure que la performance des relaxations externes. La nouvelle méthode de relaxation interne n'était pas non plus optimiste par rapport aux bornes inférieure et supérieure de la certification par WCGAIN . On observe cependant que dans les cas où un grand nombre de scénarios est généré, les cas d'incertitudes paramétriques sont restés sur un petit ensemble de valeurs, tandis que les cas d'incertitude dynamique ont été réparties sur l'ensemble du disque. Cette observation s'ajoute au fait que les techniques de relaxation externe ont une bonne performance pour l'incertitude complexe pure. Cela incite à l'étude de l'utilisation de l'approximation externe pour les incertitudes dynamiques tout en maintenant une approximation interne pour les incertitudes paramétriques. C'est l'objet de la section suivante.

Table E.5: Comparaison entre la nouvelle relaxation interne et la routine DKSYN pour $\boldsymbol{\Delta}$ redimensionné.

		inner		DKSYN				*inner*		DKSYN	
Ex	$\sigma(\Delta)$	γ	$n_x(K)$	μ	$n_x(K)$	Ex	$\sigma(\Delta)$	γ	$n_x(K)$	μ	$n_x(K)$
1	1.007	0.976	4	0.993	13	16	0.825	1.117	4	1.212	98
2	0.99	0.999	1	1.01	16	17	0.053	0.261	1	19.034	9
3	1.117	0.853	4	0.895	38	18	0.053	0.265	1	18.775	6
4	1.017	1.009	7	0.983	20	19	0.224	1.000	1	4.466	6
5	0.826	1.004	3	1.21	22	20	x	0.997	3	x	x
6	1.072	0.913	2	0.933	7	21	1.002	1.002	8	0.998	20
7	1.048	0.951	7	0.954	46	22	x	0.999	2	x	x
8	0.881	0.926	2	1.135	9	23	0.531	0.677	2	1.882	294
9	0.303	1.504	1	3.299	445	24	0.941	1.044	3	1.062	34
10	0.382	1.426	1	2.621	10	25	0.555	1.202	1	1.803	304
11	0.224	1.000	1	4.472	253	26	1.068	1.052	8	0.936	24
12	0.612	0.466	2	1.635	27	27	0.589	1.092	1	1.698	25
13	1.005	1.002	7	0.995	99	28	0.005	0.012	1	220	7
14	1.001	1.000	8	0.999	120	29	0.854	0.872	2	1.17	18
15	0.936	1.012	2	1.069	30	30	0.914	0.838	5	1.094	30

Légende:

Ex:	Cas de test	$\sigma(\Delta)$:	nouvelle borne de l'incertitude Δ
inner :	données de *inner*	DKSYN :	données de DKSYN
γ:	performance atteinte par *inner*	μ :	performance atteinte par DKSYN
$n_x(K)$:	ordre du correcteur		

E.5 Développement et implémentation d'une nouvelle approximation hybride pour la synthèse de correcteurs structurés robustes

Afin d'utiliser l'approximation externe dérivée à la section E.3 uniquement pour les incertitudes dynamiques, le multiplieur $\Gamma(\Phi, D)$ de la proposition E.1 devrait être adapté. Le *scaling* $D \in \mathbf{D}$ reste le même de (E.14) tandis que le multiplieur Φ est remplacé par la matrice zéro dans le multiplieur Γ de (E.15) pour obtenir:

$$\Gamma(0, D) = \begin{bmatrix} 0 & 0 & I & 0 \\ 0 & 0 & 0 & D \\ I & 0 & 0 & 0 \\ 0 & D^{-1} & 0 & 0 \end{bmatrix}. \tag{E.20}$$

Le théorème E.1 de la section E.3 est alors adapté au théorème E.2 ci-dessous.

Théorème E.2. *Supposons qu'il existe $D \in \mathbf{D}$ et un correcteur structuré $K(\kappa)$ tel que le système en boucle fermée $\Delta_p \star \Gamma(0, D)^{-\star} \star P_\gamma \star K(\kappa)$ est stable et satisfait à l'estimation*

$$\left\| \Delta_p \star \Gamma(0, D)^{-\star} \star P_\gamma \star K(\kappa) \right\|_\infty < 1 \tag{E.21}$$

pour tous $\Delta_p \in \boldsymbol{\Delta}_p$. Alors le système en boucle fermée $\Delta \star P \star K(\kappa)$ est stable de façon interne et il a le pire des cas de performance γ sur $\boldsymbol{\Delta}$.

Figure E.7 illustre les interconnexions du système $\Delta_p \star \Gamma(0, D)^{-\star} \star P_\gamma \star K(\kappa)$.

Maintenant, des scénarios ne devraient être générés que pour l'incertitude paramétrique. Cela signifie que les scénarios seront générés pour le système $T_{wz}^D(\Delta_p(x)) = \Delta_p \star \Gamma(0, D)^{-\star} \star P_\gamma \star K(\kappa)$. La synthèse multimodèle qui suit remplace la synthèse multimodèle de la section E.4 étant une version adaptée du programme (E.19) de la section E.3. Pour les scénarios générées et incluses dans l'ensemble $\boldsymbol{\Delta}_{p,a}$, la nouvelle synthèse H_∞ se présente sous la forme du programme d'optimisation:

$$\begin{array}{ll} \text{minimiser} & \gamma \\ \text{soumis à} & \|\Delta_p \star \Gamma(0, D)^{-\star} \star P_\gamma \star K(\kappa)\|_\infty \leq 1 - \eta \text{ for all } \Delta_p \in \boldsymbol{\Delta}_{p,a} \\ & \Gamma(\Phi, D)^{-\star} \star P_\gamma \star K(\kappa) \text{ stable de façon interne} \\ & D \in \mathbf{D}, \kappa \in \mathbb{R}^n, \gamma \in \mathbb{R}_+. \end{array} \tag{E.22}$$

Le schéma de l'approche de la relaxation hybride, Figure E.8, comprend la relaxation externe par le multiplieur Γ (E.20) pour le bloc complexe Δ_d et génération de scénarios actifs pour set de construction

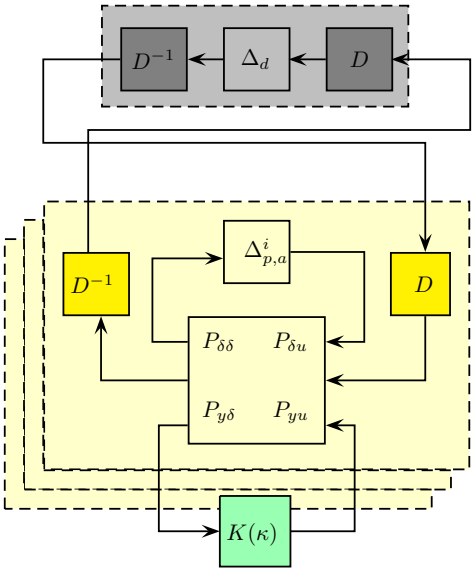

Figure E.7: Schéma d'interconnexion pour la commande robuste avec la relaxation hybride. Les couches sous-jacentes illustrent l'aspect multimodèle de la synthèse en raison des scénarios des incertitudes paramétriques.

$\mathbf{\Delta}_{p,a} \subset \mathbf{\Delta}_p$. Il y a deux possibilités pour l'application de la relaxation extérieure: Soit un multiplieur Γ est utilisé pour chaque système associée à un $\Delta_p \in \mathbf{\Delta}_{p,a}$, comme indiqué par la flèche I ou le même multiplieur Γ est utilisé pour toutes les plantes associées à l'ensemble $\mathbf{\Delta}_{p,a}$, comme indiqué par la flèche II. D'une part, la mise en œuvre de l'option I se traduit par moins de conservatisme. D'autre part, cela conduira à une croissance polynomiale du nombre des paramètres à régler pour chaque scénario ajouté.

L'implémentation de la synthèse suit les directives de l'algorithme ci-dessous:

Algorithme E.2: Synthése de lois de commande robuste par l'approximation hybride

Données: $\varepsilon > 0$, $\eta > 0$.

▷ **Instruction 1** (`Synthèse nominale`)**.**
Initialisez l'ensemble des scénarios réels actifs en tant que $\mathbf{\Delta}_{p,a} = \{0\}$.

▷ **Instruction 2** (`Synthèse Multimodèle`)**.**
Compte tenu de l'ensemble fini des scénarios réels actifs $\mathbf{\Delta}_{p,a} \subset \mathbf{\Delta}_p$, concevez un correcteur structuré $K(\kappa^*)$ en résolvant le programme multi-disques H_∞:

$$\begin{array}{ll} \text{minimiser} & \gamma \\ \text{soumis à} & \|\Delta_p \star \Gamma(0,D)^{-\star} \star P_\gamma \star K(\kappa)\|_\infty \leq 1-\eta \text{ for all } \Delta_p \in \mathbf{\Delta}_{p,a} \\ & \Gamma(\Phi,D)^{-\star} \star P_\gamma \star K(\kappa) \text{ stable} \\ & D \in \mathbf{D}, \kappa \in \mathbb{R}^n, \gamma \in \mathbb{R}_+. \end{array} \tag{E.23}$$

La solution localement optimale $(\gamma_*, D^*, \kappa^*)$ existe pour le correcteur structuré $K(\kappa^*)$.

▷ **Instruction 3** (`Calcul du pire des cas de stabilité`)**.**
Essayez de déstabiliser le système bouclé $\Delta_p \star \Gamma(0,D^*)^{-\star} \star P_{\gamma_*} \star K(\kappa^*)$ en calculant son pire des cas pour l'abscissa spectrale:

$$\alpha^* = \max_{\Delta_p \in \mathbf{\Delta}_p} \alpha\left(A(\Delta_p, \kappa^*)\right).$$

La solution est le pire scénario de stabilité Δ_p^*. Si $\alpha^* = \alpha\left(A(\Delta_p^*, \kappa^*)\right) \geq 0$, incluez Δ_p^* dans l'ensemble $\mathbf{\Delta}_{p,a}$ et revenez à l'instruction 2. Sinon, passez à l'instruction 4.

▷ **Instruction 4** (`Calcul du pire des cas de performance`)**.**
Essayez de dégrader la performance du système bouclé $\Delta_p \star \Gamma(0, D^*)^{-\star} \star P_{\gamma_*} \star K(\kappa^*)$ en calculant son pire des cas de la norme H_∞:

$$\gamma^* = \max_{\Delta_p \in \mathbf{\Delta}_p} \|\Delta_p \star \Gamma(0, D^*)^{-\star} \star P_{\gamma_*} \star K(\kappa^*)\|_\infty.$$

La solution est le pire scénario de performance $\Delta_p^\sharp$.

▷ **Instruction 5** (`Critère d'arrêt`)**.**
Si $\alpha(A(\Delta_p^\sharp, \kappa^*)) < 0$ et $\gamma^* < (1+\varepsilon)\gamma_*$, la dégradation de performance est marginale; sortez de la boucle et passez à l'étape 6 pour la certification postérieure. Sinon incluez $\Delta_p^\sharp$ dans l'ensemble $\mathbf{\Delta}_{p,a}$ et revenez à l'instruction 2.

▷ **Instruction 6** (`Certification`)**.**
Utiliser un solveur global pour certifier *a posteriori* que $T(\kappa^*)$ est robuste en performance et en stabilité $\mathbf{\Delta}$ sur l'ensemble $\mathbf{\Delta}$.

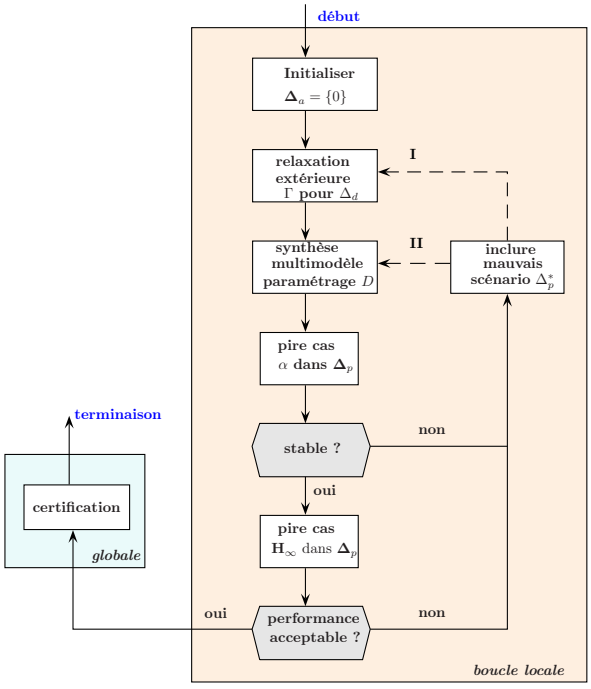

Figure E.8: Schéma de l'Algorithme E.2 pour la commande robuste avec la relaxation hybride.

L'approche avec un multiplieur unique Γ pour tous les scénarios a été mise en œuvre et les résultats obtenus pour un ensemble de 30 cas de test est présenté dans le Tableau E.6. Dans la tolérance de 5%, la borne inférieure de certification est en accord avec le γ retourné par la méthode dans tous les cas. La variation entre γ et la borne supérieure, en revanche, est inférieure à 5% dans 83% des cas. Dans le cas du test 19, la borne supérieure échoue ou atteste que le système est instable. Dans les cas de test 9, 10, 20 et 25 la borne supérieure est plus que le double de γ. Le cas de test 16 est le seul qui nécessite plus de 10 scénarios.

Contrairement à la relaxation interne, aucun des cas n'exige plus de 20 scénarios. Cela renforce l'hypothèse selon laquelle le nombre supplémentaire de scénarios requis par la technqiue de relaxation interne développée est due à l'incertitude dynamique. La Figure E.9 montre les scénarios générés pour les cas de test 7, 8, 16 et 23. Les scénarios ne sont générés que pour les incertitudes paramétriques. Dans le cas 8, où l'incertitude est purement paramétrique, le problème est exactement le même que

Table E.6: Données de la synthèse de correcteurs robustes utilisant la nouvelle relaxation hybride pour l'ensemble de cas de test.

Ex	$n_x(K)$	n_K	γ	$\underline{\gamma}$	$\overline{\gamma}$	$\lvert\Delta_a\rvert$	t_s	t_a
1	2	12	1.006	1.001	1.003	1	5	0.15
2	1	4	1.001	1.000	1.002	1	8	0.09
3	3	22	1.223	1.209	1.212	1	35	0.22
4	2	16	1.005	0.999	1.001	1	10	0.13
5	4	30	2.876	2.426	2.436	1	20	0.34
6	1	4	1.009	1.003	1.005	1	6	0.33
7	4	48	1.033	1.03	1.032	1	35	0.9
8	2	9	1.001	1.000	1.002	4	9	0.13
9	4	29	1.021	1.02	4.461	5	74	5.47
10	3	14	0.981	0.982	3.011	3	23	13.5
11	1	4	1.000	1.000	1.002	3	9	2.35
12	3	14	1.05 0	1.049	1.051	4	22	0.17
13	1	4	1.003	1.000	1.001	3	21	1.09
14	2	12	1.001	1.000	1.002	6	33	24.6
15	3	14	1.007	1.006	1.008	4	36	0.51
16	5	37	1.047	1.043	1.144	19	2165	7.61
17	3	23	1.239	1.2	1.203	4	42	1.94
18	2	9	1.158	1.155	1.158	8	106	3.88
19	1	4	1.000	1.000	Inf	3	10	2.51
20	3	14	1.088	1.083	4.572	5	73	3.99
21	1	9	1.006	1.000	1.002	3	14	0.27
22	2	9	1.396	1.415	1.42	4	105	6.68
23	3	22	3.444	3.27	3.208	3	62	1.93
24	3	14	1.188	1.186	1.189	4	34	0.26
25	4	29	1.058	1.058	5.877	5	92	7.18
26	1	9	1.008	1.000	1.002	3	22	1.05
27	3	14	1.012	1.008	1.012	6	68	0.42
28	2	12	1.001	0.999	1.006	7	38	2.53
29	2	9	0.996	0.995	0.997	4	33	0.08
30	5	24	1.144	1.119	1.122	4	85	0.26

Légende:

Ex:	Cas de test	γ :	performance atteinte par *hybrid*
$n_x(K)$:	ordre du correcteur	$\underline{\gamma}$:	borne inférieure du certificat sur la performance
n_K:	dimension du paramètre κ	$\overline{\gamma}$:	borne supérieure du certificat sur la performance
t_s:	temps ecoulé pour la synthèse [s]	$\lvert\Delta_a\rvert$:	nombre de scénarios
t_a:	temps ecoulé pour la certification [s]		

pour la relaxation interne. Le cas 7 est une incertitude dynamique pure et, en tant que tel, aucun scénario n'est généré dans l'approche hybride, tandis que pour la relaxation interne le disque est bien échantillonné. Pour les cas d'incertitude mixte 16 et 23, les scénarios pour les incertitudes paramétriques prennent plus de valeurs sur la synthèse qui utilise la relaxation interne.

Les résultats de la comparaison de l'approche hybride aux nouvelles relxations externe et interne et DKSYN sont affichés dans le Tableau E.7. L'approche hybride est équivalente à l'approche interne dans 76% des cas et il est moins performant dans les autres cas. La relaxation hybride est meilleure que la nouvelle technique de relaxation externe dans 63 % des cas, elle est moins performante dans 1 cas et elles sont équivalentes dans les autres cas. La relaxation hybride est meilleure que DKSYN dans 50% des cas, est surperformé par DKSYN dans 4 cas, et elles sont équivalents dans 37% des cas.

Le Tableau E.8 présente les résultats de la technique de relaxation hybride pour le $\boldsymbol{\Delta}$ redimensioné pour la comparaison avec DKSYN . Pour le $\boldsymbol{\Delta}$ redimensionné, l'approche de relaxation hybride ne peut pas atteindre meilleures performances que DKSYN dans les cas 3 et 26 pour un correcteur d'ordre jusqu'à 15. Ils sont équivalents dans les cas 4, 7, 13, 14 et 21 et l'approche hybride surpasse DKSYN dans 77% des cas restants.

La relaxation hybride est très proche de la relaxation interne en termes de performance. La méthode réussit dans les cas d'incertitudes mixtes où les méthodes basées sur relaxation externes ont échoué. Cependant, on peut remarquer que dans de tels cas une relaxation interne pure atteint de meilleures performances. Sur la base de ces résultats, il est conclu qu'en ce qui concerne seulement la performance la méthode de relaxation interne pure présentée dans la section E.4 est la meilleure

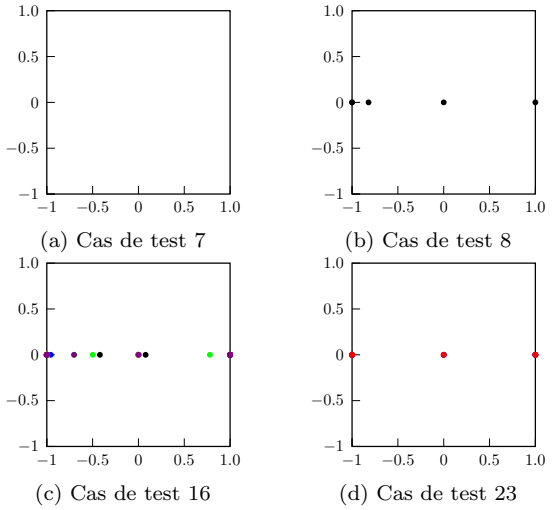

(a) Cas de test 7 (b) Cas de test 8

(c) Cas de test 16 (d) Cas de test 23

Figure E.9: Scénarios générés pour les cas de test 7, 8, 16 et 23 sur le plan complexe, avec des triangles et des cercles pour les incertitudes complexes et réelles, respectivement.

technique. En ce qui concerne le nombre de scénarios générés, comme prévu, l'approche hybride a besoin de moins de scénarios que la approche de relaxation interne. Cependent, dans la pratique, le plus grand nombre de scénarios n'a pas entraîné une dégradation de la performance.

E.6 Développement d'une methode pour la conception de correcteurs structurés basée sur la réponse frequentielle utilisant la minimisation de l'abscisse spectrale

Dans cette section et les deux suivantes, des techniques de conception de correcteurs rationnels structurés pour des systèmes de dimension infinie instables sont proposées. Ces techniques sont basées sur la réponse en fréquentielle des systèmes et permettent d'éviter complètement les approximations pour les systèmes et les correcteurs.

Ce que on vise, c'est d'obtenir un correcteur structuré $K(\kappa, s) \in \mathcal{K}$ que en boucle avec le système $G(s)$ donne $T(s) \in \hat{\mathcal{A}}_-(0)$. Pour la classe de systèmes considérée, ceci peut être assuré par l'abscisse spectrale négative du système asservi, $\alpha(T(\kappa, s)) < 0$.

Si un tel correcteur existe, il peut être trouvé par une recherche dans l'espace $\mathcal{K}$.Pour les systèmes de dimension infinie, $\alpha(T(\kappa^*, s)) < 0$ est certifié par le test de stabilité de Nyquist. Comme l'abscisse spectrale est le critère à utiliser, on propose de l'utiliser également dans une recherche comme fonction à minimiser. Pour continuer avec cette option, on propose ci-après une méthode pour calculer les abscisses spectrales positives pour les systèmes à dimension infinie dans $\hat{\mathcal{B}}_-(0)$.

On commençe par rappeler que si $G(s), K(s) \in \hat{\mathcal{B}}(0)$, alors $T(s) \in \hat{\mathcal{B}}(0)$. Cela signifie que $T(s)$ est méromorphe dans $\mathbb{C}^+$. Au fait d'avoir un nombre fini de pôles dans ce demi-plan, on peut prendre une constante réelle suffisamment grande $\mathfrak{a} > 0$ telle que $T(s)$ est maintenant holomorphe dans $\mathbb{C}^+_{\mathfrak{a}}$ et borné dans $\overline{\mathbb{C}^+_{\mathfrak{a}}}$. Si l'on définit $T_{\mathfrak{a}}(s)$ par: $T_{\mathfrak{a}}(s) = T(s + \mathfrak{a})$, alors $T_{\mathfrak{a}}$ est holomorphe dans $\mathbb{C}^+$ et borné dans $\overline{\mathbb{C}^+}$, donc stable. Si on définit de manière analogue $G_{\mathfrak{a}}$ et $K_{\mathfrak{a}}$, $F_{\mathfrak{a}}(s)$ peut être décrit en termes de $G_{\mathfrak{a}}(s)$ et $K_{\mathfrak{a}}(s)$ comme dans (E.2) ainsi comme $T_{\mathfrak{a}}$ et $f_{\mathfrak{a}}(s)$.

Les pôles de $G(s)$ et $K(s)$ contenus dans la région $\overline{\mathbb{C}^+} \cap \overline{\mathbb{C}^-_{\mathfrak{a}}}$ sont maintenant des pôles de $G_{\mathfrak{a}}(s)$ et $K_{\mathfrak{a}}(s)$ en $\overline{\mathbb{C}^-}$. Par conséquent, seuls les pôles de $G(s)$ et $K(s)$ contenus dans $\overline{\mathbb{C}^+_{\mathfrak{a}}}$ correspond à pôles instables de $G_{\mathfrak{a}}(s)$ et $K_{\mathfrak{a}}(s)$ dans $\overline{\mathbb{C}^+}$. Soit pu_G l'ensemble des pôles de $G(s)$ dans $\overline{\mathbb{C}^+}$. L'ensemble de pôles $pu_{G_{\mathfrak{a}}}$ en $\overline{\mathbb{C}^+}$ est défini comme $pu_{G_{\mathfrak{a}}} = \{v \in pu_G / Re(v) \geq \mathfrak{a}\}$ et $pu_{K_{\mathfrak{a}}}$, l'ensemble de les pôles de $K(s)$ en $\overline{\mathbb{C}^+}$ étant définis de manière analogue. Par conséquent, le nombre de pôles instable en boucle ouverte à utiliser dans le test de stabilité de Nyquist pour $f_{\mathfrak{a}}$ est $|pu_{G_{\mathfrak{a}}}| + |pu_{K_{\mathfrak{a}}}|$.

Ce que l'on recherche maintenant est la plus petite constante réelle $\mathfrak{a} > 0$ pour laquelle le test de stabilité de Nyquist pour $T_{\mathfrak{a}}(s)$ est positif. La valeur exacte $\mathfrak{a}$ correspond à la partie réelle du pôle plus à droite de $T(s)$. La manière la plus simple de calculer une telle $\mathfrak{a}$ est d'utiliser une

Table E.7: Comparaison entre la synthèse utilisant les nouvelles relaxations interne, externe et hybride et la routine DKSYN .

		hybrid		*inner*		*outer*	DKSYN	
Ex	$n_x(K^1)$	γ_i	$\lvert\Delta_{ai}\rvert$	γ_h	$\lvert\Delta_{ah}\rvert$	$\underline{\gamma}$	$n_x(K^2)$	μ
1	2	1.001	1	0.995	11	0.995	13	0.993
2	1	1.000	1	0.999	7	1.000	16	1.010
3	3	1.209	1	1.009	25	4.807	38	0.895
4	2	0.999	1	0.999	3	0.999	20	0.983
5	4	2.426	1	0.996	25	1.614	22	1.210
6	1	1.003	1	1.000	4	1.000	7	0.933
7	4	1.030	1	1.002	29	1.004	46	0.954
8	2	1.000	4	1.000	4	1.127	9	1.135
9	4	1.020	5	1.008	5	Inf	445	3.299
10	3	0.982	3	0.982	3	Inf	10	2.621
11	1	1.000	3	1.000	2	1.546*	253	4.472
12	3	1.049	4	1.000	11	1.246	27	1.635
13	1	1.000	3	1.000	3	1.008	99	0.995
14	2	1.000	6	1.006	4	1.000	120	0.999
15	3	1.006	4	0.996	8	9.148	30	1.069
16	5	1.043	19	1.020	31	1.948	98	1.212
17	3	1.200	4	0.999	18	2.078	9	19.034
18	2	1.155	8	1.007	7	19.636	6	18.775
19	1	1.000	3	1.000	2	1.000	6	4.466
20	3	1.083	5	0.997	8	8.057	x	x
21	1	1.000	3	1.000	3	1.000	20	0.998
22	2	1.415	4	0.999	7	49510	x	x
23	3	3.270	3	1.043	36	Inf	294	1.882
24	3	1.186	4	1.088	8	1.959	34	1.062
25	4	1.058	5	0.989	13	2692	304	1.803
26	1	1.000	3	1.000	3	1.000	24	0.936
27	3	1.008	6	1.002	8	1.588	25	1.698
28	2	0.999	7	1.000	8	162984	7	220.000
29	2	0.995	4	1.000	6	1.538	18	1.170
30	5	1.119	4	1.001	13	7.988	30	1.094

Légende:

Ex:	Cas de test	$n_x(K^1)$:	ordre du correcteur pour *hybrid* , *inner* and *outer*
γ_h :	performance atteinte par *hybrid*	γ_i :	performance atteinte par *inner*
$\lvert\Delta_{ah}\rvert$:	nombre de scénarios par *hybrid*	$\lvert\Delta_{ai}\rvert$:	nombre de scénarios par *inner*
$\underline{\gamma}$:	borne inférieure du certificat pour *outer*	μ:	performance atteinte par DKSYN
$n_x(K^2)$:	ordre du correcteur pour DKSYN		

Table E.8: Comparaison entre la nouvelle relaxation hybride et la routine DKSYN pour $\boldsymbol{\Delta}$ redimensionné.

		hybrid		DKSYN				*hybrid*		DKSYN	
Ex	$\sigma(\Delta)$	$\underline{\gamma}$	$n_x(K)$	μ	$n_x(K)$	Ex	$\sigma(\Delta)$	$\underline{\gamma}$	$n_x(K)$	μ	$n_x(K)$
1	1.007	0.989	8	0.993	13	16	0.825	1.132	4	1.212	98
2	0.99	1.000	1	1.01	16	17	0.053	0.261	1	19.034	9
3	1.117	1.070	9	0.895	38	18	0.053	0.264	1	18.775	6
4	1.017	1.009	14	0.983	20	19	0.224	1.000	1	4.466	6
5	0.826	1.055	3	1.21	22	20	x	1.083	3	x	x
6	1.072	0.923	2	0.933	7	21	1.002	1.001	10	0.998	20
7	1.048	0.974	15	0.954	46	22	x	1.415	2	x	x
8	0.881	0.926	2	1.135	9	23	0.531	0.981	1	1.882	294
9	0.303	1.507	1	3.299	445	24	0.941	1.017	2	1.062	34
10	0.382	1.426	1	2.621	10	25	0.555	1.206	1	1.803	304
11	0.224	1.000	1	4.472	253	26	1.068	1.052	15	0.936	24
12	0.612	0.474	2	1.635	27	27	0.589	1.091	1	1.698	25
13	1.005	1.002	15	0.995	99	28	0.005	0.012	1	220	7
14	1.001	1.000	10	0.999	120	29	0.854	0.871	2	1.17	18
15	0.936	1.015	2	1.069	30	30	0.914	0.905	5	1.094	30

Légende:

Ex:	Cas de test	$\sigma(\Delta)$:	nouvelle borne de l'incertitude Δ
hybrid :	données de *hybrid*	DKSYN :	donnés de DKSYN
$\underline{\gamma}$:	borne inférieure du certificat pour *hybrid*	μ :	performance atteinte par DKSYN
$n_x(K)$:	ordre du correcteur		

méthode de bissection avec la stabilité comme critère pour prendre la borne supérieure ou inférieure, en commençant par une $\overline{\mathfrak{a}} > 0$ suffisamment grand et $\underline{\mathfrak{a}} = 0$. La procédure est implémentée par l'Algorithme E.3 ci-dessous, où $\kappa^\sharp$ est fixe et $K(\kappa^\sharp, s)$ est supposé stable. L'extension à $K(s)$ instable est simple.

Algorithme E.3: Estimation of positive spectral abcissa $\alpha(S)$ of a closed-loop system S

Données: $\epsilon > 0$.

▷ **Step 1** (`Initialisation`).
Appliquer le test de stabilité de Nyquist de la section E.2 à $T(\kappa^\sharp, s)$.
Si stable, quittez. Sinon, définissez $\overline{\mathfrak{a}} = 1$, $\underline{\mathfrak{a}} = 0$ et passez à l'instruction 2.

▷ **Instruction 2** (`Recherche du décalage stabilisant`).
Appliquer le test de stabilité de Nyquist de la section E.2 au système décalé par $\overline{\mathfrak{a}}$ $T(\kappa^\sharp, s + \overline{\mathfrak{a}})$.
Si stable, passez à l'instruction 3. Sinon définissez $\underline{\mathfrak{a}} = \overline{\mathfrak{a}}$, $\overline{\mathfrak{a}} = 2\overline{\mathfrak{a}}$ et répétez l'instruction 2.

▷ **Instruction 3** (`Raffinement de l'estimation`).
$\mathfrak{a} = 0.5 \cdot (\mathfrak{a} + \underline{\mathfrak{a}})$.
Appliquer le test de stabilité de Nyquist au système décalé par $\overline{\mathfrak{a}}$ $T(\kappa^\sharp, s + \overline{\mathfrak{a}})$.
Si stable, définissez $\overline{\mathfrak{a}} = \mathfrak{a}$. Sinonm définissez $\underline{\mathfrak{a}} = \mathfrak{a}$.
Répétez l'instruction 3 jusque $\overline{\mathfrak{a}} - \underline{\mathfrak{a}} < \epsilon \cdot \max\{10^{-4}, \min\{\underline{\mathfrak{a}}, 1\}\}$. Puis retournez $\overline{\mathfrak{a}}$.

Le critère $\alpha(T(\kappa))$ calculé dans l'Algorithme E.3 doit maintenant être minimisé jusqu'à un paramètre κ^* avec $\alpha_\epsilon(T(\kappa^*)) \leq 0$ soit trouvé. En raison du fait d'utiliser uniquement la réponse frequentielle des systèmes, des méthodes de recherche directe sont plus recommandés. La technique choisie était la recherche multidirectionnelle, qui avait déjà été utilisée avec succès dans [Apkarian and Noll, 2006c] pour la commande H_∞ des systèmes de dimension finie. La routine pour la recherche multidirectionnelle de Higham [2002] est utilisé dans la synthèse. La synthèse échoue si aucun correcteur ne peut être trouvé tel que $\alpha_\epsilon(T(\kappa^*, s)) < 0$. Afin d'éviter d'être bloqué aux minima locaux, il peut être nécessaire de redémarrer la recherche avec différents points initiaux.

La méthode developpée est testée pour un ensemble de systèmes instables de dimension finie extraits de COMPLEIB [Leibfritz, 2004] et un ensemble de systèmes à dimension infinie extraits de la littérature. L'abscisse spectrale est estimée avec une tolérance de 1% et un maximum de 4 redémarrages est permis. La grille de fréquences est dans l'intervalle $[10^{-3}, 10^{4}]$ rad/s avec une densité maximale de 50 000 points par décennie. Notez qu'une grille plus grossière est utilisée dans l'optimisation par suite de la méthode présentée dans la section E.2 pour affiner la grille de fréquences. Le correcteur initial, pas forcément stable, est obtenu de manière aléatoire. La méthode de référence utilisée est SYSTUNE de MATLAB ™.

Le Tableau E.9 montre les résultats de la synthèse d'un correcteur en representation d'état de troisième ordre et tridiagonal. La stabilisation des systèmes par la technique développée est suivie par une méthode d'optimisation de la norme H_∞ basée sur la réponse frequentielle introduite dans Apkarian and Noll [2018]. Dans chaque cas, toutes les normes H_∞ ont été normalisées par la norme H_∞ obtenue par SYSTUNE.

La méthode basée sur la réponse frequentielle n'a pas réussi à trouver un correcteur stabilisant dans les cas 20 et 21 où il a été observé que les 2 ou plusieurs pôles les plus à droite sont alignés verticalement près de l'abscisse spectrale. La norme H_∞ finale après l'étape d'optimisation atteint des valeurs similaires à la méthode de référence SYSTUNE dans tous les systèmes stabilisés sauf dans les cas 4 et 36, où la différence en pourcentage était 69% et 44%, respectivement. L'analyse de ces 2 cas révèle que les correcteurs conçu par SYSTUNE ont des gains élevés tandis que ceux conçus par la méthode basée sur la réponse fréquentielle a des gains inférieurs.

Les résultats pour l'ensemble des systèmes de dimension infinie et linéaire invariant dans le temps (en anglais, IDLTI) sont présentés dans le Tableau E.10. Pour la synthèse avec SYSTUNE, les systèmes

Table E.9: Comparaison entre la methode basée sur la réponse frequentielle utilisant l'abscisse spectrale et SYSTUNE pour systèmes de dimension finie instables.

		FRD_α					SYSTUNE	
		κ^0	$\kappa^\sharp$		κ^*			
Ex	n_K	α	α	$\|.\|_\infty$	α	$\|.\|_\infty$	α	$\|.\|_\infty$
1	18	62.473	-0.024	549.75	-0.05	1.000	-0.05	1.000
2	18	0.523	-0.045	40.344	-0.049	0.997	-0.048	1.000
3	30	1.292	-0.095	3.738	-0.445	1.000	-0.445	1.000
4	40	3.102	-0.054	6.18e5	-0.045	3.26	-0.084	1.000
5	40	0.634	-0.001	18.257	-0.022	1.003	-0.017	1.000
6	40	0.614	-0.001	46.233	-0.006	1.000	-0.006	1.000
7	18	0.635	-0.016	24.422	-0.017	1.008	-0.148	1.000
8	61	0.248	-0.016	99.73	-0.177	1.000	-0.136	1.000
9	61	3.62	-0.005	268.91	-0.061	1.000	-0.076	1.000
10	33	0.223	-0.038	20.448	-0.089	0.906	-0.042	1.000
11	61	0.239	-0.005	534.1	-0.001	1.002	-0.001	1.000
12	28	1.444	-0.157	4.277	-0.737	1.000	-2.069	1.000
13	23	2.038	-0.021	72.546	-2.162	1.000	-2.972	1.000
14	23	2.504	-0.111	46.471	-1.219	1.002	-2.02	1.000
15	61	6.332	-0.221	14.498	-2.427	1.001	-1.383	1.000
16	23	10.505	-0.003	183.22	-0.39	1.022	-0.218	1.000
17	40	-0.191	-0.191	46.428	-1.094	1.000	-2.084	1.000
18	63	0.155	-0.009	26.566	-0.098	1.001	-0.01	1.000
19	28	14.065	-0.036	1404.51	-0.645	0.998	-0.63	1.000
20	23	12.707	0.34	-	-	-	-2.64	1.000
21	23	132.45	6.464	-	-	-	-3.691	1.000
22	18	1.104	-0.395	3.203	-1.988	0.998	-1.995	1.000
23	33	0.621	-0.01	72.23	-1.413	0.992	-1.776	1.000
24	33	1.429	-0.006	501.88	-2.027	1.002	-1.948	1.000
25	23	42.617	-0.396	1.847	-0.457	1.000	-3.262	1.000
26	23	52.945	-0.235	8.935	-0.564	1.000	-1.638	1.000
27	23	9.828	-0.328	15.56	-1.279	1.000	-1.927	1.000
28	23	12.534	-0.261	6.394	-0.907	1.002	-0.628	1.000
29	23	51.703	-0.041	375.61	-0.544	1.000	-0.879	1.000
30	28	0.46	-0.227	1.47	-0.963	1.001	-0.968	1.000
31	28	0.491	-0.022	221.5	-1.227	1.004	-1.499	1.000
32	33	9.422	-0.061	6.695	-1.185	1.004	-2.204	1.000
33	33	0.244	-0.068	17.57	-3.806	1.001	-3.861	1.000
34	33	0.766	-0.144	2.07	-1.548	1.000	-1.504	1.000
35	33	8.778	-0.141	6.044	-3.525	1.000	-7.346	1.000
36	23	16.985	-0.039	2.087	-0.051	1.443	-0.105	1.000

Légende:

Ex:	Cas de test	κ^0:	donnés pour le système asservi initial
α:	abscisse spectrale de $T(\kappa^i, s)$	$\kappa^\sharp$:	donnés pour le système asservi après la stabilisation
$\|.\|_\infty$:	$\|T(\kappa^i, s)\|_\infty$	κ^*:	donnés pour le système asservi après la optimisation
systune:	norme H_∞ atteinte par SYSTUNE	FRD_α:	résultats pour la methode utilisant l'abscisse spectrale
n_K:	dimension du paramètre κ		

IDLTI ont été approximés par des systèmes rationnels utilisant des approximations de Padé de 10ème ordre pour les systèmes à retard et approximations Oustaloup d'ordre 10 pour les termes d'ordre fractionnaire. La méthode developpée a échoué dans 4 cas de test. Des tests supplémentaires sont nécessaires pour clarifier les causes de cette défaillance. Deux raisons possibles sont l'utilisation d'une structure inappropriée pour le correcteur et l'échec de la méthode de recherche. Pour la même structure des correcteurs, SYSTUNE a échoué dans 6 cas pour les approximations d'ordre 10 du retard et des termes fractionnaires. Dans 4 de ces cas, en augmentant l'ordre du correcteur, la stabilisation est réussie. Dans 6 cas, augmentant l'ordre de l'approximation entraîne l'échec de la synthèse. L'inspection des résultats de l'application du correcteur conçu au système réel montre que ceci est un exemple clair du *spillover effect* décrit dans Balas [1982].

Table E.10: Comparaison entre la methode basée sur la réponse frequentielle utilisant l'abscisse spectrale pour systèmes de dimension infinie et SYSTUNE pour leurs approximations.

			FRD_α		SYSTUNE	
Ex	K	n_K	$\alpha_0(.)$	$\alpha(.)$	$\alpha_{apx}(.)$	$\alpha_{act}(.)$
1	2-SS	9	91.13	0	-36.49	0
2	2,1-TF	4	1.742	0	-0.005	0
3	3,0-TF	9	5e-6	0	-0.121	6e-5
4	2-SS0	8	u	0	-0.001	0
5	3,1-TF	5	1.382	0	-8e-5	0
6	2,1-TF	4	2.159	1.488	0.965	x
7	2-SS	9	u	0	-0.001	0
8	1-SS	4	0.265	0	-0.109	0
9	1-SS	4	4.072	0	-3.086	0
10	3-SS	14	1.545	0.165	0.004	x
11	3-SS0	19	2.030	2.030	2.298	x
12	2-SS	9	0.442	0	-0.001	0
13	2-SS0	12	u	0	-0.059	0
14	2-SS0	12	3.906	0	-0.398	3.397
15	2-SS0	16	0.812	0	-0.001	0.733
16	2-SS0	20	4.265	0	-0.002	0
17	1-SS0	3	2.726	0	-0.002	0
18	1-SS0	3	4.101	0	-0.001	0
19	1-SS0	3	3.351	0	0.029	0.286
20	1-SS0	3	4.531	0	1.599	1.575
21	3-SS	14	u	0.063	-0.132	0.747
22	3,1-TF	5	0.259	0	0.0483	x
23	1,0-TF	2	1.099	0	-3.055	7.071
24	2-SS0	8	u	0	-2.303	0
25	2-SS	9	u	0	-0.001	0.038

Légende:

Ex:	Cas de test		
n_K:	dimension du paramètre κ	K:	structure du correcteur
SYSTUNE :	results obtained by SYSTUNE	FRD_α:	résultats pour la methode utilisant l'abscisse spectrale
$\alpha_{apx}(.)$:	abscisse spectrale de l'approximatif $T_{app}(\kappa^*, s)$	$\alpha_0(.)$:	abscisse spectrale de $T(\kappa^0, s)$
$\alpha_{act}(.)$:	abscisse spectrale de l'effectif $T(\kappa^*, s)$	$\alpha(.)$:	abscisse spectrale de $T(\kappa^*, s)$
u:	correcteur instable	x:	pas calculé

E.7 Développement d'une methode pour la conception de correcteurs structurés basée sur la réponse frequentielle utilisant la minimisation de la norme H_2

La réponse impulsionnelle d'un système est directement liée à ses pôles. L'énergie de la réponse impulsionnelle d'un système strictement rationnel est finie si le système est stable et infinie sinon. L'énergie de la réponse impulsionnelle est le carré de la norme L_2, qui est calculé dans le domaine temporel. Pour un système stable, il est possible de calculer l'énergie par la norme H_2, dans le domaine fréquentiel. La norme H_2 d'une fonction de transfert stable est lisse et facile à calculer, ce qui la rend facile à minimiser par les procédures d'optimisation. Cela la place comme un choix idéal pour une fonction objective sur une recherche d'optimisation.

Soit $g(t)$ la réponse impulsionnelle associée à un système $G(s)$. L'énergie du système $G(s)$ est définie par $E(G) = \|g(t)\|_2^2$. Pour un $G(s)$ propre et stable avec une limite à l'infini G_∞, l'énergie du système moins sa limite peut également être calculée par $E(G) = \int_{-\infty}^{\infty} Tr((G(j\omega) - G_\infty)^H (G(j\omega) - G_\infty))d\omega$, que discrétisée sur la grille de fréquence Ω devient:

$$E_\omega(G) = \sum_{\omega \in \Omega} Tr(G_p(j\omega) G_p^H(j\omega)) \cdot \Delta\omega, \tag{E.24}$$

où $G_p(s) = G(j\omega) - G_\infty$.

Soit $q(\omega) = Tr((G(j\omega) - G_\infty)^H (G(j\omega) - G_\infty))$, et $Q_\omega(\omega)$ le polygone d'interpolation linéaire de $q(\omega)$ sur la grille $0 = \omega_0 < \omega_1 < \cdots < \omega_N = \overline{\omega}$. On define l'erreur de troncature $\upsilon_{\overline{\omega}} = 2\int_{\overline{\omega}}^{\infty} q(\omega)d\omega$ et l'erreur d'interpolation $\upsilon_\omega = 2\left|\int_0^{\overline{\omega}} q(\omega)d\omega - \int_0^{\overline{\omega}} Q_\omega(\omega)d\omega\right|$. L'erreur entre l'intégrale et la sommation est $\upsilon = \|E(G) - E_\omega(G)\| = \upsilon_{\overline{\omega}} + \upsilon_\omega$.

Pour une fonction de transfert strictement propre et instable $G(s)$, l'énergie $E(G)$ n'est pas finie et ne peut pas être calculée dans le domaine fréquentiel. Pourtant, si $G(s) \in \hat{\mathcal{B}}(0)$ il existe une constante réelle suffisamment grande $\mathfrak{a} > 0$ telle que $G_\mathfrak{a}(s) = G(s + \mathfrak{a})$ est holomorphe dans $\mathbb{C}_\mathfrak{a}^+$ et borné dans $\overline{\mathbb{C}_\mathfrak{a}^+}$. Soit $g_\mathfrak{a}(t)$ la réponse impulsionnelle associée à $G_\mathfrak{a}(s)$. On a que $\|g_\mathfrak{a}(t)\|_2 = \|G_\mathfrak{a}(s)\|_2$ et l'énergie $E(G_\mathfrak{a})$ est fini.

La méthode proposée consiste alors à minimiser $E(T_\mathfrak{a}\ (\kappa, s))$ jusqu'à trouver un $K(\kappa^*, s) \in \mathcal{K}$ tel que $E(T(\kappa^*, s))$ est fini, c'est-à-dire, $T_\mathfrak{a}\ (\kappa^*, s) \in \hat{\mathcal{A}}(-\mathfrak{a})$, où encore, $T(\kappa^*, s) \in H^\infty$. La constante réelle $\mathfrak{a}$ est itérativement réduite jusqu'à $\mathfrak{a} = 0$, étant donné que $\alpha(T(\kappa, s)) < \mathfrak{a}$ à chaque itération.

Cette procédure est implémenté par l'Algorithme E.4 ci-dessous:

Algorithme E.4: Synthèse basée sur la réponse frequentielle utilisant la minimisation de l'énergie.

Données: $\varepsilon > 0$.

▷ **Instruction 1** (`Initialisation`).
Sélectionnez aléatoirement κ^c.
Appliquer le test de stabilité de Nyquist à $T(\kappa^c, s)$.
Si stable, retournez $\kappa^* = \kappa^c$ et quittez. Sinon passez à l'instruction 2.

▷ **Instruction 2** (`Calcul du décalage`).
Obtenir $\overline{\mathfrak{a}}$ avec l'aide de l'Algorithme E.3 pour l'estimation de l'abscisse spectrale de $T(\kappa^c, s)$.

▷ **Instruction 3** (`Minimisation de l'énergie`).

$$\begin{array}{ll} \text{minimiser} & E(T(\kappa, s + \overline{\mathfrak{a}})) \\ \text{soumis à} & \text{test de stabilité de Nyquist positif pour} T(\kappa, s + \overline{\mathfrak{a}}) \\ & K(\kappa, s) \in \mathcal{K} \end{array} \tag{E.25}$$

en utilisant (E.24) pour calculer l'énergie et avec κ^c comme point initial et κ^+ comme solution.

▷ **Instruction 4** (`Critère d'arrêt`).
Appliquer le test de stabilité de Nyquist à $T(\kappa^+, s)$.
Si stable, retournez $\kappa^* = \kappa^+$ et quittez. Sinon définez $\kappa^c = \kappa^+$ et revenez à l'instruction 2.

Le programme d'optimisation E.25 à l'étape 3 peut être résolu par des routines qui implémentent une recherche du minimum d'une fonction. L'énergie définie ci-dessus est une fonction lisse du paramètre κ. Pour la synthèse basée sur la réponse frequentielle où la seule information disponible est l'estimation de la fonction ponctuellement, des méthodes itératives telles que les méthodes de Gauss-Newton ou de quasi-Newton peuvent être utilisées, l'estimation de l'énergie étant calculée par (E.24). Dans le présent travail, la routine FMINCON [MathWorks, 2017] de MATLAB ™ a été utilisée pour la recherche. La grille de fréquences est une grille dense mais un algorithme de sélection d'une grille de fréquences appropriée afin de garantir une erreur de tolérance souhaitée υ dans l'estimation de la norme H_2 peut être développé comme Apkarian and Noll [2018] ont fait pour la norme H_∞.

La méthode développée dans cette section est testée selon les mêmes règles que celles du test de la section précédente. Pour le calcul de l'énergie, la grille de fréquences est dans l'intervalle $[10^{-3}\ ,10^4]$ rad/s échantillonné par 10 000 points distribués logarithmiquement. Pour l'estimation de l'abscisse spectrale, on a utilisé une grille de fréquences dans le même intervalle avec une densité maximale de 50 000 points par décennie et une tolérance de 10% pour les systèmes rationels et de de 1% pour les système de dimension finie. Cette grille de fréquences est raffinée par la méthode présentée dans la

Table E.11: Comparaison entre la methode basée sur la réponse frequentielle utilisant la norme H_2 et SYSTUNE pour systèmes de dimension finie instables.

		FRD_2					SYSTUNE	
		κ^0	$\kappa^\sharp$		κ^*			
Ex	n_K	α	α	$\|.\|_\infty$	α	$\|.\|_\infty$	α	$\|.\|_\infty$
1	18	62.473	-0.05	400.54	-0.05	1.000	-0.05	1.000
2	18	0.523	-0.005	1205.13	-0.048	0.99	-0.048	1.000
3	30	1.292	-0.021	14.529	-0.325	0.997	-0.445	1.000
4	40	3.102	-0.002	7.34e6	-0.062	1.056	-0.084	1.000
5	40	0.634	-0.009	71.404	-0.025	1.001	-0.017	1.000
6	40	0.614	-0.003	5.606	-0.006	1.000	-0.006	1.000
7	18	0.635	-0.018	11.844	-0.148	1.002	-0.148	1.000
8	61	0.248	-0.039	5.362	-0.207	0.998	-0.136	1.000
9	61	3.62	-0.174	12.477	-0.056	1.000	-0.076	1.000
10	33	0.223	0.199	-	-	-	-0.042	1.000
11	61	0.239	-0.005	354.21	-0.001	1.000	-0.001	1.000
12	28	1.444	-0.351	2.234	-0.629	1.000	-2.069	1.000
13	23	2.038	-0.005	16.484	-1.599	1.000	-2.972	1.000
14	23	2.504	-0.61	2.327	-0.599	1.002	-2.02	1.000
15	61	6.332	-0.194	5.774	-1.918	0.998	-1.383	1.000
16	23	1.008	1.016	-	-	-	-0.218	1.000
17	40	-0.191	-0.191	46.428	-1.094	1.000	-2.084	1.000
18	63	0.155	-0.127	1.115	-0.129	1.000	-0.01	1.000
19	28	1.9	-0.042	69.434	-0.641	0.998	-0.63	1.000
20	23	12.328	36.041	-	-	-	-2.64	1.000
21	23	6.223	67.23	-	-	-	-3.691	1.000
22	18	1.104	-0.242	2.582	-1.993	0.998	-1.995	1.000
23	33	0.621	-0.027	73.051	-1.363	1.003	-1.776	1.000
24	33	1.429	1.455	-	-	-	-1.948	1.000
25	23	42.617	-0.33	1.909	-0.532	1.000	-3.262	1.000
26	23	52.945	-0.451	3.491	-0.536	1.000	-1.638	1.000
27	23	9.828	-0.506	2.272	-1.042	1.000	-1.927	1.000
28	23	12.534	-0.147	6.575	-0.976	1.003	-0.628	1.000
29	23	51.703	-0.005	4.465	-0.729	1.000	-0.879	1.000
30	28	0.46	-0.097	3.828	-0.936	1.004	-0.968	1.000
31	28	0.491	-0.157	2.174	-1.25	1.005	-1.499	1.000
32	33	9.422	-0.027	17.349	-2.222	1.004	-2.204	1.000
33	33	0.244	-0.704	1.903	-3.859	1.000	-3.861	1.000
34	33	0.766	-0.266	1.743	-1.613	1.000	-1.504	1.000
35	33	8.778	-0.626	2.557	-1.924	1.000	-7.346	1.000
36	23	16.985	-0.04	2.017	-0.046	1.429	-0.105	1.000

Légende:

Ex:	Cas de test	κ^0:	donnés pour le système asservi initial
α:	abscisse spectrale de $T(\kappa^i, s)$	$\kappa^\sharp$:	donnés pour le système asservi après la stabilisation
$\|.\|_\infty$:	$\|T(\kappa^i, s)\|_\infty$	κ^*:	donnés pour le système asservi après la optimisation
systune:	norme H_∞ atteinte par SYSTUNE	FRD_2:	résultats de la methode utilisant la norme H_2
n_K:	dimension du paramètre κ		

Table E.12: Comparaison entre la methode basée sur la réponse frequentielle utilisant la norme H_2 pour systèmes de dimension infinie et SYSTUNE pour leurs approximations.

			FRD_2		SYSTUNE	
Ex	K	n_K	$\alpha_0(.)$	$\alpha(.)$	$\alpha_{apx}(.)$	$\alpha_{act}(.)$
1	2-SS	9	24.37	0	-36.49	0
2	2,1-TF	4	0.437	0	-0.005	0
3	3,0-TF	9	0	0	-0.121	6e-5
4	2-SS0	8	0.21	0	-0.001	0
5	3,1-TF	5	0.305	0	-8e-5	0
6	2,1-TF	4	1.020	1.020	0.965	x
7	2-SS	9	1.437	0	-0.001	0
8	1-SS	4	0.132	0	-0.109	0
9	1-SS	4	1.02	0	-3.086	0
10	3-SS	14	0.988	0.978	0.004	x
11	5-SS0	33	2.326	2.301	2.298	x
12	2-SS	9	1.052	1.021	-0.001	0
13	2-SS0	12	0	0	-0.059	0
14	2-SS0	12	3.906	0	-0.398	3.397
15	2-SS0	16	0.812	0	-0.001	0.733
16	2-SS0	20	4.265	0	-0.002	0
17	1-SS0	3	0	0	-0.002	0
18	1-SS0	3	0	0	-0.001	0
19	1-SS0	3	0.289	0	0.029	0.286
20	1-SS0	3	0	0	1.599	1.575
21	3-SS	14	0.839	0.063	-0.132	0.747
22	3,1-TF	5	0.140	0	0.048	x
23	1,0-TF	2	1.020	0	-3.055	7.071
24	2-SS0	8	0	0	-2.055	0
25	2-SS	9	0	0	-0.001	0.038

Légende:

Ex:	Cas de test		
n_K:	dimension du paramètre κ	K:	structure du correcteur
SYSTUNE :	données de SYSTUNE	FRD_2:	résultats de la methode utilisant la norme H_2
$\alpha_{apx}(.)$:	abscisse spectrale de l'approximatif $T_{app}(\kappa^*, s)$	$\alpha_0(.)$:	abscisse spectrale de $T(\kappa^0, s)$
$\alpha_{act}(.)$:	abscisse spectrale de l'effectif $T(\kappa^*, s)$	$\alpha(.)$:	abscisse spectrale de $T(\kappa^*, s)$
x:	pas calculé		

section E.2. La recherche peut être redémarrée un maximum de 10 fois à différents points initiaux. Le correcteur initial est obtenu aléatoirement mais il doit être stable depuis le début de la recherche.

Les résultats pour les cas de test rationnels sont présentés dans le Tableau E.11. Dans les cas 10, 16, 20, 21 et 24, la nouvelle méthode ne permet pas de trouver une solution stabilisatant après 10 redémarrages. Le résultat final après l'optimisation a atteint des valeurs similaires à la méthode de référence SYSTUNE dans tous les systèmes stabilisés, sauf dans le cas 36, où la différence était de 43 %. L'inspection des solutions a montré que contrairement à la méthode basée sur l'abscisse spectrale, la cause de la défaillance n'est pas liée à l'alignement des pôles les plus à droite, une fois que ce n'était pas le cas dans les cas de défaillance. Ce qui s'est produit, c'est que la minimisation de la norme H_2 n'implique pas une réduction supplémentaire de l'abscisse spectrale. Une solution possible consiste à créer de nouvelles heuristiques pour le choix du décalage.

Les systèmes de dimension infinie ont été approximés pour utiliser la routine SYSTUNE. Les approximations de Padé ont été utilisées pour les systèmes à retard et les approximations Oustaloup de Tepljakov et al. [2011], pour les systèmes d'ordre fractionnaire. La méthode basée sur la minimisation de la norme H_2 échoue dans 5 cas. Dans 7 cas, le correcteur initial est déjà stabilisant.

La technique developée dans cette section a obtenu le taux de succès le plus faible parmi les techniques de synthèse basée sur la réponse frequentielle. La méthode est également la plus lente en raison de la densité élevée de la grille de fréquences. La bonne efficacité de la méthode elle-même corrobore l'argument empirique selon lequel la minimisation de la norme H_2 des systèmes peut effectivement conduire à la stabilisation. Même avec des taux de réussite plus faibles que la méthode précédente, sa fonction objective, l'énergie, est facilement calculée et la recherche est également simplifiée en raison

du fait que la fonction est lisse. Cependant, la contrainte de la recherche est toujours difficile à gérer.

E.8 Développement d'une methode pour la conception de correcteurs structurés basée sur la réponse frequentielle utilisant la minimisation de la norme H_∞

La norme H_∞ d'un système $G(s)$ est le gain maximal de sa réponse fréquentielle $G(j\omega)$. De même, les valeurs singulières $\bar{\sigma}(G(j\omega))$ pour $\omega \in \Omega$ sont liées aux pôles du système dans la mesure où les pôles mal amortis provoquent des pics de résonance. Dans de nombreux cas, les pôles mal amortis sont très proches des axes imaginaires, contribuant à une faible marge de stabilité. En minimisant la norme H_∞ d'un système stable, nous finissons par augmenter l'amortissement des pôles du système. Cela, dans certains cas, se fait en poussant ces pôles faiblement amortis dans $\mathbb{C}^-$ et se traduit par une augmentation des marges de stabilité. Une relation indirecte entre la norme H_∞ et la stabilité peut également être obtenue par la marge de module. La marge de module d'un système bouclé est la distance minimale entre la courbe de ce système et l'origine dans le graphique de Nyquist et elle est définie par $\|S(s)\|_\infty^{-1}$, $S(s) = (I + G(s)K(s))^{-1}$.

Inspirée par le fait que la minimisation de la norme H_∞ peut augmenter les marges de stabilité et pousser les pôles dans le demi-plan gauche, une méthode de conception de correcteurs structurés stabilisants $K(\kappa, s)$ pour les systèmes instables exploitant une minimisation itérative de la norme H_∞ décalée est développé. La justification en est qu'une fois que les pôles instables proche de l'axe imaginaire du système en boucle fermée $T(\kappa, s)$ sont décalés vers le demi-plan gauche, l'optimisation de la norme H_∞ décalé les poussera plus loin. Cela implique que le système réel, non décalé, aura une abscisse spectrale plus petite $\alpha(T(\kappa^*, s)) < \alpha(T(\kappa, s))$.

Afin de maximiser l'effet de la minimisation de la norme H_∞ sur les pics ressonants causés par des pôles mal amortis, on doit assurer que les pôles sont suffisamment proches de l'axe imaginaire. On y parvient en calculant l'abscisse spectrale $\mathfrak{a}_S$ du système en boucle fermée réel, par l'algorithme estimateur E.3, puis en déplaçant le système de $\mathfrak{a}_S + \zeta$. Cela signifie que les pôles, correspondant auparavant à l'abscisse spectrale, sont maintenant sur $\mathbb{C}_\zeta^-$. Plus le ζ est petit, plus les pôles sont proches de l'axe imaginaire. En minimisant la norme H_∞ décalé, on s'attend à obtenir un nouveau κ_{+1} tel que $\alpha(S(\kappa_{+1}, s)) = \mathfrak{a}_S - \xi$. On continue jusqu'à $\alpha(S(\kappa_{+n}, s)) < 0$.

La technique de conception des correcteurs est implémentée par l'Algorithme E.5 ci-dessous.

Algorithme E.5: Synthèse basée sur la réponse frequentielle utilisant la minimisation de la norme H_∞.

Données: $\varepsilon > 0$.

▷ **Instruction 1** (`Initialisation`).
Définez $\mathfrak{a} = \alpha(G(s))$.
Trouvez $SG = \max_{\omega\in\Omega} \bar{\sigma}(G(\mathfrak{a} + j\omega))$.
Initialisez $K(\kappa^0, s) \in \mathcal{K}$.
Réduisez le gain du correcteur $K(\kappa^0, s + \mathfrak{a})$ jusque $\|K(\kappa^c, s + \mathfrak{a})\|_\infty < SG^{-1}$.
Appliquer le test de stabilité de Nyquist à $T(\kappa^c, s)$.
Si stable, retournez $\kappa^* = \kappa^c$ et quittez. Sinon passez à l'instruction 2.

▷ **Instruction 2** (`Calcul du décalage`).
Obtenir $\mathfrak{a}$ avec l'aide de l'Algorithme E.3 pour l'estimation de l'abscisse spectrale de $T(\kappa^c, s)$.

▷ **Instruction 3** (`Minimisation de la norme` H_∞).

$$\begin{array}{ll} \text{minimiser} & \max\limits_{\omega\in\Omega} \overline{\sigma}(T(\kappa, \mathfrak{a}+\varepsilon+j\omega)) \\ \text{soumis à} & \text{test de stabilité de Nyquist positif pour } T(\kappa, s+\mathfrak{a}\,) \\ & K(\kappa,s)\in\mathcal{K} \end{array} \tag{E.26}$$

avec κ^c comme point initial et κ^+ comme solution.

▷ **Instruction 4** (`Critère d'arrêt`).
Appliquer le test de stabilité de Nyquist à $T(\kappa^+, s)$.
Si stable, retournez $\kappa^* = \kappa^+$ et quittez. Sinon définez $\kappa^c = \kappa^+$ et revenez à l'instruction 2.

Le programme E.26 de l'étape 3 pour l'optimisation de la norme H_∞ peut être résolu par n'importe quelle technique, à condition que la norme H_∞ soit calculée pour une grille de fréquences discrète. Ce problème est non convexe et non lisse et la technique de Apkarian and Noll [2018] est choisie car elle ne convexifie pas le problème et est adaptée aux grilles de fréquences discrètes et finies. Dans cette approche, la grille de fréquences Ω est raffinée pour chaque κ, garantissant une tolérance souhaitée pour erreur d'estimation de la norme H_∞. La grille Ω est mise à jour pour $T(\kappa, s+\varepsilon+\mathfrak{a}\,)$, où $\mathfrak{a}$ est constante à l'étape 3. La petite constante ε assure que le système n'a pas de pôles sur $\mathfrak{a}\, + j\mathbb{R}$.

Les pics de la norme H_∞ sont également dues à un conrrecteur mal amorti. Ces pôles ne contribuent toutefois pas à la méthode de stabilisation. Pour éviter tels correcteurs, certaines contraintes peuvent être posées à la classe $\mathcal{K}$. En plus de la structure, les pôles correcteurs peuvent être limités à une région conique dans $\mathbb{C}^-$, pour des pôles stables avec une décroissance négative $\alpha(K(\kappa,s)) \leq -\tau$ et un amortissement fixe $\min\{Re(\lambda)/|\lambda|\} = \psi$.

L'efficacité de la méthode pour la conception de correcteurs structurés basée sur la réponse fréquentielle utilisant la minimisation de la norme H_∞ est testée selon le même termes des sections précédentes. La grille de fréquences se situe dans l'interval $[10^{-3}\ ,10^{3}]$ rad/s pour un maximum de 10 000 points distribués de manière logarithmique, raffinée par la méthode introduite dans Apkarian and Noll [2018]. Le paramètre ε est mis à jour de manière itérative à 3% du décalage actuel $\mathfrak{a}$. L'abscisse spectrale a été estimée avec une tolérance de 2% et une grille de fréquences dans le même intervalle avec une densité maximale de 50 000 points par décennie et adaptée à chaque itération par la méthode présentée dans la section E.2.

Les résultats pour les systèmes rationnels instables sont présentés dans le Tableau E.13. Le taux de réussite de la technique est similaire à ceux des autres autres techniques basée sur la réponse frequentielle développées. Un résultat surprenant qui n'est pas entièrement compris est le fait que cette technique est celle qui atteint la pire norme H_∞ après l'optimisation, parmi les 3 techniques.

Les résultats des tests pour les systèmes de dimension infinie sont présentés dans le Tableau E.14. La méthode de conception basée sur la minimisation de la norme H_∞ échoue dans 6 cas. Comme prévu, pour les 12 systèmes déjà stables, l'étape initiale basée sur un faible gain est suffisante pour garantir la conception d'un correcteur stabilisant.

E.9 Étude de cas

On considère maintenant l'exemple du papier Aguiar et al. [2018], inspiré par le probème de commande d'un missile décrit en Krueger [1993]. L'interconnexion en boucle fermée est présentée dans la Figure E.10, montrant le correcteur à concevoir K, le système généralisée P, composée de 5 blocs, les incertitudes et les pondérations pour la performance, W_e et W_d.

La dynamique du missile comprend la dynamique du corps rigide G_r, les trois modes flexibles du système G_f en parallèle avec G_r, et la dynamique des actionneurs et des capteurs, qui sont représentés par des systèmes de second ordre G_{act},G_{acc}, G_{gyr}. Le système P comporte deux pondérations supplémentaires pour la performance et de robustesse W_e, W_d, ce qui donne un total de $n_x(P) = 29$ d'états. L'entrée de commande du missile est l'angle de déflexion de l'empennage d_f à travers de l'actionneur G_{act} et la sortie mesurée est $y = [\eta_m \ \ q_m]^T$, avec accélération η_m obtenue à partir de l'accéléromètre G_{acc} et la vitesse de tangage q_m obtenue à partir du gyroscope G_{gyr}. L'actionneur est décrit par $u_{act} = G_{act} \cdot d_f$ avec $G_{act}(s) = \frac{\omega_{act}^2}{s^2+2\cdot 0.7\cdot\omega_{act}s+\omega_{act}^2}$ et il a un limite de déflexion des ailettes de 40 deg. et un limite de 300 deg./s pour la vitesse.

Table E.13: Comparaison entre la methode basée sur la réponse frequentielle utilisant la norme H_∞ et SYSTUNE pour systèmes de dimension finie instables.

		FRD_∞					SYSTUNE	
		κ^0	$\kappa^\sharp$		κ^*			
Ex	n_K	α	α	$\|.\|_\infty$	α	$\|.\|_\infty$	α	$\|.\|_\infty$
1	18	2.676	-0.05	67.461	-0.05	1.000	-0.05	1.000
2	18	0.177	-0.007	2249.13	-0.035	1.245	-0.048	1.000
3	30	-0.007	-0.035	331.89	-0.445	1.015	-0.445	1.000
4	40	0.006	-0.088	1.95e7	-0.167	3.311	-0.084	1.000
5	40	0.588	-0.001	121.479	-0.018	1.001	-0.017	1.000
6	40	0.632	-0.006	107.828	-0.006	1.000	-0.006	1.000
7	18	0.08	-0.058	9.782	-0.149	1.369	-0.148	1.000
8	61	0.092	-0.011	224.025	-0.028	1.247	-0.136	1.000
9	61	0.228	-0.007	275.896	-0.071	1.000	-0.076	1.000
10	33	0.242	0.016	-	-	-	-0.042	1.000
11	61	0.243	-0.002	43.797	-0.001	1.058	-0.001	1.000
12	28	2.008	-0.566	1.907	-0.251	1.000	-2.069	1.000
13	23	1.996	-1.19	1.184	-2.616	1.000	-2.972	1.000
14	23	1.754	-0.223	1.864	-0.983	1.220	-2.02	1.000
15	61	1.402	-0.365	5.712	-2.372	1.005	-1.383	1.000
16	23	1.115	-0.929	9.012	-0.383	1.022	-0.218	1.000
17	40	0.007	-4.317	105.073	-1.721	1.003	-2.084	1.000
18	63	-0.002	-0.066	2.121	-0.011	1.006	-0.01	1.000
19	28	3.286	-0.46	168.176	-0.636	1.002	-0.63	1.000
20	23	1.981	0.615	-	-	-	-2.64	1.000
21	23	1.859	-4.116	34.168	-4.109	1.458	-3.691	1.000
22	18	1.059	-0.276	4.797	-1.997	0.998	-1.995	1.000
23	33	0.738	-0.148	16.146	-1.698	0.988	-1.776	1.000
24	33	1.662	-1.148	6.267	-2.043	1.005	-1.948	1.000
25	23	1.333	-20.419	14.291	-2.797	1.000	-3.262	1.000
26	23	0.546	-0.268	9.05	-1.217	1.000	-1.638	1.000
27	23	-2.558	-2.559	8.679	-1.762	1.001	-1.927	1.000
28	23	0.251	0.067	-	-	-	-0.628	1.000
29	23	2.012	-7.614	4.497	-1.073	1.001	-0.879	1.000
30	28	0.139	-0.492	2.162	-0.99	0.999	-0.968	1.000
31	28	0.254	-1.523	1.056	-2.225	1.002	-1.499	1.000
32	33	0.191	-0.414	1.905	-2.222	0.998	-2.204	1.000
33	33	1.629	-1.102	3.045	-3.888	1.002	-3.861	1.000
34	33	0.117	-0.118	2.835	-1.667	1.000	-1.504	1.000
35	33	0.55	-0.523	3.516	-6.014	1.000	-7.346	1.000
36	23	0.26	-0.04	2.01	-0.054	1.482	-0.105	1.000

Légende:

Ex:	Cas de test	κ^0:	donnés pour le système asservi initial
α:	abscisse spectrale de $T(\kappa^i, s)$	$\kappa^\sharp$:	donnés pour le système asservi après la stabilisation
$\|.\|_\infty$:	$\|T(\kappa^i, s)\|_\infty$	κ^*:	donnés pour le système asservi après la optimisation
systune:	norme H_∞ atteinte par SYSTUNE	FRD_∞:	résultats de la methode utilisant la norme H_∞
n_K:	dimension du paramètre κ		

Des modèles de second ordre similaires sont utilisés pour l'accéléromètre G_{acc} et le gyroscope G_{gyr}, les valeurs numériques indiquées dans le Tableau E.15. Les incertitudes sur les parametres sont de $\pm 30\%$ pour Z_a et M_q et de $\pm 15\%$ pour M_a. La dynamique rigide du corps, G_r du missile est décrite par la représentation d'état ci-dessous, où l'entrée est fournie par l'actionneur et la sortie est le vecteur $[\eta_{rigid}\ q_{rigid}]^\mathsf{T}$:

$$G_r: \quad \begin{bmatrix}\dot\alpha\\ \dot q\end{bmatrix} = \begin{bmatrix}Z_\alpha & 1\\ M_\alpha & M_q\end{bmatrix}\begin{bmatrix}\alpha\\ q\end{bmatrix} + \begin{bmatrix}Z_d\\ M_d\end{bmatrix} u_{act}$$

$$\begin{bmatrix}\eta_{\text{rigid}}\\ q_{\text{rigid}}\end{bmatrix} = \begin{bmatrix}V/kG\, Z_\alpha & 0\\ 0 & 1\end{bmatrix}\begin{bmatrix}\alpha\\ q\end{bmatrix} + \begin{bmatrix}V/kG\, Z_d\\ 0\end{bmatrix} u_{act}.$$

Trois modes flexibles sont ajoutés pour représenter la dynamique de flexion du missile.

$$G_f: \begin{bmatrix}\eta_{\text{flex}}\\ q_{\text{flex}}\end{bmatrix} = \sum_{i=1}^{3}\begin{bmatrix}\eta_i(s)\\ q_i(s)\end{bmatrix} u_{act},$$

Table E.14: Comparaison entre la methode basée sur la réponse frequentielle utilisant la norme H_∞ pour systèmes de dimension infinie et SYSTUNE pour leurs approximations.

			FRD_∞		SYSTUNE	
Ex	K	n_K	$\alpha_0(.)$	$\alpha(.)$	$\alpha_{apx}(.)$	$\alpha_{act}(.)$
1	2-SS	9	0	0	-36.49	0
2	2,1-TF	4	0	0	-0.006	0
3	3,0-TF	9	1e-4	9e-5	-0.121	6e-5
4	2-SS0	8	0.004	0	-0.001	0
5	3,1-TF	5	0	0	-8e-5	0
6	2,1-TF	4	1.609	1.591	0.965	x
7	2-SS	9	0.712	0	-0.001	0
8	1-SS	4	0.101	0	-0.109	0
9	1-SS	4	1.073	0	-3.086	0
10	3-SS	14	1.196	1.037	0.004	x
11	5-SS0	33	2.300	2.301	2.298	x
12	2-SS	9	0.459	0	-0.001	0
13	2-SS0	12	0	0	-0.060	0
14	2-SS0	12	0	0	-0.398	3.397
15	2-SS0	16	0	0	-0.001	0.733
16	2-SS0	20	0	0	-0.002	0
17	1-SS0	3	0	0	-0.002	0
18	1-SS0	3	0	0	-0.001	0
19	1-SS0	3	0	0	0.029	0.286
20	1-SS0	3	0	0	1.599	1.575
21	3-SS	14	0.839	0.013	-0.132	0.747
22	3,1-TF	5	0.135	0.134	0.048	x
23	1,0-TF	2	1.010	0	-3.055	7.071
24	2-SS0	8	0	0	-2.303	0
25	2-SS	9	0.014	0	-0.001	0.038

Légende:

Ex:	Cas de test		
n_K:	dimension du paramètre κ	K:	structure du correcteur
SYSTUNE :	données de SYSTUNE	FRD_∞:	résultats de la methode utilisant la norme H_∞
$\alpha_{apx}(.)$:	abscisse spectrale de l'approximatif $T_{app}(\kappa^*, s)$	$\alpha_0(.)$:	abscisse spectrale de $T(\kappa^0, s)$
$\alpha_{act}(.)$:	abscisse spectrale de l'effectif $T(\kappa^*, s)$	$\alpha(.)$:	abscisse spectrale de $T(\kappa^*, s)$
x:	pas calculé		

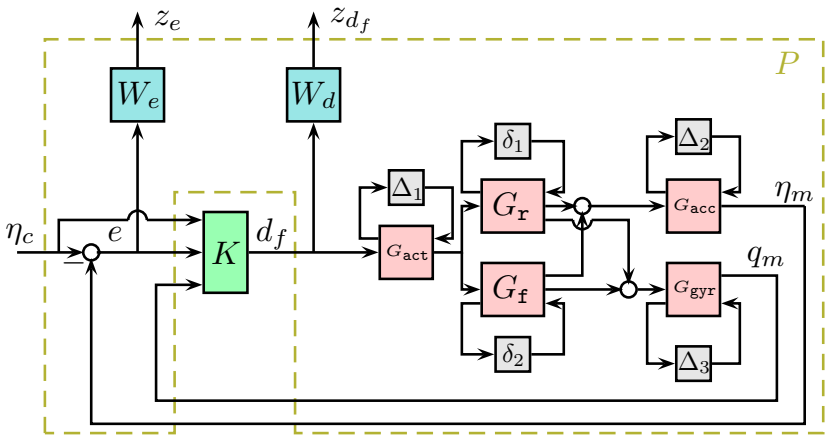

Figure E.10: Interconnexion des sous-systèmes, des blocs d'incertitude et du correcteur.

où

$$\begin{bmatrix}\eta_i(s)\\ q_i(s)\end{bmatrix} = \frac{1}{s^2 + 2\cdot 0.02\cdot\omega_i s + \omega_i^2}\begin{bmatrix}s^2 K_{\eta_i}\\ s K_{q_i}\end{bmatrix},$$

Table E.15: Values and uncertainty of the missile parameters

Var	Value	Var	Value	Var	Value	Var	Value
Z_a	-5.24	Z_d	-0.73	M_a	-46.97	M_d	-1134
M_q	-4.69	V/kG	1.182	ω_1	368	ω_2	937
ω_3	1924	ω_{act}	377.0	ω_{acc}	188.5	ω_{gyr}	500.0
K_{η_1}	-0.943	K_{η_2}	0.561	K_{η_3}	-0.312	K_{q_1}	1024.1
K_{q_2}	406.5	K_{q_3}	-1408.4				

$i = 1, 2, 3$, et puis la dynamique globale est

$$\begin{bmatrix} \eta \\ q \end{bmatrix} = \begin{bmatrix} \eta_{\text{rigid}} \\ q_{\text{rigid}} \end{bmatrix} + \begin{bmatrix} \eta_{\text{flex}} \\ q_{\text{flex}} \end{bmatrix}.$$

Les sorties finales mesurées sont alors $\eta_m = G_{acc} \cdot \eta$ et $q_m = G_{gyr} \cdot q$. Les valeurs des paramètres du système sont présentés au Tableau E.15.

La dynamique en haute fréquence non modélisée de l'actionneur et du capteur est supposée être 0,1% incertain à basse fréquence et 100 % à haute fréquence. Cela correspond à inclure le pondération $W^{\Delta}_{act}(s) = \frac{(s+\omega_{act})^2}{(s+10\cdot\omega_{act})(s+100\cdot\omega_{act})}$, pour l'actionneur, et de même, pour l'accéléromètre et le gyromètre avec leurs fréquences respectives ω_{acc} et ω_{gyr}, indiquées dans le Tableau E.15, chacune avec 15 % d'incertitude par rapport à la valeur nominale. En rassemblant tous les blocs incertains du missile, $\Delta = \text{diag}\left[\Delta_p, \Delta_d\right]$, avec $\Delta_p = \text{diag}\left[\delta_{Z_\alpha}, \delta_{M_\alpha}, \delta_{M_q}; \delta_{\omega_1} I_6, \delta_{\omega_2} I_6, \delta_{\omega_3} I_6\right]$ et $\Delta_d = \text{diag}\left[\Delta_{act}, \Delta_{acc}, \Delta_{gyr}\right]$.

Enfin, les pondérations de performance ont été choisies de manière à refléter les exigences de conception suivantes : Tout d'abord, l'accélération η_m doit suivre la commande η_c avec un temps de montée d'environ 0,5 seconde. D'où la fonction de pondération $W_e(s)$ pour la fonction de transfert de η_c vers la fonction tracking error $e := \eta_c - \eta_m$ a été choisi comme $W_e(s) := \frac{1}{100}\frac{s/10+100}{s/10+0.05}$.

Deuxièmement, pour la robustesse, le taux de variation à haute fréquence du signal de commande et du *roll-off* sont capturées et pénalisées par la contrainte $||W_d(s)T_{d_f\eta_c}||_\infty \leq 1$, où $W_d(s)$ est une pondération passe-haut $W_d(s) := (s/200(0.001s+1))^2$. Cela permet également de répondre aux exigences imposées par la les limites de déflexion de l'actionneur et les limites de vitesse. Au total, la sortie régulée est $z = [W_e e \;\; W_d d_f]^\mathsf{T} = [z_e \;\; z_{d_f}]^\mathsf{T}$.

A l'aide des méthodes décrites dans ce travail, on calcule des compensateurs robustes K d'ordre 6 avec 3 entrées η_c, $e = \eta_c - \eta_m$, et q_m, et une sortie d_f.

Les méthodes de relaxation hybrides et interne ont atteint performances très similaires, 0.4416 et 0.4310, alors que l'approche en relaxation extérieure n'était pas en mesure de trouver une solution. La valeur de performance retournée par DKSYN était Inf, ce qui signifie qu'elle n'a pas pu trouver de solution non plus. Le nombre de scénarios généré par la relaxation interne était 13 tandis que pour l'hybride était 6. Les réponses indicielles η_m, q_m and δ_c to η_c obtenues sont indiquées sur la Figure E.11. Les deux techniques ont permis d'atteindre les exigences de conception prescrites.

E.10 Conclusion

Cette thèse présentait trois nouvelles relaxations pour le problème de commande robuste et trois nouvelles méthodes pour la synthèse de correcteurs basée sur la réponse fréquentielle.

Le développement d'une nouvelle approximation externe a permis les multiplieurs et le compensateur d'être calculés simultanément pour stabiliser et améliorer les performances. Le développement d'un nouvelle relaxation interne a permis d'obtenir les meilleures performances parmi toutes les méthodes testées dans cette thèse et réduire le conservatisme tout en assurant la robustesse. Le développement d'une relaxation hybride combinant les relaxations interne et externe a conduit à la deuxième meilleure performance de tous les méthodes testées tout en générant moins de scénarios. Les trois relaxations n'exigent pas que $\boldsymbol{\Delta}$ soit redimensioné, ce qui signifie que la performance est calculée pour le système tel que modélisé. Les contributions à la commande de systèmes de dimension infinie sont le développement d'un estimateur de l'abscisse spectrale pour les systèmes IDLTI qui sont méromorphes sur le plan complexe de la moitié gauche et le développement de trois techniques pour la synthèse de correcteurs structurés basée sur la réponse frequentielle pour des systèmes IDLTI instables ou stables.

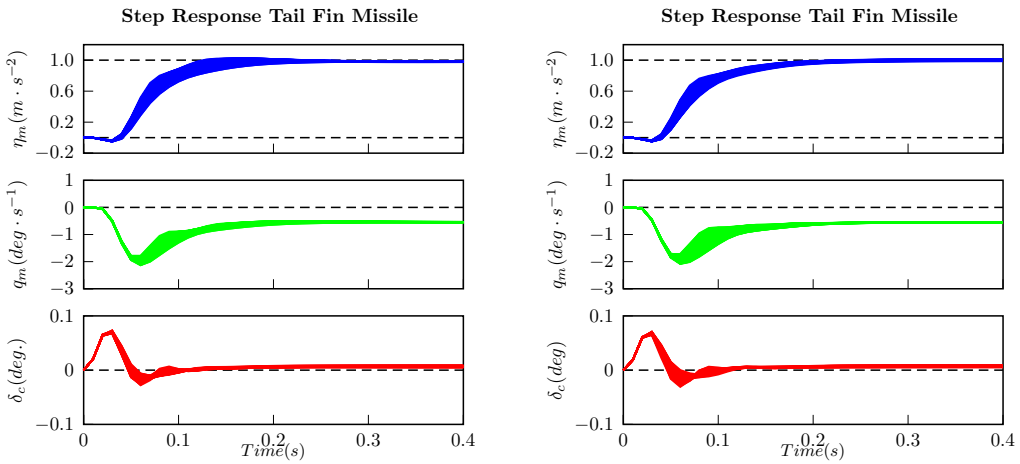

(a) Réponses indicielles obtained by inner relaxation technique

(b) Réponses indicielles obtained by hybrid relaxation technique

Figure E.11: Réponses indicielles of the closed-loop system for the Tail Fin Missile.

La principale limitation de la relaxation externe est la grande quantité de conservatisme introduite pour les systèmes soumis à une incertitude structurée avec des blocs d'incertitude paramétrique avec un grand nombre de répétitions, ce qui implique que les multiplieurs ont un grand nombre de paramètres à régler et constituera un défi pour pour les outils d'optimisation actuels. La principale limitation de l'approche basée sur la minimisation de l'abscisse spectrale est le caractère non lisse de la fonction minimisée. Ceci peut être la cause d'une perturbation dans des cas spécifiques, empêchant le progrès de la recherche.

Comme suggestions de travaux futurs, les relaxation proposés peuvent s'appliquer à la commande H_2 conduisant à une synthèse mixte H_2/H_∞ et l'estimateur spectral peut être amélioré par l'implémentation d'heuristiques plus sophistiquées à la place de l'algorithme de bissection. L'estimateur pourrait également être étendu à l'estimation des valeurs négatives de l'abscisse spectrale, ou à l'estimation sans connaissance préalable de l'emplacement des pôles grâce à grille de fréquence appropriée et un décalage initial suffisamment important. Une autre suggestion pour améliorer les résultats en termes de taux de succès des méthodes basées sur l'énergie et l'abscisse spectrale est la spécialisation de routines d'optimisation.